

Pre-applied bonded waterproofing membranes: Influences of nonwovens on filtration and bonding properties

Ulli Heinlein

Vollständiger Abdruck der von der Fakultät für Bauingenieurwesen und Umweltwissenschaften der Universität der Bundeswehr München zur Erlangung des akademischen Grades eines

Doktors der Ingenieurwissenschaften (Dr.-Ing.)

genehmigten Dissertation.

Gutachter:

1. Gutachter: Prof. Dr.-Ing. Thomas Freimann
2. Gutachter: Univ.-Prof. Dr.-Ing. Christian Thienel
3. Gutachter: Univ.-Prof. Dr.-Ing. Wolfgang Breit

Die Dissertation wurde am 03.03.2023 bei der Universität der Bundeswehr München eingereicht und durch die Fakultät für Bauingenieurwesen und Umweltwissenschaften am 14.09.2023 angenommen. Die mündliche Prüfung fand am 13.11.2023 statt.

Danksagung

Die vorliegende Arbeit entstand während meiner Zeit als wissenschaftlicher Mitarbeiter an der Technischen Hochschule Nürnberg im Labor für Beton- und Baustofftechnologie zwischen 2018 bis 2023.

Ganz herzlich möchte ich Herrn Prof. Dr.-Ing. Thomas Freimann für die langjährige fachliche Betreuung und Zusammenarbeit danken, die für mich ursprünglich vor 10 Jahren als Tutor für das Baustoffpraktikum begonnen hat. Über die Jahre hinweg haben sich zahlreiche Projekte, Veröffentlichungen und Erfindungen entwickelt, die schließlich auch zu dieser Dissertation geführt haben.

Ebenso herzlich bedanke ich mich bei Prof. Dr.-Ing. Christian Thienel für sein Interesse an der Themenstellung und seiner Bereitschaft, meine Arbeit an der Universität der Bundeswehr München zu betreuen. Die anregenden Diskussionen haben immer wieder neue Sichtweisen und Ideen für ergänzende Versuche hervorgebracht. Auch die Möglichkeit das μ CT zu nutzen, hat die Arbeit bereichert.

Herrn Prof. Dr.-Ing. Wolfgang Breit danke ich sehr für die Bereitschaft die Arbeit als dritter Gutachter zu bewerten. Auch Herrn Prof. Dr.-Ing. Thomas Braml bin ich für die Übernahme des Vorsitzes des Promotionsverfahrens sehr verbunden.

Weiterhin sind Frau Dr.-Ing. Nancy Beuntner und Herr Wolfgang Saur hervorzuheben, die mich bei meinen μ CT-Versuchen unterstützt und die Labornutzung so unkompliziert möglich gemacht haben. Auch durch die gute Arbeitsatmosphäre am Institut hat es immer Spaß gemacht, nach Neubiberg zu kommen.

Ganz besonders möchte ich mich bei meiner Familie und Freundin bedanken. Vor allem meinen Eltern gilt besonderer Dank, die mich bis heute immer unterstützt und gefördert haben.

Abstract

Pre-applied bonded membranes are used to waterproof concrete basements and are installed before reinforcement works, e.g., in a formwork. The membranes form a bond with the subsequently poured fresh concrete and often use nonwovens as a bonding layer, which must be filled with cement paste during concrete placement. However, due to limited studies, the cement paste separation process and paste properties in the nonwoven are unknown. Also, no recommendations for optimized nonwovens are possible, and advice for practice is limited.

This thesis aims to optimize the membrane products and understand processes during concrete placement. It first examines currently used pre-applied membranes for their essential nonwoven and fiber properties using thickness measurements, infrared spectrometry (FTIR), and microscopic analysis.

In the second part of the thesis, the nonwoven deformation behavior during concrete placement is studied by measuring the thickness change of nonwovens using microsections and an incident light microscope. Also, porosity is analyzed via micro-computed tomography scans (micro-CT scans). During concrete placement, the nonwoven is initially compressed due to the fresh concrete load and relaxes again during vibration compaction as cement paste increasingly fills the nonwoven. The cement paste transfers the fresh concrete load, enabling the nonwoven to recover due to the residual stress in the nonwoven fibers.

The separation of cement paste from fresh concrete and its properties in the nonwoven are investigated in the third part of the thesis using a customized filtration test stand, 'loose' nonwovens, and a practice-oriented concrete placement. The separated cement paste is analyzed for water content, solid density, and particle size. Video recordings supplement the tests and show that nonwovens are characterized by water movements during concrete placement. Similar to Controlled Permeable Formworks, excess water separates from the fresh concrete during concrete placement, filling the nonwoven pores in a short time. Simultaneously, a limited amount of fine solids enter the nonwoven, while unseparated particles on the nonwoven surface form a filter cake and stop the separation of solids, resulting in a water-rich cement paste within the nonwoven. It is upon vibration compaction that the filter cake is loosened and more solids enter the nonwoven. Water is displaced, the water-solid ratio in the nonwoven is reduced and is low for small nonwoven pore volumes, high compaction energies in the vicinity of the nonwoven, and high fresh concrete spreads.

In order to identify overall good nonwoven properties, the fourth part of the thesis focuses on the bond strength between nonwoven and concrete by performing pull-off tests according to DIN EN 1542. The bond strength develops proportionally to the concrete tensile splitting strength and is influenced by the mortar strength in the bonding zone, which in turn is affected by the water content in the nonwoven. High bond strengths are achieved for nonwovens with low basis weights and concretes with high tensile splitting strengths. Vibration compaction displaces water accumulations and thus increases the bond strength, e.g., at formwork corners.

This thesis provides an in-depth understanding of the time-dependent processes within nonwovens of pre-applied membranes during concrete placement and the impact of various boundary conditions. Based on the results, advantageous nonwoven properties for pre-applied bonded membranes and favorable installation conditions for the construction site are formulated.

Kurzfassung

Frischbetonverbundsysteme (FBVS) werden als ergänzende Abdichtung bei wasserundurchlässigen Bauwerken aus Beton eingesetzt. Sie werden vor dem Betoneinbau verlegt, und nutzen eine Verbundschicht um einen lagesichereren wie wasserundurchlässigen Verbund (Hinterlaufschutz) zum Bauwerk auszubilden. Dafür werden häufig Vliese eingesetzt, die während des Betoneinbaus mit Zementleim gefüllt werden müssen. Allerdings sind die dabei ablaufenden Prozesse und die betontechnologischen Eigenschaften des Zementleims im Vlies bisher unbekannt. Auch gibt es noch keine Empfehlungen zu optimierten Vlieseigenschaften.

Die vorliegende Thesis soll helfen, die Bauweise zu verbessern und Vorgänge in mechanisch-adhäsiven FBVS nachzuvollziehen. Im ersten Teil werden dazu Vliese von FBVS mit Hilfe von Dickenmessungen, FTIR-Analysen und mikroskopischen Betrachtungen charakterisiert.

Anschließend wird im zweiten Teil der Arbeit das Deformationsverhalten von Vliesen im Betonierprozess nachvollzogen, indem die Vliesdicke vor und nach dem Betoneinbau unter einem Auflichtmikroskop vermessen wird. Außerdem wird die Porosität durch Mikro-CT Aufnahmen ermittelt. Die Vliese werden beim Betoneinbau durch den Frischbetondruck komprimiert, vergleichbar zu einer mechanischen Belastung, aber dekomprimieren wieder bei Vibrationsverdichtung. Die Vliesstruktur füllt sich während des Betoneinbaus zunehmend mit Zementleim, sodass der Frischbetondruck über den Zementleim abgetragen und die Vliesfasern entlastet werden. Schließlich führt die Eigenspannung in den Vliesfasern dazu, dass die initiale Kompression zurückgeht.

Die Abtrennung von Zementleim aus dem Frischbeton und seine betontechnologischen Eigenschaften werden anschließend in einem eigens entwickelten Versuchsstand untersucht. ‚Lose‘ Vliese werden dazu in einem Filtertest praxisnah mit Frischbeton verbaut und der abgetrennte Zementleim auf Menge, Wassergehalt, Feststoffdichte und Partikelgröße bestimmt. Videoaufnahmen der Verbundschicht ergänzen die Versuche und zeigen, dass sich bei Betoneinbau Überschusswasser aus dem Frischbeton abtrennt; vergleichbar zu wasserabführenden Schalungsbahnen. Das Überschusswasser füllt die Vliesporen in kurzer Zeit und kann sich lateral im Vlies bewegen. Gleichzeitig gelangt eine begrenzte Menge an feinen Feststoffen in das Vlies, wobei zurückbleibende Partikel einen Filterkuchen auf der Vliesoberfläche bilden und die weitere Feststoffabtrennung verlangsamen. Dadurch bildet sich im Vlies zu Beginn des Betoneinbaus ein wasserreicher Zementleim. Erst bei einsetzender Vibrationsverdichtung wird der Filterkuchen gelockert, weiterer Feststoff in das Vlies eingetragen und Wasser aus dem Vlies verdrängt. Das Wasser-Feststoffverhältnis im Vlies sinkt und ist für geringe Porenvolumina der Vliese, hohe Verdichtungsenergien und hohe Frischbetonkonsistenzen niedrig.

Um übergreifend gute Vlieseigenschaften für FBVS zu identifizieren, wird im letzten Teil der Thesis der Haftverbund verschiedener Vliese zu Beton in Abreißversuchen nach DIN EN 1542 untersucht. Der Haftverbund entwickelt sich dabei proportional zur Spaltzugfestigkeit des Betons und wird durch die Zementsteifigkeit in der Verbundschicht beeinflusst. Höhere Zementfestigkeiten und längere Erhärtungsdauern führen daher zu größeren Haftzugfestigkeiten. Die Zementsteifigkeit in der Verbundschicht hängt zusätzlich von der abgetrennten Wassermenge im Vlies ab, sodass höhere Haftzugfestigkeiten letztlich für leichtere Vliese erreicht werden. Außerdem ist eine Vibrationsverdichtung vorteilhaft, da sie Wasseransammlungen verdrängt und dadurch die Haftzugfestigkeit z.B. an Schalungsecken erhöht.

Die vorliegende Arbeit ermöglicht ein vertieftes Verständnis zu den Vorgängen in Vliesen von FBVS während des Betoneinbaus und den Einflüssen verschiedener Randbedingungen. Darauf aufbauend werden vorteilhafte Vlieseigenschaften für FBVS, geeignete Einbaubedingungen sowie Einbauempfehlungen für die Baustelle formuliert.

Table of Contents

Danksagung	I
Abstract	II
Kurzfassung	III
Table of Contents	IV
List of Abbreviations	VI
List of Figures	VII
1 Introduction	1
1.1 Thesis background.....	1
1.2 Scope of the thesis.....	1
2 State of knowledge	3
2.1 Pre-applied bonded waterproofing membranes	3
2.1.1 Overview	3
2.1.2 Mode of action and differentiation of pre-applied bonded membranes.....	4
2.1.3 Application aims and regulations of pre-applied bonded membranes	5
2.2 Studies on nonwoven bonded pre-applied membranes	6
2.2.1 Studies on the waterproof bond.....	6
2.2.2 Studies on the bond strength.....	6
2.3 Nonwovens	7
2.3.1 General information.....	7
2.3.2 Nonwoven production.....	7
2.3.3 Nonwovens under mechanical load.....	8
2.3.4 Filtration using nonwovens	9
2.3.5 Nonwoven geotextiles	10
2.3.6 Nonwovens for Controlled Permeable Formworks.....	11
3 Summary of the methods applied	12
4 Main results	19
4.1 Characterization of nonwovens on pre-applied bonded membranes	19
4.2 Macroscopic nonwoven behavior during concrete placement.....	19
4.2.1 Change under compression during concrete placement.....	19
4.2.2 Porosity in the nonwoven during concrete placement.....	22
4.3 Materials for filtration and pull-off tests	22
4.4 Cement paste filtration and processes within nonwovens during concrete placement	23
4.4.1 Temporal sequence of solids and water intrusion.....	23
4.4.2 Water flow within nonwovens	25

- 4.4.3 Particle size distribution in nonwovens 26
- 4.4.4 Influences on the separated solid mass..... 28
- 4.5 Bond strength of nonwovens to concrete..... 30
 - 4.5.1 Influence of hardened concrete properties 30
 - 4.5.2 Influence of concrete placement conditions 33
 - 4.5.3 Influence of nonwoven properties 35
- 4.6 Hypothesis on cement paste separation and bond strength development 36
 - 4.6.1 Cement paste separation after fresh concrete placement 36
 - 4.6.2 Cement paste separation during vibration compaction 37
 - 4.6.3 Bond strength development..... 38
- 5 Conclusions..... 40**
- 6 Recommendations for practice 40**
- 7 Perspectives 41**
- 8 References..... 43**
- 9 Publications..... 51**
 - 9.1 Pre-applied bonded waterproofing membranes: A review of the history and state-of-the-art in Europe and North America 51
 - 9.2 Pre-applied mechanical bonded waterproofing membranes: Macroscopic nonwoven behavior during the concreting process 63
 - 9.3 Pre-applied mechanically bonded waterproofing membranes: Cement paste filtration process and influencing parameters..... 75
 - 9.4 Pre-applied mechanically bonded waterproofing membranes: Bond strength of nonwovens to concrete and influencing parameters 93
- 10 Appendix A 111**
- 11 Appendix B 112**

List of Abbreviations

Material abbreviations

PCE	Polycarboxylate ether
PP	Polypropylene
PE	Polyethylene
LDPE	Low-density polyethylene
PVC	Polyvinylchloride
TPO	Thermoplastic polyolefins
FPO	Flexible polyolefins
EPDM	Ethylene-propylene-diene rubber
SIS	Styrene-isoprene-styrene block polymer
SBS	Styrene-butadiene-styrene block polymer

Mathematical abbreviations

T_{Total}	Total thickness of a pre-applied bonded membrane
T_{NW}	Nonwoven thickness
V_{pore}	Nonwoven pore volume on 1 m ²
ε	Nonwoven porosity
C_{nw}	Nonwoven compression
$C_{\text{nw,loss}}$	Thickness loss of a nonwoven following a loading cycle
f_{cm}	Compressive strength of concrete at 28 days
$f_{\text{ct,sp}}$	Splitting strength of concrete
s	Cement-specific coefficient depending on its strength class
t_{T}	Temperature-adjusted concrete age
Δt_i	Time period during concrete curing
$T(\Delta t_i)$	Mean temperature during the time period Δt_i
$f_{\text{nw,pull-off}}(t)$	Bond strength of nonwovens to concrete over time
v	Nonwoven-specific coefficient for bond strength approximation
ρ	Density of nonwoven fibers

Other abbreviations

w/c ratio	Water/cement ratio of fresh concrete
w/s ratio	Water/solids ratio (by mass) of cement paste within nonwovens
CPF	Controlled Permeable Formwork
ETA	European Technical Assessment
FTIR	Fourier transform infrared spectroscopy
ATR	Attenuated total reflection
CE	Conformité Européenne
UV	Ultraviolet
Micro-CT	Micro-computed tomography
SEM	Scanning electron microscope
fib	Fédération internationale du béton

List of Figures

Fig. 1	Pre-applied bonded membranes are installed previous to placing the fresh concrete and prevent lateral water migrations due to a waterproof bond achieved by different bonding mechanisms	3
Fig. 2	Differentiation of pre-applied bonded membranes by the sealing layer and the bonding mechanism (based on [4,5,11]).....	4
Fig. 3	Microsections of different bonding mechanisms. (a,b) fiber bonded membrane with polymer barrier; (c) fiber bonded membrane with a swellable barrier; (d,e) synthetic adhesive bonded membranes, and (f) bonding zone of a bituminous bonded membrane	4
Fig. 4	Models of filtration mechanisms: (a) straining, (b) cake filtration, and (c) depth filtration (based on [60, p. 145]).....	10
Fig. 5	Section of a 50 mm long image to determine the average thickness of a nonwoven...	13
Fig. 6	Setup of the filtration test stand and first steps in the experimental procedure	15
Fig. 7	The nonwoven surface was not changed by the lamination process using epoxy resin. SEM images of the nonwovens N4 with calender bonding (a), N6 with needle bonding (b), and N9 with hydroentanglement and large openings (c) are shown.....	16
Fig. 8	Experimental procedure of the pull-off tests on concrete bonded nonwovens.....	17
Fig. 9	Top view of a reference specimen after testing (a) and a larger specimen with increasing testing distance to the point of concrete placement and compaction in concentric circles (b).....	17
Fig. 10	Compression of a vertically-oriented membrane during ongoing compaction with an internal vibrator.....	20
Fig. 11	Compressional change per time of the nonwovens S1-S7 during the initial 2.5 s compaction with an internal vibrator.....	21
Fig. 12	Compression of a vertically-oriented membrane during ongoing compaction with an internal vibrator.....	21
Fig. 13	Micro-CT scans of cylindrical specimens with the pre-applied membrane S3 ($\varnothing/h = 20/10$ mm) visualizing (a) and determining (b) the change in porosity during ongoing compaction.....	22
Fig. 14	Filtration of excess water in the static intrusion test at different fresh concrete loads and w/c ratios using N1	24
Fig. 15	Time-dependent processes in the nonwoven N1 during static loading (a) and subsequent vibration compaction (b).....	24
Fig. 16	Nonwoven N1 during and after concrete placement. Color dots with red to green coloring indicate water movement in the nonwoven. Noticeable is the flow of filtrated excess water in the nonwoven before and after concrete compaction.	25
Fig. 17	Water/solid ratio in the nonwovens N1&N2 in relation to the distance to the internal vibrator axis	26

Fig. 18 Particle size distribution in the nonwovens N1-8&10. Nonwoven N9 was not included in the above evaluation due to its wider openings..... 27

Fig. 19 Influence of varying fresh concrete spreads on the solid mass in the filtrate 28

Fig. 20 Textile influences due to variable pore volumes in the nonwovens 29

Fig. 21 Nomogram for estimating the w/s ratio in a nonwoven considering the relevant influences during concrete placement. Note that the nomogram is only valid for concrete mixtures with excess water. 31

Fig. 22 (a) Development of the bond strength and concrete tensile splitting strength during ongoing concrete curing considering the concrete temperature according to Equation 12. Approximation started 12 h after concrete placement. (b, c) Typical failure mode in the pull-off tests. 32

Fig. 23 Nonwoven bond strength and concrete tensile splitting strength for varying w/c ratios two days after concrete casting. 33

Fig. 24 Comparison of the bond strength of nonwovens to the tensile splitting strength of concrete for N1-N10. 33

Fig. 25 Comparison of the bond strength in horizontal and vertical orientation 34

Fig. 26 Bond strength with increasing distance from the internal vibrator and location of concrete placement..... 34

Fig. 27 The nonwoven bond strengths on a column is affected by varying w/c ratios of the fresh concrete in the bonding zone. Similar to CPF, excess water separates in the column center and accumulates at the formwork bottom..... 35

Fig. 28 Bond strength of nonwovens N1-N10 at a w/c ratio of the fresh concrete of 0.55 (a) and 0.40 (b) 36

Fig. 29 Hypothesis on the time-dependent processes in the nonwoven during concrete placement..... 37

1 Introduction

1.1 Thesis background

Basements create additional space to accommodate technical equipment, parking areas, and living space and are especially important in densely populated inner cities [1]. In order to protect the structure from deterioration and ensure its suitability for the intended use, basements must be waterproofed depending on the water exposure [2]. If the basement is exposed to groundwater, waterproofing can be done using barrier protection or structural integral waterproofing [3,4].

Barrier protections use continuous watertight layers and should be arranged outside of new buildings (positive side) [5]. They can either be installed loosely in front of a structure or bonded to the basement surface, e.g., as a hot-applied bituminous membrane. International guidelines [4,6] point out that bonded membranes prevent lateral water movement between the membrane and a concrete basement surface. If there is a local damage in the waterproofing layer, this effect improves redundancy. Bonded waterproofing membranes can be post-applied on finished basement walls [5] and need a working trench around the basement.

In the new millennium, cities' population grew and raised the demand for living space in densely populated areas. As a result, basements were extended to the property line. To avoid working trenches, 'blindside' waterproofing membranes were introduced that were applied directly on a soil retention system and bonded with a later-built basement wall made of concrete. Similar waterproofing membranes were used below base slabs and in formwork and ensured a waterproof and adhesive bond with the subsequently poured fresh concrete by providing a bonding layer [7–10]. These 'pre-applied bonded waterproofing membranes' were first used in North America [5] and also widely used in Europe during the last decade [11]. They are applied as stand-alone waterproofing measures or combined with waterproof concrete structures and improve redundancy, seal separation cracks in the concrete, or ensure high usage requirements or gas impermeability [4,12]. The growing interest in the world market is visible by increasing sales figures, manufacturers [13], patents, and the integration into regulations [4].

The bonding layer of pre-applied bonded membranes is made of synthetic adhesives, bitumen, or nonwovens [12,14] and has a non-stick surface allowing walkability and horizontal installation directly below base slabs. Bonding layers made of synthetic adhesives and bitumen are understood in their mode of action and can essentially be described as cold-bonding adhesives with a non-stick surface. In contrast, the mode of action of nonwovens has not yet been conclusively clarified. In the past, phenomenological investigations have been carried out and the waterproof bond was tested under various manufacturing conditions using hydrostatic tests. It was found that nonwovens are filled with cement paste during the concrete placement and that vibration compaction in the vicinity of the nonwoven is necessary for a waterproof bond [15]. Although these are already important guidelines for concrete placement, no recommendations on favorable nonwoven properties for pre-applied bonded membranes are possible thus far. Also, the processes in nonwovens during concrete placement, cement paste properties within nonwovens, and their bond strength to the concrete surface need further investigation.

1.2 Scope of the thesis

Research works by *Meyer et al.* [15] and *Freimann and Heinlein* [16] were the starting point for this thesis, as the authors investigated various pre-applied membranes and provided initial

findings on the bonding mechanisms. However, the nonwoven properties were unknown, and processes within the nonwoven were not understood due to the closed structure of the pre-applied membranes. Also, the bond strength measurements were influenced by the adhesion between the nonwoven and sealing layer.

This thesis aims to gain an in-depth understanding of nonwoven bonded pre-applied membranes, internal processes during concrete placement, and bond strength development. The newly gained knowledge is intended to enable optimization of the nonwovens and allow recommendations for concrete placement conditions and stripping times on-site. For that, the following research questions are addressed:

1. *Nonwoven properties:* What are the essential properties of nonwovens of currently used pre-applied bonded membranes?
2. *Macroscopic behavior:* What is the deformation behavior of nonwovens during concrete placement? Can it be linked to the behavior under mechanical load?
3. *Cement paste separation:* How is cement paste separating from fresh concrete into a nonwoven during concrete placement and vibration, and what processes occur within the nonwoven? What are the properties of the separated cement paste?
4. *Influences on the bond:* How is the bond influenced by nonwoven and fresh concrete properties? How is the bond developing, and what are the effects of concrete placement and nonwoven orientation?

Each research question was addressed in one peer-reviewed journal paper listed in Chapter 9, with the main findings summarized and discussed in Chapter 4.

The **first paper** reviews the historical development, current patents, characteristics, regulations, and previous investigations of pre-applied bonded membranes since there exists limited international literature. Chapters 2.1 and 2.2 are based on this review focusing on mechanically bonded membranes. Also, nonwoven properties of currently used pre-applied membranes were tested (Chapters 4.1 and 9.1). In the **second paper**, the nonwoven deformation behavior during concrete placement is determined using microsections and compared with the behavior under mechanical load. Furthermore, micro-CT scans determined the porosity change caused by concrete placement (Chapters 4.2 and 9.2). The **third paper** uses filtration tests to examine the separation of cement paste, its properties, and the processes within nonwovens during concrete placement (Chapters 4.4 and 9.3). The results were supplemented by video recordings of the nonwoven taken during concrete placement for the fourth paper visualizing internal processes. Furthermore, the **fourth paper** determines the bond strength of nonwovens to concrete in pull-off tests in relation to the concrete tensile splitting strength and cement paste properties in the bonding zone (Chapters 4.5 and 9.4). Chapter 4.6 provides an overarching discussion of the results of Chapters 4.2, 4.4, and 4.5. In combination, a working model of the time-dependent processes in the nonwoven is proposed, and recommendations on favorable nonwoven properties and concrete placement conditions on-site are given. Essential findings and recommendations for practice are summarized in Chapters 5 and 6, and further research needs are stated in Chapter 7.

2 State of knowledge

2.1 Pre-applied bonded waterproofing membranes

2.1.1 Overview

Pre-applied bonded membranes are used as positive-side barrier protection on concrete structures. Before the concrete works, they are placed on a mud slab, vertically on a formwork, or in blindside applications onto a soil retention system. The membrane sheets are hereby joined at seams and penetrations are sealed to achieve a waterproof layer. During further construction, fresh concrete is applied directly onto the membranes, and a bond is achieved [12].

The membranes essentially comprise a sealing and a bonding layer. The single-ply sealing layer is hydrostatic pressure resistant and enables crack bridging of the adjoining concrete structure. The bonding layer achieves a two-fold bond with the concrete surface [17]: First, a waterproof bond is created, which prevents lateral water migrations between the membrane and the concrete surface even in case of local damage. Thus, separating cracks in the concrete cannot be saturated, which increases the redundancy of the waterproofing compared to unbonded barrier protections [4,18]. Second, an adhesive bond secures the position during stripping and use, so fasteners, soil settlements, or degradation in the soil cannot harm the sealing layer [5].

The bond is created mechanically using nonwovens or geogrids, adhesively using coated synthetic adhesives, or bituminous using sanded bituminous membranes [12]. Due to their non-stick surface, the membranes can be walked on during horizontal installation, and base slabs can be constructed directly on them. Fig. 1 shows the mode of action of pre-applied membranes and the different bonding mechanisms.

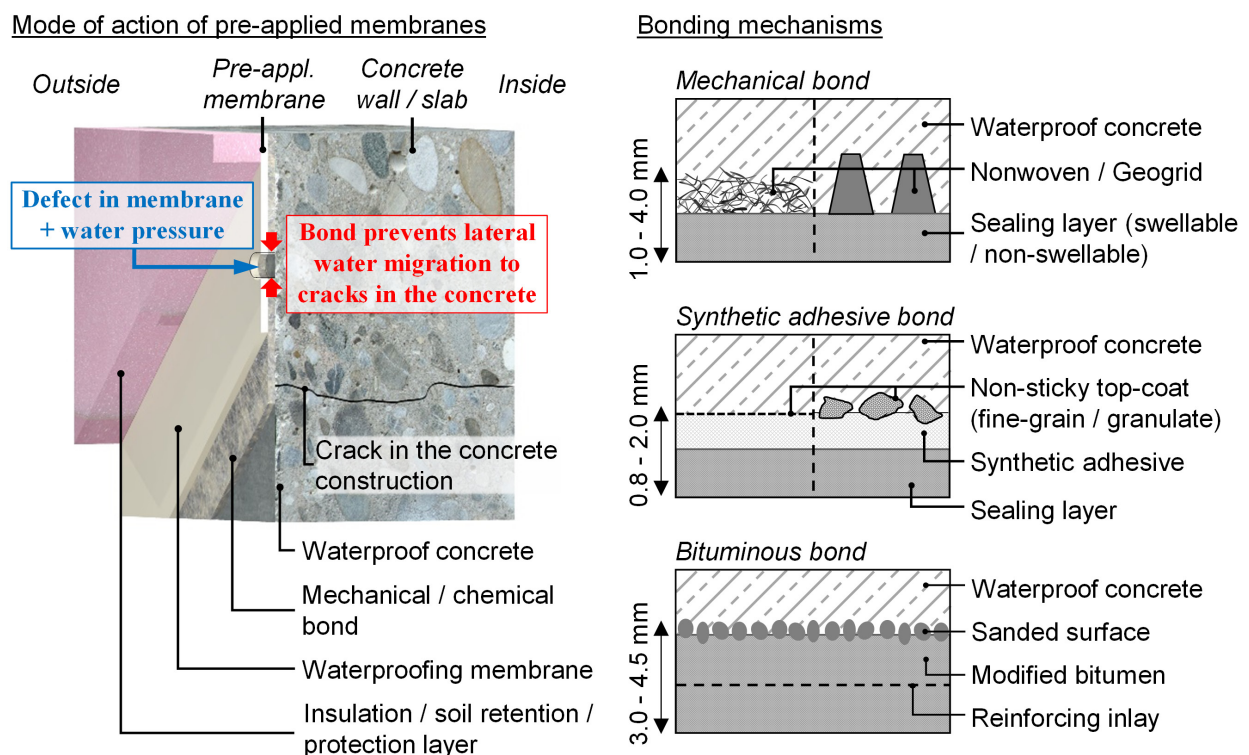


Fig. 1 - Pre-applied bonded membranes are installed previous to placing the fresh concrete and prevent lateral water migrations due to a waterproof bond achieved by different bonding mechanisms

2.1.2 Mode of action and differentiation of pre-applied bonded membranes

Pre-applied bonded membranes can be differentiated according to their sealing layer and bonding mechanism. Fig. 2 shows a possible distinction, and Fig. 3 cross-sections of various commercially available pre-applied membranes bonded to concrete.

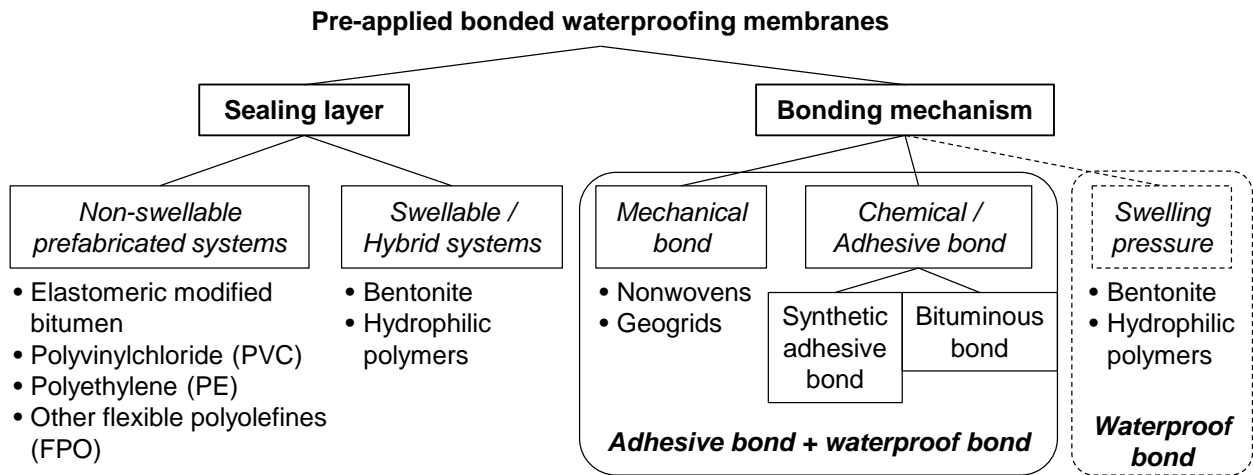


Fig. 2 - Differentiation of pre-applied bonded membranes by the sealing layer and the bonding mechanism (based on [4,5,11])

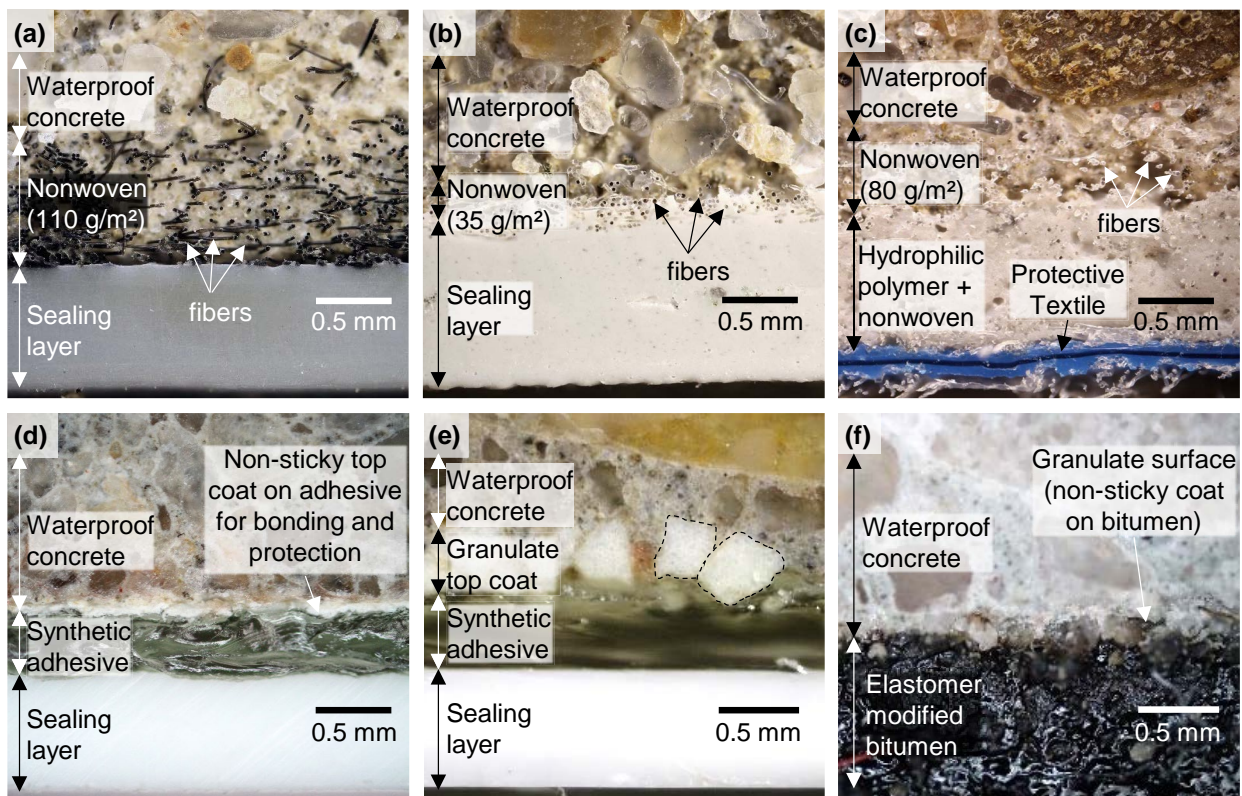


Fig. 3 - Microsections of different bonding mechanisms. (a,b) fiber bonded membrane with polymer barrier; (c) fiber bonded membrane with a swellable barrier; (d,e) synthetic adhesive bonded membranes, and (f) bonding zone of a bituminous bonded membrane

The product review in Chapter 9.1 shows sealing layers made of non-swellable thermoplastic materials such as polyvinylchloride (PVC), thermoplastic and flexible polyolefins (TPO, FPO) like polyethylene (PE), or elastomeric materials like ethylene-propylene-diene rubber (EPDM) [19 p. 2.50 ff.,20] with thicknesses between 0.5-2.2 mm. Also, elastomer-modified bitumen is used as

sheet membranes with thicknesses between 3.0-4.5 mm and a reinforcing inlay, e.g., polyester fleece [15,21].

In a few cases, swellable materials are formed or added to pre-applied membranes. Hydrophilic polymers, based on acrylamide or acrylic acid, are used as superabsorbent [22,23] and added to nonwovens or polymer waterproofing membranes. Like bentonite, the swellable materials become waterproof by absorbing water as they create a swelling pressure, thus, requiring sufficient confining pressure between the building and the substrate [5].

The bond to the concrete surface is achieved mechanically using nonwovens or chemically using synthetic adhesives or modified bitumen. Chemically bonded membranes are understood in their mode of action and can essentially be described as cold-bonding adhesives with a non-stick surface [24]. Synthetically bonded membranes use pressure-sensitive adhesives and are based, for example, on styrene-isoprene block polymers (SIS) or dimethylnaphthalene-formaldehyde resin with thicknesses of approx. 0.3-0.6 mm [25]. An additional top coating acts as a bonding bridge between the adhesive and the fresh concrete, enables a non-stick surface and walkability in horizontal applications, prevents the membrane roll from sticking together during delivery, and protects against UV rays [26]. The top coating is, e.g., made of calcium carbonate, calcium silicate, or acrylic latex with mineral substances. Bituminous bonded membranes are modified by elastomers such as styrene-butadiene-block polymers (SBS) and are topped with sand [27]. More information on adhesively bonded membranes can be found in Chapter 9.1.

A mechanical bond is achieved via nonwovens or, in a few cases, using structures similar to geogrids [28]. They are embedded during the concrete placement and interlock with fresh concrete [29]. Especially nonwovens with a pronounced porosity require cement paste to separate from the fresh concrete. The cement paste must fill the nonwoven pores and close capillaries to form a waterproof fiber-cement composite [14]. It is believed that cement paste separates from fresh concrete during vibration compaction and has similar properties in nonwovens as in fresh concrete [16].

2.1.3 Application aims and regulations of pre-applied bonded membranes

Pre-applied bonded membranes are often used worldwide as a stand-alone waterproofing system and must meet the requirements of national codes, such as ASTM D7832 [30] in the United States. If the waterproofing membranes shall be distributed within the European Union and the European Economic Area, CE marking is required by a Declaration of Performance [31]. Groundwater barriers (Type T) made of plastic and rubber must comply with EN 13967 [32]; bituminous membranes with EN 13969 [33]. Besides, a product declaration via a European Technical Assessment (ETA) [34] is possible, and additional national regulations have to be considered.

Besides the application as primary waterproofing, pre-applied membranes are also used as an additional measure on waterproof concrete structures to improve the basement's overall waterproofing and provide more redundancy. This combination of waterproofing systems is, for example, considered in the United Kingdom in BS 8102 as Type A+B and can achieve very high usage requirements in the basement, such as the Grade 3 waterproofing according to BS 8102:2009. It is also the common application of pre-applied membranes in Germany. Besides that, pre-applied membranes can be used on waterproof concrete structures to seal cracks and substitute crack injections [12].

2.2 Studies on nonwoven bonded pre-applied membranes

2.2.1 Studies on the waterproof bond

The first experimental investigations on nonwoven bonded pre-applied membranes were carried out by *Freimann and Heinlein* [16]. They placed the membranes with fresh concrete and tested the waterproof bond after concrete hardening by applying water pressure to a defect in the bonding layer. The hydrostatic tests were carried out following DIN EN 12390-8 [35] and ASTM D5385 [36] with 5.0-6.9 bar water pressure. A colorant was added to the water to evaluate the water migration between the sealing layer and the concrete after the test. The authors found longer compaction times and higher fresh concrete spreads resulting in smaller water migrations. It was argued that vibration compaction is necessary to separate cement paste as it lowers the yield point of the fresh concrete and that higher fresh concrete spreads facilitate cement paste separation. Furthermore, it was assumed that the cement paste in the nonwoven is similar to that in the fresh concrete.

Meyer et al. [15] also investigated the waterproof bond in 312 hydrostatic tests following DIN EN 12390-8. High compaction energies in the vicinity of the nonwoven and high fresh concrete spreads were again favorable for the waterproof bond, as the yield point of the fresh concrete was lowered. In combination with 760 pull-off tests according to DIN EN 1542 [37], it was further recognized that mechanically bonded pre-applied membranes could simultaneously have a good bond strength but a poor waterproof bond. This discrepancy was explained by the porous structure of nonwovens, which can interlock with concrete in their upper fiber layer but still have water-bearing capillaries. Lighter or thinner nonwovens were assumed to be advantageous as they fill more quickly with cement paste.

Nonwoven bonded membranes have also been investigated for shotcrete applications by *Leslie and Carter* [38]. They constructed a wall in situ and found shotcrete overspray and poorly compacted concrete resulting in poor bonding. Hydrostatic tests according to ASTM D5385 [36] ($n = 6$) verified the observation. Only shotcrete specimens with good concrete compaction had a waterproof bond.

In summary, the literature review in Chapter 9.1 highlights concrete compaction as a vital element for the waterproof bond of nonwovens, with higher fresh concrete spreads and thinner nonwovens being advantageous. However, the processes and cement paste properties in the nonwoven remain unknown.

2.2.2 Studies on the bond strength

Meyer et al. [15] investigated the bond strength of six mechanically bonded pre-applied membranes in pull-off tests according to DIN EN 1542. The membranes were horizontally placed with fresh concrete and compacted on a vibration table. Variations were made regarding the concrete age (2, 7, 28 d), the cement type, and the fresh concrete load. In addition, wet nonwovens were included in the tests. The following results were obtained:

- The bond strengths in the reference test were between 0.40-0.93 MPa after two days using a CEM II/A-LL 32.5 R. Afterward, the strength developed slower and increased about 23 % between 2 and 7 days and about 10 % between 7 and 28 days.
- Using a CEM III/A 32.5 N with a lower early strength resulted in lower initial bond strength. The reference values of the CEM II were reached after seven days.
- The bond strength was reduced if the nonwovens were wet during concrete placement.

- Higher fresh concrete loads led to increased bond strengths. Across a column with 2.5 m height, the bond strength increased by 35 % between the column head and base.
- Failure often occurred between the nonwoven and the concrete surface. At higher concrete strengths, however, the bond between the waterproofing layer and the nonwoven was partly decisive.

Schreiber [39] additionally found that the bond strength development is slower for lower concrete temperatures. Combined with the results of *Meyer et al.* [15], it suggests that the bond strength between nonwoven and concrete surface depends on the concrete strength development. However, other effects on the bond strength could not be assigned due to unknown nonwoven properties and processes during concrete placement. Also, a weak adhesive bond between the sealing layer and the nonwoven partly influenced the pull-off tests.

2.3 Nonwovens

2.3.1 General information

Nonwovens are bonded fiber webs and differ from textiles by individual fibers instead of yarns, pronounced anisotropy in structure and properties, and a high porosity [40,41]. Furthermore, they are distinguished from stitch-bonded fabrics and paper based on their formation technology and fiber properties. According to ISO 9092 [42], a nonwoven is "an engineered fibrous assembly, primarily planar, which has been given a designed level of structural integrity by physical and/or chemical means, excluding weaving, knitting or paper making."

The following is a brief presentation of nonwoven production and related products, which is necessary to understand nonwovens on pre-applied bonded membranes.

2.3.2 Nonwoven production

Today, nonwovens are used in most areas of life with widely varying properties. Various manufacturing techniques have been established in recent decades, which can be summarized in the following four steps [43–45] with the processes relevant to this work illustrated in Appendix A.

1. *Fiber preparation*: Fibers for technical nonwovens are usually derived from synthetic materials and are spun out of melts or solvents, e.g., by dragging them through nozzles. Fibers can be manufactured with different properties, e.g., in terms of fineness, cross-section, or crimp, and are produced with unlimited lengths (filaments) during the web formation process or with limited lengths (staple fibers) in a separate production step.
2. *Web formation*: Individual fibers are manipulated two- or three-dimensionally into a voluminous web with little mechanical strength. During the web formation process, fibers are first separated or spun and then arranged in the desired orientation. Fibers are moved dry, wet, or directly out of the melt - in a dry-laid, wet-laid, or polymer-laid process:
 - *Dry-laid*: Especially carding and aerodynamic forming (air-laid) are used. In carding, staple fibers are separated using serrated cylinders (cards) and then aligned parallel to the production direction to form a fibrous web. An illustration is displayed in Appendix A. In the air-laid process, staple fibers are pre-separated on a card, dispersed in an air stream, and finally deposited on an air-permeable conveyor belt.
 - *Wet-laid*: Similar to paper production, staple fibers are dispersed in water. Subsequently, fibers are filtered using an inclined conveyor belt and a vacuum, then pressed and dried.

- *Polymer-laid*: The fiber and web formation processes are combined, and fibers are blown directly out of the melt onto a conveyor belt using air. Depending on the airflow, the fibers in the nonwoven can be filaments (spun-laid process, see Appendix A) or microfibers (melt-blown process).
3. *Web bonding*: The voluminous web is stabilized by creating friction, interlocking, or adhesive or cohesive bonds between the fibers using mechanical, chemical, and/or thermal methods. The bonding method and the degree of bonding are primary factors for mechanical properties, porosity, flexibility, softness, and density. The following procedures are used:
- *Mechanical bonding*: Fibers are reoriented in the fibrous web using needle-punching and hydroentanglement, creating friction and interlocking between fibers. In needle-punching, numerous barbed needles are inserted vertically through the nonwoven web, drawing fibers into the puncture channel and creating friction with surrounding fibers. In hydroentangling, thin high-pressure water jets are directed perpendicularly onto the web, where they reorient and entangle fibers (see Appendix A).
 - *Chemical bonding*: Fiber crossing points are adhesively bonded by chemical binders introduced by impregnation, spraying, or foaming.
 - *Thermal bonding*: Thermoplastic fibers are cohesively bonded using heat and often pressure. For example, calender bonding is used to bond lightweight webs. The nonwoven is passed through two cylinders, one of which is heated and engraved. At the positive engraving points, fibers are plasticized and welded together (see Appendix A).
4. *Finishing*: Nonwovens are finally finished in various ways and, for example, printed, coated, laminated, or made antistatic or flame retardant. For pre-applied membranes, plasma and corona treatment are particularly relevant, making the surface of polypropylene (PP) fibers hydrophilic by forming radical sites. Also, the production of pre-applied membranes can be interpreted as a finishing process, as the nonwoven is laminated to a sealing layer. Thermoplastics are extruded onto nonwovens using wide slot nozzles, or nonwovens are laminated onto sealing layers using adhesives.

Nonwovens are primarily differentiated by their formation process, basis weight, and, if applicable, special properties. For this thesis, dry-laid and polymer-laid nonwovens are relevant, with mechanical and thermal web bonding and basis weights between 35-130 g/m², representing the nonwovens on pre-applied membranes.

2.3.3 Nonwovens under mechanical load

Nonwovens generally cannot withstand high mechanical forces due to their rather unordered fiber structure and do not reach the mechanical resistance of thread materials (textiles) [45]. However, as production can alter fibers, web formation, and web bonding, the mechanical strength can be improved by varying the fiber properties, orientation, bonding type, and bonding degree. Also, the bonding type mainly affects the deformation behavior as it controls whether fibers reorient under load [43].

Nonwovens show pronounced compressions when loaded as fibers bend elastically between fiber bonding points, which were created during web bonding [46,47]. The compression factor C_{nw} is calculated according to Equation 1 and is commonly shown as a positive value in nonwoven studies [48]:

$$C_{nw} = \frac{\Delta T_{nw}}{T_{nw,0}} = \frac{T_{nw,0} - T_{nw,loaded}}{T_{nw,0}} \quad [-] \quad (1)$$

where $T_{nw,0}$ is the initial (unloaded) thickness, and $T_{nw,loaded}$ is the loaded thickness.

During compression, nonwoven fibers are bent and altered in their three-dimensional orientation. As a result, fiber bonding points are reoriented, and slippage can occur at friction-based fiber bonding points. When the nonwoven is subsequently unloaded, the thickness recovers due to the elasticity of the fibers. However, the reoriented fiber bonding points lead to a plastic deformation known as thickness loss [49,50]. The thickness loss $C_{nw,loss}$ is calculated according to Equation 2.

$$C_{nw,loss} = \frac{T_{total,0} - T_{total,rec}}{T_{total,0}} \quad [-] \quad (2)$$

where $T_{total,0}$ is the initial total nonwoven thickness at 0.5 kPa, and $T_{total,rec}$ is the recovered thickness after cyclic loading.

The thickness loss depends, on the one hand, on external influences such as the loading level [51], the number of loading cycles [52], and the holding time of the load [53]. On the other hand, the properties of the nonwovens are relevant. A higher thickness loss occurs for a higher nonwoven thickness and porosity [51] and a lower number of fiber bonds with weaker bonding forces [52,54,55]. For example, needle-punched nonwovens show a high compressibility and thickness loss due to their low number of friction-based fiber bonds. In contrast, thin calendered nonwovens with thermal bonding points show less thickness loss.

Due to the characteristic deformation behavior, nonwoven properties are partly specified in relation to the compressive load. Relevant to this thesis, the porosity ε (Equation 3) as well as the nonwoven pore volume V_{pore} (Equation 4) change with the nonwoven thickness T [56, p. 352 ff.].

$$\varepsilon = 1 - \frac{m}{\rho \cdot T \cdot A} \quad [-] \quad (3)$$

where m is the nonwoven basis weight in the area A , and ρ the density of the fiber material.

$$V_{pore} = \varepsilon \cdot T \quad [\text{dm}^3/\text{m}^2] \quad (4)$$

2.3.4 Filtration using nonwovens

In process engineering and geotechnical applications, nonwovens are used as a filter medium in dry or wet environments [57,58]. They retain solids from gas streams or suspensions using two filtration mechanisms: On the one hand, particles are retained on individual fibers as they break out of the fluid streamlines and adhere to the fiber surface, e.g., due to their electrostatic charge. This mechanism is usually used in solid-gas filtration [56]. On the other hand, particles are retained in the pore structure of the filter medium, either on the surface or in the depth in constricting pores [58,59]. It is usually relevant for solid-liquid filtration and distinguishes between three model conceptions, explained in the following and presented in Fig. 4 [60,61]:

1. *Straining*: Comparable to a sieve, solids are retained in the pores of the filter medium due to their size. Particles remain either on the surface of a filter medium (surface straining) or inside in constricting pores (depth straining). The particles accumulate over time and reduce permeability and filter performance, known as clogging [62]. Particles smaller than the opening widths of the pores pass through the filter.
2. *Cake filtration*: Solids are retained on the surface of the filter medium, forming solid bridges and, finally, a filter cake. After consolidation, the filter cake itself acts as a filter medium. Cake filtration can be performed with thin nonwovens and is usually used for high solid

contents in the suspension. The filtration rate depends on the filter cake thickness, compression, and external pressure.

3. *Depth filtration*: Particles remain on pore walls and fiber surfaces mainly due to interparticle forces, so retained particles can be smaller than the opening width of the pores. Filtration can achieve high separation efficiencies and clear filtrates. However, the total filtration volume is limited to the filter media's storage capacity, requiring nonwovens with a high pore volume.

In real filtrations, the described models superimpose and change over the filtration time. For example, cake filtration initially behaves as surface straining. Until the filter cake is formed, the filter medium retains particles due to their size, while fine particles can initially pass, known as turbidity run [60].

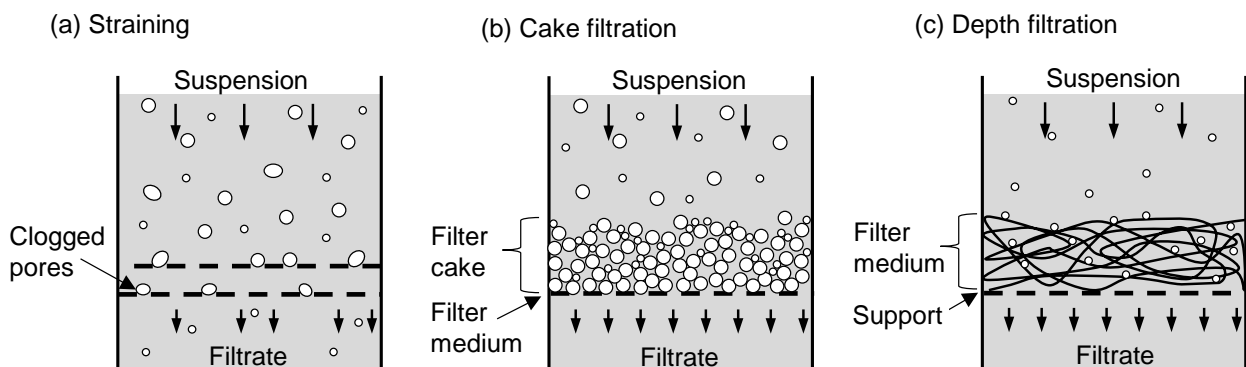


Fig. 4 - Models of filtration mechanisms: (a) straining, (b) cake filtration, and (c) depth filtration (based on [60, p. 145])

Different filtration tasks use varying filtration media. The suitability of a filter medium for a particular suspension is usually tested in pressure filtration tests under laboratory conditions [63]. A test filtration is carried out in a pressure cell, and parameters like filter resistance and permeability are determined over time. Permeability during filtration can be described using *Darcy's* equation in Equation 5 or with similar proportionalities from *Kozeny-Carman* [41].

$$Q = -\frac{k}{\eta} \cdot \frac{\Delta p}{L} \quad [\text{m}^3/\text{s}] \quad (5)$$

where Q is the volumetric flow rate, k is the specific permeability coefficient of the filter, η is the fluid viscosity, and Δp is the pressure difference over the conduit length of fluid flow L . For nonwovens, the specific permeability depends on its pore properties [64–66] and decreases when the nonwoven thickness, density, basis weight, or generally, the ‘bonding energy’ increases [67–71]. Additionally, the filtration parameters change over the filtration time as the filter medium's initial filter resistance and permeability are increasingly altered by particle entrapment or accumulation. For example, during a cake filtration at constant pressure, the filtrate flow rate decreases over time as clogging reduces permeability and solid particles accumulate on the filter surface, increasing the length of fluid flow [58].

2.3.5 Nonwoven geotextiles

Nonwovens are also used as a geotechnical element for nonwoven geotextiles. According to ISO 10318-1 [72], they are used for filtration, drainage, separation, reinforcement, and erosion control. Furthermore, they are applied for sludge dewatering [73–75] and are characterized based on their water permeability, filtration efficiency, opening width, and mechanical properties [76]. The nonwovens must retain fines, remain sufficiently permeable to water, and should not be

clogged by particles [77,78]. Depending on the application, nonwovens with 50-1700 g/m², 0.25-9 mm thickness, 75-850 μm opening size with fibers made of polypropylene (PP), polyester (PES), polyethylene (PE), or polyamide (PA) are used. Their functionality is designed based on geometric and hydraulic experience values [79] or tested in the laboratory via pressure tests [80]. *Cazzuffi et al.* [81] summarize further standard test methods.

When geotextiles are used for filtration via static load, they are initially compressed. As a result, the characteristic opening width is reduced, and water paths are reoriented [82]. During filtration, the first particles are retained within the structure. Further solids form bridges on top of fibers, reducing the geotextile's opening widths and permeability [83,84]. Pronounced filter cakes were observed during sludge dewatering combined with initial turbidity during the filter cake formation [85–87]. A few studies investigated the influence of pulsating hydrostatic load [88,89], finding more solids passing through nonwovens than under static load.

2.3.6 Nonwovens for Controlled Permeable Formworks

Nonwovens are also used as filters in Controlled Permeable Formworks (CPF). CPFs are placed on formworks and remove excess water and air voids from the adjacent fresh concrete during concrete placement. In this way, they decrease the capillary porosity of the concrete surface, increasing the mechanical properties, strength, density, and durability [90].

CPF either store excess water from the concrete surface in absorptive sheets or discharge excess water via a filter and a drain element. In the latter case, nonwovens are arranged facing the fresh concrete, filtrating excess water and air but retaining cement particles due to small opening widths (4-35 μm) [91]. A water-permeable drainage layer is arranged on the back of the filter, discharging the filtrated excess water and air outside the formwork [92]. Nonwovens for CPF have thicknesses between 0.35-2.0 mm, basis weights up to 400 g/m², are usually made of PP or PE, and often have calendered surfaces [91,93,94].

The amount of separated excess water depends on the w/c ratio of the fresh concrete and was measured between 0.7-2.5 l/m² at a w/c of 0.5 [95,96]. The excess water separates without compaction [94,97] and lowers the w/c ratio of the adjacent concrete. This improves, for example, the surface tensile strength by 30 % (w/c 0.50) [98] or by 50 % (w/c 0.55) [93] compared to a formwork with a smooth and non-absorbent surface.

3 Summary of the methods applied

Fourier transform infrared spectroscopy in attenuated total reflection mode (ATR-FTIR)

In order to characterize the nonwovens on pre-applied membranes, the fiber material was identified by infrared spectroscopy. FTIR spectra were obtained with a 'Nicolet 6700' FTIR spectrometer from the 'ThermoFisher Scientific' company in ATR mode.

Mechanical thickness measurement

Nonwoven thickness was measured mechanically following DIN EN 1849-2 [99] using the 'Hildebrand HTG-A' thickness gauge with a measuring accuracy of 0.001 mm. The load during measurement was set between 0.5-20 kPa, and the nonwoven thickness was determined after 30 s load duration. The compression at different loads was calculated according to Equation 1 (p. 8).

The mechanical thickness measurement is designed for loose nonwovens. However, nonwovens of pre-applied membranes cannot be separated from their sealing layer without damage for measurement. Thus, the nonwovens were measured using whole pre-applied membranes. The unloaded nonwoven thickness was initially measured using optical methods (see next Chapter). Then, the behavior under compressive load was determined using the thickness gauge, considering the sealing layer thickness and compression by measuring an uncoated edge strip, extending Equation 1 to Equation 6:

$$C_{nw} = \frac{T_{total,0} - T_{total,loaded} - \Delta T_{SL}}{T_{total,0} - T_{SL,0}} \quad [-] \quad (6)$$

where $T_{total,0}$ and $T_{SL,0}$ correspond to the unloaded total and sealing layer thickness, $T_{total,loaded}$ to the total thickness at higher loading, and ΔT_{SL} to the change in thickness of the sealing layer due to loading.

For selected nonwovens, the thickness loss was determined in a mechanical loading cycle [54,100]. One load cycle of 0.5-20-0.5 kPa was applied in 8 stages (0.5-1-2-4-7-10-15-20 kPa), with each load level maintained for 30 s. The thickness loss $C_{nw,loss}$ is usually obtained according to Equation 7 [101]:

$$C_{nw,loss} = \frac{T_{nw,0} - T_{nw,rec}}{T_{nw,0}} \quad [-] \quad (7)$$

where $T_{nw,0}$ is the initial unloaded nonwoven thickness, and $T_{nw,rec}$ is the recovered nonwoven thickness after unloading. Again, the sealing layer had to be considered. Since it exhibited elastic material behavior in the test, the thickness loss of nonwovens of pre-applied membranes was calculated according to Equation 8:

$$C_{nw,loss} = \frac{T_{total,0} - T_{total,rec}}{T_{total,0} - T_{SL,0}} \quad [-] \quad (8)$$

where $T_{total,0}$ and $T_{SL,0}$ are the initial total and sealing layer thicknesses at 0.5 kPa, and $T_{total,rec}$ is the recovered thickness after cyclic loading. Equations 6 and 8 have an increased inaccuracy compared to direct measurements by considering the sealing layer in separate measurements. However, the higher inaccuracy was acceptable since the tests merely aimed at comparing the results in the following optical thickness measurements.

Optical thickness measurement

The nonwoven thickness was measured using an incident light microscope to determine the unloaded nonwoven thickness and its deformation behavior during concrete placement. Measurement was done following DIN EN 1849-2 by taking overlapping photos over a length of $l \geq 50$ mm

The photos were connected using the algorithm in [102] and measured using the known pixel size.

The nonwoven thickness was measured on ‘loose’ membranes before concrete placement and again on microsections after concrete placement to evaluate the deformation behavior. Since nonwovens have a high scatter in thickness due to the manufacturing process, measurements had to be done in the same position before and after concrete placement to ensure direct comparison. A membrane strip with 8 mm width was removed from the center of a 200/200 mm membrane specimen and measured on its cut edges. The strip was reinserted into the specimen at its original position, fixed on the reverse side, and used in the concreting process. After concrete hardening, the specimen was separated through the initially measured strip. The adjacent cut edges were then prepared as microsections by wet grinding processes and measured again.

Measurements were also carried out on specimens without or with low compaction (0-1 s vibration compaction time) that had to be stabilized before specimen preparation. Hoses were placed onto the nonwoven from the outside of the formwork before the concrete was placed. After concrete hardening, a viscous, low-shrinkage epoxy resin with a high working time was passed through the hoses by gravity. Fig. 5 shows the thickness measurement on a detail of a microsection that was stabilized with a red epoxy resin. Chapter 9.2 provides a detailed description of the procedure and a verification of the method.

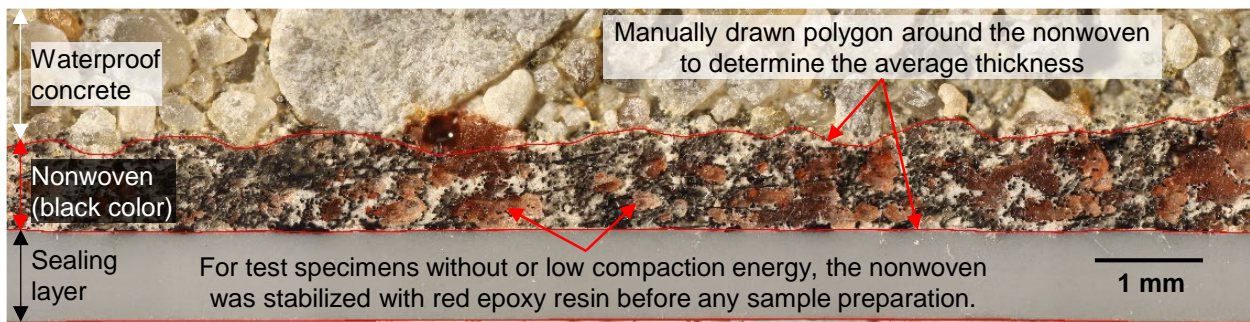


Fig. 5 - Section of a 50 mm long image to determine the average thickness of a nonwoven

Vibration compaction using internal vibrators

In order to ensure reproducible compaction times, an internal vibrator (\varnothing 55 mm) was equipped with time and location control. The time was controlled using a contactor between the transducer and the internal vibrator, and the height position using a pneumatic cylinder. Both were operated via programmable time-switching relays. The internal vibrator could be used close to the pre-applied membrane with a temporal accuracy of 0.1 s and removed immediately afterward. An image of the assembly is displayed in the second own paper in Chapter 9.2.

Micro Computed Tomography (Micro-CT)

Micro-CT scans analyzed the porosity in nonwovens of pre-applied membranes after varying vibration compaction times. Basic information on micro-CT scans can be found for nonwovens in [103], for concrete in [104], and for concrete specimens with synthetic microfibers (\varnothing 35 μ m) in [105].

The pre-applied membranes were scanned using cores with the dimensions $\varnothing/h = 25/10$ mm that were taken adjacent to the microsections used for optical measurements. Influences from drilling were avoided by cutting the membranes initially by hand and analyzing only the inner 20 mm of the core diameter. The scans were taken with the ‘Bruker SkyScan micro-CT 1173’ with a 130 kV

X-ray source and a flat-panel sensor with 2240 x 2240 pixels. The samples were examined with 80 kV voltage and 80 μ A current, a Brass filter with 0.25 mm thickness, and a rotational path of 360°. The voxel resolution in the scans was 17 μ m. The 3D volume reconstruction and subsequent segmentation and analysis were performed with Bruker software 'NRecon' and 'CTAnalyser'. The spatial representation was realized with 'CTVox'.

During analysis, the distribution of gray values from the synthetic components and artifacts overlapped in the histogram. Therefore, a two-step binarization was applied to interpret all synthetic materials as solids and minimize pores' artifacts. First, global thresholding was used. Second, appearing artifacts were removed by adaptive thresholding with a two-dimensional Otsu algorithm. The binary pore structure then matched the grayscale images.

Hydrostatic testing of the waterproof bond

The waterproof bond between the membrane and concrete surface was tested following a modified version of DIN EN 12390-8 [35] by applying water pressure to a defined defect in the membrane. For the tests, specimens with dimensions of $l/w/h = 200/200/100$ mm were produced, with the membrane having a central defect with a diameter of 25 mm. After 28 days of water storage, 5 bar water pressure was applied to the defect in the sealing layer. A fluorescent tracer (Uranine AP, CAS No. 518-48-8; 0.17 g/l) was added to the water. The pressure was raised stepwise by 1 bar/h and maintained for three days. After testing, the membrane was removed from the concrete, and lateral water movements became visible under UV light. The test is similar to the modified version of ASTM D5385 [36], is recommended for testing pre-applied membranes [12], and is described in detail in [16].

Static and dynamic intrusion tests

The process of cement paste separation was investigated with a self-developed test stand, enabling a practice-oriented fresh concrete placement on loose nonwovens and the collection of separated cement paste. The setup was based on a static filtration test and is comparable with concrete filter presses [106–108], the testing of the filtration resistance of geotextiles [80], or filter fabrics [63]. In order to ensure a practice-oriented concrete placement, it was supplemented with an internal vibrator and dimensioned for fresh concrete mixtures typical for the construction site. Fig. 6 shows the setup, comprising a grating (30 mm aperture), the nonwoven on a supporting mesh (\varnothing 340 mm, 2.5 mm aperture), and a two-part pressure chamber consisting of a steel tube (\varnothing 320 mm). Below the grating was a scale with a collection tray (\varnothing 360 mm).

During testing, the nonwoven was placed on the grating, the lower part of the pressure pot was fixed, and fresh concrete was mixed and poured into the pressure chamber. Then, the upper part of the pressure chamber was lowered, fixed, sealed, and compressed air was applied to simulate higher fresh concrete loads. Afterward, the test procedure varied to examine the sequences during concrete placement. First, 'static intrusion tests' determined the processes in the nonwoven due to concrete load before vibration compaction. Varying loads were applied via compressed air, and the filtrate mass in the collection tray was recorded for up to 30 min. Second, 'dynamic intrusion tests' examined the cement paste separation during vibration compaction. However, a static load was applied first to simulate an actual concrete pour, and since the static load already caused filtration effects. The static load was maintained until stationary masses were reached within the nonwoven, and the concrete was subsequently vibrated with an internal vibrator for 1-30 s.

The filtrate was then weighed and analyzed for its properties: First, the particle size was investigated using laser granulometry. Second, the water mass in the filtrate was determined by oven drying at 105 °C until mass constancy was reached. Then, the water-to-solids ratio in the nonwoven was calculated according to Equation 9 to compare the cement paste properties in the nonwoven with those in the fresh concrete:

$$w/s = \frac{m_w}{m_s} \quad [-] \quad (9)$$

where m_w is the water mass, and m_s is the solid mass. Third, the solids density ρ_s was determined using the pycnometer according to DIN EN 1097-7 [109]. A detailed description of the test and a verification of the method is given in the third own paper in Chapter 9.3.

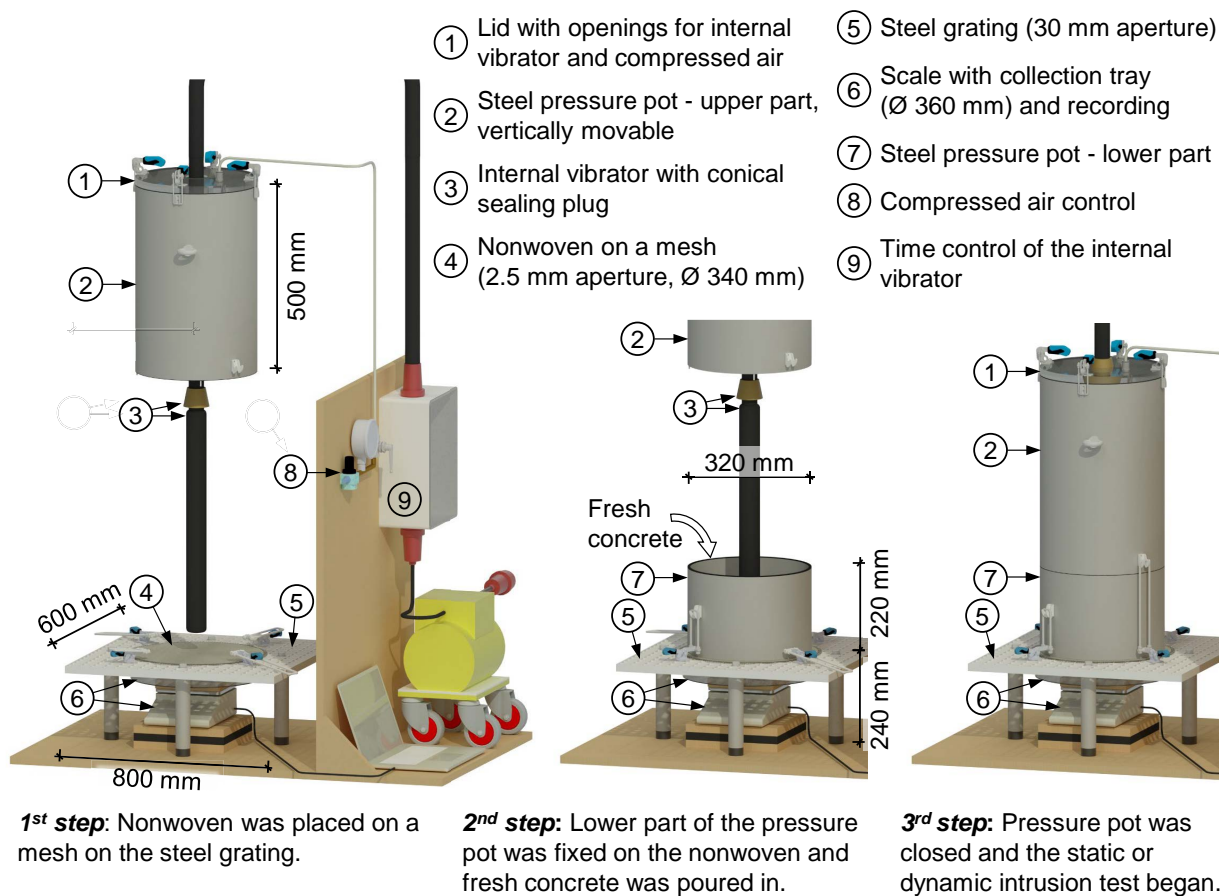


Fig. 6 - Setup of the filtration test stand and first steps in the experimental procedure

Laser granulometry of separated cement paste

Separated cement paste was analyzed for particle size distribution using the laser diffraction method according to ISO 13320 [110]. The laser particle sizer 'Analysette 22' from 'Fritsch GmbH' with a measuring range between 0.01-2100 μm and an inverse Fourier setup was used. Samples were measured in wet dispersion in deionized water after being exposed to ultrasound for 60 s. Each filtration test was analyzed using two samples with three measurements. The results were evaluated using the software 'MaS control' based on the Fraunhofer theory.

Lamination of loose nonwovens to a sealing layer

The filtration tests used loose nonwovens to enable the collection of cement paste. However, for a reliable determination of the w/s ratio inside the nonwovens, water and cement paste leakage through the nonwoven had to be prevented during concrete placement. For this purpose, the

build-up of pre-applied membranes was reproduced by laminating the loose nonwovens onto a plastic film made of low-density polyethylene (LDPE, 125 μm thickness). Epoxy resin was used and applied to the plastic film at around 50 g/m^2 . After curing, a second layer of epoxy resin was applied at about 50 g/m^2 , and the nonwoven was placed on top and lightly pressed down with a roller. This two-step procedure resulted in a full-surface bond between the nonwoven and the epoxy resin and a closed surface on the reverse side. The nonwoven surface was afterward unaltered, as shown in Fig. 7. In contrast to pre-applied membranes, this method ensured known nonwoven properties and variations independent of pre-applied membranes on the market.

Scanning electron microscopy (SEM)

SEM images gave an impression of the nonwoven surface texture and proved an unchanged surface after the lamination onto the plastic film (see Fig. 7). SEM images were obtained with the 'JSM-6510' from 'Jeol Ltd.' with an acceleration voltage of 2.0 kV and a working distance of 44-47 mm. For preparation, the samples were sprinkled with silver for 30 s in an 'Auto Sputter Coater' from 'Cressington'.

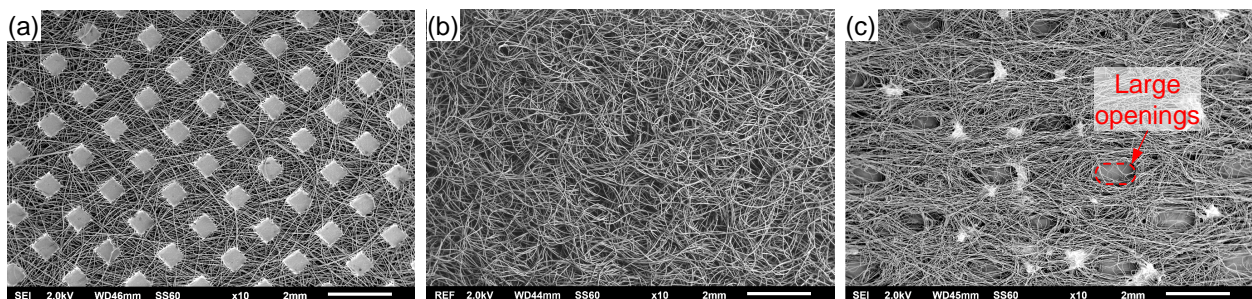


Fig. 7 - The nonwoven surface was not changed by the lamination process using epoxy resin. SEM images of the nonwovens N4 with calender bonding (a), N6 with needle bonding (b), and N9 with hydroentanglement and large openings (c) are shown.

Nonwoven bond strength to concrete

Nonwoven bond strength to concrete was determined in pull-off tests according to DIN EN 1542 [37] using loose nonwovens laminated to a sealing layer. The laminated specimen ensured known nonwoven properties and enough stability for the pull-off tests. Also, the plastic film could be removed after concrete hardening, so test stamps were applied directly on the nonwovens, and the test force acted directly on the bonding zone. Thus, the test results were not influenced by the material strength between the nonwoven and sealing layer, as was in previous studies using pre-applied membranes [15,39]. The test procedure yielded bond strength values comparable to previous studies in [15,39] (see Chapter 9.4).

Fig. 8 shows the experimental procedure, with the laminated nonwovens placed in sealed formworks with horizontal or vertical orientation. The specimen size was chosen according to DIN EN 1542 with $l/w = 300/300$ mm in the reference tests. The concrete height was set to 200 mm for horizontally-oriented nonwovens to ensure good compaction with an internal vibrator. Vertically-oriented nonwovens were tested with 300 mm concrete height for an equal testing area. A few specimens were chosen bigger ($l/w/h = 600/600/200$ mm or $300/300/1200$ mm) to investigate the impact of a larger distance to internal vibrators or increased fresh concrete heights. A practice-oriented fresh concrete mixture was poured and compacted with an internal vibrator. The specimens stayed in the formwork for one day and were then stripped and subsequently cured under wrapping foil at 23-25 $^{\circ}\text{C}$.

At least five pull-off tests per specimen were conducted according to DIN EN 1542. For preparation, the circumferences of the test positions were drilled, the plastic film removed, and the test surface lightly roughened and dried. Then, a steel stamp (\varnothing 50 mm) was applied with a fast-curing epoxy resin, and the pull-off test was finally carried out with a stress rate of 0.05 MPa/s, using the automatic pull-off tester 'Proceq DY-206'. If the specimens were younger than one day, the test positions were not drilled, as the bond could be damaged. Instead, the stamp was applied, and the nonwoven cut by hand. Fig. 9 shows the arrangement of pull-off tests for reference and larger specimens. A detailed description of the test and further test photos are provided in the fourth own paper in Chapter 9.4.

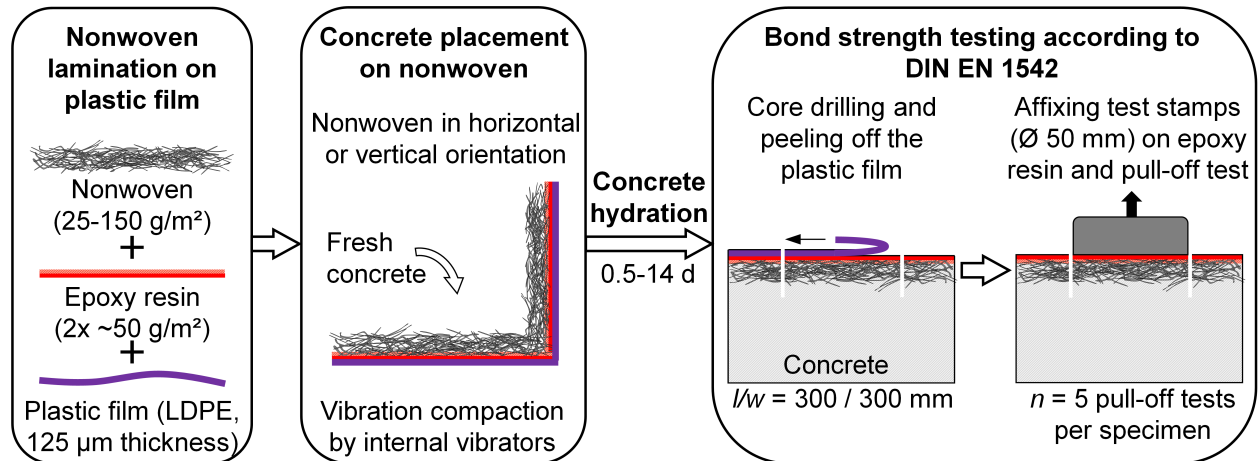


Fig. 8 - Experimental procedure of the pull-off tests on concrete bonded nonwovens

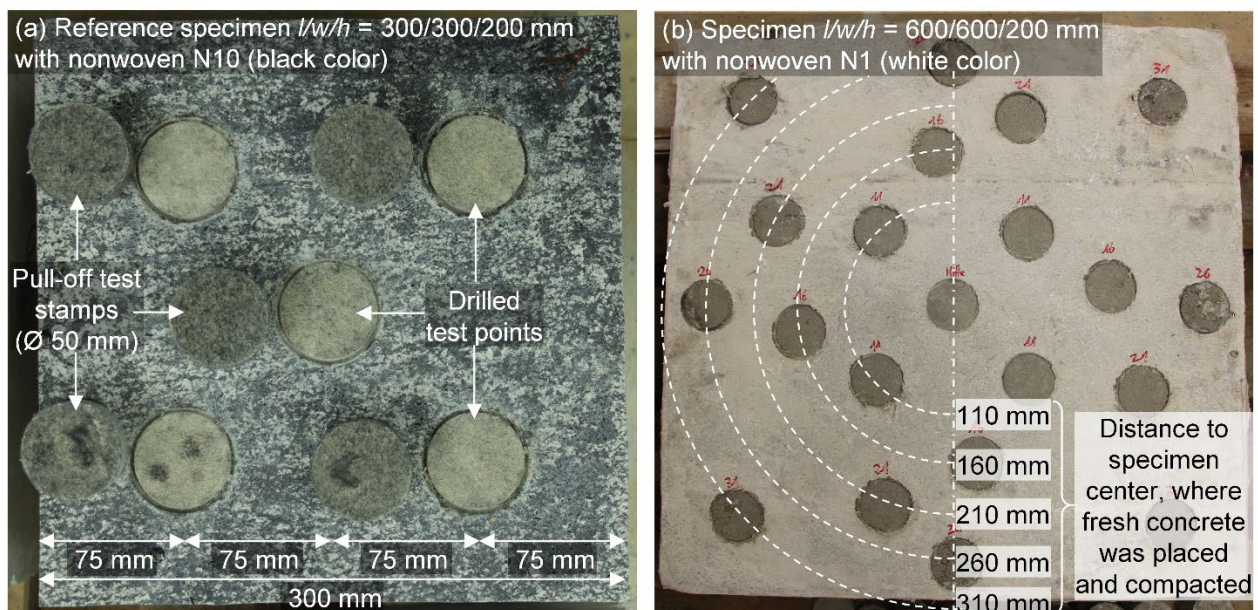


Fig. 9 - Top view of a reference specimen after testing (a) and a larger specimen with increasing testing distance to the point of concrete placement and compaction in concentric circles (b)

Tensile splitting tests

In order to compare the bond strength to the concrete strength, tensile splitting tests were performed according to DIN EN 12390-6 [111] using concrete cylinders with $\varnothing/h = 150/300$ mm. For each concrete mixture and test date, three specimens were tested.

Approximation of the strength development

The development of the concrete tensile splitting strength was approximated using a mathematical approach of the model code of the *fédération internationale du béton (fib)* [112]. The mathematical approach is designed to approximate the compressive strength development of normal concretes $f_{cm}(t)$ according to Equation 10. It uses the mean compressive strength f_{cm} at 28 days, the strength class of the cement considered with the coefficient s , and the temperature-adjusted concrete age t_T .

$$f_{cm}(t) = f_{cm} \cdot e^{s \cdot \left[1 - \left(\frac{28}{t_T}\right)^{0.5}\right]} \quad [\text{MPa}] \quad (10)$$

In Chapter 4.5, Equation 10 was used to approximate the tensile splitting tests. Hence, it was adjusted to Equation 11 for the purposes of this thesis:

$$f_{ct,sp}(t) = f_{ct,sp} \cdot e^{s \cdot \left[1 - \left(\frac{14}{t_T}\right)^{0.5}\right]} \quad [\text{MPa}] \quad (11)$$

where $f_{ct,sp}$ is the concrete tensile splitting strength after 14 days as the maximum test duration, and $f_{ct,sp}(t)$ is the tensile splitting strength over time. The approximation started at the beginning of concrete hardening. The concrete temperature during curing was considered using Equation 12:

$$t_T = \sum_{i=1}^n \Delta t_i \cdot e^{13.65 - \frac{4000}{273 + T(\Delta t_i)}} \quad [\text{d}] \quad (12)$$

where t_T is the temperature-adjusted concrete age, and $T(\Delta t_i)$ is the mean temperature during the time period Δt_i .

The nonwoven bond strength showed proportionality to the concrete tensile splitting strength in Chapter 4.5. Thus, the bond strength over time $f_{NW,pull-off}(t)$ was expressed in relation to the tensile splitting strength using a nonwoven-specific coefficient v according to Equation 13:

$$f_{NW,pull-off}(t) = v \cdot f_{ct,sp}(t) \quad [\text{MPa}] \quad (13)$$

Concrete temperature measurement

The concrete temperature for Equation 12 was measured on bond strength specimens ($l/w/h = 300/300/200$ mm) with embedded temperature sensors and a data logger. NiCr-Ni thermowires were embedded in the specimen core and 20 mm below the concrete surface, and the temperature was recorded at one-hour intervals with the 'Almemo 2890-9' data logger from 'Ahlborn GmbH'. Two specimens were measured for each cement type. Also, the air temperature was recorded.

4 Main results

4.1 Characterization of nonwovens on pre-applied bonded membranes

The range of essential nonwoven properties was covered using seven internationally available pre-applied bonded membranes, as presented in Table 1. Further information on the test method is given in the first own paper in Chapter 9.1

Table 1 – Properties of nonwovens of pre-applied bonded membranes

Property	Unit	Individual mean values of 7 tested products							Test method, number of specimen n , and standard deviation \bar{s}
		S1	S2	S3	S4	S5	S6	S7	
Nonwoven basis weight	g/m ²	62	47	129	36	113	92	83	ISO 9073-1 [113], $n = 8$, $\bar{s} = 7.1$ g/m ²
Fiber diameter	μm	24/35	13	33	25	23	26	11/21	DIN 65571-2 [114], $n = 35$, $\bar{s} = 2.7$ μm
Fiber material		PE/PP	PES	PP	PP	PP	PP	PES	FTIR, $n = 2$
Nonwoven thickness (unloaded)	mm	0.52	0.20	0.82	0.31	1.08	0.50	0.68	Optical measurement, DIN EN 1849-2 [99], $n = 8$, $\bar{s} = 0.08$ mm
Mean nonwoven compression at 2.0 kPa load	[-]	0.04	0.10	0.10	0.16	0.08	0.06	0.12	Mech. measurement, Equation 6, $n = 8$, $\bar{s} = 0.03$
Range of nonwoven compression at 20 kPa load	[-]	0.21-0.36	0.26-0.58	0.30-0.42	0.32-0.49	0.24-0.34	0.20-0.45	0.33-0.41	Mech. measurement, Equation 6, $n = 8-15$, $\bar{s} = 0.06$
Thickness loss, measured for S3&S5 in 1 cycle	[-]	-	-	0.18	-	0.14	-	-	Mech. cyclic loading, Equation 8, $n = 5$, $\bar{s} = 0.02$
Nonwoven porosity ϵ (unloaded)	[-]	0.87	0.82	0.83	0.87	0.87	0.80	0.91	Calculated acc. to Equation 3
Nonwoven bonding		NP	CB	NP	HE	NP	HE	NP	NP: Needle-punched; CB: Calender bonded; HE: Hydroentangled.

The nonwovens on pre-applied membranes have basis weights between 35-130 g/m² and unloaded thicknesses between 0.2-1.1 mm. Fibers usually are monofilament staple fibers with a round cross-section made of PP, PE, or PES with a diameter of 11-35 μm and are bonded mechanically or thermally using a calender. The nonwoven S1 additionally contains filaments. The pronounced deformation behavior results in a nonwoven compression between 0.20-0.58 at 20 kPa load and a thickness loss between 0.14-0.18, determined for the needle-punched nonwovens S3 and S5. Nonwovens with similar weights and production methods are also used for thin geotextiles for filtering applications in housing construction, see, e.g., [115,116].

4.2 Macroscopic nonwoven behavior during concrete placement

4.2.1 Change under compression during concrete placement

The pre-applied bonded membranes S1-S7, characterized in Table 1 (Chapter 9.1), were used in Chapter 9.2 to examine their change under compression during concrete placement. The nonwoven thickness was measured before and after concrete placement on 192 microsections using an incident light microscope.

The membranes were initially measured and then placed with a practice-oriented waterproof concrete mixture with 320 kg/m³ cement (CEM II/A-LL 32.5 R), a w/c ratio of 0.55, and a grading curve A/B 32 ($k = 4.81$) with quarzitic round aggregate. Compaction was carried out with an internal vibrator ($\varnothing 55$ mm). Additional variations were made in terms of fresh concrete load via the fresh concrete height (2/20 kPa), the compaction time (0-20 s), and the orientation of the nonwovens during concrete placement (horizontal/vertical). Chapter 9.2 provides method verification, measurement scatter, and all results.

Fig. 10 displays the compression of S3&S5 during concrete placement with a vertical orientation in the formwork. The nonwovens are compressed after pouring the fresh concrete ($t = 0$ s), depending on the fresh concrete load, with the compression being comparable to a mechanical load. For example, S5 exhibits a compression between 0.28-0.32 at 20 kPa fresh concrete load, which is within the compression of a 20 kPa mechanical measurement with 0.24-0.34 (see Table 1). Nonwoven geotextiles are also compressed during filtration depending on the static load, reducing pore sizes in the nonwoven [82].

With the onset of vibration compaction, the compression decreases similarly to a viscoelastic retardation curve and is primarily completed after 8 s compaction time for vertically-oriented nonwovens. The compression recovery ends with a nonwoven typical thickness loss, which is again comparable to a mechanical thickness measurement. For example, S3 showed a thickness loss of 0.187 at 20 kPa fresh concrete load, comparable to a mechanical measurement of 0.18 (see Table 1).

The nonwoven compression change during vibration compaction is proportional to the development of the waterproof bond, as was found comparing the compression recovery (Fig. 10) with lateral water migrations (Chapter 9.2). At the same time, it is known from [15,16] that the waterproof bond forms by filling the nonwoven pores with cement paste. Due to the proportional behavior, it can be argued that the compression recovery is also a result of the cement paste filling. The fresh concrete load is increasingly transferred to the cement paste in the nonwoven pores, removing the load from the nonwoven fibers and allowing them to recover due to their residual stress.

Based on this hypothesis, nonwovens for pre-applied membranes should show a rapid compression recovery as it would achieve a waterproof bond more rapidly. In order to investigate this assumption and identify beneficial nonwoven properties, the membranes S1-S7 were used in concrete placements with short compaction times ($t = 0.5/ 1.0/ 1.5/ 2.5$ s). The resulting compression recovery curves were compared by expressing them as a summed compressional change per time $\Delta C_{NW,i}/\Delta t_i$ during the four vibration time intervals (0-0.5 s; 0.5-1.0 s; 1.0-1.5 s; 1.5-2.5 s) according to Equation 10:

$$a_{nw} = \sum \frac{\Delta C_{nw,i}}{\Delta t_i} \quad [1/s] \quad (10)$$

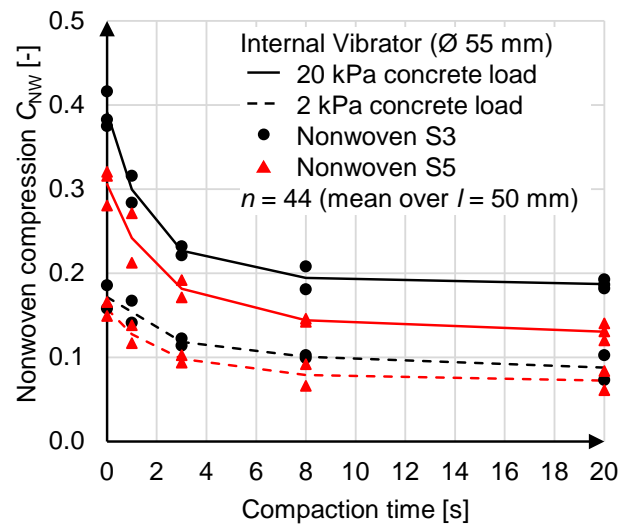


Fig. 10 - Compression of a vertically-oriented membrane during ongoing compaction with an internal vibrator

where the index i denotes the four compaction time intervals and the index nw the different nonwovens.

The values a_{nw} for the nonwovens S1-S7 were then plotted against various nonwoven properties to identify possible correlations. Fig. 11 shows the best correlation against the nonwoven pore volume with a logarithmic trend and a coefficient of determination of $r^2 = 0.82$ [117]. Accordingly, nonwovens with a lower pore volume exhibit a faster compression recovery, most likely due to a faster cement paste filling. This finding fits the hydrostatic tests of *Meyer et al.* [15], where thicker nonwovens needed longer compaction times for a waterproof bond.

Horizontally-oriented nonwovens in Fig. 12 showed a similar compression change in the first seconds of vibration compared to the vertically-oriented nonwovens in Fig. 10. However, with long compaction times, no thickness loss remains; the nonwovens reach their unloaded thicknesses with a remaining compression of $-0.016 \leq C_{NW} \leq 0.037$ and the nonwovens' typical thickness loss is overcome. All investigated pre-applied membranes S1-S7 exhibit this effect for a compaction time of 20 s with a remaining compression of $-0.021 \leq C_{nw} \leq 0.039$ (see Chapter 9.2). The deviation to the vertically-oriented nonwovens can possibly be explained by the vibration amplitude of the internal vibrator. The amplitude is horizontally oriented in the concrete, thus, acting as a radial shear force on horizontally-oriented nonwovens. This shear force may loosen fiber friction points in the nonwoven that were responsible for the thickness loss, allowing the fibers to return to their original position.

If vibration compaction was carried out using a vibration table, the nonwoven compression also decreased - but significantly slower (see second own paper in Chapter 9.2). This finding is comparable to the results of hydrostatic tests from *Meyer et al.* [15], where samples compacted on a vibration table needed long compaction times for a waterproof bond. The authors linked the long necessary compaction times to dampening effects of the formwork and the nonwoven, reducing the compaction energy in the vicinity of the nonwoven.

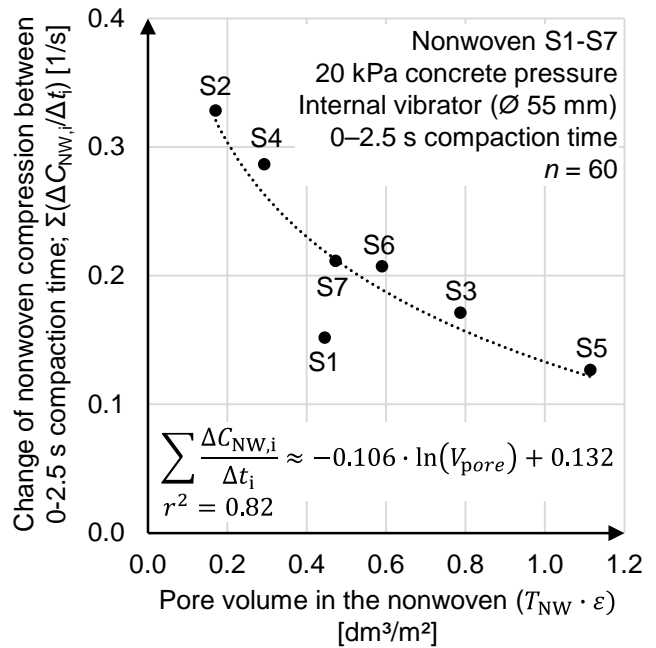


Fig. 11 - Compressional change per time of the nonwovens S1-S7 during the initial 2.5 s compaction with an internal vibrator

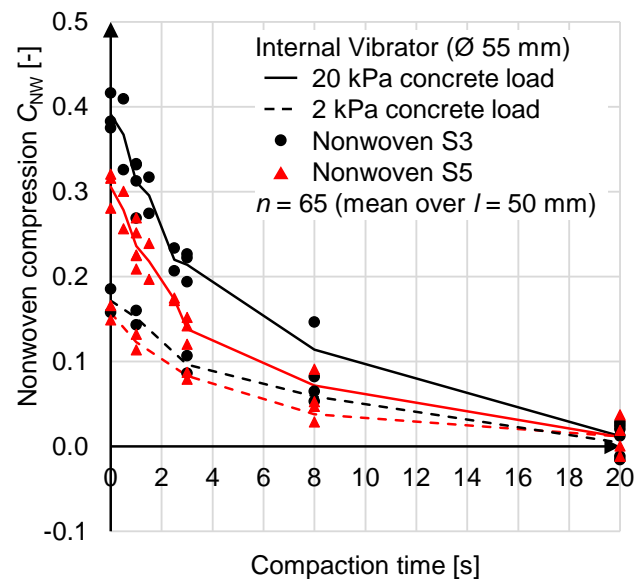


Fig. 12 - Compression of a vertically-oriented membrane during ongoing compaction with an internal vibrator

4.2.2 Porosity in the nonwoven during concrete placement

Four micro-CT scans were performed to examine the porosity change during sustained vibration compaction for membrane S3. Fig. 13-a shows the spatial distribution of the specimens' open and closed pore structures with open pores extending to the specimen edge; Fig. 13-b shows the distribution of the measured porosity over the nonwoven height. Note that the voxel resolution in the scans was $17\ \mu\text{m}$ and, thus, no capillary pores ($\leq 5\ \mu\text{m}$ [118]) were detected, and the displayed porosity describes air and compaction pores.

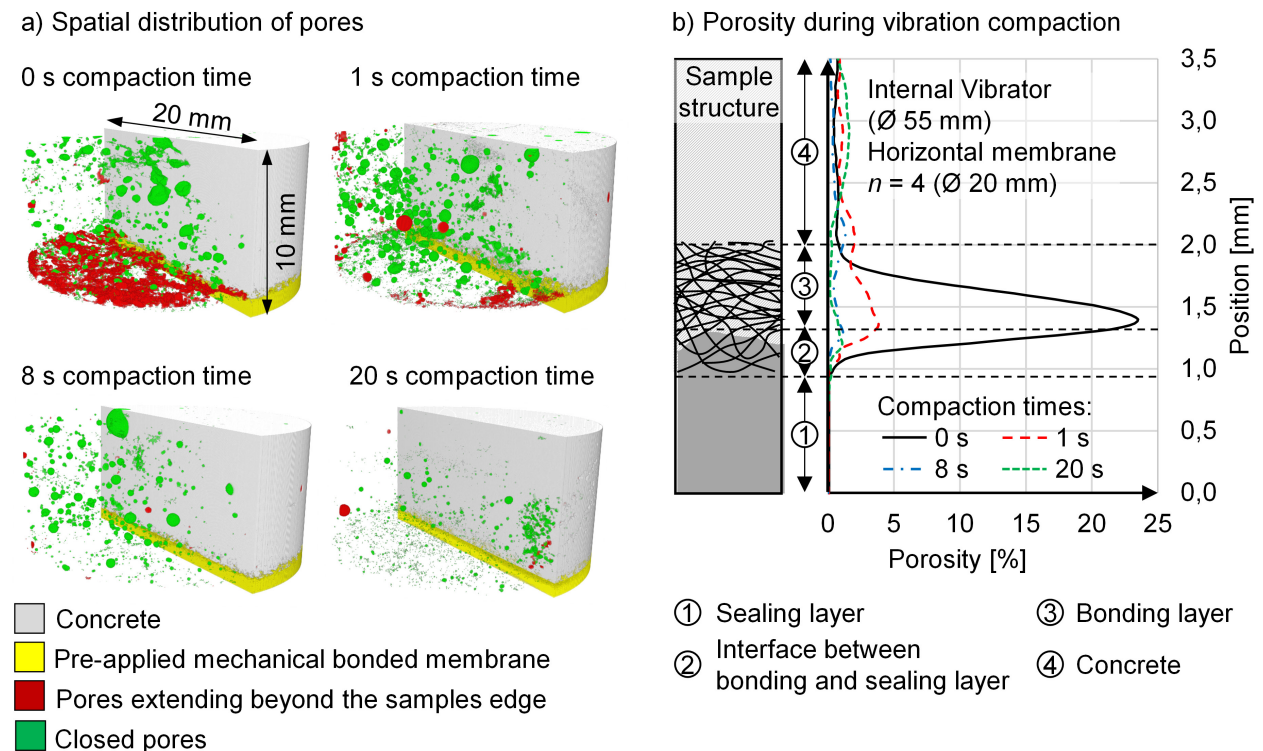


Fig. 13 - Micro-CT scans of cylindrical specimens with the pre-applied membrane S3 ($\text{Ø}/h = 20/10\ \text{mm}$) visualizing (a) and determining (b) the change in porosity during ongoing compaction

Without compaction ($t = 0\ \text{s}$), the porosity in the nonwoven reaches a maximum of 23.5 % at the interface between the nonwoven and the sealing layer. No waterproof bond is then present, as is confirmed in hydrostatic tests (see Chapter 9.2). After 1 s vibration compaction, the porosity in the bonding layer drastically decreases, while displaced air and water appear to rise into the adjacent concrete and increase its local porosity. However, according to the hydrostatic tests, a waterproof bond is not yet present and needs 3-5 s vibration compaction to form. Interpolating the results in Fig. 13-b, this vibration time correlates with about 1.5-2 % porosity in the nonwoven. For vibration compaction times longer than 8 s, the spatial distribution showed a decreasing concrete porosity but no significant change within the nonwovens. A certain number of closed pores remain in the nonwoven even after extensive vibration compaction. This finding fits the compression change in Fig. 10 and the hydrostatic tests in Chapter 9.2, where no change in thickness and waterproof bond occurred with more than 8 s of vibration compaction.

4.3 Materials for filtration and pull-off tests

The following filtration and pull-off tests in Chapters 4.4 and 4.5 investigate ten loose nonwovens N1-N10. In order to ensure comparability to pre-applied membranes, they were mainly selected within the property range of pre-applied membranes provided in Table 1 but with varying weights,

bonding methods, and surface structures. Also, N1&N2 were derived from the production line of internationally available pre-applied membranes and are identical to the nonwovens of S1&S5 in Table 1. In order to widen the property range, the nonwoven N6 with a high pore volume and the nonwoven N9 with a large opening width of 1.2 mm were additionally included. Table 2 lists the relevant nonwoven properties determined as in Table 1. The standard deviations are listed in Chapter 9.3.

Table 2 - Properties of nonwovens N1-N10 in Chapters 4.4 and 4.5

Property	Unit	Individual mean values of the tested nonwovens									
		N1	N2	N3	N4	N5	N6	N7	N8	N9	N10
Basis weight	g/m ²	64	97	24	53	117	153	110	37	60	87
Fiber material		PP	PP	PP	PP	PP	PP	PP	PES	PES	PES
Thickness at 0.5 kPa load	mm	0.83	1.50	0.23	0.35	1.33	3.23	0.49	0.43	0.61	1.15
Thickness at 15 kPa load	mm	0.60	1.07	0.16	0.28	1.06	1.86	0.39	0.29	0.45	0.81
Porosity at 15 kPa load (Equation 3)	[-]	0.88	0.90	0.84	0.80	0.88	0.91	0.69	0.91	0.90	0.92
Pore volume at 15 kPa load (Equation 4)	[dm ³ /m ²]	0.53	0.96	0.14	0.22	0.93	1.70	0.27	0.27	0.41	0.75
Type of bonding NP: Needle-punched; CB: Calender bonded; HE: Hydroentangled.		NP	NP	CB	CB	NP +CB	NP	NP +CB	HE	HE	HE
Charact. opening size of pores O_{90}	[μ m]	-	-	-	-	115	121	100	-	-	-

The fresh concrete mixture was varied in Chapters 4.4 and 4.5 within limits for waterproof concrete. The reference mixture used a CEM II/A-LL 42.5 N, with a cement content of 320 kg/m³, a w/c ratio of 0.55, and an A/B 32 grading curve with quarzitic round grain. The spread was adjusted to 460 mm according to DIN EN 12350-5 [119] using a PCE-based superplasticizer. Further mix designs are given in the third and fourth own papers in Chapters 9.3 and 9.4.

4.4 Cement paste filtration and processes within nonwovens during concrete placement

4.4.1 Temporal sequence of solids and water intrusion

The cement paste separation and processes within nonwovens during concrete placement were investigated using a filtration test stand. The tests were divided into static intrusion tests without vibration compaction and dynamic intrusion tests with compaction in order to replicate the processes during concrete placement. The reference test was carried out with the reference concrete mixture from Chapter 4.3, 15 kPa fresh concrete load, a high-frequency internal vibrator \varnothing 55 mm, and loose nonwovens, as is common for filtration tests.

Fig. 15 shows the solid and water mass content within the nonwoven N1, divided into the two test procedures. In the static intrusion test, about 0.4-0.5 kg/m² of water and an equal mass of solids separated from the fresh concrete into nonwoven N1 within the first minute. Subsequently, the nonwoven was saturated, and no further change occurred. The w/s ratio in the nonwoven N1 was then about 1.0, and thus, significantly higher than the w/c ratio of the fresh concrete. If the tests were repeated with a nonwoven laminated to a sealing layer for verification, comparable w/s ratios were determined (see Chapter 9.3). When the fresh concrete was removed after the test, a dense

layer of small aggregates was found on top of the nonwovens. It represents a filter cake responsible for the limited solids separation during the turbidity run.

Vibration compaction started after stationary masses were reached; thus, for nonwoven N1 after 1 min static load. About 0.5 kg/m² more solids were then separated from the fresh concrete within 30 s decreasing the w/s ratio continuously to about 0.6. The solid separation follows a power function ($r^2 = 0.94$) with a decreasing separation rate, most likely caused by embedded particles in the filter cake and the nonwoven. This ‘clogging’ is known to lower permeability and leads to a decreasing particle size distribution, as the opening widths of the filter cake and the nonwoven are reduced. An in-depth discussion follows in Chapter 4.6.

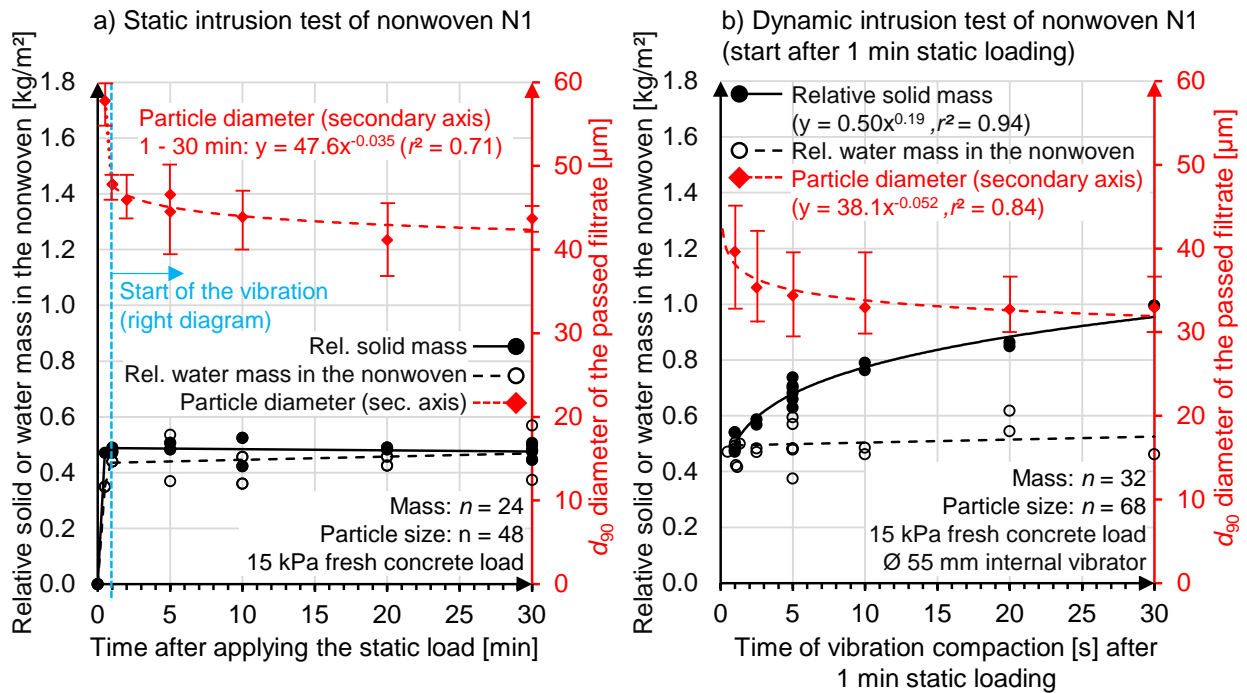


Fig. 15 - Time-dependent processes in the nonwoven N1 during static loading (a) and subsequent vibration compaction (b)

Similar results were obtained using the thicker nonwoven N2, but with more excess water separating from the fresh concrete. After the static intrusion test, the solid mass in the nonwoven was again about 0.5 kg/m², but the water content was about 1.2 kg/m². After 30 s vibration compaction, the solids content increased to 1.0 kg/m², and the water content decreased to 0.9 kg/m². Thus, the w/s ratio in the nonwoven developed from 2.1-2.8 after the static intrusion test to 0.9-1.2 after compaction. The higher w/s ratios compared to N1 are due to the higher pore volume in the nonwoven, allowing more excess water to separate from the fresh concrete.

Nonwovens of pre-applied membranes have pore volumes of up to 1 dm³/m², as seen in

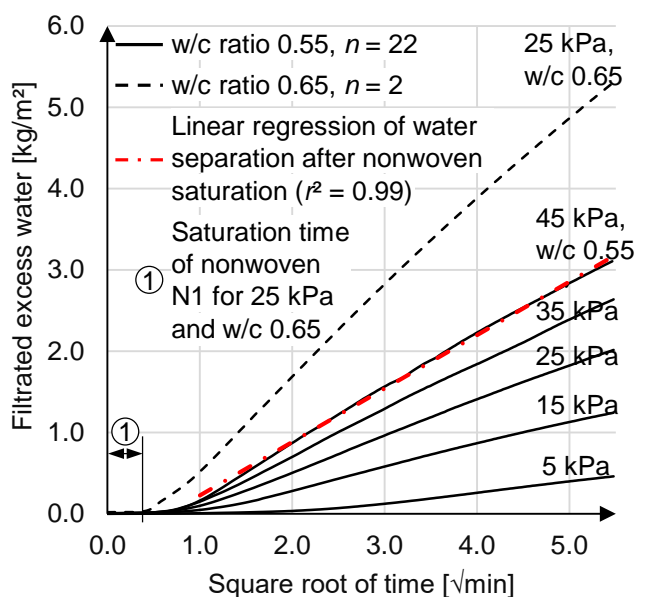


Fig. 14 - Filtration of excess water in the static intrusion test at different fresh concrete loads and w/c ratios using N1

Table 1 from the nonwoven thickness and porosity. Typical waterproof concrete mixtures contain enough excess water to fill this pore volume, as shown in Fig. 14 with the filtrated water in the collection tray of the filtration test stand. The filtration rate follows a square root time curve and is influenced by the fresh concrete load and the excess water content in the fresh concrete, as was similarly determined in [106,107]. Thus, depending on the fresh concrete load and w/c ratio, nonwovens can be saturated with filtrated excess water after a few minutes.

4.4.2 Water flow within nonwovens

The processes within a nonwoven during concrete placement were recorded using the nonwoven N1 laminated onto a transparent plastic film and placed in a formwork made of acrylic glass. For better visualization of water movements, three dots of water-soluble color powder were applied onto the nonwoven having a red to green color depending on the dilution. The reference concrete from Chapter 4.3 was placed in one layer and compacted with an internal vibrator (\varnothing 55 mm).

Fig. 16 shows the vertically-oriented nonwoven in a column-formwork during concrete placement. Excess water separates from the fresh concrete into the nonwoven after concrete pouring, sinks within the nonwoven, and collects at the base. Note that the water accumulation was only possible because the formwork was sealed. Common formwork would allow excess water to drain. During compaction, more solids enter the nonwoven, and the standing water is displaced partly upwards within the nonwoven and partially back into the fresh concrete, as seen from the changing cement paste color. Water movements also occur after compaction. However, it is unclear whether the water rises within the nonwoven due to its lower density or between the laminated nonwoven and the acrylic glass due to a leaking sealing. Due to the color changes of the cement paste and the water accumulation at the right column edge, both effects are plausible.

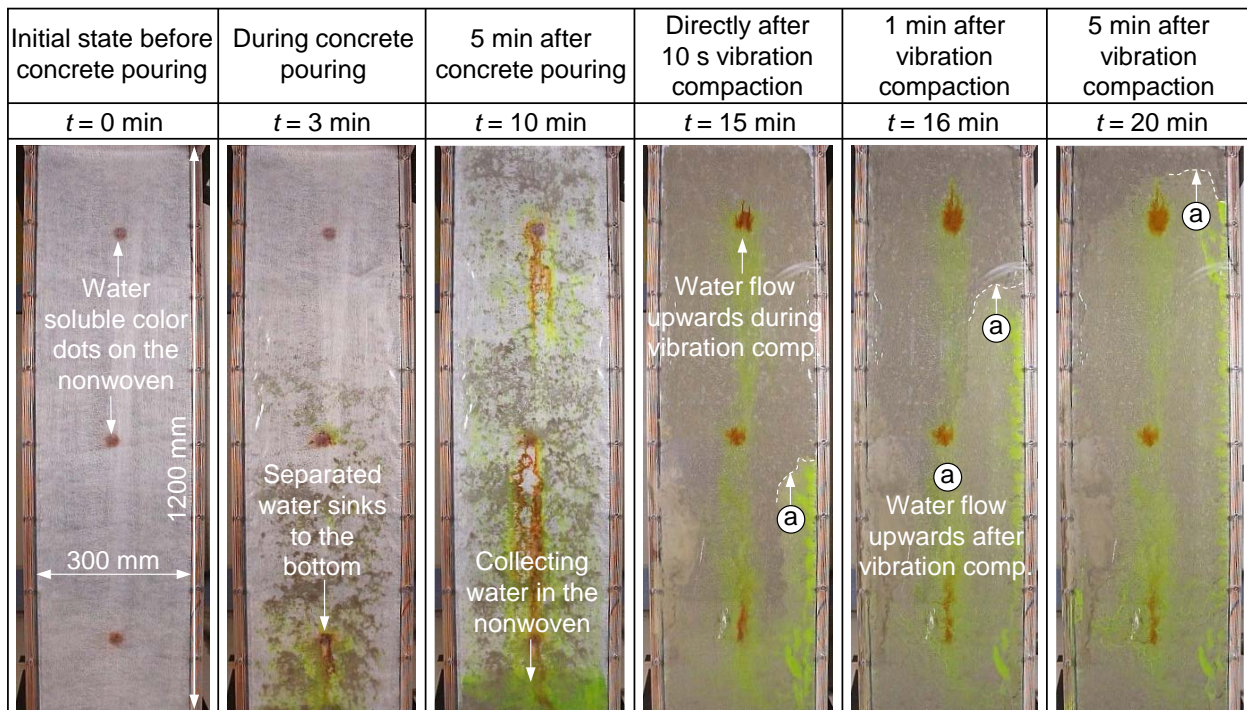


Fig. 16 - Nonwoven N1 during and after concrete placement. Color dots with red to green coloring indicate water movement in the nonwoven. Noticeable is the flow of filtrated excess water in the nonwoven before and after concrete compaction.

The behavior of the nonwoven N1 was also recorded in horizontal orientation during concrete placement, shown in the fourth own paper in Chapter 9.4. After concrete pouring, water collects at the specimen edges and rises upwards along the formwork during compaction.

The water movements possibly influence the cement paste within the nonwoven and result in varying w/s ratios across a specimen. This effect was investigated in Chapter 9.4 across horizontally-oriented specimens by measuring the w/s ratio of several subsamples. Disks (\varnothing 50 mm) were punched out of a laminated nonwoven specimen before concrete placement, placed back in the overall sample, taped on the reverse side, and individually tested for their w/s ratio after concrete placement. Fig. 17 shows the w/s ratio of the nonwovens N1 and N2 with increasing distance from the position of concrete pouring and vibration compaction. Note that the concrete was poured and compacted at the specimen center, and the w/s ratio was measured as a mean value over the nonwoven height. Three points become apparent:

- N2 has higher w/s ratios as more excess water separates from the fresh concrete due to its larger pore volume compared to N1.
- The w/s ratio is lowest at the point of concrete pouring. Since this effect is also present for uncompacted specimens, it is probably because the fresh concrete movement at the specimen center carries more fine particles into the nonwoven during concrete placement. At the specimen edge, the solids content is lower, resulting in higher w/s ratios.
- Vibration compaction reduces the w/s ratio in the nonwoven as solids are carried in, and excess water is displaced. Internal vibrators with larger diameters exhibit greater effects.

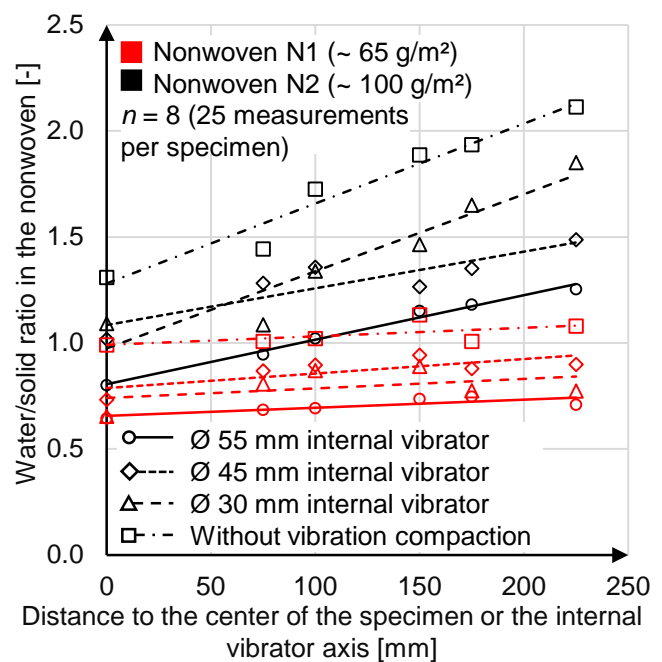


Fig. 17 - Water/solid ratio in the nonwovens N1&N2 in relation to the distance to the internal vibrator axis

In summary, the processes in the nonwoven during concrete placement are characterized by water movement, varying the w/s ratio of the cement paste. Similar to Controlled Permeable Formworks (CPF), excess water separates from the fresh concrete and fills the nonwoven pores. The filtrated water moves in the nonwoven before and during compaction, changing the w/s ratio of the cement paste in the bonding zone.

4.4.3 Particle size distribution in nonwovens

During the filtration test, a variable particle size distribution in the separated filtrate was observed (see Fig. 15, p. 24, Chapter 4.4.1). The particle size decreased during fresh concrete loading and vibration compaction, presumably due to entrapped particles in the filter cake and the nonwoven.

For a more detailed analysis, Fig. 18 shows the particle size distribution over the nonwoven height (top side facing concrete/bottom/passed filtrate) at varying compactions (static/dynamic intrusion test). The particle size distributions are presented as mean values for the nonwovens N1-8&10 since they are comparable. The measurements allow four observations:

- The particle size distributions of all nine nonwovens vary only slightly. For example, the standard deviation of the passed filtrate is between 4.5-5.9 μm . Further standard deviations are listed in Table 3.
- The particle size in the filtrate d is smaller than the characteristic opening sizes O of the nonwoven. For the nonwovens N5-N7, the manufacturer determined the 90 % percentile of the opening sizes to $O_{90} = 100\text{-}121 \mu\text{m}$ in a hydrodynamic sieving test according to ISO 12956 [120] (see Table 2). The corresponding particle sizes of the filtrate are $d_{90} = 30\text{-}34 \mu\text{m}$. The particle size distribution is thus not determined by the nonwoven but by the filter cake.
- The particle size distribution varies over the height of the nonwoven and is smaller the lower the particles are measured within the nonwoven. Coarser particles ($d > 90 \mu\text{m}$) are retained in the upper nonwoven structure, representing depth straining. In combination with measurements of the particle size distributions of cement and aggregate fines, more sand particles are present in the upper nonwoven. Thus, a varying cement-aggregate ratio and a variable paste composition result.
- The particle size varies with the compaction. Smaller particle sizes are present in the dynamic intrusion test as more fine aggregates and cement particles ($d < 10 \mu\text{m}$) are separated than in the static intrusion test. This effect is probably due to dissolved agglomerations during vibration compaction and an increasingly clogged filter cake that leads to decreasing opening widths during the compaction period.

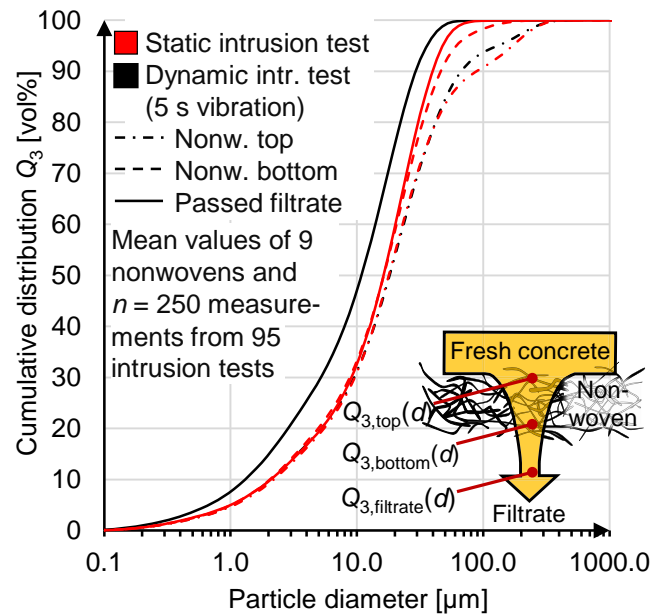


Fig. 18 - Particle size distribution in the nonwovens N1-8&10. Nonwoven N9 was not included in the above evaluation due to its wider openings.

Table 3 - Particle diameter in Fig. 18. Average \bar{d}_{90} diameter and standard deviation \bar{s} of the particles in the nonwoven [μm]

Testing area	Particle diameter [μm] in the nonwoven	
	Static intrusion test	Dynamic intr. test
Nonwoven top	$\bar{d}_{90} = 89.2$ ($\bar{s} = 72.5$)	$\bar{d}_{90} = 94.0$ ($\bar{s} = 49.2$)
Nonwoven bottom	$\bar{d}_{90} = 49.7$ ($\bar{s} = 16.5$)	-
Passed filtrate	$\bar{d}_{90} = 39.9$ ($\bar{s} = 5.9$)	$\bar{d}_{90} = 29.2$ ($\bar{s} = 4.5$)

Nonwoven N9 is not included in the above evaluation since it had much wider openings (1.2 mm). In the static intrusion test, the particle diameters in the filtrate are $d_{90} \approx 170\text{-}190 \mu\text{m}$ and, thus, smaller than the opening widths of around 1.2 mm. The filter cake again determines the particle size distribution.

In summary, filter cake filtration and depth straining determine the particle size in the nonwoven. The particle size varies due to different loading conditions (static/dynamic intrusion), time, and position in the nonwoven. The decreasing particle size over time was presumably due to an increasingly compacted and clogged filter cake and nonwoven, as was similarly observed for filtering geotextiles [78,83,88]. Simultaneously, the cement paste composition in the nonwoven is variable in terms of w/s ratio and cement-aggregate ratio due to more sand particles in the upper part of the nonwoven. Due to the variable composition, varying cement paste rheology must be expected.

4.4.4 Influences on the separated solid mass

In Chapter 4.2, longer compaction times significantly reduced the nonwoven porosity in micro-CT scans and improved the waterproof bond in hydrostatic tests. Additionally, in Chapter 4.4.1, longer compaction times resulted in a higher separated solid mass that reduced the w/s ratio in the nonwoven. In combination, it can be argued that the separated solid mass impacts the waterproof bond by influencing the cement paste's w/s ratio and capillary porosity. The impact of other practice-oriented boundary conditions was investigated via the following variations in 379 intrusion tests:

- *Fresh concrete properties:* Fresh concrete spread (420-550 mm), cement content (280-380 kg/m³), and water content (w/c ratios 0.40-0.65).
- *Concrete placement:* Fresh concrete load (5-45 kPa), diameter of the internal vibrator (38-58 mm), vertical distance between nonwoven and internal vibrator (0-100 mm), duration of fresh concrete loading before compaction (1-20 min), and vibration compaction time (1-30 s).
- *Nonwoven:* N1-N10 (Pore volume 0.14-1.70 dm³/m² at 15 kPa load).

Fig. 19 shows the solid mass in the nonwoven for different fresh concrete spreads that were adjusted by adding varying amounts of PCE-based superplasticizer. Higher additions of superplasticizers increase the separated solid mass in the static and dynamic intrusion tests. It is known that superplasticizers dissolve agglomerations of cement particles, increase workability, reduce shear resistance and lower the yield point [121,122]. Accordingly, separated solids could enter the nonwoven easier as the friction and filtration resistance is reduced. The effect is similar to dispersants in typical filtration applications [123].

Furthermore, nonwovens themselves have a strong influence on the separated solid mass. Fig. 20 shows the nonwovens N1-N10 in the static and dynamic intrusion tests, with nonwovens with higher pore volumes separating more solids. A similar effect was seen in [87], where thicker geotextiles separated higher solid masses. It was argued that thicker nonwovens are leading to a slower stabilization of the filter cake, resulting in a lower filter cake compaction and a higher permeability. However, nonwovens with low pore volumes are filled faster with solids, as seen by comparing the separated solid volume to the nonwoven pore volume - or by the deviation of the linear regression to the angle bisector. As a result, nonwovens with lower pore volumes have lower w/s ratios, closer to the w/c ratio of the fresh concrete.

During vibration compaction, the linear regressions in Fig. 20 shifted, indicating more additional solids separated for nonwovens with a higher pore volume. Nevertheless, they still have higher w/s ratios compared to nonwovens with lower pore volumes, as proven with laminated nonwovens. The nonwoven N6 with a 'high' pore volume ($V_{\text{pore}} = 1.7 \text{ dm}^3/\text{m}^2$) had w/s ratios of

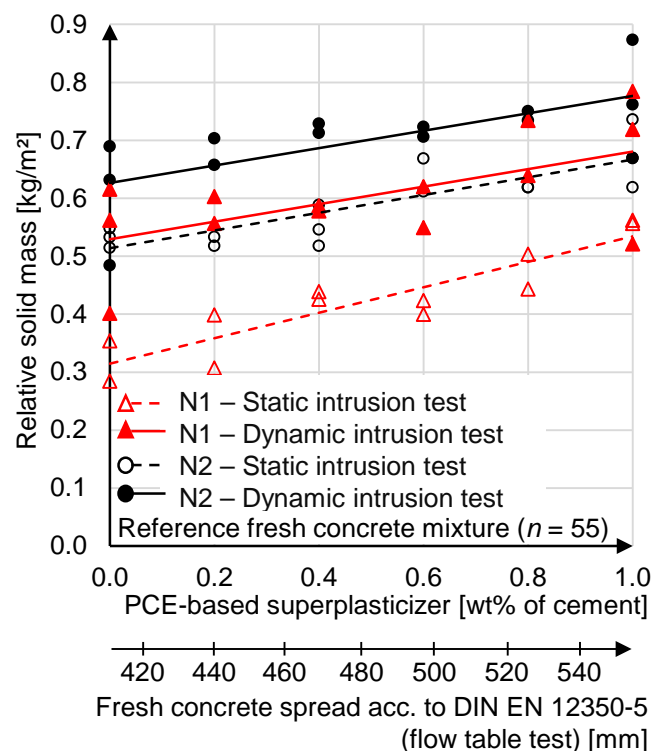


Fig. 19 - Influence of varying fresh concrete spreads on the solid mass in the filtrate

1.1-1.3 after 5 s compaction time, whereas the nonwoven N3 with a lower pore volume ($V_{\text{pore}} = 0.14 \text{ dm}^3/\text{m}^2$) had a w/s ratio of 0.55-0.60, approximately equal to the fresh concrete. Similar effects were seen in the hydrostatic tests in second own paper provided in Chapter 9.2, where thicker nonwovens had poorer waterproof bonds, corresponding to unfilled nonwovens parts or a cement paste with higher capillary porosity. Also, the thickness measurements in Chapter 4.2.1 showed nonwovens with higher pore volumes providing a slower compression recovery. This effect was most likely because nonwovens with higher pore volumes need disproportionately more solids to build up a supporting framework in the pores.

The internal vibrator and its position also affect the separated solid mass, with smaller internal vibrators and increasing distances leading to less separated solids. This finding fits the report of the *American Concrete Institute* [124] on the behavior of fresh concrete during vibration. Smaller unbalanced masses of internal vibrators and bigger distances in the fresh concrete lead to a decreasing compaction effect due to lower wave amplitudes. On pre-applied membranes, lower wave amplitudes may lead to a less pronounced loosening of the filter cake and, thus, a lower filter cake permeability during the dynamic intrusion.

All investigated variables are compared in Table 4 by listing their solid mass ranges. The solid mass range was determined as the starting and end values of the linear regressions across one variable. The results were additionally averaged over the nonwovens studied to obtain a representative mean value.

Table 4 - Comparison of the investigated variables. The listed values represent the starting and end values of the linear regression of each variation, averaged over the investigated nonwovens.

Variables	Range of the relative solid mass [kg/m ²]	
	Static intrusion test	Dynamic intr. test
Reference tests	0.51 (± 0.04)	0.70 (± 0.04)
Cement paste volume (230-330 dm ³ /m ³)	0.38-0.70	0.67-0.74
Fresh concrete spread (0-1 wt% superplasticizer)	0.41-0.60	0.58-0.73
Fresh concrete load (5-45 kPa)	0.51-0.55	0.66-0.69
Sustained static loading duration (1-20 min)	0.47-0.50	-
Time of vibration compaction (1-30 s)	-	0.52-0.95
Distance nonwoven - internal vibrator (0-100 mm)	-	0.60-0.72
Diameter of the internal vibrator (38-58 mm)	-	0.63-0.69
Textile influences (0.14-1.84 dm ³ /m ² pore volume)	0.25-0.78	0.39-1.13

Based on the solid mass ranges in Table 4, the *static intrusion* is influenced by the following variables, ranked according to their relevance:

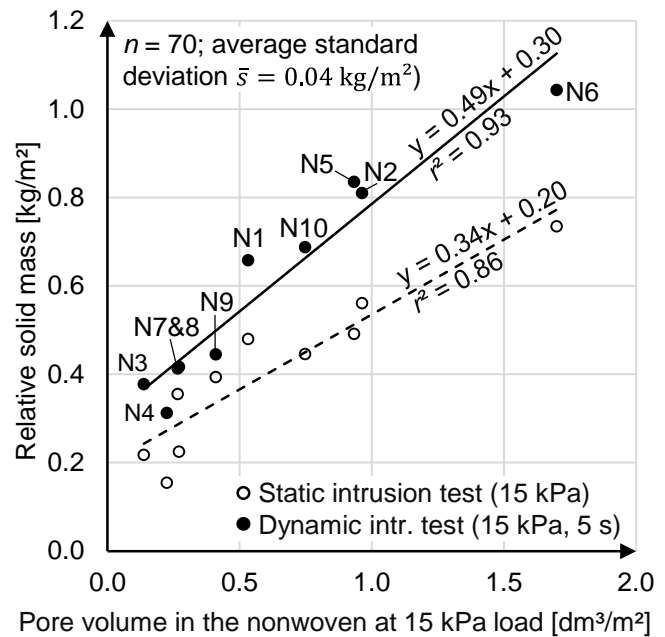


Fig. 20 - Textile influences due to variable pore volumes in the nonwovens

1. Pore volume in the nonwoven.
2. Workability of the fresh concrete (see variable cement paste volume and fresh concrete spread).

The relative solid mass in the *dynamic intrusion* is affected by the following variables, ranked according to their relevance:

1. Pore volume in the nonwoven.
2. Vibration compaction time with an internal vibrator.
3. Workability of the fresh concrete (variable quantity of superplasticizer).
4. The vertical distance between the internal vibrator and the nonwoven.

In summary, more solids are separated on the construction site for longer vibration compaction times, higher fresh concrete spreads, and smaller distances to the internal vibrator. The separated solid mass also increases with a higher nonwoven pore volume. However, the filtrated excess water rises disproportionately, resulting in an overall increased w/s ratio for nonwovens with high pore volumes.

Fig. 21 shows a nomogram based on the dynamic intrusion test to better visualize relevant influences on the solid mass and w/s ratio. The nomogram shows the impact of the pore volume of the nonwoven, the compaction parameters, and the fresh concrete spread in split images a and b. Split image c transforms the solid mass into the w/s ratio, based on the solids volume in the nonwoven and the premise that the remaining nonwoven pore volume is filled with excess water. The solid volume is calculated based on its known mass and density (see the third own paper in Chapter 9.3). Also, the following limitations apply:

- The nomogram is only valid for fresh concrete mixtures with excess water ($w/c > 0.40$).
- The nomogram is based on average values measured in the filtration test stand in a circular formwork with \varnothing 320 mm. At the same time, it is known from the fourth own paper given in Chapter 9.4 that the w/s ratios vary with their distance to the internal vibrator.
- Only the graph for 5 s vibration compaction was measured for all nonwovens. Other compaction graphs are calculated based on the compaction progress for nonwoven N1 and N2.

4.5 Bond strength of nonwovens to concrete

4.5.1 Influence of hardened concrete properties

The bond strength of nonwovens to concrete was determined according to DIN EN 1542 in pull-off tests with nonwovens laminated on a plastic film. The test procedure is described in Chapter 3, and verification of the method and all results are given in Chapter 9.4. Nonwovens were mainly investigated on test specimens with $l/w/h = 300/300/200$ mm in horizontal orientation since air voids did not affect the bond strength. Furthermore, the following variations were tested:

- *Concrete properties:* Concrete age (0.5-14 d), water content (w/c ratio 0.40-0.65), cement content (280-380 kg/m³), cement type (CEM II/A-LL 42.5 N, CEM III/A 42.5 N-LH), and fresh concrete spread, varied by means of PCE-based superplasticizer (420-610 mm according to DIN EN 12390-5).
- *Concrete placement:* Nonwoven orientation (horizontal/vertical), fresh concrete height (0-1200 mm), vibration compaction time (0-10 s), and distance to different internal vibrators (0-310 mm distance of pull-off tests to the axis of internal vibrators \varnothing 30/45/55 mm).
- *Nonwovens:* N1-N10 from Chapter 4.3

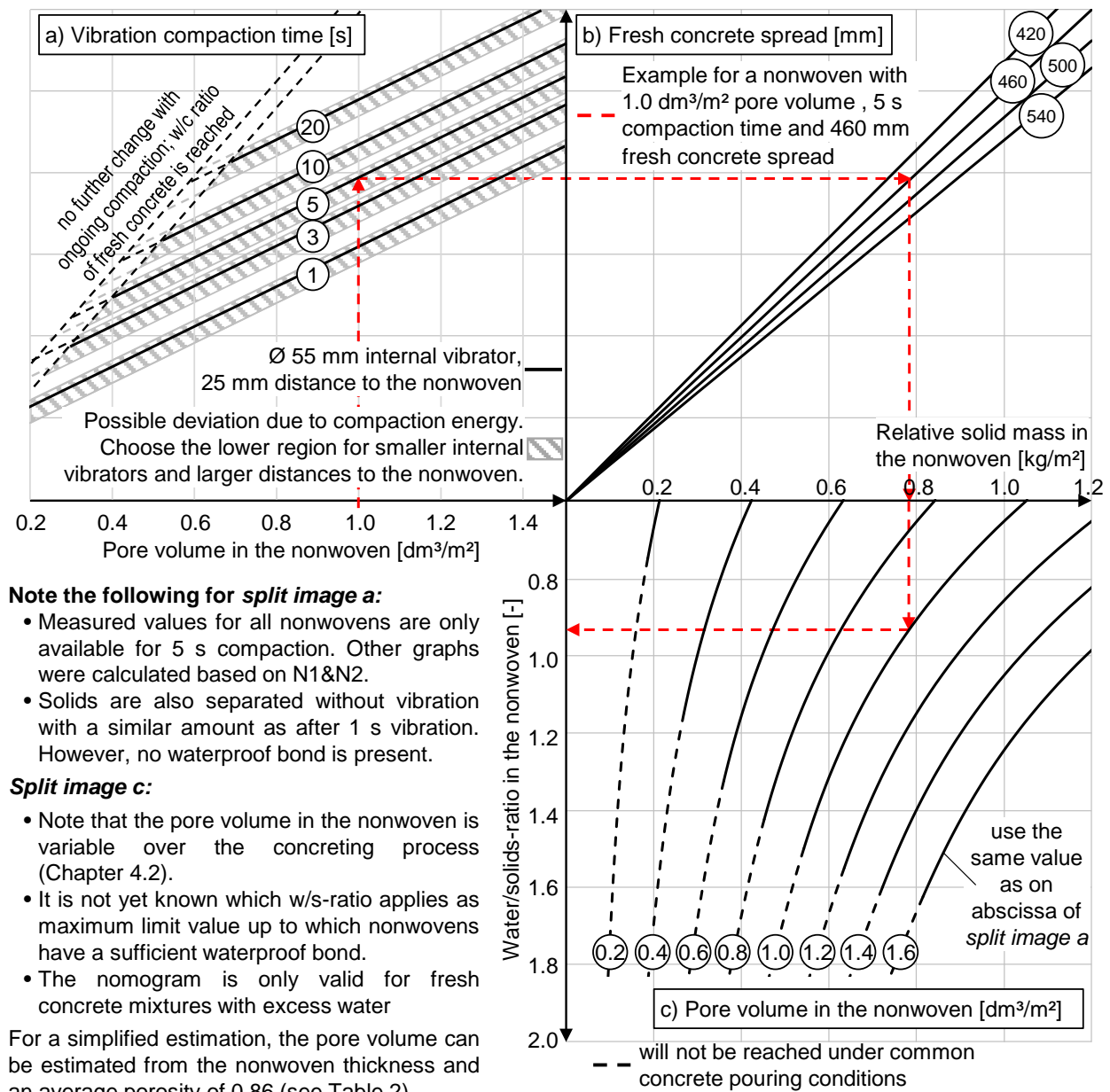


Fig. 21 - Nomogram for estimating the w/s ratio in a nonwoven considering the relevant influences during concrete placement. Note that the nomogram is only valid for concrete mixtures with excess water.

Fig. 22-a displays the development of the concrete tensile splitting strength and the nonwoven bond strength using a CEM II/A-LL 42.5 N. The tensile splitting strength was approximated after concrete setting according to the *fib* model code using Equation 11 (p. 18), considering the concrete temperature during curing according to Equation 12 (p. 18). The *fib* model code approach also showed a good fit to the nonwoven bond strength after a nonwoven-specific coefficient v was introduced in Equation 13 (p. 18). The coefficient v acts as a proportionality constant and shifts the tensile splitting trend. Table 5 lists the variables used for Equations 11 and 13, with the cement-specific values s chosen close to the values suggested in the model code for the used cement type.

The nonwoven bond strength is lower than the concrete tensile splitting strength and ranges between 0.28-0.94 MPa after two days using a CEM II/A-LL 42.5 N. Thus, the bond strength varies at a factor of 0.18-0.52 of the concrete tensile splitting strength (see Table 5). The scatter of mean values in the reference tests was at a maximum of 0.17 MPa (see Chapter 9.4) and thus

sufficiently low compared to the influencing variables. The consistent results also confirmed a uniform lamination process of the nonwovens. Furthermore, the results are comparable to the investigations of Meyer *et al.* [15], where the bond strength of six mechanically bonded pre-applied membranes was between 0.40-0.93 MPa after two days using a CEM II/A-LL 32.5 R.

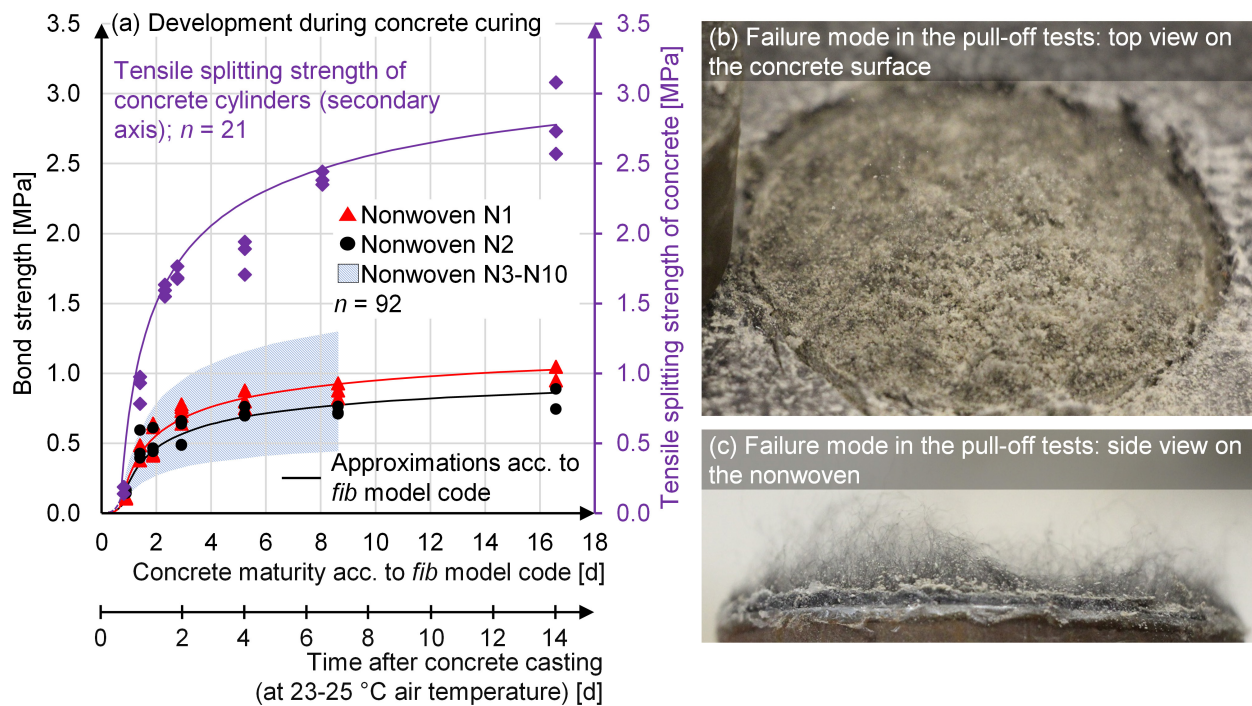


Fig. 22 - (a) Development of the bond strength and concrete tensile splitting strength during ongoing concrete curing considering the concrete temperature according to Equation 12. Approximation started 12 h after concrete placement. (b, c) Typical failure mode in the pull-off tests.

Table 5 – Coefficients in Equations 11 and 13 used to approximate the results in the tensile splitting and pull-off tests in Fig. 22-a

Cement type	Mean tensile splitting strength $f_{ct,sp}$, 14 d after concrete casting for Equation 11	Cement-specific coefficient s in Equation 11	Nonwoven-specific coefficient v in Equation 13		
			Nonwoven N1	Nonwoven N2	Nonwoven N3-N10
CEM II/A-LL 42.5 N	2.79	0.25	0.37	0.31	0.18-0.52
CEM III/A 42.5 N-LH	2.71	0.42	0.37	0.31	-

The debonding generally occurred in the interface between the concrete surface and the nonwoven, as the uppermost nonwoven fibers remained in the concrete and were pulled out of the nonwoven. The nonwoven disintegrated, and the cement paste in the nonwoven pores was released and remained on the concrete surface as sandy residue. Fig. 22-b shows the concrete surface after testing, and Fig. 22-c the disintegrated nonwoven for N2 two days after concrete casting.

Varying the fresh concrete mixture influenced the bond strength, especially by changing the w/c ratio, with lower w/c ratios improving the tensile splitting and bond strength (see Fig. 23). Nevertheless, the bond strength was still proportional to the tensile splitting strength. Furthermore, the CEM III with lower early strength led to slower bond strength development, as seen from the coefficient s in Table 5. However, the bond strength of the reference concrete mixture was reached after about 10 d. Also, the bond strength values could still be approximated with the *fib* model code approach with unchanged nonwoven-specific coefficients. In contrast, varying fresh

concrete spreads and cement contents within limits for waterproof concrete structures had little influence on the tensile splitting or bond strength (see Chapter 9.4).

For a better illustration of the relationship between bond strength and tensile splitting strength, pull-off test results were plotted against the related tensile splitting strengths in Fig. 24. The values were approximated with linear regression (min $r^2 = 0.82$), showing slopes between 0.18-0.56, close to the coefficients ν in Table 5. The correlation between bond strength and concrete tensile splitting strength is plausible: the bond is achieved by embedded nonwoven fibers in the cement matrix, with the cement matrix also influencing the concrete strength [125,126]. Nevertheless, the bond strength is still clearly below the concrete tensile splitting strength, presumably because the nonwoven fibers are mostly arranged parallel to the concrete surface, weakening the cement matrix. Also, results vary clearly between the different nonwovens, which will be discussed in Chapter 4.5.3.

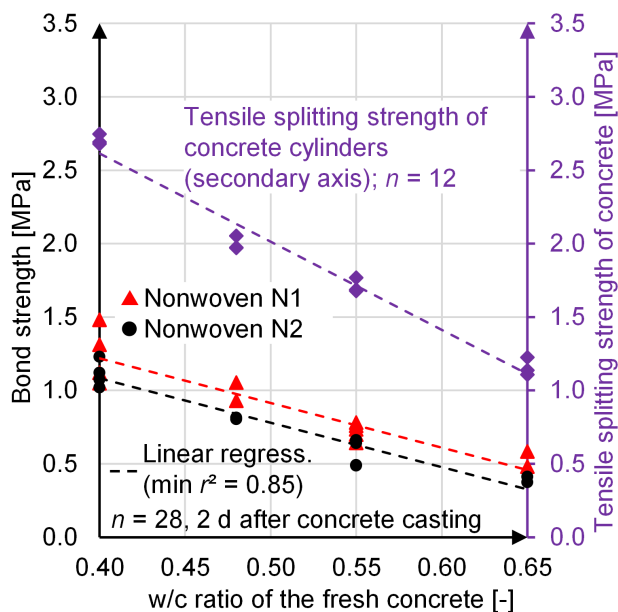


Fig. 23 - Nonwoven bond strength and concrete tensile splitting strength for varying w/c ratios two days after concrete casting.

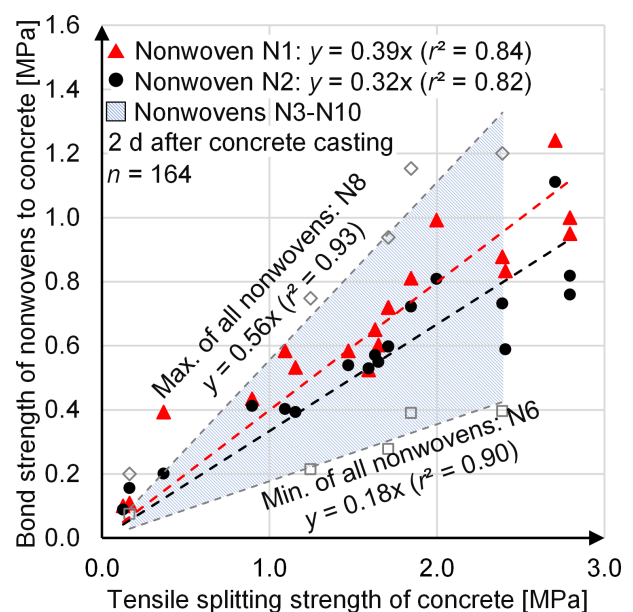


Fig. 24 - Comparison of the bond strength of nonwovens to the tensile splitting strength of concrete for N1-N10.

4.5.2 Influence of concrete placement conditions

The concrete placement conditions alter the w/s ratio and cement paste properties within the nonwovens, as was shown in Chapter 4.4. The impact on the bond strength was first investigated using reference specimens ($l/w = 300/300$ mm) with varying the nonwoven orientation (horizontal/vertical) and vibration compaction time (0-10 s).

Higher compaction times increase the bond strength slightly, as shown in the fourth own paper in Chapter 9.4. However, the bond strength without any vibration compaction is nearly as high as after 2 s compaction, with the failure zone still being in the upper nonwoven area. Thus, it is plausible that the upper nonwoven fibers interlock with the filter cake and fine solids that enter the nonwoven within the first minutes after concrete pouring (see Fig. 15, p. 24, Chapter 4.4). The following vibration compaction does not improve the fiber embedment in the concrete surface, and separated solids fill deeper located nonwoven pores without significantly impacting the bond strength. In contrast, the orientation of the nonwoven influences the bond strength, with vertically-oriented nonwovens having lower bond strengths. On average, the bond strength was reduced

by 25 % for the nonwovens N1-N10, as shown in Fig. 25, with visible reasons being voids, water channels, and cement paste washouts at the lower half of the specimen.

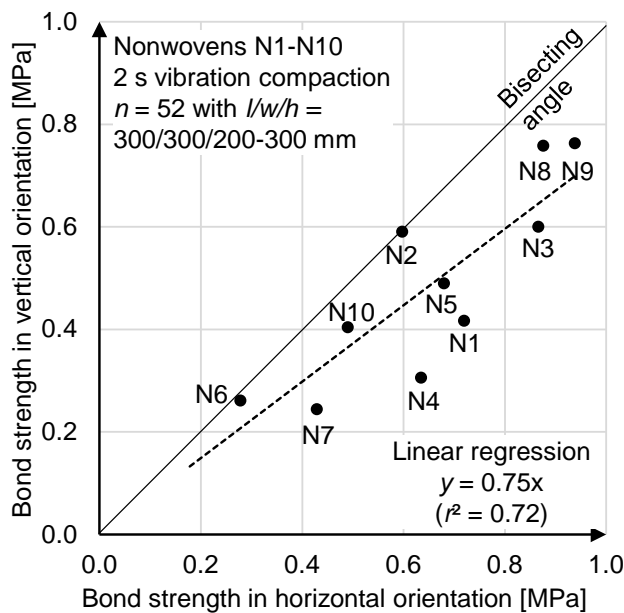


Fig. 25 - Comparison of the bond strength in horizontal and vertical orientation

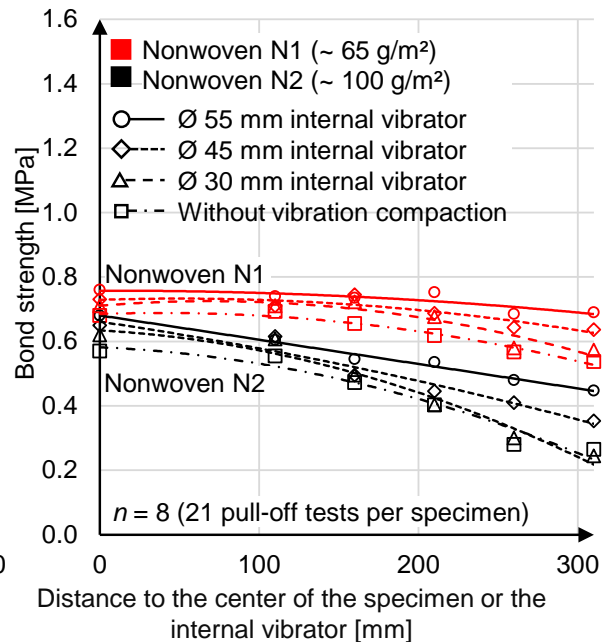


Fig. 26 - Bond strength with increasing distance from the internal vibrator and location of concrete placement

In the filtration tests and video recordings in Chapter 4.4, water movements became visible during concrete placement. They affected the w/s ratio across the nonwovens, with horizontally-oriented nonwovens showing higher w/s ratios towards the specimen edge (Fig. 17, p. 26, Chapter 4.4). In order to investigate the influence of the changing w/s ratios on the bond strength, pull-off tests were performed across larger samples ($l/w/h = 600/600/200$ mm). The concrete was placed and compacted at the specimen center. Fig. 26 displays the bond strength across a specimen with horizontally-oriented nonwovens, allowing the following observations:

- The bond strength at the specimen center was equal to reference tests. Towards the specimen edge, the bond strength decreased especially for uncompacted specimens. At the same time, Fig. 17 (p. 26) showed higher w/s ratios towards the specimen edge.
- The nonwoven N2 exhibited lower bond strengths than N1 and had higher w/s ratios in Chapter 4.4.
- Vibration compaction improved the bond strength at the specimen edge and reduced the w/s ratio in Fig. 17, as water accumulations were displaced.

After examining the impact of horizontal water movements, the influence of vertical water movements was investigated with pull-off tests over a column with 1.2 m height at 80 mm intervals. This column was also used to record vertical water movements in Fig. 16 (p. 25, Chapter 4.4), showing filtrated excess water in the column center and collecting water at the column base. Fig. 27 shows the bond strength over the column height, with the bond strength at the column head corresponding to the reference tests. For example, the bond strength at the column head was 0.75 MPa for N1 compared to the reference test with 0.72 MPa. Towards the center of the column, the bond strength increased by 30-40 % and was 0.98 MPa for N1. At the base of the column, the bond strength decreased to about 0.5 MPa. Comparing the bond strengths of the

column with those at varying w/c ratios of the fresh concrete in Fig. 23, the column center corresponds to w/c 0.48-0.50 and the column base to 0.60. Thus, it can be argued that the visible filtration of excess water during the concrete placement lowered the w/c ratio of the adjacent fresh concrete and increased the bond strength. It is also known from Fig. 14 (p. 24) that water filtration is faster at higher loads, explaining the increasing strength towards the column center. As the formwork was sealed, the filtrated excess water collected at the column base, raising its w/c ratio in the bonding zone and reducing the matrix strength.

In summary, the results of the larger specimens suggest an indirect proportionality between the w/s ratio of the cement paste in the nonwoven and the bond strength. Further discussion will follow in Chapter 4.6.3.

4.5.3 Influence of nonwoven properties

In Chapter 4.4, nonwovens with higher pore volumes separated more solids but led to higher w/s ratios in total. In order to identify nonwoven properties that influence the bond strength, results of pull-off test were plotted against various nonwoven properties. The bond strengths were based on the reference test two days after concrete pouring using a fresh concrete mixture with a w/c ratio of 0.55. Fig. 28-a shows the regression with the best coefficient of determination being $r^2 = 0.69$, with nonwovens with higher basis weights having lower bond strength values.

The regression against nonwoven thickness led to a low coefficient of determination of $r^2 = 0.48$; against pore volume of $r^2 = 0.39$.

Previous pull-off test results of larger specimens suggest an influence of the w/s ratio on bond strength (Chapter 4.5.2). However, the w/s ratio itself is influenced by the nonwoven pore volume as it controls the separable amount of excess water (Chapter 4.4). In order to separate those two influences, the tests from Fig. 28-a were repeated using a fresh concrete mixture that can be assumed having no excess water with a w/c of 0.40. Then, the w/s ratios in all nonwovens approximately correspond to the w/c ratio of the fresh concrete, as was proven in Chapter 9.3. Fig. 28-b displays the test results with only slight differences between the nonwovens or slightly higher values for nonwovens with higher basis weights. For comparison with Fig. 28-a, the bond strength values were plotted against basis weights leading to a poor correlation ($r^2 = 0.28$). A slightly better but still poor correlation was obtained versus nonwoven pore volume ($r^2 = 0.48$).

The trend of Fig. 28-b can be physically explained. Heavier nonwovens are usually mechanically bonded by needling or hydroentanglement and thus have rougher surface textures and more fibers in the z-direction than calendared nonwovens. As a result, they interlock better with the cement matrix [127].

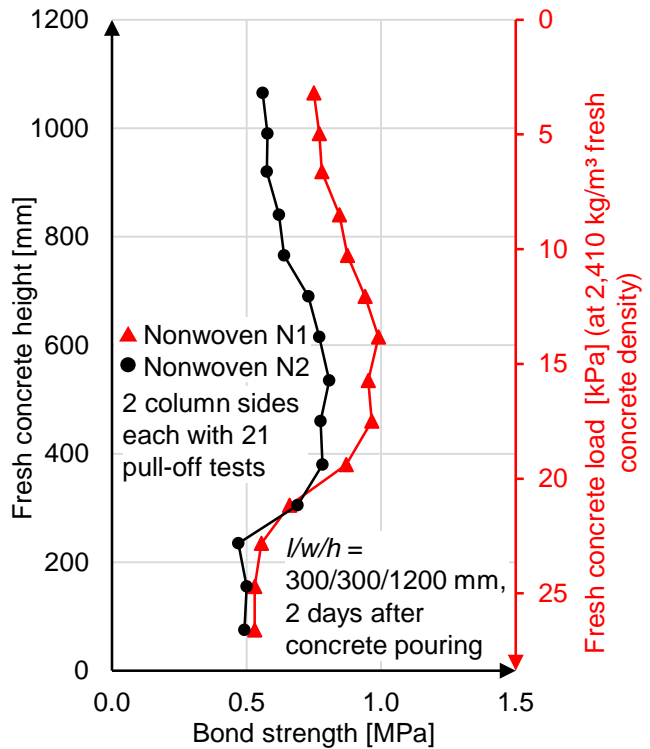


Fig. 27 - The nonwoven bond strengths on a column is affected by varying w/c ratios of the fresh concrete in the bonding zone. Similar to CPF, excess water separates in the column center and accumulates at the formwork bottom.

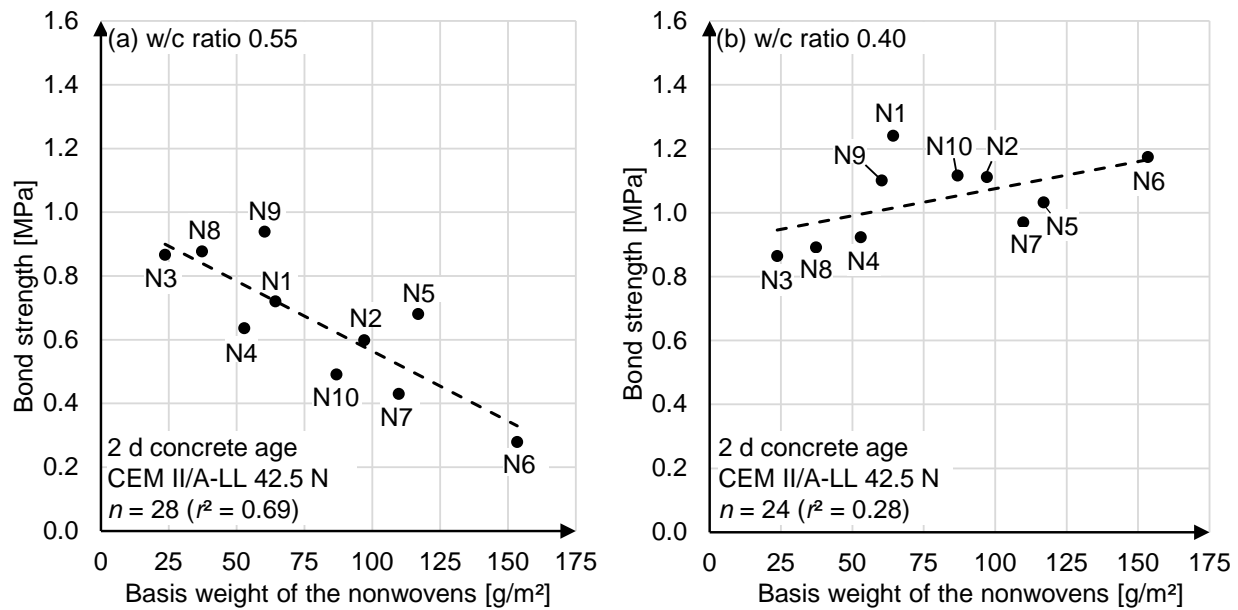


Fig. 28 - Bond strength of nonwovens N1-N10 at a w/c ratio of the fresh concrete of 0.55 (a) and 0.40 (b)

4.6 Hypothesis on cement paste separation and bond strength development

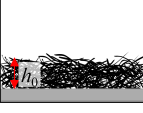
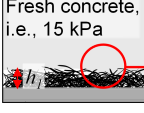
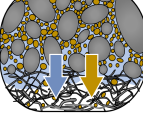
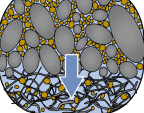
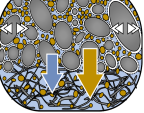
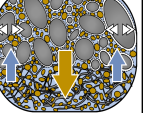

4.6.1 Cement paste separation after fresh concrete placement

Based on the information provided in Chapters 4.2, 4.4, and 4.5, a hypothesis on the time-dependent processes in the nonwoven during concrete placement and the bond strength formation is presented and discussed. The hypothesis is divided into initial processes in the nonwoven after fresh concrete pouring (Chapter 4.6.1), subsequent processes during the vibration compaction (Chapter 4.6.2), and the following development of the bond strength (Chapter 4.6.3).

At the beginning of the fresh concrete placement, the nonwoven is compressed, and its pore volume is reduced, as shown in Chapter 4.2 and described for the filtration using geotextiles [82]. Simultaneously, water and a limited solid mass are separated from the fresh concrete leading to a filter cake and a water-rich cement paste within the nonwoven (see Chapter 4.4). Fig. 29 shows a graphical summary with examples of nonwovens N1 and N2. Note that the w/s ratios apply to the location of concrete placement.

The initial separation of solids is common for the beginning of filter cake filtration, with fine solids passing through the filter medium, known as turbidity run [58]. It was also observed during sludge dewatering using geotextiles [85,86] and may be driven by the solid density and the flow of filtrated water for pre-applied membranes. Larger solids remain on top of the nonwoven due to straining, forming the filter cake rapidly, most likely due to the high solids content of concrete and its graded aggregate size distribution.

At this stage, nonwovens are not waterproof, as verified with hydrostatic tests in Chapter 9.2. On the one hand, nonwovens still have high porosity due to air and compaction pores, as shown in micro-CT scans in Chapter 4.2. The high w/s ratios in the nonwovens will also result in high capillary porosity in the hardened cement paste, as known from *Powers et al.* [128]. On the other hand, vibration compaction is probably needed to disperse solids in the nonwoven. *Palmeira and Trejos* [82] also argued for geotextiles that vibration moves particles within the nonwoven structure. A similar effect was observed and described in Chapter 9.3 for fresh concrete mixtures with low water contents, where vibration was needed to transport particles through the nonwoven.

External influences and effects	Initial state	Static intrusion via fresh concrete load (i.e., 15 kPa)			Dynamic intrusion via vibration compaction		
		Compression due to concr. load	Build up of filter cake	Final filter cake due to static load	Loosening of the filter cake	Return flow of water from nonwoven	Final state in the concrete
Processes in the nonwoven (Schemes show sections of pre-applied membranes)							
	Unloaded nonwov. with thickness h_0	Empty, but compressed nonwoven, $h_1 < h_0$	Water and fines into nonwoven	High water/solids ratio in nonwoven	Cement paste into nonwoven	Water from nonwoven into fresh concrete	Filled nonwoven, $h_{fin} \approx h_0$
„Thin“ nonwoven N1	$m \approx 65 \text{ g/m}^2$ $V_{\text{pore}} = 0.76 \text{ dm}^3/\text{m}^2$	$t = 0$ $V_{\text{pore}} = 0.53 \text{ dm}^3/\text{m}^2$	$t_{\text{static}} < 1 \text{ min}$ $w/s \approx 0.7$	$t_{\text{static}} \geq 1 \text{ min}$ $w/s \approx 1.0$	$t_{\text{vibr}} = 1 \text{ s}$ $w/s \approx 0.9$	$t_{\text{vibr}} = 5 \text{ s}$ $w/s \approx 0.6^*$	$t_{\text{vibr}} = 10 \text{ s}$ $w/s \approx 0.55^*$
„Thick“ nonwoven N2	$m \approx 100 \text{ g/m}^2$ $V_{\text{pore}} = 1.40 \text{ dm}^3/\text{m}^2$	$t = 0$ $V_{\text{pore}} = 0.96 \text{ dm}^3/\text{m}^2$	$t_{\text{static}} < 5 \text{ min}$ $w/s \approx 1.6$	$t_{\text{static}} \geq 5 \text{ min}$ $w/s \approx 2.3$	$t_{\text{vibr}} = 1 \text{ s}$ $w/s \approx 1.2$	$t_{\text{vibr}} = 5 \text{ s}$ $w/s \approx 0.9^*$	$t_{\text{vibr}} = 10 \text{ s}$ $w/s \approx 0.8^*$

*Nonwovens N1&N2 have a sufficient waterproof bond. The maximum limit value of the w/s-ratio is unknown so far.

Fig. 29 - Hypothesis on the time-dependent processes in the nonwoven during concrete placement

4.6.2 Cement paste separation during vibration compaction

With the onset of vibration compaction, more solids enter the nonwoven, the nonwoven decompresses, and its porosity decreases. Similarly, *Narejo and Koerner* [88] as well as *Hong and Wu* [89] tested geotextiles under pulsating hydrodynamic load and found excessive soil loss through the geotextile compared to static loading. On pre-applied membranes, higher solid separation may be due to four effects:

- The vibration compaction loosens the existing filter cake and raises its permeability.
- Dynamic action is known to reduce the yield point of cement paste and dissolve interparticle forces [124], lowering filtration resistance.
- As the solid volume in the nonwoven increases, water from the nonwoven is forced back upwards due to its lower density and passes the filter cake, as seen in the spatial distribution of the micro-CT scans. The method of "backflows" or filter cake washing is used in standard filtration applications to loosen the filter cake in cyclic intervals [123].
- Nonwovens are compressed due to the fresh concrete load but recover during vibration compaction (Chapter 4.2). Due to the compression recovery, pore sizes may expand, and permeability increases again. A change in pore size due to compression was also observed by *Palmeira et al.* [82].

With vibration compaction and the entry of solids, separated water is displaced laterally within the nonwoven and back into the fresh concrete. Nevertheless, a high w/s ratio remains in the nonwovens. After 5 s of compaction, it ranges from 0.6-0.9 for the nonwovens N1 and N2 at the point of concrete placement. Evaluating this w/s ratio must consider two points: On the one hand, N1 and N2 are waterproof after 5 s of vibration compaction (see second own paper in Chapter 9.2). On the other hand, *Powers et al.* [128] showed increasing permeability of hardened cement paste above w/c 0.6, even when complete cement hydration was accomplished. It is not yet clear why nonwovens have a waterproof bond even with high w/s ratios, for which three effects are plausible:

- An inhomogeneous solids distribution in the nonwoven may result in locally fluctuating w/s ratios, leading to nonwoven areas with w/s ratios < 0.6 . On the one hand, this effect may occur across the nonwoven surface. So far, the smallest test area had a diameter of 50 mm and did not verify this (Chapter 4.4.2). On the other hand, a fluctuating w/s ratio is also plausible over the nonwoven height, as suggested by the varying porosity over the nonwoven height observed in the micro-CT scans in Chapter 4.2.2 for short compaction times.
- The waterproof bond has, so far, always been measured at the concrete placement and compaction position. According to Fig. 17, this position has the lowest w/s ratio across the specimen. Thus, previous hydrostatic tests are not valid across the nonwoven and most likely overestimate the waterproof bond at specimen edges.
- The nonwoven-cement composite may have enhanced waterproofing. *Ramezani-anpour et al.* [129] investigated normal concretes with PP microfibers and found reduced permeability in hydrostatic tests up to addition rates of 0.9 kg/m^3 . The authors attributed the decreased permeability to pore-blocking effects caused by the fibers. With increasing fiber additions, however, permeability increased again due to increased air void content and porosity. In comparison, nonwovens of pre-applied membranes have higher ‘fiber addition rates’, so an enhanced waterproofing effect has to be questioned. *Hannawi et al.* [130] also found higher permeabilities around macro-fibers and attributed them to a porous interfacial transition zone comparable to the mortar-aggregate interface in normal concretes [131].

4.6.3 Bond strength development

The bond strength of nonwovens to concrete develops proportionally to the concrete tensile splitting strength. The debonding occurs in the uppermost nonwoven layer so that the relevant bonding area is to be expected in the interface between nonwoven and concrete. Fibers deeper in the nonwoven seem to have little effect on the bond, presumably due to the high fiber content and their parallel arrangement to the concrete surface, weakening the cement matrix. Also, nonwovens achieve a bond even without vibration compaction. This effect is presumably because the upper nonwoven fibers bond with the filter cake and with fine particles separated during filter cake formation.

The results in Chapters 4.5.2 and 4.5.3 also suggest an impact of the w/s ratio in the nonwoven on the bond strength. Discussing this observation must consider two points:

- The investigated bonding zone consists of the nonwoven surface filled with cement paste, so the cement strength will influence the overall bond strength.
- According to Abrams Law, cement strength is generally inversely affected by its w/c ratio (see Fig. 23 or [132,133]). Hence, it is plausible that water movements and varying w/s ratios in the bonding zone impact the bond strength. The effect is similar to CPFs that increase the concrete’s surface strength by decreasing the adjacent w/c ratio [93,98]. Similar effects were seen for wet nonwovens that exhibited reduced bond strengths in the investigations of *Meyer et al.* [15] and wet geotextiles that had reduced peel strength values to concrete in the investigations of *Long and Paul* [134].

The bond strength of varying nonwovens also fits this assumption. For fresh concretes with excess water, nonwovens showed lower bond strength values with rising nonwoven basis weights (Chapter 4.5) but greater w/s ratios with higher pore volumes (Chapter 4.4). Thus, the w/s ratio in the nonwoven again influences the cement matrix strength in the bonding zone. Furthermore, the bond is probably influenced by the nonwoven structure, as observed using a concrete mixture

without excess water. The surface roughness and fiber ratio in the z-direction are likely important but could not be assigned due to the scatter in the tests.

In conclusion, the nonwoven bond strength is most likely influenced by the cement strength in the interface between the nonwoven and concrete surface, which in turn is affected by the local w/s ratio in the upper nonwoven. The nonwoven structure may also have a secondary influence, which could not be assigned so far. For the development of new pre-applied membranes, nonwovens with low basis weights can be recommended. As they usually have low pore volumes, they also are favorable for a good waterproof bond, as shown in Chapter 4.4. Higher bond strength values are also achieved for fresh concrete mixtures with low w/c ratios and vibration compaction as water accumulations are displaced. However, long compaction times are especially important for the waterproof bond as nonwovens already bond during filter cake formation. On-site, bond strength can be roughly estimated using the predicted concrete tensile strength according to the *fib* model and a nonwoven-specific coefficient.

5 Conclusions

Nonwovens are often used on pre-applied bonded membranes as a bonding layer. Nevertheless, existing research cannot fully explain their mode of action and the development of the waterproof and adhesive bond. Based on this thesis, a significant extension of the so-far known bonding mechanisms is provided. Furthermore, the sequences during the concrete placement are understood, and the nonwovens as well as the concrete pouring conditions on the construction site can be optimized.

At the beginning of this thesis, nonwovens of currently used pre-applied membranes were characterized having nonwoven basis weights between 35-130 g/m² and unloaded thicknesses of 0.2-1.1 mm. They are usually made of PP or PES staple fibers and bonded mechanically or thermally. During concrete placement, the nonwovens exhibit a deformation behavior comparable to mechanical loading, as observed using microsections. After the concrete is poured, the fresh concrete load compresses the nonwoven. During the following vibration compaction, cement paste fills the nonwoven pores and increasingly transfers the fresh concrete load, so the nonwoven decompresses due to the residual stress of its fibers. However, the final thickness depends on the nonwoven orientation. Vertically-oriented nonwovens show a thickness loss. This effect is typical for nonwovens after a loading cycle as fiber friction points are reoriented. Horizontally-oriented nonwovens, in contrast, decompress fully. The vibration amplitude of the internal vibrator probably acts as a radial shear force on horizontal nonwovens and loosens fiber friction points. As the nonwoven pore volume increases with decompression, its w/s ratio changes with nonwoven compression.

The compression cycle is accompanied by filtration processes filling the nonwoven pores, observed in filtration tests and video recordings through transparent acrylic glass formworks. After the concrete is poured, excess water is filtrated from the fresh concrete, comparable to CPF. It fills the nonwoven pores within minutes and can move freely in the nonwoven pore structure. Simultaneously, a limited amount of fine solids enter the nonwoven. Coarser particles remain on top of the nonwoven, forming solid bridges and finally a filter cake that determines further solid separation. Finally, the w/s ratio in the nonwoven is above the w/c ratio of the fresh concrete, leading to high capillary porosity and a water-permeable bond. Upon vibration compaction, the filter cake is loosened, more solids enter the nonwoven, and water is displaced, reducing the w/s ratio and the porosity of the cement paste within the nonwoven. However, the solid separation rate and particle size decrease with continued compaction as the filter cake and nonwoven are increasingly clogged. The final w/s ratio in the nonwoven is lower for small nonwoven pore volumes, high fresh concrete spreads, and high compaction energies in the vicinity of the nonwoven.

The bond strength develops proportionally to the concrete tensile splitting strength at a factor of 0.18-0.58, measured in pull-off and concrete tensile splitting tests. It is achieved by embedding the concrete-facing nonwoven fibers in the cement matrix and thus is mainly influenced by the cement matrix strength in the bonding zone. The cement strength, in turn, is affected by the nonwoven basis weight, as it controls the separable amount of excess water that deteriorates the cement strength.

6 Recommendations for practice

Based on the results of this thesis, the following practice recommendations can be given:

Nonwovens: Nonwovens with low pore volumes and low basis weights are advantageous for pre-applied membranes as they separate less excess water from the fresh concrete. The excess water would otherwise deteriorate the properties of the cement paste in the bonding zone resulting in higher capillary porosity and lower tensile strength. Surface texture may have a secondary influence on the bond strength but needs further investigation.

Fresh concrete: Fresh concrete mixtures with a higher spread separate more solids into the nonwoven, allowing a waterproof bond to be achieved more quickly. A higher fresh concrete spread is linked to a reduced yield point and shear resistance [121,122], presumably leading to a reduced filtration resistance. Hence, the recommendation from [12] is still valid to use fresh concrete mixtures with a spread of at least 420 mm following the flow table test in DIN EN 12350-5 [119]. In contrast, higher fresh concrete loads do not separate more solids but rather filtrate excess water more quickly. Also, fresh concrete mixtures with a high tensile splitting strength lead to high nonwoven bond strength, e.g., with low w/c ratios and high cement strength.

Vibration compaction: The solids separation into the nonwoven is limited by a filter cake. However, vibration compaction loosens the filter cake, allowing more solids to enter the nonwoven. A few seconds of vibration compaction close to the nonwoven is recommended. Longer compaction times are required for nonwovens with a higher pore volume, smaller internal vibrators, and greater distances to the nonwoven.

Filtrated excess water accumulates in areas of uncompacted fresh concrete, so vibration compaction should be done as soon as possible and carefully in the corner and base areas of formworks. Also, the spacing between compaction points should be relatively small and not exceed ten times the diameter of the internal vibrator. Otherwise, the w/s ratio in the nonwoven is rising with increasing distances to the internal vibrator.

Time of stripping: The time of stripping depends on the bond strength and the forces acting, e.g., at fasteners. The bond strength develops proportionally to the concrete tensile splitting strength at 18-56 % for practice-oriented normal concretes. It varies for vertically-oriented nonwovens between -25 % to +35 % of the reference values due to vertical water movements and air voids. Thus, the bond strength can be estimated using the equation for concrete tensile splitting strength and a nonwoven-specific coefficient, as seen in Fig. 24 (p. 33) and Fig. 28-a (p. 35).

For the formulation of times of stripping, stripping forces must be known, but have been little investigated so far. Thus, the recommendation of *Heinlein et al.* [17] remains valid. Pre-applied membranes should remain in the formwork for two days in good weather conditions ($T \geq 20$ °C) and cement types with medium or rapid strength development. At lower temperatures or with cement types with low early strength, the stripping time should be extended, e.g., to four days. The stripping time can be estimated based on the concrete strength development according to the *fib* model code approach and the concrete maturity using Equations 10 and 12 (p. 18).

7 Perspectives

An important contribution to understanding the mechanisms of nonwoven bonded membranes is the variable w/s ratio, influenced by filtrated excess water and water movements in the nonwovens. However, it was not possible to determine the maximum w/s ratio up to which the nonwovens are waterproof. In order to identify maximum w/s ratios, nonwovens can separately be filled with a defined cement paste to ensure uniform cement paste properties and be tested

for their permeability, e.g., in hydrostatic tests. Furthermore, the w/s ratio in a nonwoven is most likely not uniform and, e.g., shows a gradient over the nonwoven height. It can be indirectly determined via the cement paste pore structure, e.g. via mercury intrusion porosimetry. Also, backscattered SEM images of polished microsections can be analyzed, as known for investigating the interfacial transition zone (see, e.g., [135]).

The waterproof bond of pre-applied membranes is usually analyzed in hydrostatic tests performed at the point of concrete pouring and compaction. However, this thesis showed varying w/s ratios depending on the distance to the point of concrete placement. Previous test results are thus not applicable for all nonwoven areas and most likely overestimate the waterproof bond at specimen edges. In order to identify the influence of the test position, hydrostatic tests should be carried out across larger samples.

Nonwovens with low pore volume and low basis weights are advantageous for pre-applied bonded membranes in terms of the waterproof bond and the bond strengths, as they separate less excess water from the fresh concrete. In order to use low pore volume and thus thin nonwovens on the construction site, their resistance to on-site stresses must be further tested, e.g., against abrasion and cleaning. The abrasion resistance can be tested following existing standards, which are given for textiles in ISO 12947-2 [136] and geosynthetics in ISO 13427 [137]. In both standards, the materials are moved with pressure on a substrate, and their integrity is inspected at intervals. A procedure for testing cleanability was published in 2023 in the leaflet "Frischbetonverbundsysteme" of the "Deutscher Beton- und Bautechnikverein E.V." (DBV) [138]. The bonding layer is contaminated by clays and cement paste, gently cleaned with high-pressure water jets, used for concrete composite specimens, and tested for the waterproof bond following DIN EN 12390-8. After cleaning, the waterproof bond must not be significantly deteriorated compared to an uncontaminated reference.

The work presented here can be regarded as fundamental laboratory work on nonwovens of pre-applied membranes, whose results must be verified on construction sites and extended to include the influences of soiling and weather. The tests carried out in this thesis should be repeated at different temperatures and with wet and soiled nonwovens. The bond strengths should also be tested using standard formworks, and acting forces during stripping have to be determined. Furthermore, the experimental limitations of the tests listed in the own papers in Chapters 9.2-9.4 should be considered.

8 References

- [1] Henshell J. The Manual of Below-Grade Waterproofing Systems. 1st Edition: Wiley & Sons, Inc; 2000.
- [2] Bonk M. Aufgabe von Bauwerksabdichtungen. In: Lufsky K, editor. Bauwerksabdichtung. 7. Auflage, Wiesbaden: Vieweg+Teubner Verlag / GWV Fachverlage GmbH, Wiesbaden; 2009, p. 1–4.
- [3] Lufsky K (ed.). Bauwerksabdichtung. 7. Auflage, Wiesbaden: Vieweg+Teubner Verlag / GWV Fachverlage GmbH, Wiesbaden; 2009.
- [4] BS 8102:2009-11-30, Code of practice for protection of below ground structures against water from the ground. British Standards Institution, London.
- [5] Henshell J. The Manual of Below-Grade Waterproofing. 2nd Edition. New York.: Routledge; 2016.
- [6] National Roofing Contractors Association. The NRCA Roofing and Waterproofing Manual. 5th ed. Rosemont; 2006.
- [7] Barlett K, Jenkins R (1994) Waterproofing Membrane (US 5,316,848). United States Patent. <https://depatisnet.dpma.de/DepatisNet/depatisnet?action=pdf&docid=US000005316848A>.
- [8] Wolf R, Gebhards G (1997) Tiefbauabdichtungen (DE 196 11 297 A1) Deutsches Patentamt. <https://depatisnet.dpma.de/DepatisNet/depatisnet?action=pdf&docid=DE000019611297A1>.
- [9] White A (1992) Water-barrier of water-swellable clay sandwiched between interconnected layers of flexible fabric needled together using a lubricant (US 5,174,231) United States Patent. <https://depatisnet.dpma.de/DepatisNet/depatisnet?action=pdf&docid=US000005174231A>.
- [10] Barlett et al. (1996) Waterproofing Membrane (US 5,496,615) United States Patent. <https://depatisnet.dpma.de/DepatisNet/depatisnet?action=pdf&docid=US000005496615A>.
- [11] Kloster M. Bauen im Bestand mittels Frischbetonverbundsystem. Abdichtung – neuer Weg zur Sanierung eines Kühlturms. Beton- und Stahlbetonbau 2006;101(12):1006–9. <https://doi.org/10.1002/best.200608191>.
- [12] Deutscher Beton- und Bautechnik-Verein E.V. DBV-Heft 44 Frischbetonverbundsysteme (FBV-Systeme) - Sachstand und Handlungsempfehlungen. Fassung Oktober 2018. Eigenverlag DBV; 2018.
- [13] Bloch M, Zitzelsberger T. WU-Konstruktionen mit Frischbetonverbundsystem. In: Fouad NA, editor. Bauphysik Kalender 2018: Feuchteschutz und Bauwerksabdichtung. Berlin, Germany: Ernst & Sohn; 2018, p. 285–308.
- [14] Freimann T, Heinlein U. Planung und Anwendung der Frischbetonverbundsysteme bei wasserundurchlässigen Baukonstruktionen aus Beton. In: Bergmeister K, Fingerloos F, Wörner J-D, editors. Beton-Kalender 2018: Bautenschutz, Brandschutz. Berlin, Germany: Ernst & Sohn a Wiley brand; 2018, p. 227–258.
- [15] Meyer L, Bilgin S, Filusch S, Freimann T, Heinlein U, Herrmann K. Bauwerksabdichtung mit Frischbetonverbundfolie - Grundlagen zur Erstellung eines Regelwerks für eine innovative Bauart: Abschlussbericht F 3183. Stuttgart: Fraunhofer IRB Verlag; 2020.
- [16] Freimann T, Heinlein U. Frischbetonverbundtechnologie. Beton- und Stahlbetonbau 2018;113(5):368–84. <https://doi.org/10.1002/best.201700098>.

- [17] Heinlein U, Freimann T, Bilgin S, Filusch S, Meyer L, Herrmann K. Frischbetonverbundsysteme – Neue Erkenntnisse aus Forschung und Praxis. Beton- und Stahlbetonbau 2020. <https://doi.org/10.1002/best.202000031>.
- [18] Haack A, Kessler D. Abdichtungen bei unterirdischen Bauwerken unter Berücksichtigung neuer Normen. In: Bergmeister K, Fingerloos F, Wörner J-D, editors. Beton Kalender 2019. Wiley; 2018, p. 795–861.
- [19] Kubal MT. Construction waterproofing handbook. 2nd ed. New York: McGraw-Hill; 2008.
- [20] Buccellato P, Henshell J. Recent Developments in Below-Grade and Plaza Waterproofing Systems: 31st RCI International Convention and trade show 2016:153–62.
- [21] Soprema AG. Frischbetonverbund-Abdichtungsbahn Colphene BSW. [October 04, 2022]; Available from: <https://www.soprema.ch/de/product/ingenieurbau/bauten-unter-terrain/bituminoese-systeme/abdichtungen/colphene-bsw-unilay-hp>.
- [22] Kogel A (2014) Verwendung eines Dichtungselements zur Bauwerksabdichtung (EP 2 665 791 BW) Europäische Patentschrift. <https://depatisnet.dpma.de/DepatisNet/depatisnet?action=pdf&docid=EP000002665791B1>.
- [23] Friedrich S. Chapter 3, Superabsorbent Polymers (SAP). In: Mechtcherine V, Reinhardt H-W, editors. Application of Super Absorbent Polymers (SAP) in Concrete Construction: State-of-the-Art Report Prepared by Technical Committee 225-SAP. 1st Edition. Springer Netherlands; 2012, p. 13–19.
- [24] Cogliano J (1991) Waterproofing Membrane (US 4,994,328) United States Patent. <https://depatisnet.dpma.de/DepatisNet/depatisnet?action=pdf&docid=US000004994328A>.
- [25] Wiercinski et al. (2012) Waterproofing Membrane (WO 2013/063197 A1) World Intellectual Property Organization. <https://depatisnet.dpma.de/DepatisNet/depatisnet?action=pdf&docid=WO002013063197A1>.
- [26] Wiercinski R, Ranganathan A (2012) Waterproofing Membrane (WO 2012/092019 A1) World Intellectual Property Organization. <https://depatisnet.dpma.de/DepatisNet/depatisnet?action=pdf&docid=WO002012092019A1>.
- [27] Roland Wolf GmbH. Broschüre FBV-Abdichtungssysteme. [October 04, 2022]; Available from: https://www.wolfseal.de/de/downloads/fbv-thepro-schottwand/fbv_abdichtungssysteme_roland_wolf_gmbh.pdf.
- [28] Feldmeier J, Gürster H (2015) Flächenabdichtelement für Baukörper (DE 10 2014 107 423 A1) Deutsches Patent- und Markenamt. <https://depatisnet.dpma.de/DepatisNet/depatisnet?action=pdf&docid=DE102014107423A1>.
- [29] Feldmeier J, Weißenbach N (2017) Flächenabdichtelement für Baukörper (DE 10 2015 120 401 A1) Deutsches Patent- und Markenamt. <https://depatisnet.dpma.de/DepatisNet/depatisnet?action=pdf&docid=DE102015120401A1>.
- [30] ASTM D7832/D7832M-14: Standard Guide for Performance Attributes of Waterproofing Membranes Applied to Below-Grade Walls / Vertical Surfaces (Enclosing Interior Spaces). West Conshohocken, PA: American Society for Testing and Materials.
- [31] Regulation (EU) No 305/2011 of the European Parliament and of the Council. Official Journal of the European Union 2011.
- [32] DIN EN 13967. Abdichtungsbahnen - Kunststoff- und Elastomerbahnen für die Bauwerksabdichtung gegen Bodenfeuchte und Wasser - Definition und Eigenschaften; Deutsche Fassung EN 13967:2012 + A1:2017. Berlin: Beuth Verlag GmbH.
- [33] DIN EN 13969. Abdichtungsbahnen - Bitumenbahnen für die Bauwerksabdichtung gegen Bodenfeuchte und Wasser - Definition und Eigenschaften; Deutsche Fassung EN 13969:2004 + A1:2006. Berlin: Beuth Verlag GmbH.

- [34] European Assessment Document EAD 030378-00-0605. Fully Bonded, Pre-applied Flexible Sheet for Waterproofing. May 2018: European Organisation for Technical Assessment.
- [35] DIN EN 12390-8. Prüfung von Festbeton - Teil 8: Wassereindringtiefe unter Druck; Deutsche Fassung EN 12390-8:2019. Berlin: Beuth Verlag GmbH.
- [36] ASTM D5385-93. Standard Test Method for Hydrostatic Pressure Resistance of Waterproofing Membranes. American Society for Testing and Materials.
- [37] DIN EN 1542:1999-07, Produkte und Systeme für den Schutz und die Instandsetzung von Betontragwerken - Prüfverfahren - Messung der Haftfestigkeit im Abreiversuch; Deutsche Fassung EN 1542:1999. Berlin: Beuth Verlag GmbH.
<https://doi.org/10.31030/8086119>.
- [38] Leslie D, Carter J JR. The Physics Behind Lessons Learned in a Full-Size Blindside Mock-Up. 2019 IIBEC Building Enclosure Symposium:87–104.
- [39] Schreiber P. Frischbetonverbundtechnologie - Vergleichende Untersuchungen zum Einfluss des Betonalters auf die Haftspannung in der Grenzschicht von vertikal applizierten FBV-Systemen. Unpublished Master Thesis at the Nuremberg Institute of Technology, Germany. 2019.
- [40] Wilson A. Development of the nonwovens industry. In: Russell SJ, editor. Handbook of nonwovens. Boca Raton: CRC; Woodhead publishing limited; 2007, p. 1–15.
- [41] Mao N, Russell SJ. Characterisation, testing and modelling of nonwoven fabrics. In: Russell SJ, editor. Handbook of nonwovens. Boca Raton: CRC; Woodhead publishing limited; 2007, p. 401–514.
- [42] DIN EN ISO 9092:2019-08, Vliesstoffe - Wrterbuch (ISO 9092:2019); Deutsche Fassung EN ISO 9092:2019. Berlin: Beuth Verlag GmbH. <https://doi.org/10.31030/3030558>.
- [43] Russell SJ (ed.). Handbook of nonwovens. Boca Raton: CRC; Woodhead publishing limited; 2007.
- [44] Fuchs H, Albrecht W. Vliesstoffe: Rohstoffe, Herstellung, Anwendung, Eigenschaften, Prfung. 2nd ed. Weinheim: Wiley-VCH; 2012.
- [45] Pietsch K, Fuchs H. Vliesstoffhalbzeuge und Vliesbildungstechniken. In: Cherif C, editor. Textile Werkstoffe fr den Leichtbau: Techniken - Verfahren - Materialien - Eigenschaften. Berlin, Heidelberg: Springer-Verlag Berlin Heidelberg; 2011, p. 327–366.
- [46] van Wyk CM. 20—Note on the Compressibility of Wool. *Journal of the Textile Institute Transactions* 1946;37(12):T285-T292. <https://doi.org/10.1080/19447024608659279>.
- [47] Kothari VK, Das A. An approach to the theory of compression of nonwoven fabrics. *Indian Journal of Fibre & Textile Research* 1996(21):235–43.
- [48] Kothari VK, Das A. The Compressional Behaviour of Spunbonded Nonwoven Fabrics. *The Journal of The Textile Institute* 1993;84(1):16–30.
<https://doi.org/10.1080/00405009308631243>.
- [49] Dunlop JI. On the Compression Characteristics of Fibre Masses. *The Journal of The Textile Institute* 1983;74(2):92–7. <https://doi.org/10.1080/00405008308631770>.
- [50] Carnaby GA, Pan N. Theory of the Compression Hysteresis of Fibrous Assemblies. *Textile Research Journal* 1989;59(5):275–84. <https://doi.org/10.1177/004051758905900505>.
- [51] Asanovic KA, Kostic MM, Mihailovic TV, Cerovic DD. Compression and strength behaviour of viscose/polypropylene nonwoven fabrics. *Indian Journal of Fibre & Textile Research* 2019(44):329–37.
- [52] Sengupta S, Ray P, Majumdar PK. Effect of dynamic loading on jute-based needle-punched nonwoven fabrics. *Indian Journal of Fibre & Textile Research* 2005;30:389–95.

- [53] Jafari S, Ghane M. An analytical approach for the recovery behavior of cut pile carpet after static loading by mechanical models. *Fibers Polym* 2016;17(4):651–5. <https://doi.org/10.1007/s12221-016-6191-7>.
- [54] Kothari VK, Das A. Compressional Behaviour of Nonwoven Geotextiles. *Geotextiles and Geomembranes* 1992(11):235–53.
- [55] Das A, Alagirusamy R, Banerjee B. Study on needle-punched non-woven fabrics made from shrinkable and non-shrinkable acrylic blends. Part II: transmission behaviour. *The Journal of The Textile Institute* 2009;100(4):350–7. <https://doi.org/10.1080/00405000701819691>.
- [56] Hutten IM. *Handbook of nonwoven filter media*. Kidlington, Oxford, Waltham, MA: Butterworth Heinemann an imprint of Elsevier Ltd; 2016.
- [57] Mukhopadhyay A. Composite nonwovens in filters: theory. In: *Composite Non-Woven Materials*. Elsevier; 2014, p. 120–163.
- [58] Stieß M. *Mechanische Verfahrenstechnik - Partikeltechnologie 1*. 3rd ed. Springer; 2009.
- [59] Zobel S, Gries T. The use of nonwovens as filtration materials. In: Chapman R, editor. *Applications of Nonwovens in Technical Textiles*. Elsevier; 2010, p. 160–183.
- [60] Gösele W, Leibnitz R, Oechsle D, Pongratz E, Tichy JW. Kapitel 8 Filterapparate. In: Luckert K, editor. *Handbuch der mechanischen Fest-Flüssig-Trennung*, 1st ed. Essen: Vulkan-Verlag; 2016, p. 143–268.
- [61] Hardman E. Textiles in filtration. In: Horrocks AR, Anand S, editors. *Handbook of technical textiles*. Boca Raton, FL: CRC Press/Woodhead Pub; 2000, p. 316–357.
- [62] Rankilor P. Textiles in civil engineering. Part 1 - geotextiles. In: Horrocks AR, Anand S, editors. *Handbook of technical textiles*. Boca Raton, FL: CRC Press/Woodhead Pub; 2000, p. 358–371.
- [63] Verein Deutscher Ingenieure. VDI 2762-1 - Mechanical solid-liquid-separation by cake filtration - Overview; 2006.
- [64] Vallabh R. *Modeling Tortuosity in Fibrous Porous Media using Computational Fluid Dynamics*. Dissertation at the North Carolina State University; 2009.
- [65] Dixit P, Ishtiaque SM, Roy R. Influence of sequential punching in layered structure of needle punched nonwoven on the filtration behavior. *Composites Part B: Engineering* 2020;182:107654. <https://doi.org/10.1016/j.compositesb.2019.107654>.
- [66] Soltani P, Johari MS, Zarrebini M. Tomography-based determination of transverse permeability in fibrous porous media. *Journal of Industrial Textiles* 2015;44(5):738–56. <https://doi.org/10.1177/1528083713512357>.
- [67] Ventura H, Ardanuy M, Capdevila X, Cano F, Tornero JA. Effects of needling parameters on some structural and physico-mechanical properties of needle-punched nonwovens. *The Journal of The Textile Institute* 2014;105(10):1065–75. <https://doi.org/10.1080/00405000.2013.874628>.
- [68] Berkalp OB. Air Permeability & Porosity in Spun-laced Fabrics. *Fibres & Textiles in Eastern Europe* 2006;14(3):81–5.
- [69] Rawal A. A cross-plane permeability model for needle-punched nonwoven structures. *The Journal of The Textile Institute* 2006;97(6):527–32. <https://doi.org/10.1533/joti.2005.0219>.
- [70] Hwang G-S, Hwu B-L, Hsing W-H, Lu C-K. Manufacturing effects on the hydraulic properties of needlepunched nonwoven geotextiles. *Geotextiles and Geomembranes* 1998(16):355–63.
- [71] Roy R, Ishtiaque SM. Effect of fibre orientation on mechanical and functional properties of needle-punched nonwoven. *Indian Journal of Fibre & Textile Research* 2019;44:321–8.

- [72] DIN EN ISO 10318-1:2018-10, Geokunststoffe - Teil 1: Begriffe (ISO 10318-1:2015 + Amd 1:2018); Dreisprachige Fassung EN ISO 10318-1:2015 + A1:2018. Berlin: Beuth Verlag GmbH. <https://doi.org/10.31030/2838687>.
- [73] Barrett RJ. Use of plastic filters in coastal structures. 10th Conference on Coastal Engineering, Tokyo, Japan 1966:3-22.
- [74] Christopher BR, Fischer GR. Geotextile filtration principles, practices and problems. *Geotextiles and Geomembranes* 1992;11(4-6):337–53. [https://doi.org/10.1016/0266-1144\(92\)90018-6](https://doi.org/10.1016/0266-1144(92)90018-6).
- [75] Liao K, Bhatia S. Geotextile tube: Filtration performance of woven geotextile under pressure. *Proceedings of NAGS* 2005:1–15.
- [76] Bundesanstalt für Wasserbau. Merkblatt Anwendung von geotextilen Filtern an Wasserstraßen (MAG). Karlsruhe: Bundesanstalt für Wasserbau (BAW-Merkblätter, -Empfehlungen und -Richtlinien). Eigenverlag Bundesanstalt für Wasserbau; 1993.
- [77] Luettich SM, Giroud JP, Bachus RC. Geotextile filter design guide. *Geotextiles and Geomembranes* 1992;11(4-6):355–70. [https://doi.org/10.1016/0266-1144\(92\)90019-7](https://doi.org/10.1016/0266-1144(92)90019-7).
- [78] Muthukumar A, Ilamparuthi K. Laboratory studies on geotextile filters as used in geotextile tube dewatering. *Geotextiles and Geomembranes* 2006;24(4):210–9. <https://doi.org/10.1016/j.geotexmem.2006.03.002>.
- [79] Bhatia SK, Smith JL. Geotextile Characterization and Pore-Size Distribution: Part I. A Review of Manufacturing Processes. *Geosynthetics International* 1996;3(1):85–105. <https://doi.org/10.1680/gein.3.0055>.
- [80] ASTM D1434-1982, Test Method for Determining Gas Permeability Characteristics of Plastic Film and Sheeting: American Society for Testing and Materials. <https://doi.org/10.1520/D1434-82R15E01>.
- [81] Cazzuffi D, Mandaglio MC, Moraci N. Hydraulic properties, behavior, and testing of geotextiles. *Geotextiles* 2016:151–76.
- [82] Palmeira EM, Trejos Galvis HL. Opening sizes and filtration behaviour of nonwoven geotextiles under confined and partial clogging conditions. *Geosynthetics International* 2017;24(2):125–38. <https://doi.org/10.1680/jgein.16.00021>.
- [83] Gardoni MG, Palmeira EM. Microstructure and pore characteristics of synthetic filters under confinement. *Géotechnique* 2002;52(6):405–18. <https://doi.org/10.1680/geot.2002.52.6.405>.
- [84] Koerner RM, Koerner GR. Lessons learned from geotextile filter failures under challenging field conditions. *Geotextiles and Geomembranes* 2015;43(3):272–81. <https://doi.org/10.1016/j.geotexmem.2015.01.004>.
- [85] Bourgès-Gastaud S, Stoltz G, Sidjui F, Touze-Foltz N. Nonwoven geotextiles to filter clayey sludge: An experimental study. *Geotextiles and Geomembranes* 2014;42(3):214–23. <https://doi.org/10.1016/j.geotexmem.2014.03.002>.
- [86] Wilke M, Hangen H. Geotextile Container und Schläuche zur Entwässerung von Schlämmen: Funktionsprinzip - Abdichtungsmaßnahmen - Anwendungsmöglichkeiten. 27. Fachtagung 'Die sichere Deponie 2011 - Abdichtung von Deponien und Altlasten mit Kunststoffen'.
- [87] Stoltz G, Delmas P, Barral C. Comparison of the behaviour of various geotextiles used in the filtration of clayey sludge: An experimental study. *Geotextiles and Geomembranes* 2019;47(2):230–42. <https://doi.org/10.1016/j.geotexmem.2018.12.008>.
- [88] Narejo DB, Koerner RM. A dynamic filtration test for geotextile filters. *Geotextiles and Geomembranes* 1992;11(4-6):395–400. [https://doi.org/10.1016/0266-1144\(92\)90021-2](https://doi.org/10.1016/0266-1144(92)90021-2).

- [89] Hong Y-S, Wu C-S. Filtration behaviour of soil-nonwoven geotextile combinations subjected to various loads. *Geotextiles and Geomembranes* 2011;29(2):102–15. <https://doi.org/10.1016/j.geotexmem.2010.10.010>.
- [90] Price WF. *Controlled permeability formwork*. London: CIRIA; 2000.
- [91] Yang ZQ, Liu JZ, Lin W, Liu JP, Xu DG. Review of Progress and Applications of Controlled Permeability Formwork in Concrete Engineering. *Advanced Materials Research* 2013;821-822:171–8. <https://doi.org/10.4028/www.scientific.net/AMR.821-822.171>.
- [92] Schubel PJ, Warrior NA, Elliott KS, Jones M. An Investigation into the critical factors affecting the performance of composite controlled permeable formwork liners: Part I – Drainage medium. *Construction and Building Materials* 2008;22(7):1551–9. <https://doi.org/10.1016/j.conbuildmat.2007.03.030>.
- [93] Schubel PJ, Warrior NA, Elliott KS. An investigation into factors affecting the performance of composite controlled permeable formwork liners: Part II – Filter medium. *Construction and Building Materials* 2008;22(11):2235–49. <https://doi.org/10.1016/j.conbuildmat.2007.08.006>.
- [94] Figueiras H, Nunes S, Coutinho JS, Figueiras J. Combined effect of two sustainable technologies: Self-compacting concrete (SCC) and controlled permeability formwork (CPF). *Construction and Building Materials* 2009(23):2518–26. <https://doi.org/10.1016/j.conbuildmat.2009.02.035>.
- [95] Serafini F (1998) Concrete Form Liner (US 5,824,347) United States Patent. <https://depatisnet.dpma.de/DepatisNet/depatisnet?action=pdf&doid=US000005824347A>.
- [96] Beddoe R. The effect of formwork linings on surface concrete. In: 28th Research Colloquium DAfStb. Technische Universität München 1993.
- [97] Kothandaraman S, Kandasamy S, Sivaraman K. The effect of controlled permeable formwork liner on the mechanical and durability properties of self compacting concrete. *Construction and Building Materials* 2016(118):319–26. <https://doi.org/10.1016/j.conbuildmat.2016.05.083>.
- [98] Basheer L, Nanukuttan SV, Basheer PAM. The influence of reusing ‘Formtex’ controlled permeability formwork on strength and durability of concrete. *Mater Struct* 2008;41(8):1363–75. <https://doi.org/10.1617/s11527-007-9335-9>.
- [99] DIN EN 1849-2:2019-09, Abdichtungsbahnen - Bestimmung der Dicke und der flächenbezogenen Masse - Teil 2: Kunststoff- und Elastomerbahnen für Dachabdichtungen; Deutsche Fassung EN 1849-2:2019. Berlin: Beuth Verlag GmbH. <https://doi.org/10.31030/3042454>.
- [100] Debnath S, Madhusoothanan M. Compression Properties of Polyester Needle-punched Fabric. *Journal of Engineered Fibers and Fabrics* 2009;4(4). <https://doi.org/10.1177/155892500900400404>.
- [101] Kothari VK, Das A. Compressional behaviour of layered needle-punched nonwoven geotextiles. *Geotextiles and Geomembranes* 1993;12(2):179–91. [https://doi.org/10.1016/0266-1144\(93\)90005-9](https://doi.org/10.1016/0266-1144(93)90005-9).
- [102] Preibisch S, Saalfeld S, Tomancak P. Globally optimal stitching of tiled 3D microscopic image acquisitions. *Bioinformatics* 2009;25(11):1463–5. <https://doi.org/10.1093/bioinformatics/btp184>.
- [103] Ali MA, Umer R, Khan KA, Cantwell WJ. Application of X-ray computed tomography for the virtual permeability prediction of fiber reinforcements for liquid composite molding processes: A review. *Composites Science and Technology* 2019;184:107828. <https://doi.org/10.1016/j.compscitech.2019.107828>.

- [104] Du Plessis A, Boshoff WP. A review of X-ray computed tomography of concrete and asphalt construction materials. *Construction and Building Materials* 2019;199:637–51. <https://doi.org/10.1016/j.conbuildmat.2018.12.049>.
- [105] Qin Y, Wu H, Zheng Y, Wang W, Yi Z. Microscopic Texture of Polypropylene Fiber-Reinforced Concrete with X-Ray Computed Tomography. *Advances in Civil Engineering* 2019;2019:1–9. <https://doi.org/10.1155/2019/2386590>.
- [106] El Zein AR, Vanhove Y, Djelal C, Madec O, Gotteland P. Evaluation of internal bleeding in concrete foundation from the Terzaghi's effective stress postulate. *Materials and Structures* 2021;54(6). <https://doi.org/10.1617/s11527-021-01828-1>.
- [107] Djelal C, Vanhove Y, Azzi A, Madec O. Recommendation for concrete mix design to prevent bleed channels on diaphragm walls. *European Journal of Environmental and Civil Engineering* 2022;26(4):1402–14. <https://doi.org/10.1080/19648189.2020.1713900>.
- [108] ÖVBB-Merkblatt "Weiche Betone". Österreichische Vereinigung für Beton und Bautechnik. 2009.
- [109] DIN EN 1097-7:2008-06, Prüfverfahren für mechanische und physikalische Eigenschaften von Gesteinskörnungen - Teil 7: Bestimmung der Rohdichte von Füller - Pycnometer-Verfahren; Deutsche Fassung EN 1097-7:2008. Berlin: Beuth Verlag GmbH. <https://doi.org/10.31030/1426719>.
- [110] DIN EN ISO 13320:2020-01 Particle size analysis - Laser diffraction methods. 2020-01. Beuth.
- [111] DIN EN 12390-6:2010-09, Prüfung von Festbeton - Teil 6: Spaltzugfestigkeit von Probekörpern; Deutsche Fassung EN 12390-6:2009. Berlin: Beuth Verlag GmbH. <https://doi.org/10.31030/1709271>.
- [112] fib Model Code for Concrete Structures 2010. fédération internationale du béton / International Federation for Structural Concrete (fib). Berlin: Ernst & Sohn.
- [113] ISO 9073-1:1989-07 Textilien; Prüfverfahren für Vliesstoffe; Teil 1: Bestimmung der flächenbezogenen Masse. Berlin: Beuth Verlag GmbH.
- [114] DIN 65571-2:1992-11, Luft- und Raumfahrt; Verstärkungsfasern; Bestimmung des Filamentdurchmessers von Filamentgarnen; Längsprojektionsverfahren. Berlin: Beuth Verlag GmbH. <https://doi.org/10.31030/2538052>.
- [115] Bermüller & Co. GmbH. Bontec NW - Technical Datasheet. [October 04, 2022]; Available from: www.beco-bermueller.de/de/produkte/geokunststoffe-geotextilien-geobaustoffe/vliesstoffe/bontec-nw-vliesstoffe/.
- [116] Fibertex Nonwovens A/S. Product application guide, Geotextiles. [October 04, 2022]; Available from: <https://www.fibertex.com/sites/fibertex.com/files/2019-03/ProductKey.pdf>.
- [117] Kundt G, Krentz H, Glass Ä. *Epidemiologie und Medizinische Biometrie (Epidemiology and Medical Biometry)*. Aachen: Shaker Verlag; 2011. 246 p.
- [118] Locher FW. *Zement: Grundlagen der Herstellung und Verwendung*. Düsseldorf: Bau+Technik; 2000.
- [119] DIN EN 12350-5:2019-09, Prüfung von Frischbeton - Teil 5: Ausbreitmaß; Deutsche Fassung EN 12350-5:2019. Berlin: Beuth Verlag GmbH. <https://doi.org/10.31030/3045714>.
- [120] DIN EN ISO 12956:2020-05 Geotextilien und geotextilverwandte Produkte - Bestimmung der charakteristischen Öffnungsweite (ISO/DIS 12956:2018); Deutsche Fassung EN ISO 12956:2020. Berlin: Beuth Verlag GmbH.
- [121] Rickert J. Zeta-Potential und Rheologie von Zementleimen - Einfluss von Fließmitteln sowie Hüttensand und Kalkstein. *Betontechnische Berichte* 2010-2012. VDZ.

- [122] Spanka G, Grube H, Thielen G. Wirkungsmechanismen verflüssigender Betonzusatzmittel. *beton* 1995;45(11):802.
- [123] Luckert K (ed.). *Handbuch der mechanischen Fest-Flüssig-Trennung*. 1st ed. Essen: Vulkan-Verlag; 2016.
- [124] American Concrete Institute ACI Committee 309. Report on Behaviour of Fresh Concrete During Vibration. ACI 309. IR-08 2008.
- [125] Mehta PK, Monteiro P. *Concrete. Microstructure, Properties, and Materials*. 4th ed. McGraw-Hill; 2014.
- [126] RILEM REPORT 11. Interfacial Transition Zone in Concrete. State-of-the-Art Report prepared by RILEM Technical Committee 108-ICC, Interfaces in Cementitious Composites. Edited by J.C. Maso. E & FN Spon, London, 1996.
- [127] Patnaik PK, Swain PTR, Mishra SK, Purohit A, Biswas S. Recent developments on characterization of needle-punched nonwoven fabric reinforced polymer composites – A review. *Materials Today: Proceedings* 2020;26:466–70. <https://doi.org/10.1016/j.matpr.2019.12.086>.
- [128] Powers TC, Copeland LE, Hayes JC, Mann HM. Permeability of Portland Cement Paste. *Journal of the American Concrete Institute* 1954:285–98.
- [129] Ramezaniapour AA, Esmaeili M, Ghahari SA, Najafi MH. Laboratory study on the effect of polypropylene fiber on durability, and physical and mechanical characteristic of concrete for application in sleepers. *Construction and Building Materials* 2013;44:411–8. <https://doi.org/10.1016/j.conbuildmat.2013.02.076>.
- [130] Hannawi K, Bian H, Prince-Agbodjan W, Raghavan B. Effect of different types of fibers on the microstructure and the mechanical behavior of Ultra-High Performance Fiber-Reinforced Concretes. *Composites Part B: Engineering* 2016;86:214–20. <https://doi.org/10.1016/j.compositesb.2015.09.059>.
- [131] Monteiro P, Maso JC, Ollivier JP. The aggregate-mortar interface. *Cement and Concrete Research* 1985;15(6):953–8. [https://doi.org/10.1016/0008-8846\(85\)90084-5](https://doi.org/10.1016/0008-8846(85)90084-5).
- [132] Singh SB, Munjal P, Thammishetti N. Role of water/cement ratio on strength development of cement mortar. *Journal of Building Engineering* 2015;4:94–100. <https://doi.org/10.1016/j.jobbe.2015.09.003>.
- [133] Bonzel J, Dahms J. Der Einfluß des Zements, des Wasserzementwertes und der Lagerung auf die Festigkeitsentwicklung des Betons. *Betontechnische Berichte*;66:115–38.
- [134] Long JH, Paul SL. Bond Strength between Geotextiles and Concrete. *Geotextiles and Geomembranes* 1989;8:113–32.
- [135] Friedl L. Experimentelle Untersuchungen zum Transport von Wasser und Chlorid in rezykliertem Beton und zu der daraus ableitbaren Gefahr der chloridinduzierten Stahlkorrosion. Dissertation an der Technischen Universität München; 2003.
- [136] DIN EN ISO 12947-2:2017-03, Textilien - Bestimmung der Scheuerbeständigkeit von textilen Flächengebilden mit dem Martindale-Verfahren - Teil 2: Bestimmung der Probenzerstörung (ISO 12947-2:2016); Deutsche Fassung EN ISO 12947-2:2016. Berlin: Beuth Verlag GmbH. <https://doi.org/10.31030/2539223>.
- [137] DIN EN ISO 13427:2015-03, Geokunststoffe - Simulation von Scheuerbeschädigungen (Gleitblockprüfung) (ISO 13427:2014); Deutsche Fassung EN ISO 13427:2014. Berlin: Beuth Verlag GmbH. <https://doi.org/10.31030/2151674>.
- [138] Deutscher Beton- und Bautechnik-Verein E.V. DBV-Merkblatt Frischbetonverbundsysteme (publication expected in 2023).

9 Publications

9.1 Pre-applied bonded waterproofing membranes: A review of the history and state-of-the-art in Europe and North America

Reprint

Published in "Construction and Building Materials"

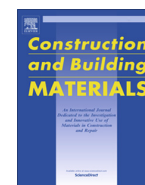
Volume 296, June 2021; DOI: 10.1016/j.conbuildmat.2021. 123751

Authors: U. Heinlein, K.-Ch. Thienel, T. Freimann



Contents lists available at ScienceDirect

Construction and Building Materials

journal homepage: www.elsevier.com/locate/conbuildmat

Review

Pre-applied bonded waterproofing membranes: A review of the history and state-of-the-art in Europe and North America

Ulli Heinlein^{a,*}, Karl-Christian Thienel^b, Thomas Freimann^a^a Technische Hochschule Nürnberg Georg Simon Ohm, Keßlerplatz 12, 90489 Nürnberg, Germany^b Universität der Bundeswehr München, Werner-Heisenberg-Weg 39, 85577 Neubiberg, Germany

HIGHLIGHTS

- Pre-applied bonded waterproofing membranes are reviewed.
- State-of-the-art properties, applications, and national regulations are presented.
- Latest investigations and further research needs are summarized.
- Insight into the history and the significance on the market is given.

ARTICLE INFO

Article history:

Received 7 December 2020

Received in revised form 29 April 2021

Accepted 2 May 2021

Available online 4 June 2021

Keywords:

Pre-applied waterproofing membranes

Bonded waterproofing membranes

Positive-side waterproofing membranes

Basement waterproofing

Blindside waterproofing

Waterproof concrete structure

ABSTRACT

Since the end of the 20th century, below-grade concrete structures can be waterproofed with sheet membranes in a pre-application process. The waterproofing membranes are installed before concrete placement, e.g., directly on a soil retention system and interact with the subsequently poured fresh concrete, thus forming an adhesive and waterproof bond. The market for this construction method is currently growing, which is why characteristics, mechanisms, and international regulations in place are reviewed. Moreover, the history of pre-applied bonded membranes is presented, based on a product and patent research. Also, recently conducted investigations and an outlook on further research needs is given.

© 2021 The Authors. Published by Elsevier Ltd. This is an open access article under the CC BY-NC-ND license (<http://creativecommons.org/licenses/by-nc-nd/4.0/>).

Contents

1. Introduction	2
2. Retrospective	3
3. State-of-the-art	3
3.1. Application and essential properties	3
3.2. Regulations	4
3.3. Testing procedures	4
4. Characteristics and investigations	5
4.1. Overview	5
4.2. Sealing layer	5
4.3. Bonding mechanisms	7
4.3.1. Overview	7
4.3.2. Characteristics of chemical bonding	7
4.3.3. Characteristics of mechanical bonding	7
4.3.4. Investigations on the bond	7
4.4. Installation	8

* Corresponding author at: Technische Hochschule Nürnberg Georg Simon Ohm, Keßlerplatz 12, 90489 Nürnberg, Germany.

E-mail address: ulli.heinlein@th-nuernberg.de (U. Heinlein).

5. Further research needs 9
 6. Summary 9
 Declaration of Competing Interest 9
 Acknowledgement 9
 References 9

1. Introduction

Basements must be damp- or waterproofed to protect the structure from deterioration and ensure that the interior is suitable for high-quality use [1]. If the basement is exposed to hydrostatic water pressure, it can be waterproofed by tanking, structural integral waterproofing, or partially by drainage measures. A suitable waterproofing concept should consider the construction requirements, such as the water pressure, the internal usage requirements, other boundary conditions, and the particular characteristics of the waterproofing method, and their curability.

Tanking applications use a continuous watertight layer in the form of sheet-membranes, bentonite clay, liquid-applied (urethanes, rubbers, etc.), or cementitious systems and are of particular interest when restraint stresses in the structure or chemicals in the embedding soil make integral waterproof concrete structures more challenging. Depending on the system, the planner must, e.g., consider the mode of action of the membrane and the quality of the seams. Depending on the material, the tanking is applied on the outside (positive-side) or the inside (negative-side) of the structure, with positive-side waterproofing having advantages for new construction in hydrostatic groundwater [2].

Positive-side waterproofing can further be distinguished into attached and non-attached systems, according to Henshell [3]. Attached (or bonded) systems are usually installed on concrete structures and achieve a bond to the substrate, e.g., with a pressure-sensitive adhesive. Compared to non-attached membranes, the bond prevents lateral water migrations between the barrier and the substrate, and thus water migrations to cracks in the concrete. Additionally, the bond secures the place of the barrier

during construction and use. This bond requires the withstanding of structural movements and a permanent bond of the membrane, whereas non-attached membranes have no constraint points with the structure.

Bonded systems can even further be distinguished according to their time of installation into pre- and post-applied systems. Pre-applied bonded systems are installed before the concrete works on a mud-slab, a soil retention system, or a formwork and later form a bond with the subsequently placed fresh concrete. They can be walked on in horizontal installations, and the concrete structure is built directly on them. These systems require special care on site since no additional protection layers are applied. Further concrete works on pre-applied membranes can lead to soiling and punctual damage, eventually affecting the bond or the waterproofing [4].

Pre-applied bonded membranes, hereafter also referred to as ‘membranes’, are currently experiencing market growth, even though the mechanisms and application limits are not yet fully understood. They usually have the form of prefabricated sheet-membranes and essentially comprise a sealing layer and a bonding mechanism and are joined by seams. The sealing layer must be a single-ply hydrostatic resistant waterproofing layer enabling crack-bridging and can be made of non-swellable and swellable materials. The bonding mechanism allows an adhesive and waterproof connection to the concrete surface and is achieved mechanically using nonwovens or chemically by means of synthetic adhesives or elastomer-modified bitumen. An additional non-sticky top-coat is applied on chemical bonding layers, enabling walking on the membranes in horizontal applications and replacing formerly used release papers (see Fig. 1). The membranes are

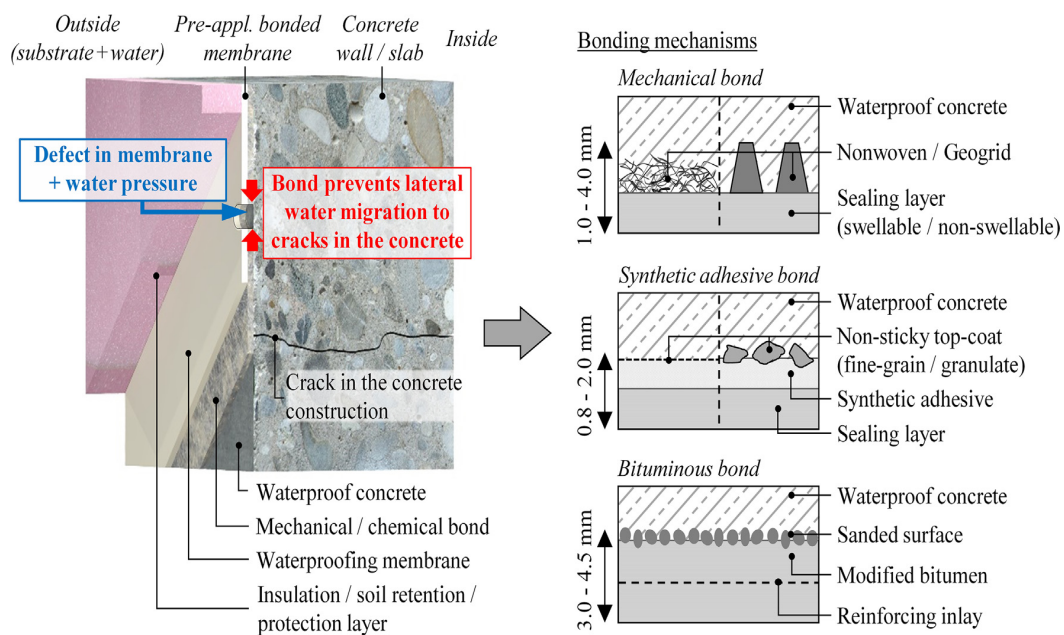


Fig. 1. Pre-applied bonded membranes prevent lateral water migrations due to a waterproof bond, which is achieved by different bonding mechanisms.

joined by various seams. As with all waterproofing membranes, they must be considered weak points and have to be waterproof, at least in contact with concrete.

Today, pre-applied bonded membranes are available from at least 35 manufacturers worldwide using several different bonding and sealing mechanisms. Due to the product variety and some particular features in the execution, the following article shall provide an international overview and give guidance for planning and execution. First, the article presents the historical background and the current regulations. Second, the characteristics and bonding mechanisms of nowadays used membranes based on a product, patent, and research review are shown. Finally, thus far known application limits and open questions are summarized.

2. Retrospective

Pre-applied bonded waterproofing membranes were first introduced to the U.S. market in the 1990s and required some development steps beforehand. An essential step was the technology to prefabricate waterproofing sheet-membranes, as it became possible from the end of the 19th century onwards [5]. Further efforts included developing synthetic membranes at the end of the 1930s [6], which were increasingly used in the waterproofing industry since the 1950s [7]. By the end of the 1960s, self-adhesive waterproofing membranes emerged, which were post-applied using cold-bonding modified bitumen [2,8]. These membranes could already be used as pre-applied bonded systems in vertical applications but did not yet provide walkability for horizontal installations. Swellable waterproofing materials in the form of bentonite clay came up in the U.S. in the 1930s and were initially used in loose layers [9]. In the 1960s, panels emerged with bentonite placed between two cardboards [10–12]. These could also be used as pre-applied systems but did not yet provide a bond to the structure.

The first attempts to achieve a bond between a pre-installed product and fresh concrete are dating back to the 1970s. In the U.S., Stokes pre-installed self-adhesive membranes in formworks to produce precast elements, using them as a reliable release agent and for surface design. The bond was achieved by a layer of polychloroprene (rubber elastomeric) [13]. Heyen described a similar attempt in 1980 in a patent. A tunnel waterproofing membrane with a synthetic adhesive layer on both sides was first attached to a shotcrete layer. Subsequently, the tunnel lining was cast directly on the inner adhesive layer [14].

Synthetic fibers, necessary for mechanically bonded membranes, were still little used in the construction industry at this time. For example, on the European construction market, synthetic fibers were limited to 1.1 Tt/a (thousand tons per annum) in 1978. In the following, the market grew quickly, so that by the start of the 1990s, around 97 Tt/a of fibers were used [15]. This increasing interest was also visible in the waterproofing industry. Various patents were filed at the end of the 1970s, including geotextiles or fibrous nonwovens as composite, protective, or drainage layers, especially in tunnel constructions. For example, for the New Austrian Tunneling Method (NATM), nonwovens were anchored on the mountain to act as a bonding and drainage layer for the subsequently installed polymeric waterproofing membrane [16–18]. Nonwovens were also used as bonding layers for shotcrete [19], in bathroom applications for fiber bonded waterproofing membranes [20], and as a bonding layer for pre-applied wall coverings [21].

Pre-applied bonded waterproofing membranes were finally introduced in the 1990s. Patents described, mostly for the U.S., pre-applied bonded membranes in the present understanding, e.g., by Cogliano, White, and Barlett [22–26]. For self-adhesive

membranes, a way was found to ensure they could be walked on in horizontal applications while avoiding release papers: Non-sticky top-coatings like water-soluble layers [27], granulates, or elastomeric acrylic-based coatings were applied on the adhesives. Also, nonwovens were used to achieve a mechanical bond between bentonite or polymeric membranes and concrete. Compared to formerly used geotextiles, the basis weights of nowadays used nonwovens are reduced to a maximum of 130 g/m². In comparison, geotextiles for protection and drainage usually have basis weights between 300 and 500 g/m² for basements [28,29] and up to 900 g/m² for tunnels [30]. The lower basis weight ensured a complete filling of the nonwovens with cement paste during concrete placement, thus forming a resistance against lateral water migration.

In the new millennium, the construction method gained importance, especially in North America. According to Henshell [2], this was due to the growing population and the construction boom in the cities. To maximize the use of building land, the membranes were used in blindside applications and therefore applied directly to a soil retention system. Subsequently, the construction method also gained a foothold in other countries. The first application in Germany was reported for 2005, but the membranes were used hesitantly initially. It was not until 2012, which is now described as the 'year of the breakthrough' that the market share increased significantly. Whereas around 100,000 m²/a of membranes were installed in Germany in 2012, the market grew to 450,000 m²/a by 2017 – and continues to grow today [31]. In Germany, the membranes are usually applied as an additional measure on waterproof concrete structures to improve the overall basement waterproofing [31,32].

The ongoing market growth is also reflected by the related manufactures, which grew in Germany from three present manufacturers in 2013 [33] to at least ten in 2019 [34]. Worldwide there are now at least 35 manufacturers, especially in Europe, North America, and China. The number of newly published patents also reflects the growing interest. In Europe and North America, more than 20 new patents for pre-applied bonded membranes were filed between 2010 and 2020 [35–58]. Furthermore, new standards and guidelines included pre-applied membranes, like the revised British code of practice for waterproofing BS 8102 in 2009 [59], contrary to the preceding version of 1990 [60]. In summary, market growth, the rising number of manufacturers, the number of filed patents, and the consideration in standards show an ever-increasing interest for pre-applied membranes both in Europe and North America in the last years.

3. State-of-the-art

3.1. Application and essential properties

Today, pre-applied bonded membranes are most often used as stand-alone positive-side waterproofing combined with concrete structures. They are applied under base slabs, in formworks and blindside applications. The advantages of pre-applied bonded systems are thereby as follows:

- The waterproof bond improves the redundancy of the tanking [59] and reduces the overall failure risk due to local defects. This allows the membranes to be embedded further down into hydrostatic water than non-attached systems with a comparable sealing layer [61]. The membranes are usually applied down to 20 m in groundwater (see, e.g. [62,63]).
- The bond secures the location of the membrane so that soil settlements or degradation in the soil cannot harm the sealing layer [2].

- In vertical applications, the properties of the final concrete surface do not influence the application procedure. In comparison to post-applied systems, preparation works on the concrete surface (primer, etc.) need not be considered.
- Protective layers or screeds between the membrane and the concrete structure do not have to be applied.

In order to achieve the above-listed features, pre-applied bonded membranes have to have the following properties [4,64]:

- Single-ply membrane - hydrostatic pressure resistant;
- Seams, to form a continuous waterproof layer;
- Adhesive bond, to secure the position during construction and use;
- Waterproof bond, to prevent leak water migrations;
- Bonding mechanism that allows walking on the membranes in horizontal applications and easy removing of soil and cement paste;
- Sufficient elongation to enable crack bridging;
- High mechanical resistance is beneficial since subsequent trades have to work on the membranes;
- Additional physical, chemical, and technological properties similar to non-attached barriers.

In comparison to other waterproofing concepts, also weak points have to be considered. Recent studies especially found seams and T-joints being weak spots since they were partly leaking even under low water pressure (see Chapter 4.4).

3.2. Regulations

If pre-applied membranes are regarded as primary waterproofing, they are considered in the same codes and guidelines as other positive-side waterproofing measures. For instance, polymer and bituminous waterproofing membranes are covered in the U.S. in ASTM D 7832 [65]. Further guidance and minimum requirements for general waterproofing systems are stated in national standards and are provided by various organizations. For the North American market, the following have to be named:

- In the U.S. and Canada, requirements for buildings are recommended in model codes on the national level, which must then be adopted and officially introduced by the jurisdiction at the state or provincial level. In the U.S., this is accomplished by the International Code Council (ICC) in the International Building Code (IBC) [66] in section 1807 and the International Residential Code (IRC) in section R406. In Canada, the National Research Council of Canada (NRC) [67] publishes the National Building Code of Canada (NBC), providing comments on waterproofing in Division B - section 9.13.3. For suitable materials, reference is made to American or Canadian testing standards.
- Testing and specification standards are provided in the U.S. by the ASTM in the subcommittee D08.22. In Canada, American regulations are partially adopted or otherwise formulated by the Canadian General Standards Board (CGSB).
- The National Roofing Contractors Association (NRCA) gives recommendations for basement waterproofing and even detail instructions for blindside applications in their "Roofing and Waterproofing Manual" [68].
- For public buildings in the U.S., minimum standards are listed in the "P.100 Facilities Standards" [69] from the Public Building Service (PBS).
- Furthermore, to facilitate communication in planning and execution, waterproofing membranes are listed in the MasterFormat of the Construction Specification Institute (CSI) in Division 07 (Thermal and Moisture Protection), in the

subdivisions 071300 (sheet waterproofing) and 071700 (ben-tonite waterproofing) [70].

If the waterproofing membranes shall be distributed within the European Union (EU) and the European Economic Area (EEA), the EU Construction Products Regulation (No. 305/2011) requires CE marking by a Declaration of Performance (DoP). The product properties have to be tested for groundwater barriers (Type T) following the harmonized European standards EN 13967 [71] for plastic and rubber membranes or EN 13969 [72] for bituminous membranes. If the product does not comply with the mentioned harmonized standards, a product declaration via a European Technical Assessment (ETA) based on the European Assessment Document EAD 030378-00-0605 [73] can be performed, resulting in CE marking. Also, national regulations and guidelines must be considered, such as BS 8102 in the UK or ÖNORM B 3664 [74] in Austria.

Besides the application as primary waterproofing, pre-applied membranes are also used as an additional measure on waterproof concrete structures to improve the basement's overall waterproofing and provide more redundancy. This combination of waterproofing systems is, for example, also considered in BS 8102 (Type A + B) and can achieve very high usage requirements in the basement, such as the Grade 3 waterproofing according to BS 8102:2009 (or Grade 4 according to BS 8102:1990) or the German utilization class A*** [75]. Besides that, pre-applied membranes can be used on waterproof concrete structures to waterproof cracks and to substitute crack injections.

In most countries, using a waterproofing barrier lowers the requirements for the concrete compared to a waterproof concrete structure. This can save concrete and reinforcing steel, and potentially improves sustainability. For example, in Austria, using a geosynthetic clay barrier can reduce the wall thickness and allows larger crack widths in the concrete [29,76]. Only in few countries like Germany, pre-applied membranes are not considered as stand-alone waterproofing since they often do not meet certain product requirements demanded by the German standard for waterproofing DIN 18533 [28] and the related product requirement standard DIN/TS 20000-202 [77]. They are usually used as an additional measure on waterproof concrete structures within an unregulated construction method.

3.3. Testing procedures

Current testing procedures for non-swellable pre-applied membranes in Europe and the U.S., which are stated within the ICS Code 91.100.50 (International Classification for Standards), are shown in Table 1. The tests listed for the U.S. are the commonly performed tests since no specific standards are applicable for pre-applied membranes. For Europe, the tests listed include the mandatory tests for CE marking according to the harmonized European standards and further German recommendations. Swellable materials are usually further tested for their swelling properties.

Also, the membranes can be used as protective layers against ground gases, such as radon [78,79] or chemicals in the soil [4]. Accordingly, they have to be tested on their radon permeability following ISO/TS 11665-12 /-13 [80] or their Methane gas permeability following ASTM D 1434 [81]. In some datasheets, reference is made to the Radon Diffusion Measurement Protocol from the Research Institute of Sweden (RISE) or the method K124/02/95 of the Czech Republic.

The listed tests are not explicitly designed for pre-applied bonded membranes and have the following weaknesses:

- In Europe, the harmonized standards do not include mandatory tests to characterize the bond.

Table 1
Comparison of the usual North American to European testing procedures for non-swellable pre-applied bonded waterproofing membranes.

Characteristic	North American procedures	European regulations and German recommendations
Resistance against water or water vapor	Resistance to hydrostatic pressure: ASTM D 5385 (≤ 6.9 bar); Water absorption: ASTM D 570; Water vapor transmission: ASTM E 96	Resistance to hydrostatic pressure: EN 1928 (4.0 bar*); Water vapor permeability: EN 1931; Seams: Resistance to hydrostatic pressure of T-joints*; Further tests on concrete specimen acc. to PG-FBB [86]*
Bond properties	Resistance to leak water migrations acc. to modified versions of ASTM D 5385 (up to 6.9 bar for 1 d); Peel-Strength test: ASTM D 903	Resistance to leak water migrations acc. to mod. versions of ASTM D 5385, EN 12390-8 or EN 1928 (5 bar for 7–28 d)*; Pull-Off test after thermal aging: EN 1542 (≥ 0.1 N/mm ²)*
Mechanical /physical properties	Thickness: ASTM D 1000 or ASTM D 1970 or ASTM D 3767; Elongation (ASTM D 412) and tensile strength (ASTM D 412, ASTM D 882); Puncture resistance: ASTM E 154; Seams: Peel Adhesion acc. ASTM D 1876	Fire behavior: EN 13501, ISO 11925-2; Mechanical resistance: EN 12310/EN 12311/EN 12691/EN 12730; Dimensions (EN 1848-2), Defects (EN 1850-2), Thickness (EN 1849-2); Seams: shear resistance acc. to EN 12317
Thermo-mechanical behavior	Low temperature flexibility: ASTM D 1970 (-29 °C, 180° bending around a 25 mm diameter mandrel)	<i>Bituminous</i> : Cold bending behavior: EN 1109 (180° bending, 30 mm diameter mandrel, lowest temperature without cracks is determined)
Chemical stability	Resistance to Deterioration (ASTM E 154), Resistance to fungi in soil according to the procedure of GSA-PBS; some products are tested for accelerated aging acc. to ASTM G 23, G 153	Resistance to artificial aging: EN 1296, EN 1928; Resistance to alkali: EN 1847, EN 1928; <i>Non-Bituminous</i> : bitumen compatibility: EN 1548, EN 1928
Crack bridging	Low temperature crack bridging: ASTM C 1305 (-26 °C, 10 cycles, crack up to 3.2 mm)	Resistance to hydrostatic pressure (5 bar) bridging a 1 mm crack: EN 14224, EN 1928*

* According to the recommendations in DBV-Heft 44 [4].

- Some membrane properties do not yet have their own standardized test procedures but are tested following existing standards, such as the waterproof bond. These tests are practice-oriented but have not yet been examined with respect to all influencing variables.
- Tests do not comprehensively cover seams and, for example, do not test them for watertightness. Especially T-joints were partly found leaking even under low water pressure due to remaining capillaries after joining and a missing bond to concrete (see Chapter 5).
- No minimum values are stated for some tests - often because forces acting, such as during stripping, are not yet known.

4. Characteristics and investigations

4.1. Overview

Worldwide there are currently at least 35 manufacturers for pre-applied bonded membranes on the market with various products. They can be mainly distinguished by the material of the sealing layer and the bonding mechanism used. Fig. 2 shows the properties and differentiation of currently available membranes, described in more detail in Chapters 4.2 and 4.3.

Furthermore, Table 2 lists the literature that deals with pre-applied bonded membranes to date, of which many simply

describe pre-applied membranes in their basic form. Many publications were made in Germany since 2016, which reflects the discussions about the construction method. Experimental investigations on pre-applied membranes have been conducted by Boucher [82], Freimann and Heinlein [83], Leslie and Carter [84] and in a significant 2,5-year research program by Meyer et al. [85]. Key results of these investigations also are presented hereafter.

4.2. Sealing layer

The sealing layer comprises a waterproof single-ply membrane, which also enables crack bridging of the adjoining concrete structure and is nowadays made of non-swellable and swellable materials. Non-swellable sealing layers are made out of thermoplastic materials such as polyvinylchloride (PVC), thermoplastic and flexible polyolefins (TPO, FPO) like polyethylene (PE), or elastomeric materials like ethylene-propylene-diene rubber (EPDM) [64,94], with thicknesses between 0.5 and 2.2 mm. Also, elastomer modified bitumen is used as sheet-membranes with thicknesses between 3.0 and 4.5 mm and a reinforcing inlay, e.g., polyester fleece [85,95].

In few cases, swellable materials are formed or added to pre-applied membranes. Hydrophilic polymers are used as superabsorbent based on acrylamide or acrylic acid [40,96], combined with

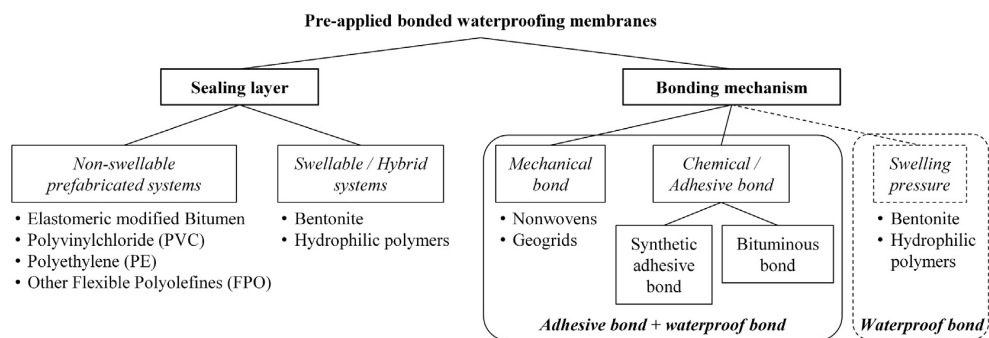


Fig. 2. Distinction of pre-applied bonded membranes by the sealing layer and the bonding mechanism (based on [2,4,59]).

Table 2
Literature regarding pre-applied bonded waterproofing membranes.

Author	Short title (partly translated)	Year	Aim of the literature
J. Henshell	The Manual of Below-Grade Waterproofing (1. Ed.)	2000	North American review and recommendations [3]
M. Kloster	Building in Existing Structures with Pre-applied Membranes	2006	First application of pre-appl. membranes in Germany [87]
K.-H. Schrod	Limitations of Waterproof Concrete Structures	2010	German description [88]
J. Henshell, P. Buccellato	Below-Grade Blindside Membranes	2011	North American practical review [89]
C. Boucher	Performance Attributes of Pre-applied Membranes	2013	Study on the bond and mechanical properties [82]
A. Haack, D. Kessler	Waterproofing of below-grade structures	2013	German description of pre-applied membranes [33]
K.-H. Schrod	Planning of Waterproof Concrete Structures with Pre-applied Membranes	2015	German discussion to the usage and regulations of pre-applied membranes [90]
J. Henshell	The Manual of Below-Grade Waterproofing (2. Ed.)	2016	North American review and recommendations [2]
Deutscher Beton- und Bautechnik-Verein E. V.	DBV-Heft 37: Pre-applied Bonded Membranes	2016	Compilation of German discussion articles [91]
T. Freimann, U. Heinlein	Design and Application of Pre-applied Membranes	2017	Research paper (influences on the bond and mechanical resistance) [83]
N. Gröske-Weißebach	Use of Pre-applied Bonded Membranes	2018	Description of German state of affairs [92]
T. Freimann, U. Heinlein	Pre-applied Waterproofing Membranes. Bonding Mechanism and General Information	2018	German review, test conditions and recommendations for installation [93]
M. Bloch, T. Zitzelsberger	Waterproof Concrete Structures with Pre-applied Waterproofing Membranes	2018	Market situation, installation, recommendations [31]
Deutscher Beton- und Bautechnik-Verein E. V.	DBV-Heft 44: Pre-applied Bonded Membranes	2018	Regulations in Germany, recommendations for planning and installation [4]
D. Leslie, J. Carter Jr.	Physics Behind Full-Size Blindside Mock-Up	2019	Study on blindside membranes in shotcrete applications [84]
L. Meyer, S. Bilgin, S. Filusch, T. Freimann, U. Heinlein, K. Herrmann	Basement waterproofing with Pre-applied Bonded Waterproofing Membranes	2020	Research report (investigations to adhesive bond, waterproof bond, seams) [85]
U. Heinlein, T. Freimann, S. Bilgin, S. Filusch, L. Meyer, K. Herrmann	Pre-applied Bonded Membranes – New Findings from Research and Practice	2020	Research paper to previous report [34]

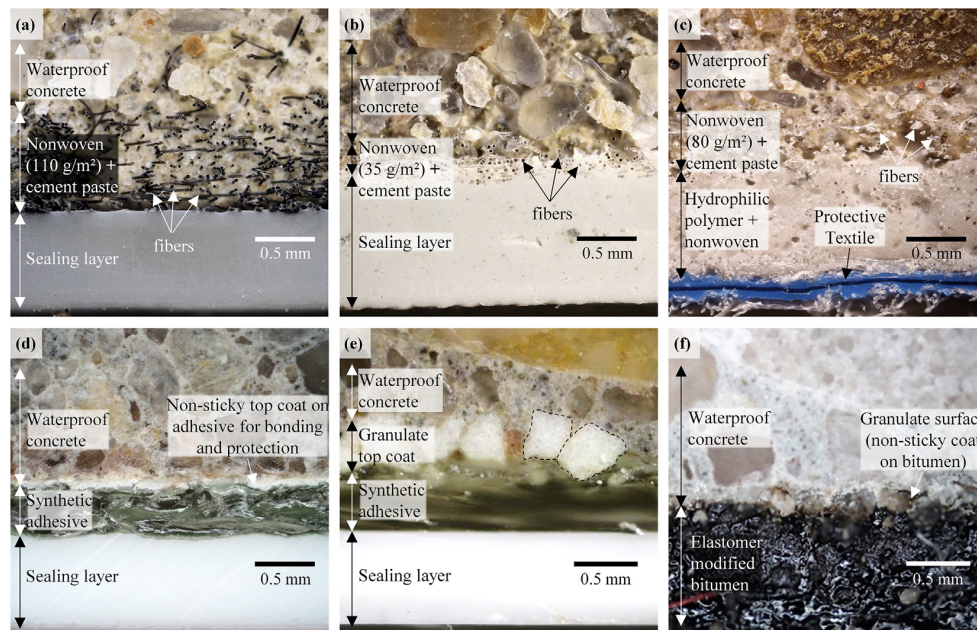


Fig. 3. The microsections show different bonding mechanisms of pre-applied waterproofing systems to concrete: the top row shows mechanical bonded, bottom row chemical bonded membranes. (a, b) Fiber bonded membranes with polymer barrier; (c) fiber bonded membrane with a swellable barrier; (d, e) synthetic adhesive-bonded membranes and (f) bituminous bonded membrane.

nonwovens or polymer waterproofing barriers. Sodium bentonite is also applied in combination with nonwovens, which is known as Geosynthetic Clay Barrier. These swellable materials are waterproofed by water absorption and a resulting swelling pressure and require a sufficient confining pressure between the building and the substrate. As a benchmark, the Austrian Guideline for

Bentonite-Protected Concrete Structures [29] states a confining pressure of more than 200 kg/m², which corresponds with a minimum cover filling of 50 cm in vertical and 20 cm in horizontal applications. Bentonite is often used in the U.S. [2], established on the European market, but in Germany only of minor importance for basement waterproofing [11,97].

4.3. Bonding mechanisms

4.3.1. Overview

The bond creates an adhesive and waterproof connection to the concrete surface and is achieved mechanically using nonwovens or chemically using synthetic adhesives or modified bitumen. Especially for mechanically bonded membranes, the adhesive and waterproof bond have to be considered independent due to the porous structure of the nonwoven [85]. Swellable materials also prevent leak water migrations by building a sufficiently high swelling pressure to the building [59]. Without additional bonding layers, however, no adhesive bond to the surface is achieved. Therefore, they are only considered fully bonded with further measures, e.g., with a nonwoven facing the fresh concrete [2]. Fig. 3 shows microsections of the bonding mechanisms in combination with concrete.

4.3.2. Characteristics of chemical bonding

Chemically bonded membranes can essentially be described as cold-bonding membranes with a non-sticky surface so that they can be walked on in horizontal applications. They either use a synthetic adhesive or modified bitumen, most often combined with an additional top-coating.

Synthetic adhesives are based, for example, on styrene-isoprene block copolymers (SIS) or dimethylnaphthalene-formaldehyde resin with thicknesses of approx. 0.3–0.6 mm and are often described as pressure-sensitive adhesives. Bitumen is modified by elastomers such as styrene-butadiene-block copolymers (SBS) [98].

Additional top-coatings are applied on top of the adhesives to replace formerly used release papers – thinly waxed or siliconized plastic films on the membranes used on post-applied bonded membranes. They usually protect the adhesive and are removed during installation [35]. The top-coatings enable a non-sticky surface and walkability in horizontal applications, prevent the membrane rolls from sticking together during delivery, and protect against UV rays. Fine-grain coatings or coarse-grain granulates are often used, which are based on calcium carbonate, calcium silicate, acrylic latex combined with mineral substances or quartzitic sand. The coating thicknesses range from several micrometers (silica, cement) [99] up to a maximum of approx. one millimeter (coarse-grained calcium carbonate) with a maximum basis weight up to approx. 450 g/m².

The adhesive surface is covered in large parts with the top-coating, thus the coating acts as a bonding bridge between the adhesive and the fresh concrete. The bond, therefore, depends on the interaction of the fresh concrete with the top-coating, which can be based on hydraulic, latent hydraulic, or pozzolanic reactions (e.g., silica top-coating) in combination with mechanical interlocking (e.g., coarse-grain granulates).

4.3.3. Characteristics of mechanical bonding

Nonwovens achieve a mechanical bond by being filled with cement paste during the concreting process, thereby interlocking with fresh concrete. This mechanism requires cement paste to separate from the concrete matrix and fill the nonwoven without voids, thus forming a waterproof fiber-cement composite. It is currently believed that this process mainly occurs during the compaction of the concrete in a filtration process [93]. In a few cases, the mechanical bond is also achieved via geogrid-like structures, as they are embedded in the fresh concrete.

To date, there are no studies available on the nonwovens of mechanically bonded membranes. This is why the nonwoven properties of seven internationally available membranes were experimentally determined and are shown in Table 3.

The fibers are usually made out of polypropylene (PP), most likely chosen due to their high chemical stability in an alkaline concrete environment. Polyester fibers (PES) are also used in some cases. Both fibers form nonwovens with basis weights between $m = 40\text{--}130\text{ g/m}^2$ and an average nonwoven thickness (unloaded) of $thk = 0.2\text{--}1.1\text{ mm}$. Based on this, the porosity of the nonwoven ε can be calculated as

$$\varepsilon = 1 - \frac{m}{\rho \cdot thk \cdot A} \quad (1)$$

where ρ is the density of the fibers and A the related area [100]. For the tested products, the porosity is between $\varepsilon = 0.80\text{--}0.91$. The required cement paste volume to completely fill the nonwoven can be calculated as

$$V_{\text{void}} = \varepsilon \cdot thk \cdot A \quad (2)$$

and is between $V_{\text{void}} = 164\text{--}756\text{ cm}^3/\text{m}^2$. The fibers are usually monofilament staple fibers with a round cross-section, a crimp, and a diameter of 13–35 μm . In one system, filaments were used in addition to staple fibers. The nonwovens are bonded by conventional methods [101] thermally on the calender, mechanically by hydroentanglement or needle-punching. Nonwovens thicker than 0.6 mm are usually bonded by needle-punching. Nonwovens with similar weight and production methods are used for thin geotextiles for filtering applications in housing construction, see, e.g. [102,103]. After the nonwoven production, the sealing layer is attached to them by heat bonding or synthetic adhesives. Table 4 summarizes and shows further sheet properties of nowadays used pre-applied bonded membranes.

4.3.4. Investigations on the bond

Early literature on attached waterproofing systems often states that a bond can prevent lateral water migration - but no information is provided on the creation or the properties of the bond. For example, the ACI "Guide to the Use of Waterproofing (...) for concrete" [103] states that (post-applied) barrier materials - fully

Table 3
Experimentally determined properties of nonwovens of n = 7 mechanical bonded pre-applied membranes.

Property	Unit	Individual mean values \bar{x} of n = 7 tested products							Test method, number of samples per product and average standard deviation \bar{s} in the test
		No. 1	No. 2	No. 3	No. 4	No. 5	No. 6	No. 7	
Nonwoven basis weight	g/m ²	62	47	129	36	113	92	83	8 samples per product, $\bar{s} = 7.1\text{ g/m}^2$
Nonwoven thickness (unloaded)	mm	0.52	0.20	0.82	0.31	1.08	0.50	0.68	DIN EN 1849-2 [104]; 8 samples per product; $\bar{s} = 0.08\text{ mm}$
Fiber diameter	μm	24 / 35	13	33	25	23	26	11 / 21	DIN 65571-2 [105]; 35 samples per product; $\bar{s} = 2.7\text{ }\mu\text{m}$
Fiber material	PE / PP	PES	PP	PP	PP	PP	PP	PES	FTIR; 2 samples per product
Nonwoven porosity	[-]	0.87	0.82	0.83	0.87	0.87	0.80	0.91	$\varepsilon = 1 - \frac{m}{\rho \cdot thk \cdot A}$ (m: nonwoven basis weight, ρ : density of fibers, thk: thickness of the nonwoven; A: area)
Nonwoven bonding		NP	CB	NP	HE	NP	HE	NP	NP: Needle-punching; CB: Calender bonding; HE: Hydroentanglement

Table 4
Sheet properties of nowadays used pre-applied bonded membranes.

Property	Unit	Barrier waterproofing		Bonding layer	
		Non-swellable	Swellable	Mechanical	Chemical/Adhesive
Material	–	Synthetic polymers or elastomer-modified bitumen, partially with reinforcing inlays	Sodium Bentonite or hydrophilic polymers, in combination with nonwovens	PP, PE, PES fibers or grid structures	<i>Synthetic:</i> Adhesive based on, e.g., SIS; top-coat based on, e.g., calcium carbonate, calcium silicates or acrylic latex <i>Bituminous:</i> Adhesive based on elastomer modified bitumen, e.g., with SBS; top-coated with sand
Thickness	mm	<i>Polymeric:</i> 0.5–2.2 <i>Bituminous:</i> 3.0–4.5	<i>Bentonite:</i> 5–7 <i>Polymers:</i> 1.2–2.5	<i>Fibers:</i> 0.2–1.1 <i>Grid:</i> 1.2–3.2	<i>Synthetic adhesive:</i> 0.3–0.5 <i>Bituminous:</i> see barrier thickness <i>Top-coat:</i> ≤1 mm
Basis weight	g/m ²	<i>Polymeric:</i> 820–2270 <i>Bituminous:</i> 3300–5000	<i>Bentonite:</i> 4000–5200 <i>Polymers:</i> 500–1200	<i>Fibers:</i> 40–130	<i>Top-coat:</i> approx. 40–450

bonded to the concrete substrate - prevent water migration in the composite layer in the event of a damaged membrane. Also, the NRCA Roofing and Waterproofing Manual [68] simply states that adhered materials reduce the possibility of lateral water migrations between the waterproofing material and substrate.

Meyer *et al.* [85] investigated ten pre-applied membranes in cast-in-place concrete applications in order to understand the bonding mechanisms. For that, the development of the adhesive tensile strength was tested in a total of $n = 760$ pull-off tests according to EN 1542 [106]. Additionally, the waterproof bond was tested in $n = 312$ hydrostatic pressure tests according to a modified version of DIN EN 12390-8 [107]. The test procedure is similar to ASTM D 5385 and applies a water pressure of 5 bar for three days on a local defect in the sealing layer. The formation of the bond was found to behave differently depending on the bonding mechanism used. Chemically bonded membranes usually showed a proportionality between the waterproof and adhesive bond. However, mechanically bonded systems behaved differently. They could achieve a good adhesive bond to the concrete - but still could not be waterproof in the bonding zone because of their porous structure. All water-bearing cavities in the nonwoven must therefore be filled with cement paste during the concreting process in order to ensure waterproofing. This filling process depends significantly on high compaction energy in the vicinity of the nonwoven. A more fluid concrete consistency was found beneficial as well. It was assumed that this is due to the lowering of the yield point of the fresh concrete during compaction. In the laboratory tests with cast-in-place concrete applications, a good waterproof bond was achieved for 5 out of 6 mechanically bonded membranes using a typical building site internal vibrator with a compaction time of 2–5 s and a fresh concrete with a flow of 48 cm, tested according to EN 12350-5 [108]. Contrary to the statements in [82], this confirms that a mechanical bond can also be waterproof.

Leslie and Carter [84] also investigated a mechanically bonded membrane - but in shotcrete application. They prepared a full-size mock-up, performed laboratory tests on the bond, and presented the acting forces during shotcrete application. It was found that shotcrete overspray and poorly compacted concrete led to a poor adhesive and waterproof bond. Laboratory tests verified this finding, where the waterproof bond was tested with $n = 6$ specimens for their resistance against pressurized and non-pressurized water following modified versions of ASTM D 5385 and D 5957.

4.4. Installation

The membranes are installed as sheets and must be waterproof at seams and details. Longitudinal seams are often realized by thermal joining methods, additional liquid sealants, or self-adhesive seams based on synthetic pressure-sensitive adhesives or cold-

bonding butyl rubber adhesives. For cross and T-joints, corners, and construction details, self-adhesive tapes or liquid applied sealing materials are also available and are sometimes used in combination with prefabricated elements, e.g., for corners [34].

Meyer *et al.* also tested the different seam variations for ten membranes. The resistance of T-joints against hydrostatic water pressure was tested without a bond to concrete, following EN 1928 (method A) [109]. In these tests, 14 of 20 seams showed leakages below one bar water pressure. This poor test result led to the assumption that water-bearing capillaries can remain in the T-joints during the joining of the seams. It was also assumed that these capillaries are probably closed by cement slurry during the concrete placement - which must be further investigated. Also, the shear resistance of 28 seam variations was tested according to EN 12317 [110] and was determined to 129–1,484 N/50 mm in the reference test. No correlation between a higher shear resistance and a higher resistance against water pressure in the seam was observed. This result confirms that the leaking of T-joints at low pressures is due to capillaries.

After the installation, concrete is cast directly on the membranes, often by pouring and sometimes by spraying. If the membranes are thereby used in formworks, the earliest possible stripping time is of interest. With this in mind, Meyer *et al.* tested the development of the adhesive tensile strength of ten pre-applied bonded membranes over the first days of concrete curing. Normal-curing cement and good weather conditions ($T = 20$ °C) resulted in adhesive tensile strengths of 0.40–0.93 MPa after two days in pull-off tests according to EN 1542. This duration is recommended by Heinlein *et al.* [34] as the stripping time, even without reference values for forces during stripping being available to date. Schreiber [111] recommended even further extending the stripping time in case of slowly curing cement or low air temperatures. Curing the specimens at an air temperature of 5 °C rather indicated more than seven days being necessary to achieve the adhesive tensile strength of the reference test ($T = 22$ °C). This also holds for chemically bonded membranes since the fresh concrete mainly interacts with the top-coating.

Furthermore, the following recommendations can be found regarding the installation:

- **Preparation:** Pre-applied bonded membranes require certain conditions for the substrate, the installation, and even the subsequent concrete placement. It is essential to follow the installation instructions and the manufacturer's specifications. Due to the specifics of the installation, the personnel should be trained in advance.
- **Spacers:** Bonding defects are formed between spacers and pre-applied membranes. For this reason, spacers should not be laid against one another but placed with an offset. Also, fiber cement spacers with notches can be used, such as those available for

fair-faced concrete. The notches face the membrane so that a waterproof bond is achieved between them. The reinforcement load and the resulting contact pressure should be considered [4,112].

- **Soiling:** Due to soil, cement paste, standing water, or leaves on the bonding layer, the bond may not develop fully during concrete placement. Consequently, soiling should be avoided or, at the latest, removed before concreting by using high-pressure cleaning as gently as possible. Permanent protective screeds or similar should not be used as they can form water-bearing layers themselves and as mechanically bonded systems may not provide a waterproof bond [85].
- **On-site testing:** After installing the membranes and before concrete works, the waterproofing can be tested, e.g., with electronic methods according to ASTM D 7877 [113] or flood testing in horizontal applications according to ASTM D 5957 [114].

5. Further research needs

Pre-applied bonded membranes have been used for around 30 years – nevertheless, the following research needs exist:

- **Testing the waterproof bond:** The waterproof bond is tested according to modified versions of ASTM D 5385 [115], EN 12390-8, or EN 1928 (method A). The applied water pressure varies between 5.0 and 6.9 bar and the duration between 1 and 28 days. A standardized procedure is needed. Also, the interaction of the acting forces is not yet clarified.
- **Correlation between the waterproof bond and contact pressure:** Karras *et al.* [116] state that the correlation between confining pressure of water and waterproof bond is not yet established. When testing the waterproof bond, high water pressures of up to 6.9 bar are used. The parallel action of high contact pressure may lead to a cushioning effect and lower water migrations.
- **Seams after concreting:** Without the bond to concrete, T-joints were partially found leaking even at low water pressures, as water-bearing capillaries remained during production. Water tightness may improve after concreting due to cement slurry impregnating capillaries, which needs further investigation.
- **Reopening of seams:** Occasionally, it is reported that seams open again after installation. The cause of this phenomenon has not yet been clarified and can be due to temperature expansions or improperly installed seams. Until further investigations have been carried out, it is advisable to follow all manufacturer's instructions when joining seams, leave the membrane open for as short a time as possible, and visually inspect seams before the concrete is placed [34,85].
- **Cleanability:** Soil and cement paste on pre-applied bonded membranes must be removed at the latest before concreting. Otherwise, the waterproof and adhesive bond will be limited. So far, it is not known whether the systems will regain their full performance after cleaning.
- **Nonwovens in the concreting process:** It is currently unknown how concrete pressure and vibration parameters impact the penetration of cement paste into nonwovens. To optimize nonwovens for pre-applied bonded membranes, the behavior of the nonwovens in the concreting process and the properties of the cement paste in the nonwoven must be understood [85].
- **Sustainability:** The recycling of concrete structures is an essential contribution to environmental protection. So far, it has not been investigated how pre-applied membranes influence the recycling of concrete components and the overall sustainability of concrete elements [34].

6. Summary

Pre-applied bonded waterproofing membranes are used as stand-alone waterproofing or additionally on waterproof concrete structures. They consist of a sealing layer and a composite layer to create an adhesive and waterproof bond. In the present appearance, they were introduced for blindside applications in North America in the 1990s and have now also gained a foothold in Europe. The interest in pre-applied bonded membranes has increased significantly in recent years, as seen from the number of manufacturers, patents, and market growth.

Recent studies have shown that the membranes work expectably – as long as trained personnel handle them with care on the construction site. Bonding problems can occur in various situations and must be avoided. Even the concrete placement requires special care, especially when mechanically bonded systems are involved. Products for pre-applied membranes should also be selected depending on whether the manufacturer can provide sufficient test reports on the functionality, including seams and detail points. Further research is needed in practical areas such as the watertightness of seams and in more academic areas such as uniform testing conditions.

Declaration of Competing Interest

The authors declare that they have no known competing financial interests or personal relationships that could have appeared to influence the work reported in this paper.

Acknowledgement

The present work is supported by the Bavarian Academic Forum BayWISS in the collegium "Infrastruktur-Bauen-Urbanisierung".

References

- [1] M. Bonk, Aufgabe von Bauwerksabdichtungen, in: K. Lufsky (Ed.), Bauwerksabdichtung, Vieweg+Teubner Verlag/GWV Fachverlage GmbH, Wiesbaden, 7. Auflage, Wiesbaden, 2009, pp. 1–4.
- [2] J. Henshell, The Manual of Below-Grade Waterproofing, Routledge, 2nd Edition, New York Routledge, 2016.
- [3] J. Henshell, The Manual of Below-Grade Waterproofing Systems, Wiley & Sons, Inc., 1st ed., 2000.
- [4] Deutscher Beton- und Bautechnik-Verein E.V., DBV-Heft 44 "Frischbetonverbundsysteme (FBV-Systeme) - Sachstand und Handlungsempfehlungen" Fassung Oktober 2018, Eigenverlag DBV, 2018.
- [5] E. Cziesielski, Geschichtliche Entwicklung der Abdichtungstechnik, in: K. Lufsky (Ed.), Bauwerksabdichtung, Vieweg+Teubner Verlag/GWV Fachverlage GmbH, Wiesbaden, 7. Auflage, Wiesbaden, 2009, pp. 5–11.
- [6] S. Hemmann, Geschichtliche Entwicklung der Bauwerksabdichtung, in: J. Weber, V. Hafkesbrink (Eds.), Bauwerksabdichtung in der Altbausanierung, Vieweg+Teubner, Wiesbaden, 2008, pp. 2–6.
- [7] K.L. Mittal, A. Pizzi, Handbook of Sealant Technology, Taylor & Francis, Boca Raton, 2009.
- [8] J. Hurst (W. R. Grace & Co.) US 3,741,856, 1973.
- [9] P. Bechtner (American Colloid Company) US 2,277,286, 1942.
- [10] K. Kuntsche, in: Geotechnik, Springer Fachmedien Wiesbaden, Wiesbaden, 2016, pp. 365–412, https://doi.org/10.1007/978-3-8348-2020-4_9.
- [11] R. Ruhnu, Abdichtung mit Bentonit, in: K. Lufsky (Ed.), Bauwerksabdichtung, Vieweg+Teubner Verlag / GWV Fachverlage GmbH, Wiesbaden, 7. Auflage, Wiesbaden, 2009, pp. 344–363.
- [12] A.G. Clem (American Colloid Company) US3,186,896, 1965.
- [13] W. Stokes US3,642,559, 1972.
- [14] J. Heyen DE2827757, 1980.
- [15] H. Fuchs, W. Albrecht (Eds.), Vliesstoffe: Rohstoffe, Herstellung, Anwendung, Eigenschaften, Prüfung, 2nd ed., Wiley-VCH, Weinheim, 2012.
- [16] P. Kolling, H. Olschak (Dynamit Nobel Aktiengesellschaft) EP0007413, 1980.
- [17] H. Wustinger (Ruhrkohle AG) DE2400866, 1975.
- [18] National Research Council, Geosynthetics, Geomembranes, and Silt Curtains in Transportation Facilities, Transportation Research Board National Research Council, Washington, DC, 1989.
- [19] US4,065,924, 1978.
- [20] T. Platts, Abdichtungen im Verbund mit Fliesen und Platten, in: K. Lufsky (Ed.), Bauwerksabdichtung, Vieweg+Teubner Verlag / GWV Fachverlage GmbH, Wiesbaden, 7. Auflage, Wiesbaden, 2009.

- [21] S. Malik DE2261401, 1974.
- [22] Barlett et al. (W.R. Grace & Co.-Conn.) US 5,316,848, 1994.
- [23] R. Wolf, G. Gebhards (Günau Illertissen GmbH; Roland Wolf GmbH) DE19611297A1, 1997.
- [24] J.A. Cogliano (W.R. Grace & Co.-Conn.) US 4,994,328, 1991.
- [25] Barlett et al. (W.R. Grace & Co.-Conn.) US 5,496,615, 1996.
- [26] A.W. White (American Colloid Company) US5,174,231, 1992.
- [27] S.W. Byrd (American Colloid Company) EP 0,610,008 A1.
- [28] DIN 18533-1:2017-07, Abdichtung von erdberührten Bauteilen - Teil 1: Anforderungen, Planungs- und Ausführungsgrundsätze, Beuth Verlag GmbH, Berlin.
- [29] **Österreichische Bautechnik Vereinigung, Bentonitgeschützte Betonbauwerke – Braune Wanne, Richtlinie, Juli, 2019.**
- [30] Bundesanstalt für Straßenwesen, Technische Lieferbedingungen und Technische Prüfvorschriften für Ingenieurbauten TL/TP-ING Teil 5 Abschnitt 5: Technische Lieferbedingungen und Technische Prüfvorschriften für Schutz- und Dränschichten aus Geokunststoffen TL/TP SD, 2017.
- [31] M. Bloch, T. Zitzelsberger, WU-Konstruktionen mit Frischbetonverbundsystem, in: N.A. Fouad (Ed.), Bauphysik Kalender 2018: Feuchteschutz und Bauwerksabdichtung, Ernst & Sohn, Berlin, Germany, 2018, pp. 285–308.
- [32] H.-J. Krause, M. Horstmann, WU-Konstruktionen mit außenliegenden Frischbetonverbundsystem, in: M. Oswald, M. Zöller (Eds.), Aachener Bausachverständigentage 2017: Bauwerks-, Dach- und Innenabdichtung: Alles geregelt?, pp. 96–105.
- [33] A. Haack, D. Kessler, Abdichtungen bei unterirdischen Bauwerken, in: K. Bergmeister, F. Fingerloos, J.-D. Wörner (Eds.), Beton-Kalender 2014 – Unterirdisches Bauen – Grundbau, John Wiley & Sons, Inc, 2014, pp. 523–584.
- [34] U. Heinlein, T. Freimann, S. Bilgin, S. Filusch, L. Meyer, K. Herrmann, Frischbetonverbundsysteme – Neue Erkenntnisse aus Forschung und Praxis, Beton- und Stahlbetonbau 115 (9) (2020) 671–683, <https://doi.org/10.1002/best.v115.9.10.1002/best.202000031>.
- [35] Wiercinski et al. (W.R. Grace & Co.-Conn.) WO 2013/063197 A1, 2013.
- [36] J.W. Muncaster, T.J. Millican (Polyguard Products, Inc.) US 7,686,903 B2.
- [37] G. Knebel (Sika Technology AG) EP 2299005 A1, 2011.
- [38] Wiercinski et al. (W.R. Grace & Co.-Conn.) WO 2012/092019 A1, 2012.
- [39] U. Weber (Sika Technology AG) EP 2349707 B1, 2013.
- [40] A. Kogel EP2665791B1, 2014.
- [41] G. Knebel, M. Eckl (Sika Technology AG) US 2015/0231863 A1, 2015.
- [42] Bertrand (Poly-America, L. P.) US 9,085,899 B1, 2015.
- [43] J. Feldmeier, H. Gürster (Max Frank GmbH & Co.KG) DE102014107423A1, 2015.
- [44] SB Bautechnik GmbH DE102015118316A1, 2017.
- [45] J. Feldmeier, N. Weißenbach (Max Frank GmbH & Co.KG) DE102015120401A1, 2017.
- [46] D. Köster (Köster Bauchemie AG) DE102015112591A1, 2017.
- [47] Ackermann et al. (Sika Technology AG) US 2018/0361716 A1, 2018.
- [48] M. Guderzo (Volteco S.p.A.) EP3283286B1, 2019.
- [49] S. Luckert, L. Schallstieg, G. Napravnik EP2907832B1, 2016.
- [50] J. Mohanraj, C. Yates GB2578740A, 2020.
- [51] J. Köster, D. Fischer, H. Looks, M. Witzke (Köster Bauchemie AG) DE102016107632A1, 2017.
- [52] FWR Solutions GmbH DE202018107450U1, 2019.
- [53] M. Bulloni, R. Z'Rotz, S. Schönbrodt, C. Bärtsch, J. von Rotz (Sika Technology AG) WO2019/106108A1, 2019.
- [54] J. Ledford, B. Gish, R. Vinson, T. Vitale, P. Digiovanni, J. Tepera, S. Velten (Carlisle Construction Materials, L. LC.) WO2020/117523A1, 2020.
- [55] R. Roskamp, S. Schoenbrodt, A. Flueck, O. Knebel (Sika Technology AG) WO2020/084096A1, 2020.
- [56] U. Weber, M. Kloster (Sika Technology AG) US2011/0197427A1, 2011.
- [57] A. Rudyan US2020/0240101A1, 2020.
- [58] E. Horstmann, C. Sovey (Tremco Incorporated) US 2016/0290375 A1, 2016.
- [59] BS 8102:2009-11-30, Code of practice for protection of below ground structures against water from the ground. British Standards Institution, London.
- [60] BS 8102:1990, Code of Practice for Protection of Structures Against Water from the Ground, British Standards Institution, London, 1990.
- [61] A. Haack, D. Kessler, Abdichtungen bei unterirdischen Bauwerken unter Berücksichtigung neuer Normen, in: K. Bergmeister, F. Fingerloos, J.-D. Wörner (Eds.), Beton Kalender 2019, Wiley, 2018, pp. 795–861.
- [62] Sika Deutschland GmbH, Frischbetonverbundtechnologie: Das SikaProof Gesamtsystem mit patentierter Hybridtechnologie, 2020. <https://deu.sika.com/dms/getdocument.get/73ff36a7-feef-4164-9953-096e95f1b11c/Das%20SikaProof%20Gesamtsystem.pdf> (accessed 11 October 2020).
- [63] BAS-de GmbH, Pre-applied waterproofing technologies. https://www.bas-de.com/images/produkte/flachenabdichtung/Englisch%20Frischbetonverbundtechnologien_Broschu%CC%88re_BAS-de%20GmbH.pdf (accessed 11 October 2020).
- [64] P. Buccellato, J. Henshell, Recent Developments in Below-Grade and Plaza Waterproofing Systems: 31st RCI International Convention and trade show (2016) 153–162.
- [65] ASTM D7832/D7832M-14: Standard Guide for Performance Attributes of Waterproofing Membranes Applied to Below-Grade Walls / Vertical Surfaces (Enclosing Interior Spaces), American Society for Testing and Materials, West Conshohocken, PA.
- [66] International building code, International Code Council, Inc, Country Club Hills, IL, 2017.
- [67] Canadian Commission of Building and Fire Codes. National Research Council of Canada, National Building Code of Canada 2015.
- [68] National Roofing Contractors Association, The NRCA Roofing and Waterproofing Manual., 5th edition, Rosemont, 2006.
- [69] U.S. General Services Administration. Public Buildings Service, P100. Facilities Standards for the Public Buildings Service, Washington, DC, 2018.
- [70] I. Construction Specification Institute, MasterFormat 2020 Edition. Master List of Numbers and Titles for the Construction Industry, 2020.
- [71] DIN EN 13967, Abdichtungsbahnen – Kunststoff- und Elastomerbahnen für die Bauwerksabdichtung gegen Bodenfeuchte und Wasser – Definition und Eigenschaften; Deutsche Fassung EN 13967:2012 + A1:2017, Beuth Verlag GmbH, Berlin.
- [72] DIN EN 13969, Abdichtungsbahnen - Bitumenbahnen für die Bauwerksabdichtung gegen Bodenfeuchte und Wasser – Definition und Eigenschaften; Deutsche Fassung EN 13969:2004 + A1:2006, Beuth Verlag GmbH, Berlin.
- [73] EAD 030378-00-0605, Fully Bonded, Pre-applied Flexible Sheet for Waterproofing, May 2018, EOTA.
- [74] ÖNORM B 3664: Abdichtungsbahnen - Kunststoffbahnen für die Bauwerksabdichtung gegen Bodenfeuchte und Wasser. Nationale Umsetzung der ÖNORM EN 13967, Austrian Standards International, Wien 91.100.50, 2019.
- [75] Deutscher Beton- und Bautechnik-Verein E.V., DBV-Merkblatt Hochwertige Nutzung von Untergeschossen - Bauphysik und Raumklima. Fassung Januar 2009.
- [76] Österreichische Bautechnik Vereinigung, Wasserundurchlässige Betonbauwerke - Weiße Wannen. Februar 2018.
- [77] DIN/TS, 20000-202:2020-11, Anwendung von Bauprodukten in Bauwerken - Teil 202: Anwendungsdokument für Abdichtungsbahnen nach Europäischen Produktnormen zur Verwendung als Abdichtung von erdberührten Bauteilen, von Innenräumen und von Behältern und Becken, Beuth Verlag GmbH, Berlin.
- [78] C. Scivyer, BRE 211: Radon. Guidance on protective measures for new buildings, 2007.
- [79] BRE 212: Construction of new buildings on gas-contaminated land. Building Research Establishment, Watford, 1991.
- [80] DIN ISO/TS 11665-12:2019-11; VDE V 0493-1-6662:2019-11. Ermittlung der Radioaktivität in der Umwelt - Luft: Radon-222 - Teil 12: Bestimmung des Diffusionskoeffizienten in wasserundurchlässigen Materialien: Prüfverfahren mit einseitiger Messung der Aktivitätskonzentrationen (ISO/TS 11665-12:2018), VDE Verlag.
- [81] ASTM D 1434-1982: Test Method for Determining Gas Permeability Characteristics of Plastic Film and Sheeting, American Society for Testing and Materials.
- [82] C. Boucher, Essential Performance Attributes of Preapplied Waterproofing, 28th RCI International Convention and Trade Show (2013) 33–42.
- [83] T. Freimann, U. Heinlein, Planung und Anwendung der Frischbetonverbundsysteme bei wasserundurchlässigen Baukonstruktionen aus Beton, in: K. Bergmeister, F. Fingerloos, J.-D. Wörner (Eds.), Beton-Kalender 2018, Bautenschutz, Brandschutz, Ernst & Sohn a Wiley brand, Berlin, Germany, 2018, pp. 227–258.
- [84] D. Leslie, J. Carter JR., The Physics Behind Lessons Learned in a Full-Size Blindside Mock-Up, 2019 IIBEC Building Enclosure Symposium 87–104.
- [85] L. Meyer, S. Bilgin, S. Filusch, T. Freimann, U. Heinlein, K. Herrmann, Bauwerksabdichtung mit Frischbetonverbundfolie - Grundlagen zur Erstellung eines Regelwerks für eine innovative Bauart: Abschlussbericht F 3183, Fraunhofer IRB Verlag, Stuttgart, 2020.
- [86] Deutsches Institut für Bautechnik DIBt, Prüfgrundsätze zur Erteilung von allgemein bauaufsichtlichen Prüfzeugnissen für Fugenabdichtungen in erdberührten Bauteilen aus Beton mit hohem Wassereindringwiderstand. PG-FBB.
- [87] M. Kloster, Bauen im Bestand mittels Frischbetonverbundsystem. Abdichtung – neuer Weg zur Sanierung eines Kühlturms, BUST 101 (2006) 1006–1009. <https://doi.org/10.1002/best.200608191>.
- [88] K.-H. Schrod, Anwendungsgrenzen von WU-Bauwerken - Sind "Weiße Wannen" wirklich dauerhaft dicht?, Beton- und Stahlbetonbau 105 (2010) 1–6.
- [89] J. Henshell, P. Buccellato, Below-Grade Blindside Waterproofing Membrane Systems: a state-of-the-art report 2011.
- [90] K.-H. Schrod, Regelgerechte WU-Planung mit Frischbeton-Verbund-Abdichtungsbahnen für WU-Konstruktionen mit hochwertiger Nutzung A***: nach DIN 18195 nicht möglich (Sonderdruck), Beton- und Stahlbetonbau 110 (2015) 1–6.
- [91] Deutscher Beton- und Bautechnik-Verein E.V., DBV-Heft 37 "Frischbetonverbundfolie" Fassung August 2016, Berlin.
- [92] N. Grüske-Weißenbach, Der Einsatz von Frischbetonverbund-systemen bei wasserundurchlässigen Betonkonstruktionen, Bauphysik 40 (3) (2018) 161–165, <https://doi.org/10.1002/bapi.v40.3.1002/bapi.201810018>.
- [93] T. Freimann, U. Heinlein, Frischbetonverbundtechnologie, Beton- und Stahlbetonbau 113 (5) (2018) 368–384, <https://doi.org/10.1002/best.201700098>.
- [94] M.T. Kubal, Construction waterproofing handbook, second ed., McGraw-Hill, New York, 2008.
- [95] Soprema AG, Frischbetonverbund-Abdichtungsbahn Colphene BSW. <https://www.soprema.ch/de/product/ingenieurbau/bauten-unter-terrain/>

- bituminoese-systeme/abdichtungen/colphene-bsw-unilay-hp (accessed 24 September 2020).
- [96] S. Friedrich, Chapter 3, Superabsorbent Polymers (SAP), in: V. Mechtcherine, H.-W. Reinhardt (Eds.), Application of Super Absorbent Polymers (SAP) in Concrete Construction: State-of-the-Art Report Prepared by Technical Committee 225-SAP. ppp, Springer Netherlands, s.l., 2012, pp. 13–19.
- [97] Deutsches Institut für Bautechnik DIBt, Muster-Verwaltungsvorschrift Technische Baubestimmungen (MVV TB). Ausgabe 2019/1, Berlin, 2019.
- [98] Roland Wolf GmbH, Broschüre FBV-Abdichtungssysteme. https://www.wolfsea.de/de/downloads/fbv-thepro-schott-wand/broschuere_fbv_thepro_schottwand_korrekturen_8juli2020_optimized.pdf (accessed 24 September 2020).
- [99] H. Chen, H. Ding, L. Xin, R. Wiercinski (GCP Applied Technologies Inc.) WO 2017/058154 A1.
- [100] I.M. Hutten, Handbook of nonwoven filter media, Second edition, Butterworth Heinemann an imprint of Elsevier Ltd, Kidlington, Oxford, Waltham, MA, 2016.
- [101] S.J. Russell, Handbook of nonwovens, CRC, Woodhead Publishing Limited, Boca Raton, 2007.
- [102] Bermüller & Co. GmbH, Bontec NW - Technical Datasheet. www.becobermueller.de/de/produkte/geokunststoffe-geotextilien-geobaustoffe/vliesstoffe/bontec-nw-vliesstoffe/ (accessed 23 September 2020).
- [103] Fibertex Nonwovens A/S, Product application guide, Geotextiles., 2018. <https://www.fibertex.com/sites/fibertex.com/files/2019-03/ProductKey.pdf> (accessed 23 September 2020).
- [104] DIN EN 1849-2:2019-09, Abdichtungsbahnen - Bestimmung der Dicke und der flächenbezogenen Masse - Teil 2: Kunststoff- und Elastomerbahnen für Dachabdichtungen; Deutsche Fassung EN 1849-2:2019, Beuth Verlag GmbH, Berlin.
- [105] DIN 65571-2:1992-11, Luft- und Raumfahrt; Verstärkungsfasern; Bestimmung des Filamentdurchmessers von Filamentgarnen; Längsprojektionsverfahren, Beuth Verlag GmbH, Berlin.
- [106] DIN EN 1542:1999-07, Produkte und Systeme für den Schutz und die Instandsetzung von Betontragwerken - Prüfverfahren - Messung der Haftfestigkeit im Abreißversuch; Deutsche Fassung EN 1542:1999, Beuth Verlag GmbH, Berlin.
- [107] DIN EN 12390-8, Prüfung von Festbeton - Teil 8: Wassereindringtiefe unter Druck; Deutsche Fassung EN 12390-8:2019, Beuth Verlag GmbH, Berlin.
- [108] DIN EN 12350-5:2019-09, Prüfung von Frischbeton - Teil 5: Ausbreitmaß; Deutsche Fassung EN 12350-5:2019, Beuth Verlag GmbH, Berlin.
- [109] DIN EN 1928, Abdichtungsbahnen. Bitumen-, Kunststoff- und Elastomerbahnen für Dachabdichtungen. Bestimmung der Wasserdichtheit. Deutsche Fassung EN 1928:2000, Beuth Verlag GmbH, Berlin.
- [110] DIN EN 12317-2:2010-12, Abdichtungsbahnen - Bestimmung des Scherwiderstandes der Fügenähte - Teil 2: Kunststoff- und Elastomerbahnen für Dachabdichtungen; Deutsche Fassung EN 12317-2:2010, Beuth Verlag GmbH, Berlin.
- [111] P. Schreiber, Frischbetonverbundtechnologie - Vergleichende Untersuchungen zum Einfluss des Betonalters auf die Haftspannung in der Grenzschicht von vertikal applizierten FBV-Systemen, Unveröffentlichte Masterthesis an der Technischen Hochschule Nürnberg, 2019.
- [112] N. Reulein, Untersuchungen zum Verbundverhalten zwischen Frischbetonverbundsystemen und Betonabstandhaltern für WU-Betonkonstruktionen, Unveröffentlichte Bachelorarbeit an der Technischen Hochschule Nürnberg, 2020.
- [113] ASTM D 7877-14: Standard Guide for Electronic Methods for Detecting and Locating Leaks in Waterproof Membranes, American Society for Testing and Materials 91.100.60, 2014.
- [114] ASTM D 5957-98 (2013): Standard Guide for Flood Testing Horizontal Waterproofing Installations, American Society for Testing and Materials, 2013.
- [115] ASTM D5385-93, Standard Test Method for Hydrostatic Pressure Resistance of Waterproofing Membranes., American Society for Testing and Materials.
- [116] J. Karras, K. Nelson, A. Nicastrò, Blindside Belowgrade Waterproofing. Lateral Water Migration, Confining Pressure and Bond Relationships, 2016. <https://www.buildingenlosureonline.com/articles/86393-blind-side-below-grade-waterproofing> (accessed 5 October 2020).

9.2 Pre-applied mechanical bonded waterproofing membranes: Macroscopic nonwoven behavior during the concreting process

Reprint

Published in “Journal of Building Engineering”

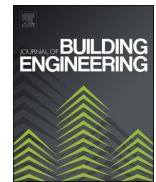
Volume 45, October 2021; DOI: [10.1016/j.jobbe.2021.103531](https://doi.org/10.1016/j.jobbe.2021.103531)

Authors: U. Heinlein, T. Freimann



Contents lists available at ScienceDirect

Journal of Building Engineering

journal homepage: www.elsevier.com/locate/jobe

Pre-applied mechanical bonded waterproofing membranes: Macroscopic nonwoven behavior during the concreting process

Ulli Heinlein^{*}, Thomas Freimann

Technische Hochschule Nürnberg Georg Simon Ohm, 90489, Nürnberg, Germany

ARTICLE INFO

Keywords:

Pre-applied waterproofing membranes
Blindside waterproofing
Waterproofing membranes
Fully-bonded waterproofing membranes
Post-cast concrete application
Nonwovens

ABSTRACT

Pre-applied bonded waterproofing membranes are used as positive-side waterproofing membranes on concrete basements. They are installed prior to concrete works and form a bond with the fresh concrete, *inter alia*, by the use of nonwovens. However, it is not yet known how the nonwovens behave during the concreting process, which is preventing any optimization. This is why this article aims to understand the macroscopic changes of nonwovens during concreting and identifies beneficial nonwoven properties for a waterproof bond. Seven nonwoven bonded pre-applied membranes are installed using fresh concrete and varying installation parameters and are afterward investigated using microsections, hydrostatic tests and micro-CT scans. During the installation process, the nonwovens are first compressed due to the fresh concrete load and behave like exposed to a mechanical load. Then, as vibration compaction begins, cement paste separates from the fresh concrete in a filtration process and fills the nonwoven. The fresh concrete pressure is then transferred via the cement paste so that the nonwovens can decompress due to the residual stress of the fibers. The final nonwoven thickness depends on compaction equipment, compaction time, and orientation of the nonwoven in the concrete. With the onset of compaction, the porosity within the nonwoven decreases fast so that acceptable lateral water migrations are present after 2–3 s using strong compaction equipment. The void volume of the nonwoven is decisive for the compaction time needed, so new nonwovens should be designed with low void volumes concerning a waterproof bond.

1. Introduction

Pre-applied bonded waterproofing membranes are applied to the outside (positive-side) of concrete basements. Already before the concrete works, they are placed on a mud-slab, vertically in a formwork or in blindside applications onto a soil retention system. In the further course of construction, fresh concrete is applied directly onto the membranes, and a tensile and waterproof bond is achieved via a bonding layer attached to the sealing layer [1]. The waterproof bond thereby increases the redundancy of the waterproofing compared to unbonded membranes. If local leakage occurs, lateral water movement between the waterproofing membrane and the concrete surface is prevented, so separating cracks in the concrete are not reached [2]. Further descriptions of the mechanisms, and types of pre-applied waterproofing membranes can be found in Ref. [3].

Pre-applied mechanically bonded membranes often use nonwovens for bonding. During concreting, the nonwovens are filled with cement paste so that capillary voids in the nonwovens are closed and a

waterproof bond is formed. These systems are widely used in the market, probably because of the simple and inexpensive production.

Meyer et al. [4] phenomenologically investigated the development of the nonwovens waterproof bond. Various membranes were installed with fresh concrete. After hardening, 5 bar water pressure were applied onto the bonding layer via a defect in the sealing layer. Especially an adequate compaction energy was found necessary to achieve a waterproof bond. However, the used test method was associated with high scatter in the results, so that it was not possible to record favorably acting nonwoven properties or the behavior of the nonwovens themselves.

Other experimental approaches to investigate the behavior of nonwovens during concreting are not available so that no nonwoven optimization is possible. Also, other research on nonwovens within concrete applications do not provide any indications. Nonwovens are used in cement-nonwoven composites as a substitute for asbestos fibers [5] or in combination with carbon-reinforced concrete [6]. In contrast to pre-applied bonded membranes, the nonwovens are impregnated

^{*} Corresponding author.

E-mail address: ulli.heinlein@th-nuernberg.de (U. Heinlein).

<https://doi.org/10.1016/j.jobe.2021.103531>

Received 30 August 2021; Received in revised form 25 October 2021; Accepted 26 October 2021

Available online 30 October 2021

2352-7102/© 2021 The Authors.

Published by Elsevier Ltd.

This is an open access article under the CC BY-NC-ND license

(<http://creativecommons.org/licenses/by-nc-nd/4.0/>).

separately in cement paste and are not subject to the concreting process. Nonwovens are also used as filters on the concrete surface in Controlled Permeable Formworks (CPF). They remove excess water and air inclusions from the concrete surface and thus improve durability [7–11], whereby the cement paste is retained by small pore radii (4–35 μm [12]). Fresh concrete is also applied to nonwovens but without forming a bond so that the CPF can be removed after concrete hardening.

Meanwhile, the behavior of loose nonwovens under mechanical load is well investigated. When exposed to compression, fiber bending between fiber bonds lead to compression, according to *van Wyk* [13]. Upon unloading, the thickness recovers due to the elasticity of the fibers, but a plastic deformation (thickness loss) can occur due to slippage at friction-based fiber bonds [14,15]. The thickness loss depends on external influences such as the loading level [16], the number of loading cycles [17], and the holding time of the load [18] and on structural properties of the nonwovens, such as the type and number of fiber bonds [17,19,20], nonwoven thickness and porosity [16]. For example, needle-punched nonwovens show a high thickness loss due to their low number of friction-based fiber bonds.

The fluid permeability of nonwovens depends on pore properties such as porosity, pore size, tortuosity, and fiber orientation [21–23]. In simplification, the permeability decreases when the nonwoven thickness, density, or basis weight increases and generally the ‘bonding energy’ of the nonwoven increases [24–28]. Another application area of nonwovens is filtration, where they are used for cake or depth filtration. Solid-liquid filtration models are based on permeability relations like described from *Darcy* in Equation (1) or with similar proportionalities from *Kozeny-Carman* [29,30].

$$Q = -\frac{k \Delta p}{\eta L} \quad (1)$$

where Q is the volumetric flow rate, k is the specific permeability coefficient of the filter, η is the fluid viscosity, and Δp is the pressure difference over the conduit length of fluid flow L . If, for example, filtration is carried out under the principles of cake filtration at constant pressure, a decrease of filtrate flow rate over time results since solid particles accumulate on the filter surface and increase the length of fluid flow. Further information on solid-liquid filtration can be found in Ref. [30].

Imaging techniques often support experimental studies on nonwovens. Early works, e.g., by *Hearly and Purdy* [31], relied on incident light microscopes. Nowadays, nonwovens are increasingly digitized by X-ray micro-computed tomography (micro-CT) [32–40]. Basic information on the use of micro-CT scans on nonwovens can be found in Ref. [41]. Micro-CT scans are also used for concrete specimens and were reviewed in Ref. [42]. Nevertheless, there are still few studies for concrete specimens with synthetic macro [43–45] or microfibers (35 μm) [46]. For the selective analysis of microfibers, high resolution (0.5 μm) became necessary due to the fibers’ small diameters and low densities resulting in high scanning efforts.

The following article aims to understand the macroscopic behavior of nonwovens during concreting to improve these often-used systems’ reliability. This article examines the change in compression, porosity, and lateral water migrations with concrete placement and compaction. The waterproof bond was thereby indirectly determined with a novel method to gain values with adequate scatter in the results. The general macroscopic nonwoven behavior during concreting was derived to identify favorable nonwoven properties and practice-oriented installation recommendations.

2. Materials and methods

2.1. Methodical approach

Four types of tests were carried out: First, the development of the waterproof bond was determined in practice-oriented hydrostatic tests.

Second, mechanical tests determined the compressional behavior of the nonwovens outside of concrete placement. Third, the nonwovens compression during concreting was determined using microsections, which indirectly led to the quality of the waterproof bond. Fourth, micro-CT scans were performed to show the change in porosity. Table 1 lists the experimental variations.

2.2. Materials

2.2.1. Nonwoven

Seven internationally available pre-applied bonded membranes were investigated with a nonwoven bonding layer (S1–S7). The membranes were analyzed using the entire pre-applied membrane since the nonwovens cannot be separated unchanged from the sealing layer, and the waterproof bond cannot be determined on loose nonwovens. Fundamental structural properties of the examined nonwovens were determined in Ref. [3] and presented in Table 2. The nonwovens are laminated to sealing layers made of non-swellable polymers like polyvinylchloride (PVC), flexible polyolefines (FPO), or ethylene-propylene-diene rubber (EPDM) (S1–S6), or swellable sealing layers (S7).

In the concreting process, all seven pre-applied bonded membranes were tested for changes in nonwoven thickness using short ($t = 0$ –2.5 s) and very long compaction times ($t = 20$ s) (see Table 1). Further investigations on the general behavior of the nonwovens in the concreting process were carried out mainly on S3 and S5. These membranes were easy to evaluate due to their relatively large nonwoven thickness and the distinct transition between the sealing layer and the nonwoven. Due to the comparable results of the seven pre-applied bonded membranes in the examined compaction times, representative results can be assumed.

2.2.2. Concrete

Pre-applied bonded membranes are usually combined with waterproof concrete mixtures. Therefore, a Portland limestone cement CEM II/A-LL 32.5 R with a cement content of 320 kg/m^3 , a water/cement ratio of 0.55, and a grading curve A/B 32 with quartzitic round grain was used [47,48]. The fresh concrete was adjusted to a flow of 48 cm according to DIN EN 12350–5 [49] and had a fresh concrete density of 2410 kg/m^3 according to DIN EN 12350–6 [50]. The vibration compaction was achieved with either a site-typical high-frequency internal vibrator (\varnothing 55 mm; frequency of 200 Hz) or a laboratory typical vibration table (frequency of 167 Hz).

2.3. Methods

2.3.1. Lateral water migration tests

Lateral water migration tests were carried out first to reproduce previous studies. The membranes S3 and S5 were installed in 48 composite specimens with dimensions of $l/w/h = 200/200/80$ mm, with the membrane having a central defect with a diameter of 25 mm. The concrete compaction was between 0 s and 15 s using an internal vibrator.

After 28 days of water storage, the waterproof bond was tested based on DIN EN 12390–8 [53]. Hydrostatic water pressure of $p = 5$ bar was applied to the defect in the sealing layer for three days. A fluorescent tracer (Uranin AP, CAS No. 518-48-8; 0.17 g/l) was added to the water. After testing, the membrane was removed from the concrete, and lateral water migrations became visible under UV light. Due to the dimensions of the test stand, the maximum penetration depth from the edge of the defect was 45 mm. The test equals the method in the previous study of *Meyer et al.* [4], was similar to the modified version of ASTM D 5385 [54] and was described in detail in Ref. [55].

2.3.2. Mechanical thickness measurements and compression properties

Mechanical measurements were done according to ISO 9073–2 [56] to determine the nonwovens’ product scatter, verify the accuracy of the

Table 1
Methodical approach and experimental variation.

Test	Variation and aim	Membrane	Load p [kPa]	Vibration compaction time t [s]	Nr. of samples
Lateral water migration tests	Change in lateral water migration resistance	S3; S5	2	0/1/2/5/10/15	48
			20	2/5	6
Mechanical properties before concreting	Thickness determination	S1 – S7	0.5	–	224
	Compression behavior under cyclic loading (2 cycles)	S3; S5	0.5–20–0.5 (8 load stages)	–	10
Optical determination of the nonwoven thickness change during concreting using microsection specimens (length $l = 50$ mm)	Thickness change during concreting using:	S3; S5	2	0/1/3/8/20	24
			20	0/0.5/1/1.5/2.5/3/8/20	50
	• Internal vibrator & horizontal orientation of the pre-applied membrane	2	0/1/3/8/20	16	
	• Internal vibrator & vertical orientation of the pre-applied membrane	20	1/3/8/20	18	
	• Vibration table & horizontal membrane	20	20/55/90	12	
	• Vibration table & vertical membrane	20	20/55/90	12	
Micro-CT scans	Porosity change and spatial presentation	S3	20	0.5/1/1.5/2.5/20	50
			20	0/1/8/20	4

Table 2
Structural properties of seven mechanical bonded pre-applied waterproofing membranes [3]

Property	Unit	Individual mean values \bar{x} of $n = 7$ tested products							Test method, number of samples per product and average standard deviation \bar{s} in the test
		S1	S2	S3	S4	S5	S6	S7	
Nonwoven basis weight	g/m ²	62	47	129	36	113	92	83	8 samples per product, $\bar{s} = 7.1$ g/m ²
Nonwoven thickness (unloaded)	mm	0.52	0.20	0.82	0.31	1.08	0.50	0.68	DIN EN 1849–2 [51]; 8 samples per product; $\bar{s} = 0.08$ mm
Fiber diameter	μm	24/35	13	33	25	23	26	11/21	DIN 65571–2 [52]; 35 samples per product; $\bar{s} = 2.7$ μm
Fiber material	–	PE/PP	PES	PP	PP	PP	PP	PES	FTIR; 2 samples per product
Nonwoven porosity	[–]	0.87	0.82	0.83	0.87	0.87	0.80	0.91	$\varepsilon = 1 - \frac{m}{\rho \cdot T \cdot A}$ (m : nonwoven basis weight, ρ : density of fibers, T : thickness of the nonwoven; A : area)
Nonwoven bonding		NP	CB	NP	HE	NP	HE	NP	NP: Needle punching; CB: Calendar bonding; HE: Hydroentenglament

optical measurement method from Chapter 2.3.3, and reproduce the compressional behavior and thickness loss of the nonwovens during concreting.

The product scatter was investigated at a compressive load of 0.5 kPa. Specimen were examined from four roll sections with eight specimens each ($n = 32$) per membrane. The mechanical measurements were performed with the Hildebrand HTG-A thickness tester with a measurement accuracy of 0.001 mm. The thickness was determined 30 s after the test stamp was placed on the nonwoven.

Next, the compressional behavior of the nonwovens was determined. The maximum pressure in the compression tests was selected to 20 kPa. On the one hand, this is a typical load level in mechanical thickness measurements. On the other hand, it corresponded to a concrete height of 0.83 m, which is not exceeded in practice in a single-layer concrete pour. The compression of the nonwovens C_{nw} is calculated in principle according to Equation (2):

$$C_{nw} = \frac{\Delta T_{nw}}{T_{nw,0}} = \frac{T_{nw,0} - T_{nw,loaded}}{T_{nw,0}} \quad (2)$$

where $T_{nw,0}$ is the initial (unloaded) thickness and $T_{nw,loaded}$ is the loaded thickness. As is common in nonwoven studies, compression is shown positive. Since the tests were carried out using the entire pre-applied membranes, the compression of the sealing layer had to be considered. The sealing layer was individually measured using an uncoated edge strip from a longitudinal joint, and the material behavior

was considered in the evaluation. The nonwoven compression was then calculated using Equation (3):

$$C_{nw} = \frac{T_{total,0} - T_{total,loaded} - \Delta T_{SL}}{T_{total,0} - T_{SL,0}} \quad (3)$$

where $T_{total,0}$ and $T_{SL,0}$ correspond to the unloaded total and sealing layer thickness, $T_{total,loaded}$ to the total thickness at higher loading, and ΔT_{SL} to the change in thickness of the sealing layer due to loading. Compared to direct measurement, Equation (3) results in an increased measurement inaccuracy, which was acceptable due to the merely comparative nature of the measured values.

Also, the thickness loss after a mechanical loading cycle was determined to simulate a concreting process. This was done for membranes S3 and S5, which were more often included in the concreting tests due to their good evaluability and large nonwoven thickness. Two load cycles of 0.5–20–0.5 kPa were applied in 8 stages (0.5–1–2–4–7–10–15–20 kPa), where each load level was maintained for 30 s. The thickness loss $C_{nw,loss}$ was obtained according to Equation (4):

$$C_{nw,loss} = \frac{T_{nw,0} - T_{nw,rec}}{T_{nw,0}} \quad (4)$$

where $T_{nw,rec}$ indicates the recovered nonwoven thickness after unloading. The sealing layer was considered according to Equation (5) under the assumption of elastic material behavior:

U. Heinlein and T. Freimann

Journal of Building Engineering 45 (2022) 103531

$$C_{nw,loss} = \frac{T_{total,0} - T_{total,rec}}{T_{total,0} - T_{SL,0}} \quad (5)$$

where $T_{total,0}$ and $T_{SL,0}$ are the initial total and sealing layer thicknesses at 0.5 kPa, and $T_{total,rec}$ is the recovered thickness after cyclic loading.

2.3.3. Optical determination of the nonwoven thickness

After concreting, the average nonwoven thickness was measured optically using an incident light microscope following DIN EN 1849-2 [51]. In order to obtain a representative average value, membrane strips were measured over a length of at least $l \geq 50$ mm with overlapping images, which were reunited via the algorithm presented in Ref. [57]. Subsequently, the average thicknesses were measured using the known pixel size. Compared to the mechanical measurement, thicknesses were independent of the nonwoven surface structure.

The change in thickness and compression indirectly measured the cement paste filling in the nonwoven and the resulting waterproof bond during the concreting process. As long as the nonwoven pores are unfilled, the fresh concrete pressure has a compressive effect on the nonwoven. As soon as the nonwoven pores are filled, the fresh concrete pressure is transferred via the stiffer cement paste, and the nonwoven thickness can recover due to the residual stress of the fibers. The link between nonwoven compression and its filling with cement paste will be proven in Chapter 3.3.3. Compared to the hydrostatic tests, the optical method is suited for comparative investigations due to a lower scatter of the results. It is also suitable to investigate a high number of specimens.

However, since the nonwoven thickness is subject to a relatively high scatter (see Chapter 3.2.1), the nonwoven thickness had to be measured at the same position before and after concreting. Thus, before concreting, a membrane strip with 8 mm width was removed from a 200/200 mm membrane center. This strip was measured optically on both cut edges, reinserted in the membrane specimen's original position, and fixed on the reverse side. After the specimen was used in the concreting process and after concrete hardening, the specimens were separated through the initially measured strip. The adjacent cut edges were then prepared as microsections and measured again (see Fig. 1).

2.3.4. Concreting and microsection preparation

A total of $n = 192$ microsection specimens were examined for changes in nonwoven thickness during concreting. The aim was to identify the influences of fresh concrete pressure ($p = 2\text{--}20$ kPa), vibration duration ($t = 0\text{--}20$ s), orientation of the nonwoven in the

formwork (vertical/horizontal) and compaction equipment (internal vibrator/vibration table).

During concreting, lateral leakage of cement paste or excess water had to be prevented since it led to fluid flow and erosion effects in the vicinity of the nonwoven. For this reason, the concrete was poured into watertight formworks. Mostly DN 200 KG pipes with a length of 1 m were used, where the membranes were fixed in the lid. For vertically oriented nonwovens, sealed column formworks were used. The compressive load was varied by the fresh concrete height (0.08–0.83 m); the concrete was placed in one layer and immediately compacted after placement. The specimens remained in the formwork for 28 days.

In order to ensure reproducible compaction times, an internal vibrator was equipped with time and location control (see Fig. 2). The time was controlled using a contactor between the transducer and the internal vibrator and the height position by a pneumatic cylinder. Both were operated via programmable time switching relays. The internal vibrator could be operated close to the pre-applied membrane with an accuracy of 0.1 s and be removed directly afterward.

Specimens without or with low compaction (0–1 s compaction time) were stabilized with epoxy resin after hardening of the concrete and before specimen preparation. For that, hoses were placed from the outside of the formwork onto the nonwoven before the concrete was placed. After the concrete hardening, a viscous, low-shrinkage epoxy resin with a high working time was passed through the hoses by gravity.

The microsections were finally prepared by wet grinding processes. In order to increase the fibers' visibility, the cement matrix on the surface was slightly removed using 18 % nitric acid for 30 s. The fibers were afterward still embedded in the matrix and not changed in the process due to their high chemical resistance of PP or PES. Fig. 3 shows an etched and analyzed specimen section in which the nonwoven was fixed with a red-colored epoxy resin.

2.3.5. X-ray micro-computed tomography

Micro-CT scans analyzed four samples of membrane S3 after varying compaction times to determine the porosity development during sustained compaction. A selective analysis of the fibers was not aimed at, so specimens with a diameter of 25 mm could be used.

The samples were taken as cores directly adjacent to the microsections from Chapter 2.3.4. In order to avoid influences from drilling, the membranes were initially cut by hand, and during analysis, the outer

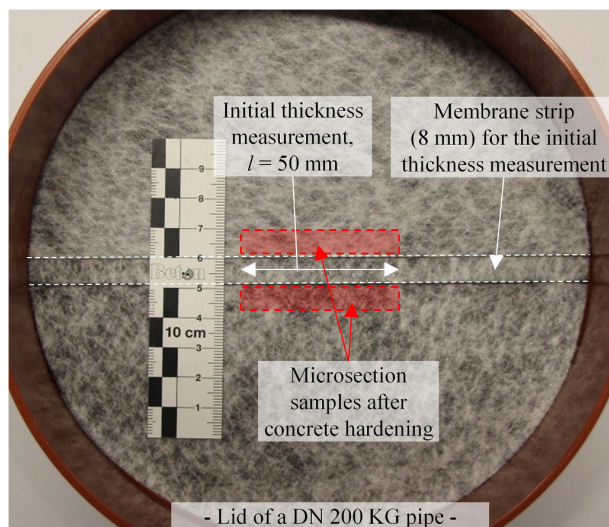


Fig. 1. Procedure for sample preparation. After the initial optical measurement, the membrane was placed in a lid of a DN 200 PVC-pipe.

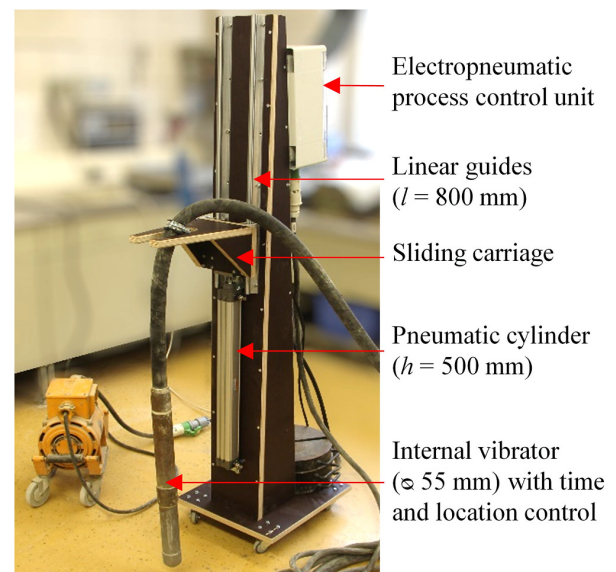


Fig. 2. Internal vibrator with time and location control.

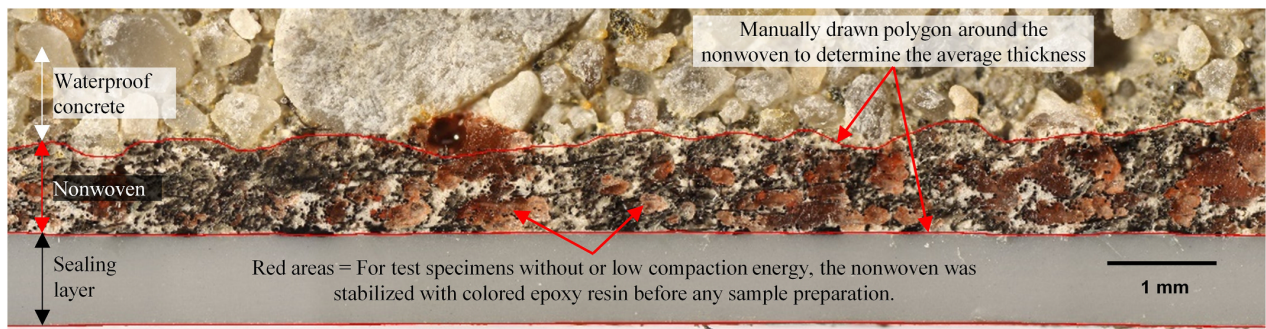


Fig. 3. Section of a 50 mm long image to determine the average thickness of the nonwoven S5 without compaction.

2 mm of the samples were not considered. The scans were done with the Bruker SkyScan micro-CT 1173 with a 130 kV X-ray source and a flat-panel sensor with 2240×2240 pixels. The voxel resolution in the scans was $14 \mu\text{m}$. The samples were examined with 80 kV voltage and 80 μA current, a Brass filter with 0.25 mm thickness, and a rotational path of 360° . The 3D volume reconstruction and subsequent segmentation and analysis were performed with Bruker software NRecon and CTAnalyser. The spatial representation was performed with CTVox.

During analysis, the distribution of gray values from the synthetic components and artifacts overlapped in the histogram. Therefore, a two-step binarization was necessary to interpret all synthetic materials as solids and minimize pores' artifacts. First, global thresholding was used. Second, appearing artifacts were removed by adaptive thresholding with a two-dimensional Otsu algorithm. The binary pore structure then matched the grayscale images. Nevertheless, the sealing layer towards the airside still showed pores since not all synthetic components could be included in the analysis. Since these pores were merely due to binarization and not physical pores, the sealing layer was not considered in Chapter 3.4.

3. Results

3.1. Lateral water migration resistance

The results of the hydrostatic tests of the membrane S3 and S5 with varying compaction times are given in Fig. 4. The graphs show linear connections of the arithmetic mean values, although the values in the tests usually scatter widely.

Without compaction, lateral water migrations of more than 45 mm occurred so that no waterproof bond was achieved. This corresponds to previous studies [4,55]. When vibration compaction began, lateral water migrations decreased. After 2–3 s compaction with a high-powered internal vibrator, no lateral water migration of more than 45 mm was detected. Upon further compaction, lateral water migration was further reduced - up to a compaction time of 10 s. Then, almost no change was measured.

3.2. Mechanical thickness measurements

3.2.1. Scatter of product thickness

The total thicknesses of the membranes S1-S7 were determined in average to $T_{\text{ges}} = 0.99\text{--}2.02$ mm, with nonwoven thicknesses between $T_{\text{nw}} = 0.19\text{--}1.07$ mm and a maximum nonwoven scatter of $\Delta T = 0.12\text{--}0.37$ mm per product (see Table 3). High product scatters are typical for nonwovens [29] and confirm that the compression change during concreting must be measured on the same specimen before and after the concreting process.

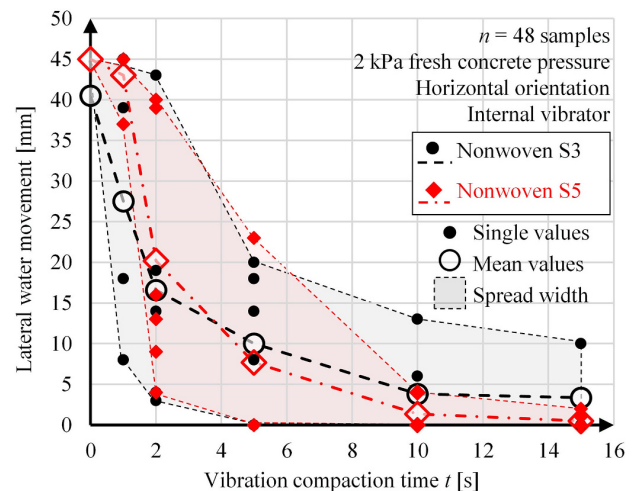


Fig. 4. Lateral water migrations after variable vibration compaction times of the nonwovens S3 and S5.

3.2.2. Change of the nonwoven thickness at 2 and 20 kPa

The thicknesses of the nonwovens changed at a compressive load of 2 kPa by $\Delta T_{\text{nw},2\text{kPa}} = 0.01\text{--}0.12$ mm and at a compressive load of 20 kPa by $\Delta T_{\text{nw},20\text{kPa}} = 0.04\text{--}0.37$ mm (see Table 3). The corresponding compressions were $C_{\text{nw},2\text{kPa}} = 0.02\text{--}0.27$ at 2 kPa compressive load and $C_{\text{nw},20\text{kPa}} = 0.20\text{--}0.58$ at 20 kPa. The compression results at 20 kPa compressive load are shown as box plots in Fig. 5.

3.2.3. Nonwoven thickness loss

The thickness losses for the membranes S3 and S5 during the mechanical measurement were found to be $C_{\text{S3,nw,loss}} = 0.181$ and $C_{\text{S5,nw,loss}} = 0.139$ in the first cycle, with a standard deviation of $s_{\text{S3}} = 0.022$ and $s_{\text{S5}} = 0.007$. The thickness loss increased by 0.027 (S3) and 0.032 (S5) with a further loading cycle. Table 3 shows the individual mean values of the mechanical measurements.

3.3. Nonwoven compression during concreting

3.3.1. Accuracy of the optical measurement method

In order to evaluate the accuracy of the optical measurement method used, eight specimens per membrane were measured both with the standardized mechanical method (Chapter 2.3.2) and the described optical method (Chapter 2.3.3).

The results of both measurement methods were very comparable for membranes with unstructured surfaces. For example, the membrane S1 showed a mechanically measured thickness of $T_{\text{mech}} = 1.46\text{--}1.58$ mm

Table 3
– Experimental determined properties of the nonwovens

Average properties	Unit	Loading [kPa]	Individual mean values \bar{x}							Samples per product n	Average standard deviation \bar{s}
			S1	S2	S3	S4	S5	S6	S7		
Product thickness T_{ges}	mm	0.5	1.50	0.99	1.92	1.51	1.94	1.97	2.02	32	0.07
Nonwoven thickness T_{nw}	mm	0	0.52	0.19	0.84	0.37	1.07	0.51	0.70	8–15	0.07
Nonwoven thickness change	mm	2.0	0.02	0.02	0.08	0.05	0.09	0.03	0.08	8–15	0.01
ΔT_{nw}		20	0.14	0.08	0.29	0.16	0.29	0.18	0.26	8–15	0.05
Thickness loss $C_{nw,loss}$ (1. cycle)	–	0.5–20	–	–	0.181	–	0.139	–	–	5	0.02

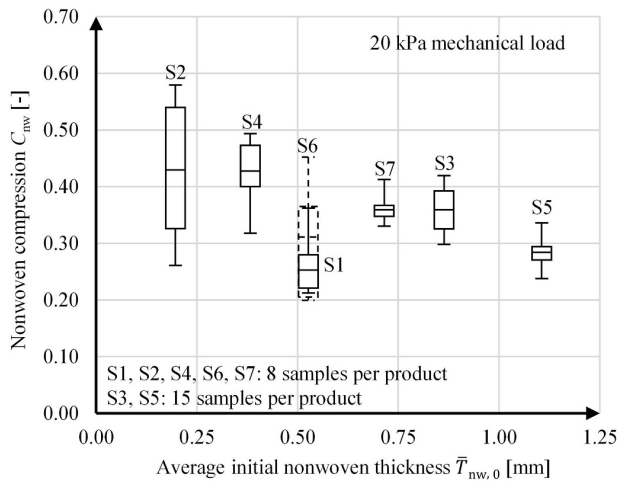


Fig. 5. Nonwoven compression of the membranes S1 – S7 as boxplots using 20 kPa load (Whisker show min/max-values).

with a mean value of $x_{mech} = 1.50$ mm. In the optical measurement, thicknesses between $T_{opt} = 1.44$ – 1.60 mm were obtained with a mean value of $x_{opt} = 1.50$ mm. The membranes S3, S5 and S6 showed similar results with a maximum deviation between the mean values of the measurement methods of $\Delta \bar{T} = \pm 0.02$ mm. Membranes with structured surfaces, i.e., from calendar bonding, yielded a maximal difference of $\Delta \bar{T}_{max} = 0.20$ mm between the mean values. This difference arises since the optical measurement determined the average thickness and the mechanical method the maximum thickness. The difference is not relevant for the optical evaluations in Chapter 3.3.2.

Furthermore, the measurement inaccuracy during the optical measurement was investigated. Two pairs of specimens (before/after concreting) of the membranes S3 and S5 were measured five times each, with at least one day interval. A maximum compression deviation of $\Delta C_{nw} = 0.031$ was obtained.

3.3.2. Compression of vertically installed nonwovens

The membranes S3 and S5 were vertically installed with 2 and 20 kPa fresh concrete pressure and sustained compaction with an internal vibrator (see Fig. 6). The longest compaction time was 20 s, which is unusual in practice but was necessary to achieve a final nonwoven compression.

After placing the fresh concrete ($t = 0$ s), the membranes were compressed depending on the fresh concrete pressure. At 20 kPa fresh concrete pressure, for example, S5 showed compression $C_{S5, NW, 0s} = 0.28$ – 0.32 , which is within the values of the mechanical measurement from Chapter 3.2.2 with $C_{S5, NW} = 0.24$ – 0.34 .

With the onset of compaction, the nonwoven thickness recovered as cement paste filled the pore structure. The load on the nonwoven decreased, allowing the nonwoven compression to recover due to the residual stress of the fibers. The resulting curve is similar to a visco-elastic retardation curve in mechanical tests with a continuous decrease

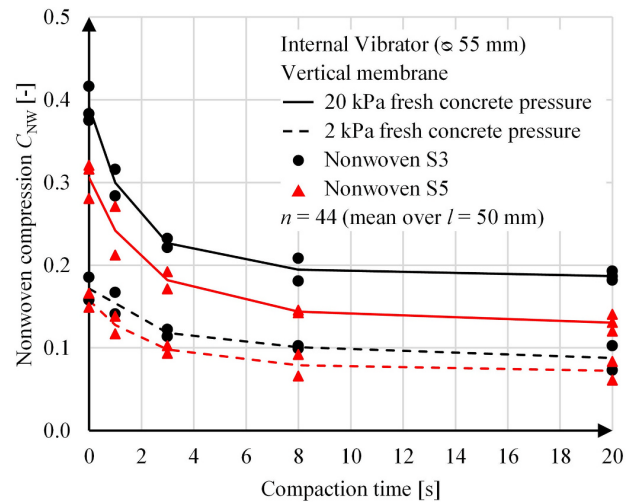


Fig. 6. Compression of a vertically placed nonwoven during ongoing compaction with an internal vibrator.

of compression.

Up to a compaction time of 8 s, higher concrete pressure resulted in faster decompression. For example, the slope ($\Delta C_{NW}/\Delta t$) of membrane S3 at a pressure of 20 kPa within 0–3 s was 2.4 times steeper in comparison to 2 kPa.

With compaction times exceeding 8 s, no further decompression occurred. This corresponds to the hydrostatic tests, where the nonwovens had a fully developed waterproof bond after this time. Furthermore, the nonwovens showed a thickness loss of $C_{S3, NW, loss} = 0.187$ for S3 and $C_{S5, NW, loss} = 0.131$ for S5. These values correspond to the mechanical cycle test. For example, the membrane S5 showed a mean mechanical thickness loss of 0.139 (see Table 3).

3.3.3. Correlation between lateral water migration and nonwoven compression

Fig. 7 compares the graphical curves for membrane S5 from the hydrostatic tests (Fig. 4) and the compression changes during concreting (Fig. 6). Note that the axis scaling was adjusted to compare the max/min values of the methods and that the lateral water migration was limited to 45 mm due to the test stand.

The graphical course of the compression change was very similar to the lateral water migrations. This was reproduced for the membrane S3 and showed that the proposed thickness measurement can be used as an indirect optical measure of the quality of the waterproof bond. Since the thickness measurement was not limited to the dimensions of the test stand nor linked to high scatter, the measurements at low compaction times were more reliable.

3.3.4. Compression of horizontally installed nonwovens

In the first seconds of compaction, the decompression slope of horizontally installed membranes was comparable to the slope of vertically

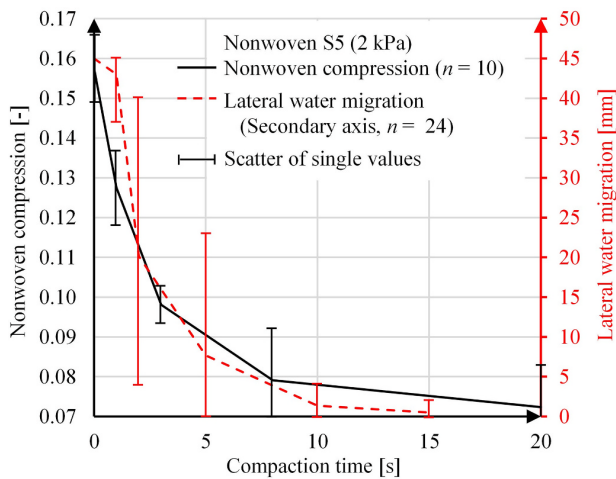


Fig. 7. Comparison of slopes of the compression change of vertical oriented nonwovens and lateral water migration resistance at 2 kPa fresh concrete pressure (Note the change in scale of the axes).

oriented specimens, as shown in Fig. 8. However, it is striking that with increasing compaction time, no thickness loss remains; the nonwoven thickness reaches the original unloaded thickness within a remaining compression of $-0.016 \leq C_{NW} \leq 0.037$. The nonwovens' typical thickness loss is therefore overcome. The difference between horizontally and vertically oriented specimens is clearly above the optical measurement inaccuracy from Chapter 3.3.1.

A fully recovered thickness was reproduced for all tested membranes S1–S7, using an internal vibrator and 20 s compaction time. Nonwoven compressions remained between $-0.021 \leq C_{NW} \leq 0.039$. Plotting the nonwoven thicknesses before and after concreting against each other lead to a linear regression with a slope of $y = 0.989x$ and a coefficient of determination of $r^2 = 0.997$ (see Fig. 9).

Compared to the vertically oriented nonwovens, which showed a thickness loss, the further decompression of horizontally oriented specimens cannot improve the waterproof bond. The hydrostatic tests and the thickness measurements from Fig. 6 showed that the nonwoven filling was completed after 8 s compaction time. The difference to vertically installed nonwovens will be further discussed in Chapter 4.

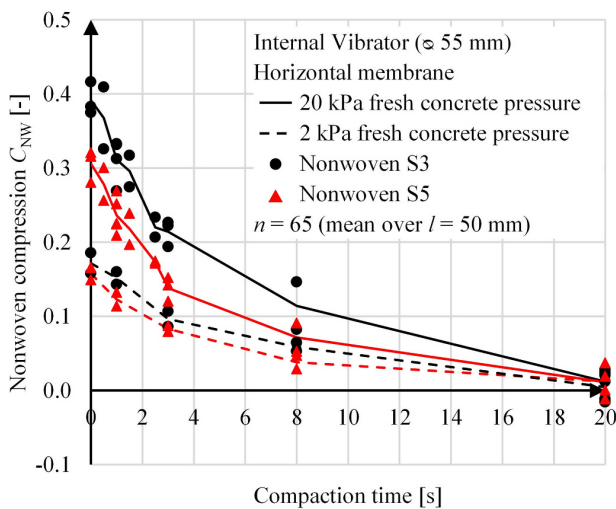


Fig. 8. Compression of a horizontally placed nonwoven during ongoing compaction with an internal vibrator.

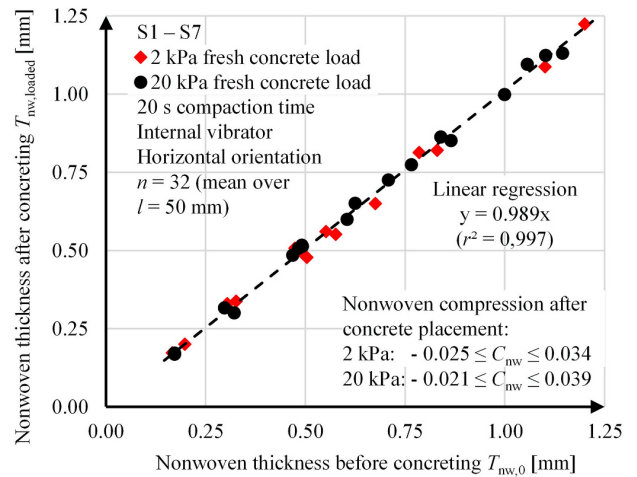


Fig. 9. Nonwoven thicknesses of S1–S7 with horizontal orientation after 20 s compaction with an internal vibrator.

3.3.5. Nonwoven compression using a vibration table

In order to investigate the influence of the compaction equipment, the S3 and S5 membranes were further installed on a vibration table - in vertical and horizontal orientation. Fig. 10 shows the compression values for S3 and, for comparison, the results using an internal vibrator. The mean values at $t = 0$ s are derived from Fig. 6.

Firstly, the vibration table's effect is significantly reduced compared to the internal vibrator as longer compaction times are required for decompression. Thus, the compaction device also strongly influenced the decompression and the development of the waterproof bond. Secondly, when the vibration table is used, the thickness loss is overcome at long compaction times, even in the vertical orientation, which will be discussed in Chapter 4. Thirdly, it can be seen that the compressions are lower for the horizontally oriented specimen. The results of the membrane S5 are comparable.

3.3.6. Influence of the nonwoven properties

In order to identify favorable nonwoven properties for cement paste penetration, all membranes S1–S7 were installed using the internal vibrator and practice-oriented compaction times ($t = 0.5/1.0/1.5/2.5$ s).

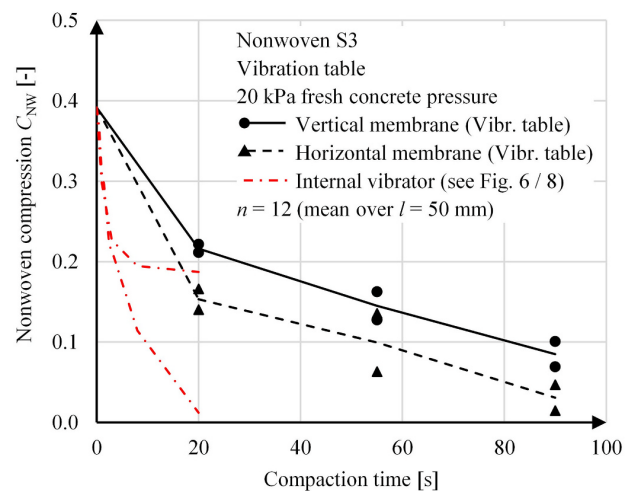


Fig. 10. Compression of the nonwoven of the membrane S3 during ongoing compaction on a vibration table.

The graphical decompression curves of all membranes were similar to those of S3 and S5 in Fig. 8 – but different slopes between the membranes became visible. A high initial slope corresponds to a fast decompression, and therefore to a fast stress release by filling the nonwoven pores with cement paste.

In order to compare the membranes with each other, the slope of each membrane was expressed as a compressional change per time $\Delta C_{NW}/\Delta t$. This coefficient was determined for the four applied time steps ($t = 0.5/1.0/1.5/2.5$ s) and then summarized, leading to one value per nonwoven expressing the overall compression change per time. The values of all nonwovens S1–S7 were then set in one diagram and plotted against various nonwoven properties to identify possible correlations. The regression approaches are listed in Table 4.

Fig. 11 shows the summarized change of the nonwoven compression per time in relation to the void volume in the nonwoven, which led to the best correlation. The void volume was calculated using the nonwoven thickness T_{NW} and porosity ϵ (see Table 2). The logarithmic approach has a coefficient of determination of $r^2 = 0.822$. Without membrane S1, the coefficient of determination would increase to $r^2 = 0.98$.

According to this correlation, nonwovens with a low void volume and a low thickness showed a faster decompression due to a faster cement paste filling. Thus, in practice, thicker and more porous nonwovens require longer compaction times to achieve a sufficient water-proof bond.

3.4. Porosity in the bonding layer

Fig. 12 shows the total porosity of four micro-CT scans over the sample height with increasing compaction times using an internal vibrator. Due to the small number of samples, it should be noted that no representativeness is given.

Without compaction, a high porosity of 23.5 % was present in the interface layer between the nonwoven and sealing layer, which fits the lateral water migrations (Chapter 3.1). After a short compaction time of 1 s with an internal vibrator, the porosity in the interface layer decreased to 3.8 %. After 8 s compaction, the porosity in the bonding layer corresponded to that of the concrete. No further change was derived with longer compaction times, which also fits the results given in Chapters 3.1 and 3.3.2.

After 1 and 8 s of compaction, a second porosity maximum can be seen in the interface between the bonding and concrete layer. This matches microscopic images, which often showed air voids on top of the nonwoven. Presumably, due to surface tension, air pores remained attached to the fibers and were released into the concrete only upon further compaction.

Fig. 13 shows the spatial distribution of the four specimens' open and closed pore structure, where open pores extend beyond the specimen edge. After 1 s compaction time, the open porosity in the bonding layer drastically decreased, and the entrapped air was released into the concrete. Further compaction decreased the total porosity in the concrete. A certain number of closed pores remained in the nonwoven even after extensive compaction.

Table 4

– Regression approaches between compression change per time and various nonwoven properties

Nonwoven properties	Regression	Coefficient of determination r^2
Void volume	$-0.106\ln(x)+0.132$	0.822
Thickness	$-0.105\ln(x)+0.150$	0.810
Basis weight	$-0.120\ln(x)+0.726$	0.591
Fiber diameter	$-0.130\ln(x)+0.630$	0.418
Porosity	$-0.392\ln(x)+0.149$	0.057

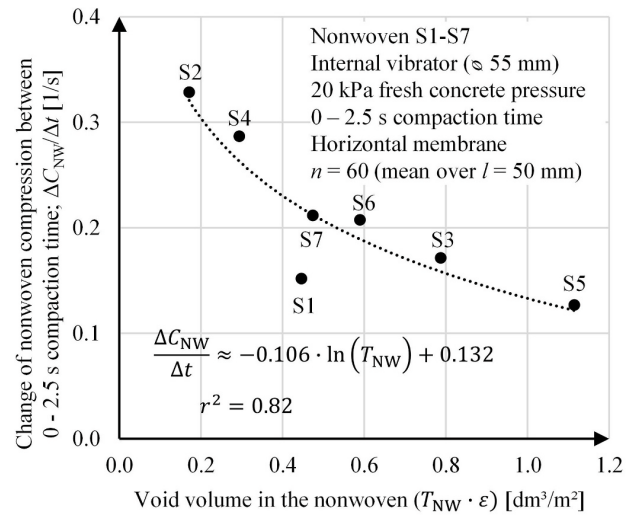


Fig. 11. Compression change per time of the nonwovens S1 – S7 during the initial 2.5 s compaction time with an internal vibrator.

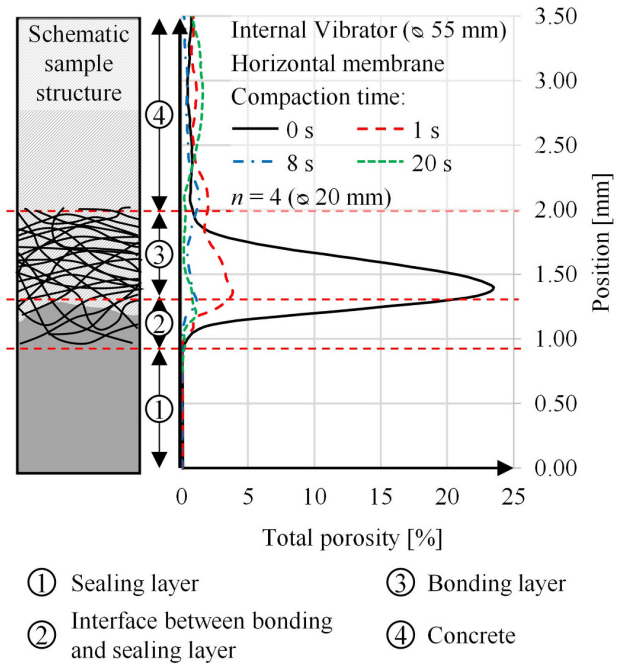


Fig. 12. Change of the total porosity within the nonwoven of the pre-applied membrane S3 during ongoing compaction with an internal vibrator and 20 kPa fresh concrete pressure.

4. Discussion

4.1. Macroscopic nonwoven behavior

Nonwovens of pre-applied bonded membranes show a load and compressional behavior that is common for technical nonwovens. In mechanical tests, they are compressed under load, recover when unloaded and suffer a remaining thickness loss. During concreting, the nonwovens behave similarly. When the fresh concrete is placed, the nonwovens are compressed depending on the fresh concrete pressure. When compaction begins, a recovery occurs, and a decrease in

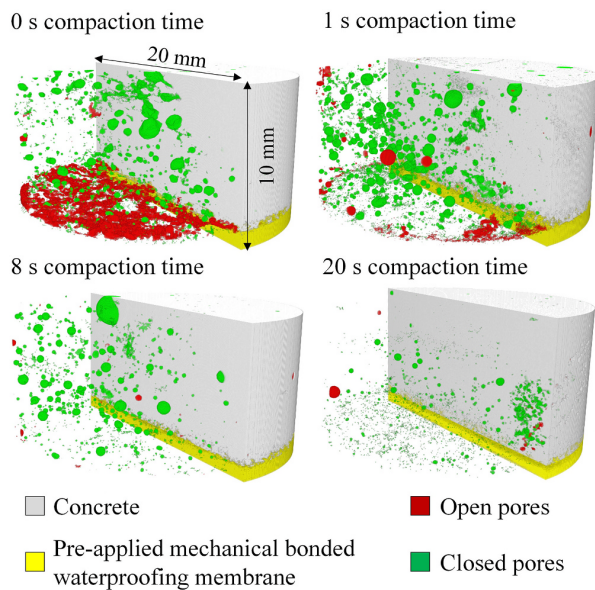


Fig. 13. Micro-CT scans of cylindrical specimen with the pre-applied membrane S3 ($\epsilon/h = 20/10$ mm) visualizing the change in porosity in the nonwoven and within their vicinity during ongoing compaction and 20 kPa fresh concrete pressure.

compression and lateral water migrations can be seen. Using an internal vibrator, no further change occurred after 8–10 s compaction. Vertically installed membranes also showed a thickness loss.

The optical measurement of the thickness change was carried out assuming that nonwovens can only recover if the fresh concrete pressure is transferred via cement paste in the nonwoven pores. Comparison with practice-oriented hydrostatic tests has shown comparability for vertically installed membranes. Furthermore, the method shows acceptable scatter and can be used for a high number of specimens.

In the concreting tests, the change in thickness showed proportionalities to the compressive load, the vibration equipment, the void volume, and the nonwoven thickness. These dependencies suggest that the separation of cement paste from concrete occurs in a filtration process. The nonwoven acts as filter medium, the cement paste as filtrate then fills up the pore structure. The following proportionalities exist in filter theories of solid-liquid filtration, which are based, for example, on Darcy's law (see Equation (1)) and were also found in the concreting process:

- $Q \sim 1/\eta$: Flow rate is indirectly proportional to fluid viscosity. This can explain the strong influence of the compaction equipment in the concreting process. Vibration lowers the yield point of cement paste. Also, a higher concrete flow was found beneficial in Ref. [4].
- $Q \sim 1/L$: Flow rate is indirectly proportional to the flow length. An increasing nonwoven thickness was also observed unfavorable in the concreting tests.
- $Q \sim \Delta p$: Flow rate is proportional to pressure difference. During concreting, higher fresh concrete pressure also led to a faster change in nonwoven thickness and thus faster cement paste filling.
- $Q \sim k$: Flow rate is proportional to permeability coefficient. Presumably, the nonwoven's average pore size and fiber orientation also matter, influencing the nonwoven permeability. However, relevant structural properties could not be reliably determined due to the sealing layer of the membranes.

If filtration would take place under stationary conditions without cake formation or clogging of the filter, a constant volume flow rate of

filtrate could be expected corresponding to the permeability. However, the high solids content of concrete suggests that cake formation initiates very quickly, which would result in a decreasing flow rate over time at constant pressure [58]. For a linear increase in nonwoven void volume, the necessary filtration time would increase more than linear. This was observed indirectly via the development of the compression change of all membranes S1–S7 in Figure 11. Due to the cake formation, increasing void volumes lead to a more than linear increase in compaction times to achieve decompression and cement paste filling. In practice, high-powered compaction equipment, high concrete flow, and fresh concrete pressure, as well as nonwovens with low void volume and thicknesses, will behave beneficially in creating a waterproof bond.

In order to further verify the filtration theorem and identify other favorable nonwoven properties, 'loose' nonwovens should be included in concrete tests under varying compressive loads and vibration modes, and filtration properties such as filter resistance and filtrate should be analyzed. Established tests are, for example, VDI 2762 [59] or using a Compression-Permeability Cell [58].

4.2. Potential microscopic nonwoven effects

Nonwovens are usually subject to pore size distribution [31]. Considering the scatter in the hydrostatic tests, it could be argued that the cement paste filling is not a homogeneous process. Instead, pores with a larger pore diameter, low tortuosity, and primarily vertical oriented fibers may reduce the local filter resistance and result in locally faster cement paste filtration – like at pores of the needle compaction. Also, in-plane permeability may contribute to cement paste distribution inside a nonwoven, which also needs further investigation.

Further effects became visible during the concreting tests. Using an internal vibrator, a distinct difference due to the nonwoven's orientation was observed. A vibrating table did not reproduce this effect. Therefore, the oriented vibration amplitude of the internal vibrator may be a relevant factor. Vertically oriented nonwovens experienced a thickness loss, while the vibration amplitude of the internal vibrator acted orthogonally and thus compressed the vertical nonwoven. Horizontal orientation left no thickness loss, while the amplitude acted parallel to the nonwoven and thus as a radial shear force. Therefore, parallel acting vibrations overcome the thickness loss, possibly due to loosening the fiber friction points in the nonwoven. This would require fibers to show movement to some degree during dynamic concrete compaction.

Another influence in concreting is the buoyancy force acting on horizontally oriented nonwovens due to the density difference between fibers ($\rho = 0.9\text{--}1.3$ g/cm³) and cement paste ($\rho \approx 1.7$ g/cm³). The buoyancy force can be estimated according to Archimedes' law using Equation (6):

$$F_A = g \cdot \rho_{\text{cement paste}} \cdot [\epsilon \cdot A \cdot T_{\text{NW}}] \quad (6)$$

where g is the acceleration due to gravity, ρ is the density of the cement paste, and the square bracket represents the nonwoven volume, which is calculated from the porosity ϵ , area A and thickness T_{NW} of the nonwoven according to Table 2. For the nonwoven S3, for example, this buoyancy force is around $F_A = 0.002$ kPa. The buoyancy acts at least on individual fibers, as can be observed from microsections. Partly, single fibers rose significantly higher into the concrete than expected due to their residual stress. However, the force is negligible compared to the compressive load. Thus, it cannot directly influence the decompression of the nonwoven - although the force may have a supportive effect on the above-discussed release of fiber friction points.

4.3. Recommendations for practice

During the filtration process, the nonwoven fills with cement paste and becomes waterproof. The porosity is rapidly reduced, and capillaries are closed. From a construction point of view, small water migrations in

the bonding layer are acceptable since they are also accepted at mounting parts. Therefore, even for currently used nonwovens with rather large void volumes, a compaction time of 2–3 s with a high-powered internal vibrator close to the membranes seems sufficient. Vast lateral water migrations are then no longer likely. Micro-CT scans showed that closed pores remain even with long compaction times – but did not contribute to extensive water movements. However, since no different internal vibrators were tested, the recommended duration should be extended for smaller, weaker devices. New nonwovens should be designed to require the shortest possible filtration time so that low thicknesses, low void volumes, and large average pore sizes are recommended. At the same time, these properties have to be considered against the adhesive tensile strength, which is required at least for formwork stripping.

4.4. Experimental limitations

Due to the experimental procedure and the samples used, the following limiting boundary conditions apply:

- The temporal change was only determined on a macroscopic level. The influence of specific nonwoven properties, micro-scale flow patterns, and fiber movements must be determined in further investigations.
- The tests were carried out with only one formwork size, concrete composition, and consistency. Also, the influence of the internal vibrator and its distance to the nonwoven was not investigated.
- The tests were carried out with undisturbed nonwoven specimens (dry, clean). The influence of water and dirt is not yet known.
- Polymers are strongly influenced by temperature. The tests were only carried out at room temperature.
- The investigations using the micro-CT were carried out without repeat samples on small samples of one membrane. Further samples are necessary for representative statements.

5. Conclusions

This paper aims to determine nonwovens' behavior during concreting and identify beneficial nonwoven properties for a waterproof bond to enable optimization. The following conclusions can be drawn:

- The proposed optical measurement based on the nonwoven thickness change during concreting has proven to be well quantifiable, simple, and correlates with lateral water migrations for vertically installed membranes.
- Nonwovens of pre-applied bonded membranes have a typical mechanical and compressional behavior for technical nonwovens. During concreting, the nonwovens first undergo compression according to the fresh concrete pressure.
- Without compaction, no waterproof bond is achieved.
- During vibration compaction, the thickness changes fast in the beginning and slower as compaction continues. If an internal vibrator is used, the decompression depends on the installation orientation. In the case of a vertical orientation, a thickness loss remains after complete filling with cement paste, corresponding to the thickness loss in cyclic loading.
- A vibration table results in slower decompression, probably due to damped vibration transmission through the formwork and membrane. Also, the nonwovens return to their original thicknesses after filling the nonwoven pores, even when arranged vertically.
- Compensation of the thickness loss may be due to vibrations that loosen fiber friction points. This assumes that fibers move in the dynamic concrete compaction.
- When compaction begins, the open porosity and lateral water migrations in the nonwoven decrease rapidly. Selective cement paste infiltration of larger pores with perpendicular fiber orientation

(needle pores) may be beneficial. Closed pores remain in the nonwoven even after extensive compaction but do not contribute to widespread lateral water movement.

- A compaction time of about 2–3 s with a high-powered internal vibrator seems sufficient for achieving a practical waterproof bond. This time has to be adjusted depending on the nonwoven thickness, void volume, concrete flow, and vibration equipment.
- In order to optimize nonwovens for cement paste filtration, they should have low thicknesses, low void volumes, and large average pore sizes. However, this may be contrary to a good adhesive tensile strength.

Author statement

The corresponding author Ulli Heinlein has acted in the following roles:

Conceptualization, Methodology, Investigation, Formal Analysis, Writing – original draft, Writing – reviewing and editing.

The author Thomas Freimann has acted in the following roles:

Funding acquisition, Resources.

Declaration of competing interest

The authors declare that they have no known competing financial interests or personal relationships that could have appeared to influence the work reported in this paper.

Acknowledgement

The authors would like to thank Prof. Dr.-Ing. K.-Ch. Thienel (Universität der Bundeswehr München) for the inspiring discussions and the possibility to use the micro-CT.

The present work is supported by the Bavarian Academic Forum in the collegium „Infrastruktur-Bauen-Urbanisierung“.

References

- [1] E.V. Deutscher Beton- und Bautechnik-Verein, DBV-Heft 44 "Frischbetonverbundsysteme (FBV-Systeme) - Sachstand und Handlungsempfehlungen" Fassung Oktober 2018, Eigenverlag DBV, 2018.
- [2] BS 8102:2009-11-30, Code of Practice for Protection of below Ground Structures against Water from the Ground. British Standards Institution, London.
- [3] U. Heinlein, K.-C. Thienel, T. Freimann, Pre-applied bonded waterproofing membranes: a review of the history and state-of-the-art in Europe and North America, *Construct. Build. Mater.* 296 (2021) 123751, <https://doi.org/10.1016/j.conbuildmat.2021.123751>.
- [4] L. Meyer, S. Bilgin, S. Filusch, T. Freimann, U. Heinlein, K. Herrmann, *Bauwerksabdichtung mit Frischbetonverbundfolie - Grundlagen zur Erstellung eines Regelwerks für eine innovative Bauart: Abschlussbericht F 3183, Fraunhofer IRB Verlag, Stuttgart, 2020.*
- [5] H. Pakravan, M. Jamshidi, M. Latifi, M. Neshastehriz, Application of polypropylene nonwoven fabrics for cement composites reinforcement, *Asian Journal of Civil Engineering (Building and Housing)* 12 (2011) 551–562.
- [6] T. Senckpiel-Peters, U. Häußler-Combe, H. Metschies, P. Eisewicht, *Entwicklung eines neuartigen leichten Deckenträgers aus Carbonbeton. Experimentelle und numerische Untersuchungen, Beton- Stahlbetonbau* 113 (2018).
- [7] W.F. Price, *Controlled Permeability Formwork*, CIRIA, London, 2000.
- [8] P.J. Schubel, N.A. Warrior, K.S. Elliott, An investigation into factors affecting the performance of composite controlled permeable formwork liners: Part II – filter medium, *Construct. Build. Mater.* 22 (11) (2008) 2235–2249, <https://doi.org/10.1016/j.conbuildmat.2007.08.006>.
- [9] H. Figueiras, S. Nunes, J.S. Coutinho, J. Figueiras, Combined effect of two sustainable technologies: self-compacting concrete (SCC) and controlled permeability formwork (CPF), *Construct. Build. Mater.* (23) (2009) 2518–2526, <https://doi.org/10.1016/j.conbuildmat.2009.02.035>.
- [10] S. Kothandaraman, S. Kandasamy, K. Sivaraman, The effect of controlled permeable formwork liner on the mechanical and durability properties of self-compacting concrete, *Construct. Build. Mater.* (118) (2016) 319–326, <https://doi.org/10.1016/j.conbuildmat.2016.05.083>.
- [11] E. Nolan, P.A.M. Basheer, A.E. Long, Effects of three durability enhancing products on some physical properties of near surface concrete, *Construct. Build. Mater.* 9 (1995) 267–272.
- [12] Z.Q. Yang, J.Z. Liu, W. Lin, J.P. Liu, D.G. Xu, Review of progress and applications of controlled permeability formwork in concrete engineering, *AMR (Adv. Magn.*

- Reson.) 821–822 (2013) 171–178, <https://doi.org/10.4028/www.scientific.net/AMR.821-822.171>.
- [13] C.M. van Wyk, 20—note ON the compressibility OF wool, *Journal of the Textile Institute Transactions* 37 (12) (1946) T285–T292, <https://doi.org/10.1080/19447024608659279>.
- [14] J.I. Dunlop, On the compression characteristics of fibre masses, *J. Textil. Inst.* 74 (2) (1983) 92–97, <https://doi.org/10.1080/00405008308631770>.
- [15] G.A. Carnaby, N. Pan, Theory of the compression hysteresis of fibrous assemblies, *Textil. Res. J.* 59 (5) (1989) 275–284, <https://doi.org/10.1177/004051758905900505>.
- [16] K.A. Asanovic, M.M. Kostic, T.V. Mihailovic, D.D. Cerovic, Compression and strength behaviour of viscose/polypropylene nonwoven fabrics, *Indian J. Fibre Text. Res.* (44) (2019) 329–337.
- [17] S. Sengupta, P. Ray, P.K. Majumdar, Effect of dynamic loading on jute-based needle-punched nonwoven fabrics, *Indian J. Fibre Text. Res.* 30 (2005) 389–395.
- [18] S. Jafari, M. Ghane, An analytical approach for the recovery behavior of cut pile carpet after static loading by mechanical models, *Fibers Polym.* 17 (4) (2016) 651–655, <https://doi.org/10.1007/s12221-016-6191-7>.
- [19] V.K. Kothari, A. Das, Compressional behaviour of nonwoven geotextiles, *Geotext. Geomembranes* (11) (1992) 235–253.
- [20] A. Das, R. Alagirusamy, B. Banerjee, Study on needle-punched non-woven fabrics made from shrinkable and non-shrinkable acrylic blends. Part II: transmission behaviour, *J. Textil. Inst.* 100 (4) (2009) 350–357, <https://doi.org/10.1080/00405000701819691>.
- [21] R. Vallabh, Modeling Tortuosity in Fibrous Porous Media Using Computational Fluid Dynamics, Dissertation at the North Carolina State University, 2009.
- [22] P. Dixit, S.M. Ishtiaque, R. Roy, Influence of sequential punching in layered structure of needle punched nonwoven on the filtration behavior, *Compos. B Eng.* 182 (2020) 107654, <https://doi.org/10.1016/j.compositesb.2019.107654>.
- [23] P. Soltani, M.S. Johari, M. Zarrebini, Tomography-based determination of transverse permeability in fibrous porous media, *J. Ind. Textil.* 44 (5) (2015) 738–756, <https://doi.org/10.1177/15280837152812357>.
- [24] H. Ventura, M. Ardanuy, X. Capdevila, F. Cano, J.A. Tornero, Effects of needling parameters on some structural and physico-mechanical properties of needle-punched nonwovens, *J. Textil. Inst.* 105 (10) (2014) 1065–1075, <https://doi.org/10.1080/00405000.2013.874628>.
- [25] O.B. Berkalp, Air permeability & porosity in spun-laced fabrics, *Fibres Text. East. Eur.* 14 (3) (2006) 81–85.
- [26] A. Rawal, A cross-plane permeability model for needle-punched nonwoven structures, *J. Textil. Inst.* 97 (6) (2006) 527–532, <https://doi.org/10.1533/joti.2005.0219>.
- [27] G.-S. Hwang, B.-L. Hwu, W.-H. Hsing, C.-K. Lu, Manufacturing effects on the hydraulic properties of needlepunched nonwoven geotextiles, *Geotext. Geomembranes* (16) (1998) 355–363.
- [28] R. Roy, S.M. Ishtiaque, Effect of fibre orientation on mechanical and functional properties of needle-punched nonwoven, *Indian J. Fibre Text. Res.* 44 (2019) 321–328.
- [29] S.J. Russell, *Handbook of Nonwovens*, (etc., CRC; Woodhead publishing limited, Boca Raton, 2007.
- [30] K. Luckert (Ed.), *Handbuch der mechanischen Fest-Flüssig-Trennung*, first ed., Vulkan-Verlag, Essen, 2016.
- [31] J.W.S. Hearle, A.T. Purdy, The structure of needle punched fabric, *Fibre Sci. Technol.* (4) (1971) 81–100.
- [32] S. S. Manickam, J.R. McCutcheon, Characterization of polymeric nonwovens using porosimetry, porometry and X-ray computed tomography, *J. Membr. Sci.* 407–408 (2012) 108–115, <https://doi.org/10.1016/j.memsci.2012.03.022>.
- [33] N. Chen, M.K. Koker, S. Uzun, M.N. Silberstein, In-situ X-ray study of the deformation mechanisms of non-woven polypropylene, *Int. J. Solid Struct.* 97–98 (2016) 200–208, <https://doi.org/10.1016/j.ijsolstr.2016.07.028>.
- [34] T. Ishikawa, K. Kim, Y. Ohkoshi, Visualization of a pillar-shaped fiber bundle in a model needle-punched nonwoven fabric using X-ray micro-computed tomography, *Textil. Res. J.* 87 (11) (2017) 1387–1393, <https://doi.org/10.1177/0040517516652351>.
- [35] F. Théron, E. Lys, A. Joubert, F. Bertrand, L. Le Coq, Characterization of the porous structure of a non-woven fibrous medium for air filtration at local and global scales using porosimetry and X-ray micro-tomography, *Powder Technol.* 320 (2017) 295–303, <https://doi.org/10.1016/j.powtec.2017.07.020>.
- [36] T. Ishikawa, Y. Ishii, K. Nakasone, Y. Ohkoshi, K. Kyong Hou, Structure analysis of needle-punched nonwoven fabrics by X-ray computed tomography, *Textil. Res. J.* 89 (1) (2019) 20–31, <https://doi.org/10.1177/0040517517736470>.
- [37] S.-Y. Jeon, W.-J. Na, Y.-O. Choi, M.-G. Lee, H.-E. Kim, W.-R. Yu, In situ monitoring of structural changes in nonwoven mats under tensile loading using X-ray computer tomography, *Compos. Appl. Sci. Manuf.* 63 (2014) 1–9, <https://doi.org/10.1016/j.compositesa.2014.03.019>.
- [38] S.-Y. Jeon, W.-R. Yu, M.S. Kim, J.S. Lee, J.W. Kim, Predicting the tensile strength of needle-punched nonwoven mats using X-ray computed tomography and a statistical model, *Fibers Polym.* 15 (6) (2014) 1202–1210, <https://doi.org/10.1007/s12221-014-1202-z>.
- [39] P. Soltani, M.S. Johari, M. Zarrebini, Effect of 3D fiber orientation on permeability of realistic fibrous porous networks, *Powder Technol.* 254 (2014) 44–56, <https://doi.org/10.1016/j.powtec.2014.01.001>.
- [40] P. Soltani, M. Zarrebini, R. Laghaei, A. Hassanpour, Prediction of permeability of realistic and virtual layered nonwovens using combined application of X-ray μ CT and computer simulation, *Chem. Eng. Res. Des.* 124 (2017) 299–312, <https://doi.org/10.1016/j.cherd.2017.06.035>.
- [41] M.A. Ali, R. Umer, K.A. Khan, W.J. Cantwell, Application of X-ray computed tomography for the virtual permeability prediction of fiber reinforcements for liquid composite molding processes: a review, *Compos. Sci. Technol.* 184 (2019) 107828, <https://doi.org/10.1016/j.compscitech.2019.107828>.
- [42] A. Du Plessis, W.P. Boshoff, A review of X-ray computed tomography of concrete and asphalt construction materials, *Construct. Build. Mater.* 199 (2019) 637–651, <https://doi.org/10.1016/j.conbuildmat.2018.12.049>.
- [43] P. Pujadas, A. Blanco, S. Cavalario, A de La Fuente, A. Aguado, Fibre distribution in macro-plastic fibre reinforced concrete slab-panels, *Construct. Build. Mater.* 64 (2014) 496–503, <https://doi.org/10.1016/j.conbuildmat.2014.04.067>.
- [44] J. Kaufmann, K. Frech, P. Schuetz, B. Münch, Rebound and orientation of fibers in wet sprayed concrete applications, *Construct. Build. Mater.* 49 (2013) 15–22, <https://doi.org/10.1016/j.conbuildmat.2013.07.051>.
- [45] A.C. Bordelon, J.R. Roesler, Spatial distribution of synthetic fibers in concrete with X-ray computed tomography, *Cement Concr. Compos.* 53 (2014) 35–43, <https://doi.org/10.1016/j.cemconcomp.2014.04.007>.
- [46] Y. Qin, H. Wu, Y. Zheng, W. Wang, Z. Yi, Microscopic texture of polypropylene fiber-reinforced concrete with X-ray computed tomography, *Adv. Civ. Eng.* 2019 (2019) 1–9, <https://doi.org/10.1155/2019/2386590>.
- [47] DIN EN 206:2013, *Beton - Festlegung, Eigenschaften, Herstellung und Konformität*; Deutsche Fassung EN 206:2013+A1:2016 (DIN EN 206). Berlin: Beuth Verlag GmbH.
- [48] DIN 1045-2:2008-08, *Tragwerke aus Beton, Stahlbeton und Spannbeton - Teil 2: Beton - Festlegung, Eigenschaften, Herstellung und Konformität - Anwendungsregeln zu DIN EN 206-1*. Berlin: Beuth Verlag GmbH. <https://doi.org/10.31030/1453177>.
- [49] DIN EN 12350-5:2019-09, *Prüfung von Frischbeton - Teil 5: Ausbreitmaß*; Deutsche Fassung EN 12350-5:2019. Berlin: Beuth Verlag GmbH. <https://doi.org/10.31030/3045714>.
- [50] DIN EN 12350-6:2019-09, *Prüfung von Frischbeton - Teil 6: Frischbetonrohddichte*; Deutsche Fassung EN 12350-6:2019. Berlin: Beuth Verlag GmbH. <https://doi.org/10.31030/3045731>.
- [51] DIN EN 1849-2:2019-09, *Abdichtungsbahnen - Bestimmung der Dicke und der flächenbezogenen Masse - Teil 2: Kunststoff- und Elastomerbahnen für Dachabdichtungen*; Deutsche Fassung EN 1849-2:2019. Berlin: Beuth Verlag GmbH. <https://doi.org/10.31030/3042454>.
- [52] DIN 65571-2:1992-11, *Luft- und Raumdichte; Verstärkungsfasern; Bestimmung des Filamentdurchmessers von Filamentgarnen; Längsprojektionsverfahren*. Berlin: Beuth Verlag GmbH. <https://doi.org/10.31030/2538052>.
- [53] DIN EN 12390-8:2019-10, *Prüfung von Festbeton - Teil 8: Wassereindringtiefe unter Druck*; Deutsche Fassung EN 12390-8:2019. Berlin: Beuth Verlag GmbH. <https://doi.org/10.31030/3045775>.
- [54] ASTM D5385-93, *Standard Test Method for Hydrostatic Pressure Resistance of Waterproofing Membranes*. American Society for Testing and Materials.
- [55] T. Freimann, U. Heinlein, Frischbetonverbundtechnologie. *Beton- und Stahlbetonbau* 113 (5) (2018) 368–384, <https://doi.org/10.1002/best.201700098>.
- [56] DIN EN ISO 9073-2:1997-02, *Textilien - Prüfverfahren für Vliesstoffe - Teil 2: Bestimmung der Dicke (ISO 9073-2:1995)*; Deutsche Fassung EN ISO 9073-2:1996. Berlin: Beuth Verlag GmbH. <https://doi.org/10.31030/7313402>.
- [57] S. Preibisch, S. Saalfeld, P. Tomanek, Globally optimal stitching of tiled 3D microscopic image acquisitions, *Bioinformatics* 25 (11) (2009) 1463–1465, <https://doi.org/10.1093/bioinformatics/btp184>.
- [58] W. Gösele, R. Leibnitz, D. Oechsle, E. Pongratz, J.W. Tichy, Kapitel 8 Filterapparate, in: K. Luckert (Ed.), *Handbuch der mechanischen Fest-Flüssig-Trennung*, first ed., Vulkan-Verlag, Essen, 2016, pp. 143–268.
- [59] Verein Deutscher Ingenieure, *VDI 2762-1 - Mechanical Solid-Liquid-Separation by Cake Filtration - Overview*, 2006.

9.3 Pre-applied mechanically bonded waterproofing membranes: Cement paste filtration process and influencing parameters

Reprint

Published in “Journal of Building Engineering”

Volume 62, October 2022; DOI: [10.1016/j.jobbe.2022.105385](https://doi.org/10.1016/j.jobbe.2022.105385)

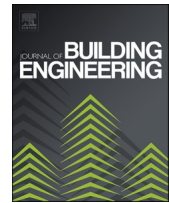
Authors: U. Heinlein, T. Freimann



ELSEVIER

Contents lists available at ScienceDirect

Journal of Building Engineering

journal homepage: www.elsevier.com/locate/job

Pre-applied mechanically bonded waterproofing membranes: Cement paste filtration process and influencing parameters

Ulli Heinlein^{*}, Thomas Freimann

Technische Hochschule Nürnberg Georg Simon Ohm, 90489, Nürnberg, Germany

ARTICLE INFO

Keywords:

Pre-applied waterproofing membranes
Blindside waterproofing
Waterproofing membranes
Fully-bonded waterproofing membranes
Post-cast concrete application
Nonwoven
Filtration
Filter cake

ABSTRACT

Pre-applied bonded waterproofing membranes are used as positive-side waterproofing on the exterior of concrete basements. They are installed on a formwork before reinforcement works and bind to the subsequently placed fresh concrete. This bond is often ensured via nonwovens as they are filled with cement paste during the concrete placement. However, it is largely unclear how the cement paste enters the nonwoven, what its properties are and how it is affected by site-specific influences and nonwoven properties. The work presented in this article used a new test stand and exposed varying nonwovens to concrete pouring conditions similar to the construction site and analyzed the filtrated cement paste. In combination with existing literature, a working model of the processes within the nonwovens was then created: After the fresh concrete is poured, a limited mass of solids and water is separated due to the mere static load, resulting in a water-rich paste within the nonwoven after a few minutes. Simultaneously, a filter cake forms on top of the nonwoven, limiting the further separation of solids. Subsequent vibration compaction loosens the filter cake, carrying more solids into the nonwoven and reducing the water/solid-ratio of the paste. The separated solid mass depends on the pore volume of the nonwoven, compaction time, and fresh concrete spread. The particle size varies over time and position in the nonwoven.

1. Introduction

Pre-applied bonded waterproofing membranes are often used to seal the outside of concrete basements (positive side). They are placed horizontally on a mud slab, vertically on a formwork, or in a blindside application onto a soil retention system. During further construction, fresh concrete is placed directly on them. A bond between membrane and concrete is formed, which improves redundancy compared to unattached waterproofing membranes [1]. If a membrane has a local defect, the waterproof bond prevents intruding water from spreading between the membrane and the concrete surface. Thus, separation cracks in the concrete are not reached [2]. [3] gives further information on the mechanisms and types of pre-applied waterproofing membranes.

In order to achieve a bond with concrete, pre-applied membranes essentially comprise a sealing layer and a bonding layer. Probably due to their low cost and easy development, nonwovens are often used for bonding. A waterproof bond is accomplished once their pores are filled with cement paste during concrete placement.

Meyer et al. [4] provided the first practice-oriented findings on nonwoven-bonded membranes by installing them with fresh concrete. After concrete hardening, the water migration resistance between membrane and concrete surface was tested by applying water pressure to a local defect in the sealing layer. For nonwovens, the most crucial factor was the vibration compaction time. The

^{*} Corresponding author.

E-mail address: ulli.heinlein@th-nuernberg.de (U. Heinlein).

<https://doi.org/10.1016/j.job.2022.105385>

Received 15 July 2022; Received in revised form 13 September 2022; Accepted 5 October 2022

Available online 8 October 2022

2352-7102/© 2022 The Authors. Published by Elsevier Ltd. This is an open access article under the CC BY-NC-ND license (<http://creativecommons.org/licenses/by-nc-nd/4.0/>).

authors argued that cement paste only infiltrates nonwovens during vibration compaction, as long as the yield point of the cement paste is reduced.

Heinlein and Freimann [5] investigated the nonwoven's macroscopic behavior during concrete placement. The nonwovens were installed with fresh concrete, and after concrete hardening, the nonwoven thickness change was measured using microsections. The nonwovens were first compressed due to fresh concrete load and subsequently decompressed during ongoing vibration compaction as cement paste filling increased. Indications arose that nonwovens with smaller pore volumes were filled disproportionately fast with cement paste and that cement paste is separated in a filtration process from the fresh concrete.

Further tests on the behavior of nonwovens in the concreting process do not exist thus far. Therefore, it is unknown which processes occur within nonwovens during concrete placement. However, it has been suspected that nonwoven filling occurs in a filtration process, which is generally well studied for nonwovens. Solid-liquid filtrations are divided into cake filtration and depth filtration [6], while mixtures with high solid contents are usually separated by cake filtration. In this process, a filter medium retains particles on its surface, forming solid bridges and, finally, a filter cake [7]. Subsequently, the filter cake itself acts as the filter medium as is shown in Fig. 1. Generally, a higher filter cake thickness and compression result in a better separation but lower performance at constant pressure. Nonwovens also show depth filtration, where particles are retained within their structure, e.g., in constricting pores. The suitability of the filter medium is usually tested in a pressure filtration test [8]. [9] provides further information on solid-liquid filtration.

Geotextiles also use nonwovens to prevent fines migration between soil layers or to dewater sludge [10–12]. They must retain fines, remain sufficiently permeable to water, and shall not be clogged by particles [13,14]. Their functionality is tested in the laboratory via pressure tests [15]. [16] summarizes further standard test methods. Geotextiles are compressed under static load, and thus, opening widths are constricted, and water paths are reoriented. During filtration, the first particles are retained within the structure; then, solid bridges form on top of fibers, reducing the geotextile's opening widths and permeability [17–19]. During sludge dewatering, pronounced filter cakes were observed together with initial turbidity and solids in the filtrate during the filter cake formation [20–22]. A few studies investigated the influence of pulsating hydrostatic load [23,24], finding more solids pass through nonwovens compared to mere static loading.

The approaches above require high water contents in the suspension and rarely use vibration, so cement paste filtration in nonwovens of pre-applied membranes cannot be derived. However, static filtration methods are also used in concrete construction to determine the water retention capacity of fresh concrete. For example, the concrete filter press is used in Austria [25] to examine concrete mixtures' suitability for diaphragm walls and drilled piles [26–28]. It is also used to determine the 'bleeding' of fresh concrete as an alternative to the 'bleeding bucket' [29], or DIN EN 480–4 [30], or ASTM C232 [31]. Furthermore, nonwovens serve as filters on concrete surfaces in Controlled Permeable Formworks (CPF). They remove water and air voids from the concrete surface, thereby increasing durability [32–36], with cement paste being retained by small pore radii (4–35 μm) [37]. However, even based on these investigations, no conclusions can be drawn on how cement paste intrudes nonwovens.

This article aims to understand the processes within nonwovens of pre-applied membranes during concrete placement in order to allow recommendations for practice and to select suitable nonwovens for pre-applied bonded membranes. For this, a purpose-built test stand was used to simulate an actual concrete pour on nonwovens. The filtrated cement paste was afterwards examined. Based on the results, a working model of the temporal processes in nonwovens during concrete placement was derived. In addition, favorable concrete placement conditions and nonwoven properties were determined.

2. Methods and materials

2.1. Methodological approach

Nonwovens were installed with fresh concrete in a newly designed test stand and subjected to static load and vibration compaction.

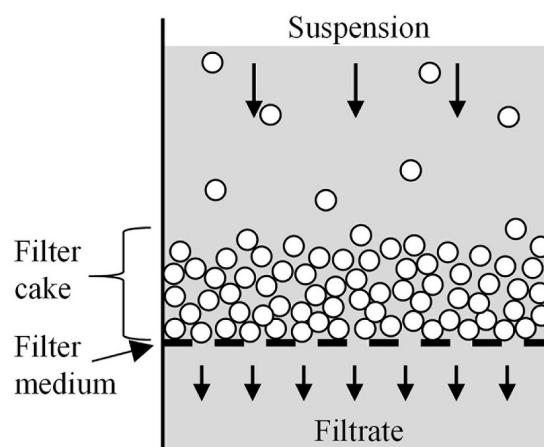


Fig. 1. Model of filter cake filtration [7].

Filtrate was filtrated through nonwovens and analyzed for its solids content, particle size distribution, and solids density. In this way, the time-dependent changes within nonwovens were determined together with the influence of fresh concrete composition, execution, and nonwoven properties. In contrast to pre-applied membranes, the tests were mainly carried out on 'loose' nonwovens without a sealing layer, as is common for filtration tests. Nonwovens with a sealing layer were included in the tests for comparison with pre-applied membranes.

2.2. Methods

2.2.1. Setup and procedure

The used test setup was designed based on a static filtration test, as generally used for concrete filter presses [25] or testing filter fabrics [8]. It was supplemented by an internal vibrator and built with dimensions to enable fresh concrete mixtures typical for construction sites. To investigate the intrusion of cement paste into nonwovens, the tests were divided into static intrusion tests using only fresh concrete load and dynamic intrusion tests using vibration compaction.

Fig. 2 shows the test stand, which essentially comprises a grating (30 mm aperture), the nonwoven on a mesh (\varnothing 340 mm, 2.5 mm aperture), and a two-part pressure chamber made of a steel tube (\varnothing 320 mm). Below the grating was a scale with a collection tray (\varnothing 360 mm). Both the scale and the grating were set up vibration damped. The test was performed according to the following procedure:

- *1st step:* The nonwoven was placed on a supporting mesh on the grating.
- *2nd step:* The lower part of the pressure chamber was fixed on the nonwoven. The gaps were sealed by ring gaskets made of Ethylene-propylene-diene-(monomer) (EPDM) rubber ($h = 10$ mm). The fresh concrete was mixed and poured into the pressure chamber with 0.21 m height (fresh concrete load $p = 5$ kPa). Gentle poking with a tamper ensured full contact between the fresh concrete and the steel tube, preventing airflow along the wall while applying compressed air.
- *3rd step:* The upper part of the pressure chamber, which was attached to a crane, was lowered and fixed in place. The internal vibrator, fixed to the ceiling, was sealed in the lid using a conical sealing plug. Compressed air was then applied ($p = 10$ –40 kPa) to simulate higher fresh concrete loads caused, e.g., in vertical applications or mass concrete slabs. Static load was applied 10 min after the mixing started.
- *Static intrusion test:* To investigate the processes in the nonwoven during concreting, static and dynamic intrusion tests were performed independently of each other. During static intrusion test, fresh concrete load was used as the primary force for filtration; no vibration compaction was applied. The filtrate mass in the collection tray was recorded for up to 30 min.
- *Dynamic intrusion test:* Fresh concrete was compacted using an internal vibrator. However, a static load was applied first to simulate an actual concrete pour, and since the static load already caused filtration effects. The static load was maintained until stationary masses were reached (1–30 min; see Chapter 3.1). Then, the concrete was vibrated with the internal vibrator for 1–30 s. To ensure exact vibration times, the internal vibrator was time programmed using a contactor. It was placed between the transducer and the internal vibrator and was operated via a programmable time switching relay.
- *4th step:* The pressure chamber was opened and the fresh concrete removed. Each batch was only used for one test.

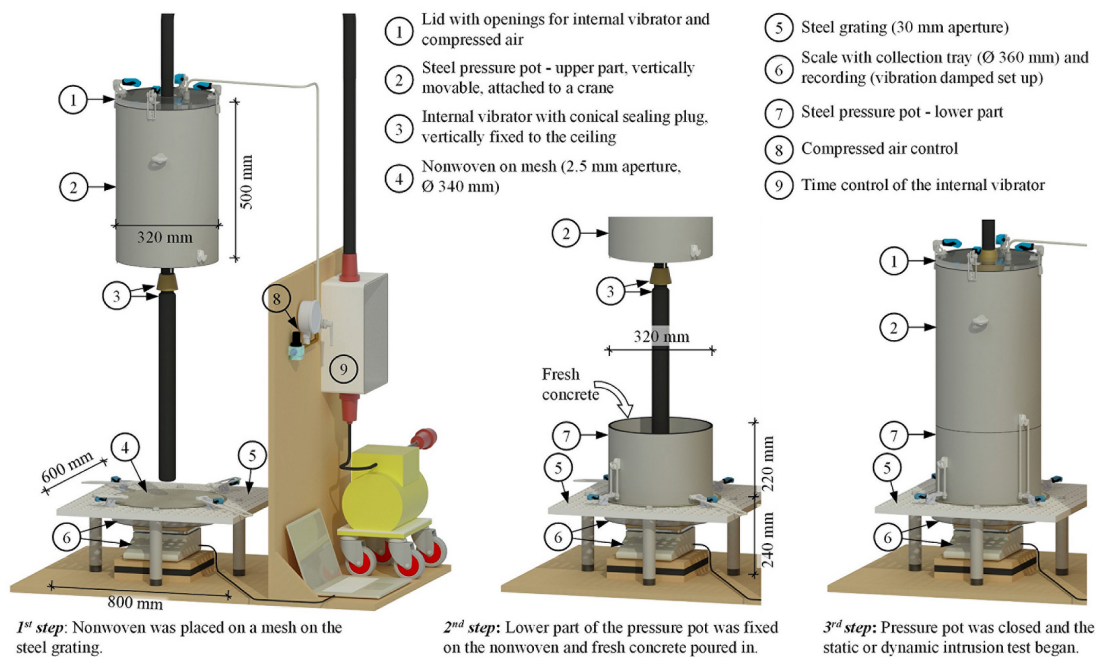


Fig. 2. Setup of the test stand and first steps in the experimental procedure.

- 5th step: The filtrates in the collection tray and nonwovens were analyzed for their solids and water content, particle diameter, and, in some cases, solids density (see Chapter 2.2.2).

2.2.2. Analysis of the filtrate

The filtrate was analyzed for particle size distribution using the laser diffraction method according to ISO 13320 [38]. The laser particle sizer 'Analysette 22' from 'Fritsch GmbH' with a measuring range between 0.01 and 2100 μm and a reverse Fourier setup was used. The sample was measured in wet dispersion in deionized water after being exposed to ultrasound for 60 s. For each concreting test, two samples with three measurement series were analyzed. The evaluation was performed with the software 'MaS control' based on the Fraunhofer theory. The particle size distributions were characterized as cumulative curves by particle volume $Q_3(d)$ or using their percentile values, e.g., at 90% passage (d_{90}). Also, particles from within the nonwovens were analyzed to provide a better insight into the processes in the nonwovens. Using deionized water, particles were washed out of the nonwoven on the top side facing the concrete and the bottom side.

The solid and water masses in the filtrate were then determined by oven drying. The residues on the mesh and the amount of filtrate required for particle size determination were considered. In the following, the masses were given as area-normalized relative quantities (kg/m^2).

After oven drying, the solid density ρ_s of the filtrate was determined randomly using the pycnometer according to DIN EN 1097-7 [39]. The samples were embedded in deionized water under vacuum and tempered in a water bath at 25 °C.

Similar to the water/cement-ratio (w/c-ratio) of concrete, the water/solids-ratio (w/s) in the nonwoven was calculated according to Equation (1). It was used to compare the paste in the nonwoven with the paste in the fresh concrete.

$$w/s = \frac{m_w}{m_s} \quad [-] \quad (1)$$

where m_w is the water mass, and m_s is the solid mass. Furthermore, the filtrates density ρ_F was calculated according to Equation (2), using the w/s-ratio and the solid density ρ_s obtained from pycnometer test.

$$\rho_F = \frac{m_s + m_w}{V_s + V_w} = \frac{m_s + m_w}{\left(\frac{m_s}{\rho_s}\right) + \left(\frac{m_w}{\rho}\right)} = \frac{1 + w/s}{\left(\frac{1}{\rho_s}\right) + w/s} \quad [\text{g}/\text{cm}^3] \quad (2)$$

where the index s indicates the solid mass and volume, and the index w the water mass and volume. The water density ρ_w was considered to be 1.0.

2.2.3. Variations

A total of $n = 379$ concreting tests were carried out. They investigated the time-dependent processes in the nonwovens and the influences of fresh concrete composition, placement, and nonwoven properties. Table 1 lists the variations.

In contrast to a real concreting process on pre-applied membranes, loose nonwovens were used, as is typical for filtration tests. Therefore, it was necessary to investigate whether the changed physical boundary conditions influenced filtration behavior. This was accomplished by reproducing the structure of pre-applied membranes by attaching loose nonwovens with epoxy resin onto a plastic film made of low-density polyethylene (LDPE, 125 μm thickness, $n = 16$). The epoxy resin was applied thinly to the plastic film, and the nonwovens were laid in place and pressed on. The resulting full-surface bond was sufficiently strong for concrete placement but could

Table 1
Methodological approach and experimental variation.

Test	Test parameters and deviations from the reference tests	Concrete mixture acc. to Table 3	Nr. of samples	
Reference static intrusion test	Static intrusion test (SIT)	Nonwoven N1&N2 (see Table 2), 15 kPa load, 46 cm fresh concrete spread, 30 min duration	Reference (1)	10
Reference dynamic intrusion test	Dynamic intrusion test (DIT)	Nonwoven N1&N2, 15 kPa load, 46 cm fresh concrete spread, static load until nonwoven is saturated - then 5 s vibration with internal vibrator \varnothing 55 mm.	1	10
Verification with nonwovens on sealing layer	SIT & DIT	Nonwovens N1&N2 were bonded to plastic film with epoxy resin to simulate the sealing layer of pre-applied membranes	1	16
Duration of fresh concrete load	SIT	1/2.5/5/10/20 min duration of static load	1	24
Vibration duration	DIT	1/2.5/10/20/30 s vibration compaction time	1	32
Diameter internal vibrator	DIT	Internal vibrator with \varnothing 38/45/55/58 mm	1	24
Distance internal vibrator to nonwoven	DIT	0/25/50/100 mm vertical distance between nonwoven and internal vibrator	1	16
Fresh concrete load	SIT & DIT	5/15/25/35/45 kPa load (0.2–1.9 m fresh concrete height)	1	58
Cement content	SIT & DIT	280/300/320/340/360/380 kg/m^3 cement content	2–6	40
Water content	SIT & DIT	0.40/0.45/0.50/0.55/0.60/0.65 water/cement ratio	7–11	40
Fresh concrete consistency	SIT & DIT	42–56 cm spread according DIN EN 12350-5	1	55
Nonwovens	SIT & DIT	N3–N10 (see Table 2) with 25–150 g/m^2 basis weight	1	54

Table 2
Structural properties of the nonwovens.

Property	Unit	Individual mean values \bar{x} of $n = 10$ tested products										Test method, number of samples per product, and average standard deviation \bar{s} in the test
		N1	N2	N3	N4	N5	N6	N7	N8	N9	N10	
Basis weight	g/m ²	64.3	97.1	23.7	52.9	116.9	153.4	109.8	37.3	60.3	86.8	6 samples per product, $\bar{s} = 8.2$ g/m ² DIN EN 1849–2 [40]; 5 samples per product; $\bar{s} = 0.04$ mm DIN EN 1849–2 [40]; 5 samples per product; $\bar{s} = 0.03$ mm DIN EN 1849–2 [40]; 5 samples per product; $\bar{s} = 0.04$ mm Manufacturer specification $\epsilon_{15\text{kPa}} = 1 - \frac{m}{\rho \cdot T_{15\text{kPa}} \cdot A}$ (m : nonwoven basis weight, ρ : density of fibers, $T_{15\text{kPa}}$: thickness of the nonwoven at 15 kPa load; A : area) $V = \epsilon_{15\text{kPa}} \cdot T_{15\text{kPa}}$ ($\epsilon_{15\text{kPa}}$: porosity at 15 kPa load, $T_{15\text{kPa}}$: thickness of the nonwoven at 15 kPa load) NP: Needle punching; CB: Calendar bonding; HE: Hydroentenglament Manufacturer specification measured acc. to ISO 12956 [41]
Thickness 0.5 kPa	mm	0.83	1.50	0.23	0.35	1.33	3.23	0.49	0.43	0.61	1.15	
Thickness 2.0 kPa	mm	0.74	1.36	0.17	0.31	1.26	2.72	0.40	0.37	0.55	1.13	
Thickness 15 kPa	mm	0.60	1.07	0.16	0.28	1.06	1.86	0.39	0.29	0.45	0.81	
Fiber material		PP	PP	PP	PP	PP	PP	PP	PES	PES	PES	
Porosity at 15 kPa load, $\epsilon_{15\text{kPa}}$	[–]	0.88	0.90	0.84	0.80	0.88	0.91	0.69	0.91	0.90	0.92	
Pore volume at 15 kPa load, $V_{15\text{kPa}}$	[dm ³ /m ²]	0.53	0.96	0.14	0.22	0.93	1.70	0.27	0.27	0.41	0.75	
Type of bonding		NP	NP	CB	CB	NP + CB	NP	NP + CB	HE	HE	HE	
Charact. opening size of pores O_{90}	[μm]	–	–	–	–	115	121	100	–	–	–	

Table 3
Fresh concrete compositions.

	Nr. of the mixture	Cement content [kg/m ³]	Water content [kg/m ³]	w/c-ratio	Aggregate A/B 32 [kg/m ³]	Cement paste volume [dm ³ /m ²]
Reference	1	320	175	0.55	1847	280
Variation of cement content	2	280	154		1937	245
	3	300	165		1891	263
	4	340	187		1799	298
	5	360	198		1753	315
	6	380	209		1707	333
Variation of w/c-ratio	7	320	128	0.40	1971	232
	8		144	0.45	1929	248
	9		160	0.50	1887	264
	10		192	0.60	1803	296
	11		208	0.65	1761	312

be separated by hand after the test. In this way, the particle diameter inside the nonwoven could be determined by washing particles out of the nonwoven.

2.3. Materials

2.3.1. Nonwoven

Ten commercially available technical nonwovens were included in the tests (N1–N10), with N1&N2 used in all variations and N3–N10 used to investigate the textile influences in Chapter 3.7. In order to ensure comparability to pre-applied membranes, N1&N2 were derived from the production line of internationally available pre-applied membranes. Fundamental structural properties of the examined nonwovens are presented in Table 2.

The nonwoven N6 was highly compressible and had a high pore volume. The nonwoven N9 had large openings with a diameter of 1.2 mm.

2.3.2. Concrete

Pre-applied membranes are usually installed with waterproof concrete. The reference concrete mixture contained a Portland limestone cement CEM II/A-LL 42.5 N with a cement content of 320 kg/m³, a w/c-ratio of 0.55, and a grading curve A/B 32 ($k = 4.81$) with quartzitic round grain. The fresh concrete was adjusted to a spread of 46 cm according to DIN EN 12350–5 [42] using a PCE-based superplasticizer. Further, it had a fresh concrete density of 2410 kg/m³ according to DIN EN 12350–6 [43]. In addition, the tests included a variation of the w/c-ratio and the cement content. Table 3 shows the compositions of the fresh concrete mixtures.

2.3.3. Internal vibrator

The concrete was compacted with high-frequency internal vibrators, as is typical for construction sites. An internal vibrator with a diameter of 55 mm was used as reference. In the variation of internal vibrators (Chapter 3.6), additional diameters of 38, 45, and 58 mm were used. They were all operated with a frequency of 200 Hz. The nominal power varied between 0.45 and 1.05 kW.

3. Results

3.1. Time-dependent processes in the nonwoven

First, the change with time of the cement paste within N1&N2 was analyzed, particularly the relative solid and water mass and particle diameter using the concrete mixture 1 of Table 3. Solid and water masses in the nonwoven were given as area-normalized relative quantities (kg/m^2). Fig. 3-a shows the results in the static intrusion test for nonwoven N1 with a load of 15 kPa. Fig. 3-b displays the results in the dynamic intrusion test using vibration compaction. The vibration started after stationary masses were reached in the nonwoven during static loading, which was the case after 1 min at 15 kPa for nonwoven N1.

In the static intrusion test, about $0.4\text{--}0.5 \text{ kg}/\text{m}^2$ of water and an equal mass of solids separated from the fresh concrete in nonwoven N1 within the first minute. Subsequently, the nonwoven was saturated, and no further change occurred. Like the mass change, the particle size change exhibited a bilinear behavior. The d_{90} diameter of the separated filtrate decreased from around $d_{90,30s} = 58 \mu\text{m}$ after 30 s to $d_{90,1\text{min}} = 48 \mu\text{m}$ after 1 min. After 30 min, the particle size had decreased to $d_{90,30\text{min}} = 42 \mu\text{m}$. When fresh concrete was removed after the test, a dense layer of small aggregates was found on top of the nonwoven, representing the filter cake. It settled within the first minute for nonwoven N1 and was responsible for the bilinear behavior in the static intrusion test.

If vibration compaction was performed after 1 min of static load, about $0.5 \text{ kg}/\text{m}^2$ more solids were separated from the fresh concrete within 30 s. The solid's separation was approximated by a power function with a good coefficient of determination of $r^2 = 0.94$, indicating the decrease in the solids' separation rate with continued vibration compaction. The d_{90} percentile of the particle diameter was further reduced to about $33 \mu\text{m}$ after 30 s vibration compaction.

A similar process was observed for nonwoven N2 as is shown in Fig. 4. During the static intrusion test, about $0.5 \text{ kg}/\text{m}^2$ of solids and about $1.2 \text{ kg}/\text{m}^2$ of water were separated within the first 5 min. Subsequently, no further change occurred. The longer saturation duration compared to nonwoven N1 was due to the higher pore volume in the nonwoven. With vibration compaction starting, the solid mass increased with a comparable progress to that of nonwoven N1. The water content in the nonwoven decreased to about $0.9 \text{ kg}/\text{m}^2$ after 30 s of vibration.

Fig. 5 shows the nonwoven N2 on a pre-applied membrane exemplarily [5]. After static loading (Fig. 5-a), the bright color of the paste in the nonwoven already indicated a high water content. Further discussion follows in Chapter 4.

3.2. Solids particle diameter in the nonwoven

Fig. 6 shows the particle size distributions of the cement paste for both test types (static/dynamic intrusion test) and different layers in the nonwoven (top side facing concrete/bottom/passed filtrate). Since the particle size distributions for nonwovens N1–N8 and N10 were very comparable, they were shown averaged in Fig. 6. Table 4 provides the scatter of the particle size distributions in Fig. 6.

The measurements allow four observations:

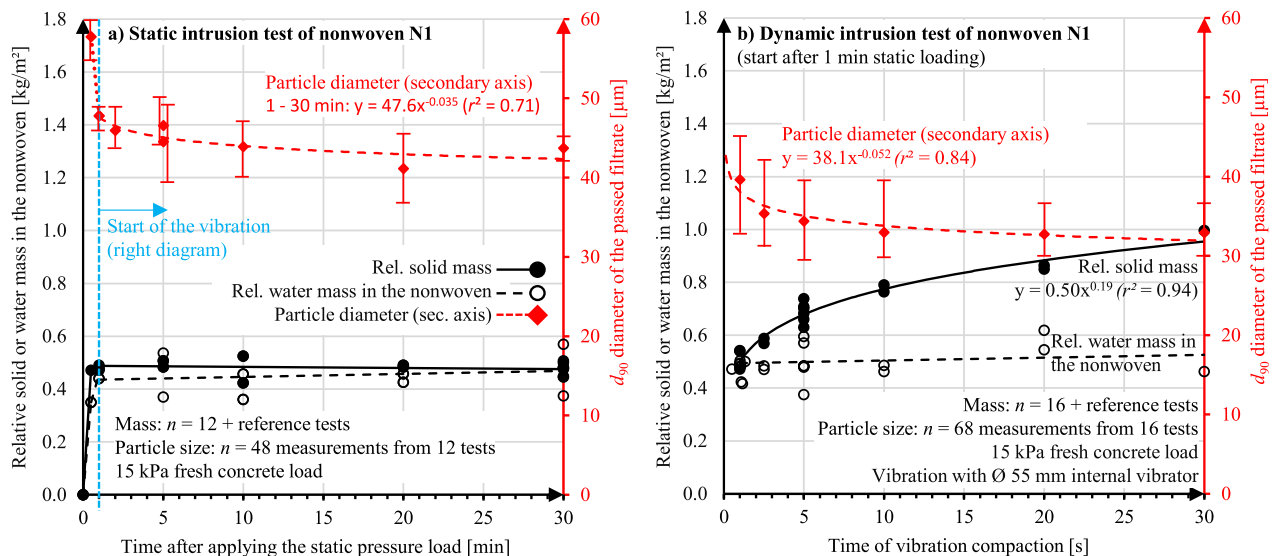


Fig. 3. Temporal processes in the nonwoven N1 during static loading (a) and subsequent vibration compaction (b) using the concrete mixture 1 of Table 3. Solid and water masses in the nonwoven were given as area-normalized relative quantities (kg/m^2). At the beginning of static loading and during compaction, the solid mass in the nonwoven increases.

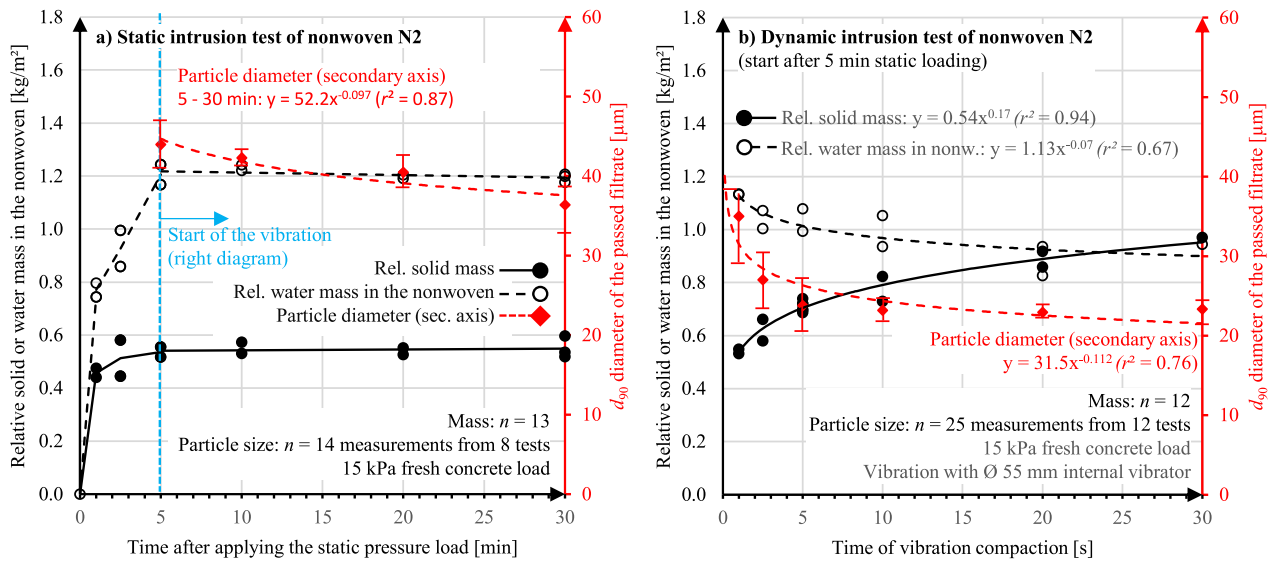


Fig. 4. Temporal processes in the nonwoven N2 during static loading (a) and subsequent vibration compaction (b) using the concrete mixture 1 of Table 3.

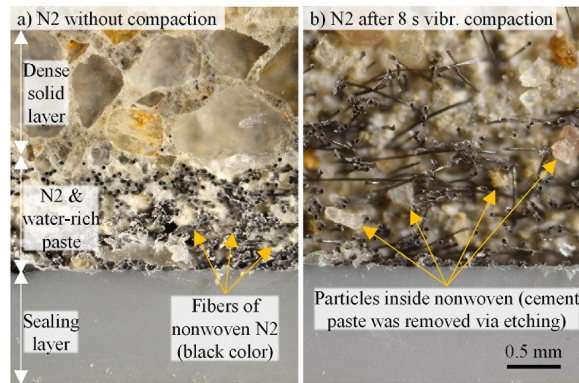


Fig. 5. Microsections of nonwoven N2 without (a) and with vibration compaction (b) [5].

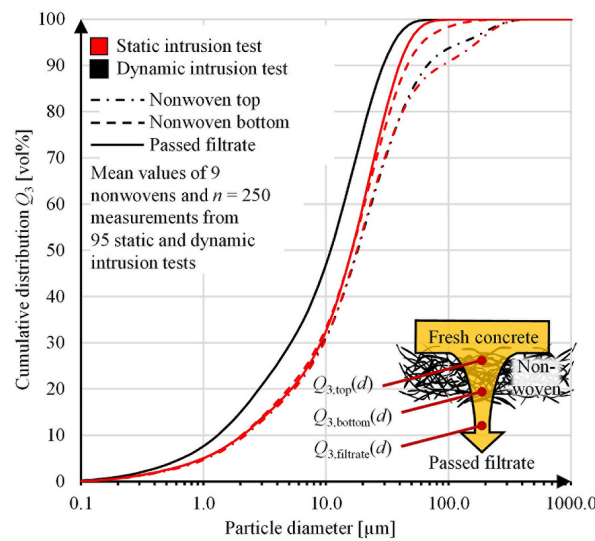


Fig. 6. Particle diameter in the nonwovens 1-8&10.

Table 4

Particle diameter in Fig. 6. Average \overline{d}_{90} diameter and standard deviation \overline{s} of the particles in the nonwoven ($n = 250$) [μm].

Area	Particle diameter [μm] in the nonwoven	
	Static intrusion test	Dynamic intr. test
Nonwoven top	$\overline{d}_{90} = 89.2$ ($\overline{s} = 72.5$)	$\overline{d}_{90} = 94.0$ ($\overline{s} = 49.2$)
Nonwoven bottom	$\overline{d}_{90} = 49.7$ ($\overline{s} = 16.5$)	–
Passed filtrate	$\overline{d}_{90} = 39.9$ ($\overline{s} = 5.9$)	$\overline{d}_{90} = 29.2$ ($\overline{s} = 4.5$)

- The particle size distribution varied over the height of the nonwoven. The particles in the upper layer of the nonwoven were coarser than in the bottom part and again coarser than in the separated filtrate. Thus, depth filtration was present. Based on the individual particle size distributions of the cement and aggregates, more sand particles were present in the upper nonwoven part.
- The particle size varied with the test type. Smaller particle sizes were present in the dynamic intrusion test as more fine aggregates and cement particles ($< 10 \mu\text{m}$) were separated than in the static intrusion test.
- The particle sizes on the top side facing the concrete exhibited an increased scatter due to the product-specific pore structure (see Table 4). In general, however, the particle sizes of all nine nonwovens were in a close range.
- d_{90} of the filtrate was smaller than the characteristic opening sizes O of the nonwovens. For the nonwovens N5–N7, the manufacturer determined the 90% percentile of the opening sizes to $O_{90} = 100\text{--}121 \mu\text{m}$ in a hydrodynamic sieving test (see Table 2). The corresponding particle sizes of the filtrate were $d_{90} = 30\text{--}34 \mu\text{m}$. In general, it is known for filter cake filtration that the particle size is determined by the filter cake and not by the filter medium's opening size, e.g. Ref. [9]. Thus, the nonwoven properties are not the main influence on the particle size distribution.

Nonwoven N9 was not included in the above evaluation since it had much wider openings (1.2 mm). In the static intrusion test, the particle diameters in the filtrate were $d_{90} \approx 170\text{--}190 \mu\text{m}$ and thus still below the opening diameter of around 1.2 mm. The particle size was again mainly determined by the filter cake.

3.3. Density of the solids in the filtrate

Table 5 lists the solid densities of the filtrate, aggregates, and cement. The density of solids in the filtrate was found to have a mean value of 2.95 g/cm^3 with a standard deviation of 0.05 g/cm^3 . It was slightly lower than the mixing density of particles $d \leq 250 \mu\text{m}$ in the fresh concrete of 3.00 g/cm^3 but within the scatter.

3.4. Reference tests and nonwovens on sealing layer

Fig. 7 shows the results of the reference tests using nonwovens N1 and N2 (parameters see Table 1). It distinguishes between relative solid and water mass in the nonwoven and the type of test. Additionally, the reference tests are compared to nonwovens bonded onto a sealing layer to verify the test procedure with changed physical boundary conditions compared to pre-applied membranes.

Nonwovens attached to a sealing layer separated comparable solid masses as loose nonwovens. The maximum deviation of the mean values was $\Delta m_{\text{solid}} = 0.05 \text{ kg/m}^2$. However, the separated water mass differed. Nonwoven N2 on sealing layer contained significantly less water mass than the loose nonwoven N2. After vibration compaction, the deviation between mean values was $\Delta m_{\text{water}} = 0.24 \text{ kg/m}^2$.

The particle sizes in the nonwovens on sealing layer were comparable to those of loose nonwovens. For example, nonwoven N1 on sealing layer showed a particle size in the upper nonwoven area of $d_{90,\text{top}} = 69 \mu\text{m}$, and on the bottom $d_{90,\text{bottom}} = 45 \mu\text{m}$. In the loose nonwoven N1, the particle size on top was $d_{90,\text{top}} = 68 \mu\text{m}$, and on the bottom $d_{90,\text{bottom}} = 46 \mu\text{m}$.

In summary, loose nonwovens separated comparable solid masses and particle sizes as nonwovens on a sealing layer – despite the changed physical boundary condition. This verifies the test method using loose nonwovens. However, the missing sealing layer led to continuous water separation since no pore water pressure could build up in the nonwoven, stopping filtration.

The water/solids-ratio inside the nonwovens could thus only be reliably determined using the nonwovens attached to a sealing layer. The w/s-ratio was calculated for the nonwovens N1 and N2 based on Equation (1). For nonwoven N1, the w/s-ratio was 1.1–1.2 after the static intrusion test and 0.6–0.8 after 5 s vibration compaction. The nonwoven N2 with a higher pore volume had a w/s-ratio between 2.1 and 2.8 after the static intrusion test and 0.9–1.2 after the vibration compaction. Compared to N1, the higher pore volume yielded a higher w/s-ratio under comparable conditions as a limited solid mass was separated during static loading, and the rest of the pore volume filled up with water.

Table 5

Density of fine aggregates and cement.

Solids	Density [g/cm^3]	Number of samples n , and range of density ρ [g/cm^3]
Cement CEM II/A-LL 42.5 N	3.07	$n = 2$ ($\rho = 3.06\text{--}3.08$)
Fine aggregates ($d \leq 250 \mu\text{m}$)	2.66	$n = 4$ ($\rho = 2.65\text{--}2.72$)
Filtered solids in the nonwoven	2.95	$n = 6$ ($\rho = 2.91\text{--}3.00$)

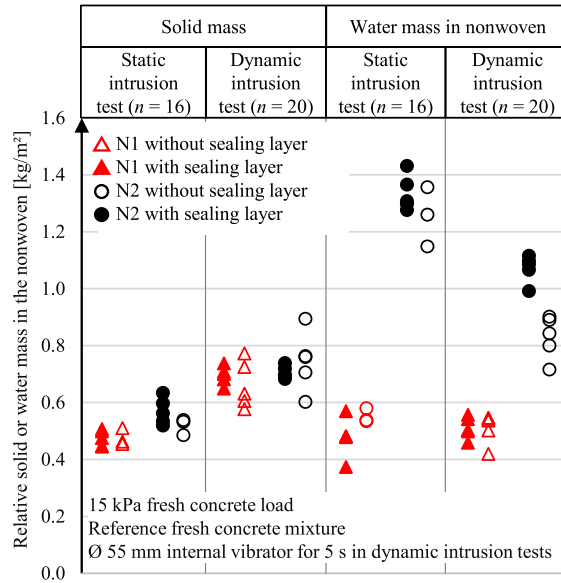


Fig. 7. ‘Loose’ nonwovens and nonwovens on a sealing layer in the reference tests.

3.5. Influences of fresh concrete properties

Fig. 8 displays the solid mass in the nonwovens for varying fresh concrete spreads. A uniform fresh concrete mixture was used, and the spread was adjusted by varying the amount of PCE-based superplasticizer added.

Higher additions of superplasticizer increased the separated solid mass in the static and dynamic intrusion tests. When the fresh concrete spread was increased from about 42 to 54 cm, the separated solid mass also rose by a factor of 1.3–1.7. For example, nonwoven N1 separated in the static intrusion test a relative solid mass of 0.31 kg/m² using a fresh concrete spread of 42 cm and 0.51 kg/m² using a spread of 54 cm.

Superplasticizers dissolve agglomerations of cement particles, increase workability, reduce shear resistance and lower the yield point [44,45]. Accordingly, separated solids could enter the nonwoven more easily as the friction and filtration resistance were reduced. The effect is similar to dispersants in typical filtration applications [9].

Furthermore, w/c-ratios and cement contents were varied according to Table 3. While varying the fresh concrete mixture, the workability had to be sufficiently high as it would be on construction sites. Therefore, the mixtures were modified with adapted superplasticizer contents to ensure a constant spread.

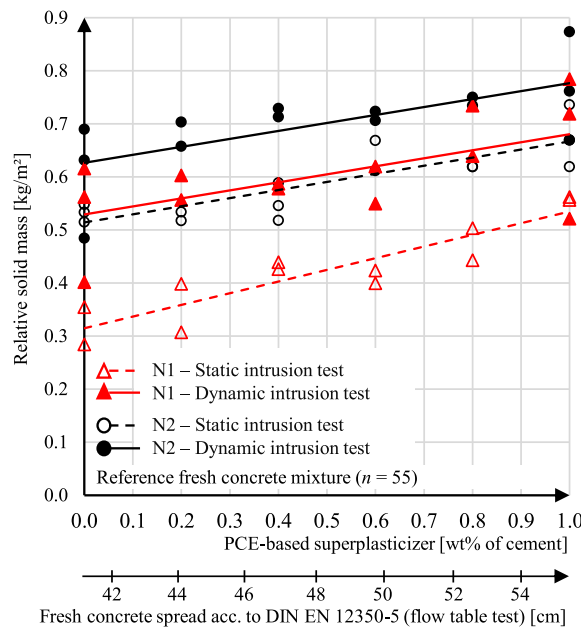


Fig. 8. Influence of varying fresh concrete spreads on the solid mass in the filtrate.

In both variations of w/c-ratio and cement content, similar results were observed. Therefore, Fig. 9 shows the results plotted versus the cement paste volume of the mixtures. For orientation, the original variations of the w/c-ratio and cement contents are listed as separate axes. Note that they have to be considered independently.

In the static intrusion test, a decreasing cement paste volume led to an increasing solid mass. The dynamic intrusion test did not reproduce this finding. Thus, the static intrusion test result was probably again influenced by the variable superplasticizer content as it increased viscosity and lowered filtration resistance as described above. When vibration compaction started, the yield point and the internal friction were reduced in all mixtures via the dynamic vibrational shear force [46]. As a result, almost the same solid mass was separated in all tests.

In contrast to Fig. 8, no increase in solid mass was achieved with rising superplasticizer content during vibration compaction. This is probably due to the superposition of the increasing superplasticizer contents with varying cement and water contents, which influence the viscosity of the different fresh concrete mixtures.

Furthermore, the fresh concrete mixtures with reduced water content released less filtrate water. This corresponds to studies of the water retention capacity of fresh concrete [47–49]. However, in the static intrusion test, less filtrate water caused the separated solids to remain in the upper part of the nonwoven and its bottom being clean. Only upon vibration compaction, the solids penetrated further into the nonwoven. Thus, vibration compaction was required to ensure good distribution of particles in the nonwoven, even if more solids were separated during static loading.

3.6. Influences during concrete placement

The fresh concrete load was varied between 5 and 45 kPa, corresponding to a fresh concrete height of 0.2–1.9 m. The actual fresh concrete height was always 0.21 m ($p = 5$ kPa), and the additional static load originated from compressed air. The separated relative solid masses are shown in Fig. 10.

Higher load in the static intrusion test resulted in a slight increase in relative solid mass. At the same time, significantly more water was separated from the fresh concrete and increased for nonwoven N1 from 1.2 kg/m² at 5 kPa to 4.3 kg/m² at 45 kPa after 30 min of static loading. It seems plausible that the higher water flow and resulting frictional forces dragged slightly more fine aggregates and cement particles into the nonwoven. In contrast, the results in the dynamic intrusion test were not influenced by higher static loads. The change for nonwoven N1 was negligible and within the scatter.

In Fig. 11-a, the vertical distance was varied between the internal vibrator and the nonwoven. Note that at a distance of 0 cm, the internal vibrator touched the nonwoven surface. With increasing distance, the separated solid mass decreased. Fig. 11-b shows the

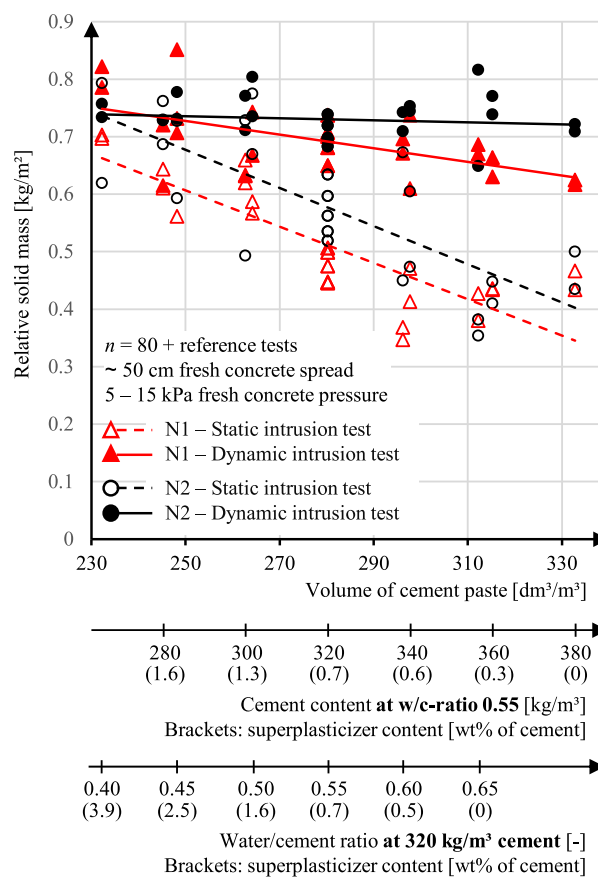


Fig. 9. Influence of fresh concrete properties due to varying cement paste volume. For orientation, the original variations of w/c-ratio and cement content were listed.

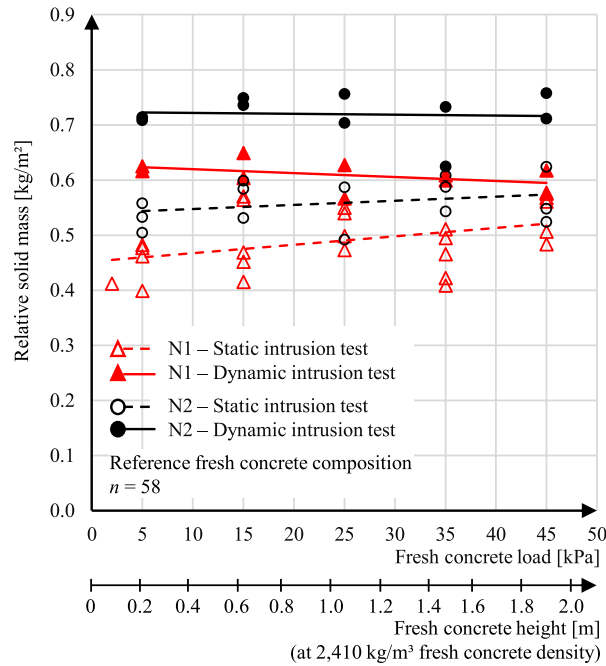


Fig. 10. Influence from varying fresh concrete loads, simulated with compressed air. For orientation, the corresponding fresh concrete heights are listed.

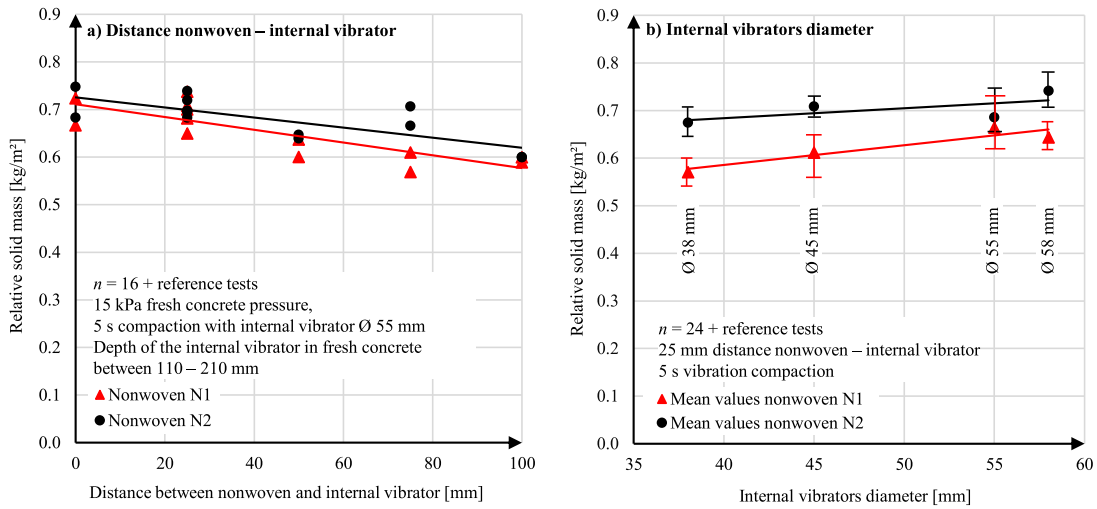


Fig. 11. Influence of varying vertical distance between internal vibrator and nonwoven (a) and varying diameters of internal vibrators (b).

influence of the diameter of the internal vibrator at a constant distance to the nonwoven. With increasing vibrator diameter, slightly more solids were recorded in the nonwoven.

In summary, higher compaction energies were beneficial in the concreting process, with the distance between the nonwoven and the internal vibrator having more influence than its diameter. Also, the diameter of the internal vibrator influenced the particle size. For example, for nonwoven N1, the filtrate was measured with $d_{90,38\text{mm}} = 51 \mu\text{m}$ using the Ø 38 mm internal vibrator and with $d_{90,58\text{mm}} = 31 \mu\text{m}$ using the Ø 58 mm internal vibrator.

3.7. Influences of textile properties

Fig. 12 shows the relative solid masses of $n = 10$ nonwovens plotted versus their pore volume. Each point represents an average value of at least three individual tests. In addition, the nonwovens N1 and N2 on the sealing layer were provided for comparison. Note that only one nonwoven (N6) was included with a pore volume $V_{\text{pore}} > 1.0 \text{ dm}^3/\text{m}^2$.

Nonwovens with higher pore volumes separated more solids in the static intrusion test. The values were approximated by linear regression with an acceptable coefficient of determination of $r^2 = 0.86$. During 5 s vibration compaction, additional solid mass was separated. Nonwovens with a higher pore volume separated disproportionately more solids.

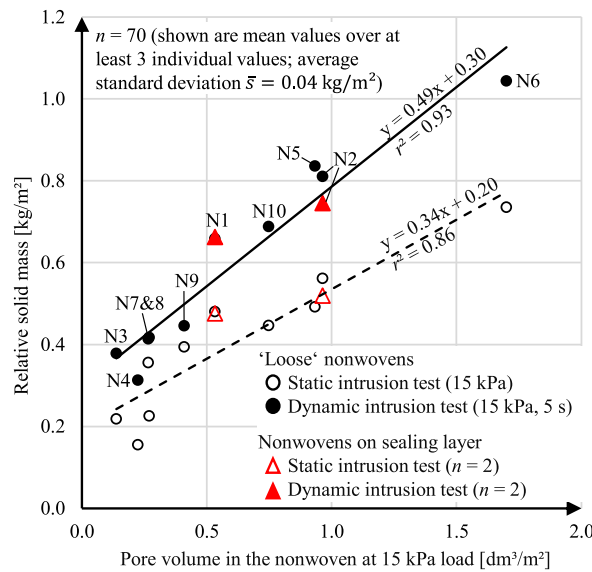


Fig. 12. Textile influences due to a variable pore volume in the nonwoven.

In Fig. 12, the relative solid masses were plotted versus the pore volume on the x-axis, resulting in a good correlation. This fits the finding in Ref. [5], where a good correlation was made to the nonwoven’s compression change during vibration compaction. If, in contrast, correlation in this study was made using the nonwoven thickness, a coefficient of determination of $r^2 = 0.81$ was obtained. The regression using nonwoven porosity showed a poorer agreement with $r^2 = 0.45$.

3.8. Comparison of the investigated variables

All variables investigated are summarized in Table 6. The values represent the starting and end values of the linear regressions in Figs. 8–12, and the mean values shown in Figs. 3 and 7. The values were averaged over the investigated nonwovens to obtain a representative mean value.

The relative solid mass in the static intrusion tests was influenced by the following factors, ranked according to their relevance:

1. Pore volume in the nonwoven.
2. Workability of the fresh concrete (see variable cement paste volume and fresh concrete spread).

The relative solid mass in the dynamic intrusion tests was affected by the following factors, ranked according to their relevance:

1. Pore volume in the nonwoven.
2. Vibration compaction time with an internal vibrator.
3. Workability of the fresh concrete (variable quantity of superplasticizer).
4. Vertical distance between the internal vibrator and nonwoven.

4. Discussion

4.1. Time-dependent progress of cement paste filtration

The processes in the nonwoven taking place during fresh concrete placing and compaction are summarized in Fig. 13,

Table 6 Comparison of the investigated variables. Values represent the starting and end values of trend lines of each considered variation as mean value of all investigated nonwovens.

Variables	Relative solid mass [kg/m ²]	
	Static intrusion test	Dynamic intr. test
Reference tests and nonwoven on sealing layer	0.51 (± 0.04)	0.70 (± 0.04)
Cement paste volume (230–330 dm ³ /m ³)	0.38–0.70 (Δ 0.32)	0.67–0.74 (Δ 0.07)
Fresh concrete spread (0–1 wt% superplasticizer)	0.41–0.60 (Δ 0.19)	0.58–0.73 (Δ 0.15)
Fresh concrete pressure (5–45 kPa)	0.51–0.55 (Δ 0.04)	0.66–0.69 (Δ 0.03)
Sustained static loading duration (1–20min)	0.47–0.50 (Δ 0.03)	–
Time of vibration compaction (1–30 s)	–	0.52–0.95 (Δ 0.43)
Distance between nonwoven and internal vibrator (0–10 cm)	–	0.60–0.72 (Δ 0.12)
Diameter of internal vibrator (38–58 mm)	–	0.63–0.69 (Δ 0.06)
Textile influences (0.14–1.84 dm ³ /m ² pore volume)	0.25–0.78 (Δ 0.53)	0.42–0.95 (Δ 0.53)

External influences and effects	Initial state	Static intrusion test via fresh concrete load (i.e., 15 kPa)			Dynamic intrusion test via vibration compaction		
		Compression due to concrete load [5]	Build up of filter cake	Final filter cake due to static load	Loosening of the filter cake	Return flow of water from nonw.	Final state in the concrete
Processes in the nonwoven (Schemes show sections of pre-applied membranes)		Fresh concrete, i.e., 15 kPa 					
	Nonwoven with unloaded thickness h_0 on sealing layer	Empty, but compressed nonwoven, $h_1 < h_0$	Water + fines into nonwoven	High water/solids ratio in nonwoven	Cement paste into nonwoven	Water from nonw. into fresh concrete	Filled and decompressed nonwoven, $h_{fin} \approx h_0$
„Thin“ nonwoven N1	$I_{pore}^* = 0.76 \text{ dm}^3/\text{m}^2$	$t = 0$ $I_{pore}^* = 0.53 \text{ dm}^3/\text{m}^2$	$t_{static} = 0.5 - 1 \text{ min}$ $w/s \approx 0.7$	$t_{static} \geq 1 \text{ min}$ $w/s \approx 1.0$	$t_{vibr} = 1 \text{ s}$ $w/s \approx 0.9$	$t_{vibr} = 5 \text{ s}$ $w/s \approx 0.6^*$	$t_{vibr} = 10 \text{ s}$ $w/s \approx 0.55^*$
„Thick“ nonwoven N2	$I_{pore}^* = 1.40 \text{ dm}^3/\text{m}^2$	$t = 0$ $I_{pore}^* = 0.96 \text{ dm}^3/\text{m}^2$	$t_{static} = 1 - 5 \text{ min}$ $w/s \approx 1.6$	$t_{static} \geq 5 \text{ min}$ $w/s \approx 2.3$	$t_{vibr} = 1 \text{ s}$ $w/s \approx 1.2$	$t_{vibr} = 5 \text{ s}$ $w/s \approx 0.9^*$	$t_{vibr} = 10 \text{ s}$ $w/s \approx 0.8^*$

*Nonwovens N1&N2 have a sufficient lateral water migration resistance. The maximum limit value of the w/s-ratio is unknown so far.

Fig. 13. Hypothesis on the temporal processes in the nonwoven after application of the fresh concrete. The nonwoven with an initial thickness h_0 is compressed due to the fresh concrete ($h_1 < h_0$), filled with water and fines after concrete placement and in the final state decompressed ($h_{fin} \approx h_0$).

supplemented with examples of nonwovens N1 and N2. Based on the tests, a hypothesis regarding the cement paste filtration and intrusion was formulated, splitting the entire process into two stages: initial processes due to fresh concrete load and subsequent processes during the vibration compaction.

After the fresh concrete is placed, the nonwoven is initially compressed, and its pore volume is reduced [5]. Simultaneously, water and a limited mass of solids are separated from the fresh concrete, as seen in Fig. 3. After a few minutes, a dense solid layer had formed on the nonwoven, clear filtrate was separated, and the nonwoven was filled with a water-rich paste. This finding contradicts the existing working model for mechanical bonded pre-applied membranes where filtration only occurs during vibration compaction [4, 50,51].

Initial separation of solids is known for common filter cake filtration [7] and was also observed during sludge dewatering using geotextiles [20,21]. Fine solids can pass through the filter medium during filter cake formation, causing turbidity. Larger solids stay on top of the nonwoven and form a filter cake, preventing further solid separation and resulting in a clear filtrate.

For nonwovens on pre-applied membranes, it is plausible that filter cake formation occurs rapidly due to concrete’s high solids content. The rapid attainment of stationary masses in the nonwoven and decrease in particle size at the beginning of static loading supports this assumption. In this stage, particle movement may be driven by the higher density of aggregates and cement particles, similar to sedimentation, and be supported by the flow of the separated water. Subsequently, depth filtration led to finer particle sizes over the nonwoven height, resulting in smaller particles in the bottom of the nonwoven. It is known from earlier studies that concrete bonded nonwovens are not waterproof after static loading [4,5], presumably because vibration is needed to disperse the solids in the nonwoven.

With the onset of vibration compaction, more solids from the fresh concrete were penetrating the nonwoven. Similarly [23,24], tested geotextiles under pulsating hydrodynamic load and found excessive soil loss through the nonwoven compared to static loading. On pre-applied membranes, higher solid separation may be due to five effects:

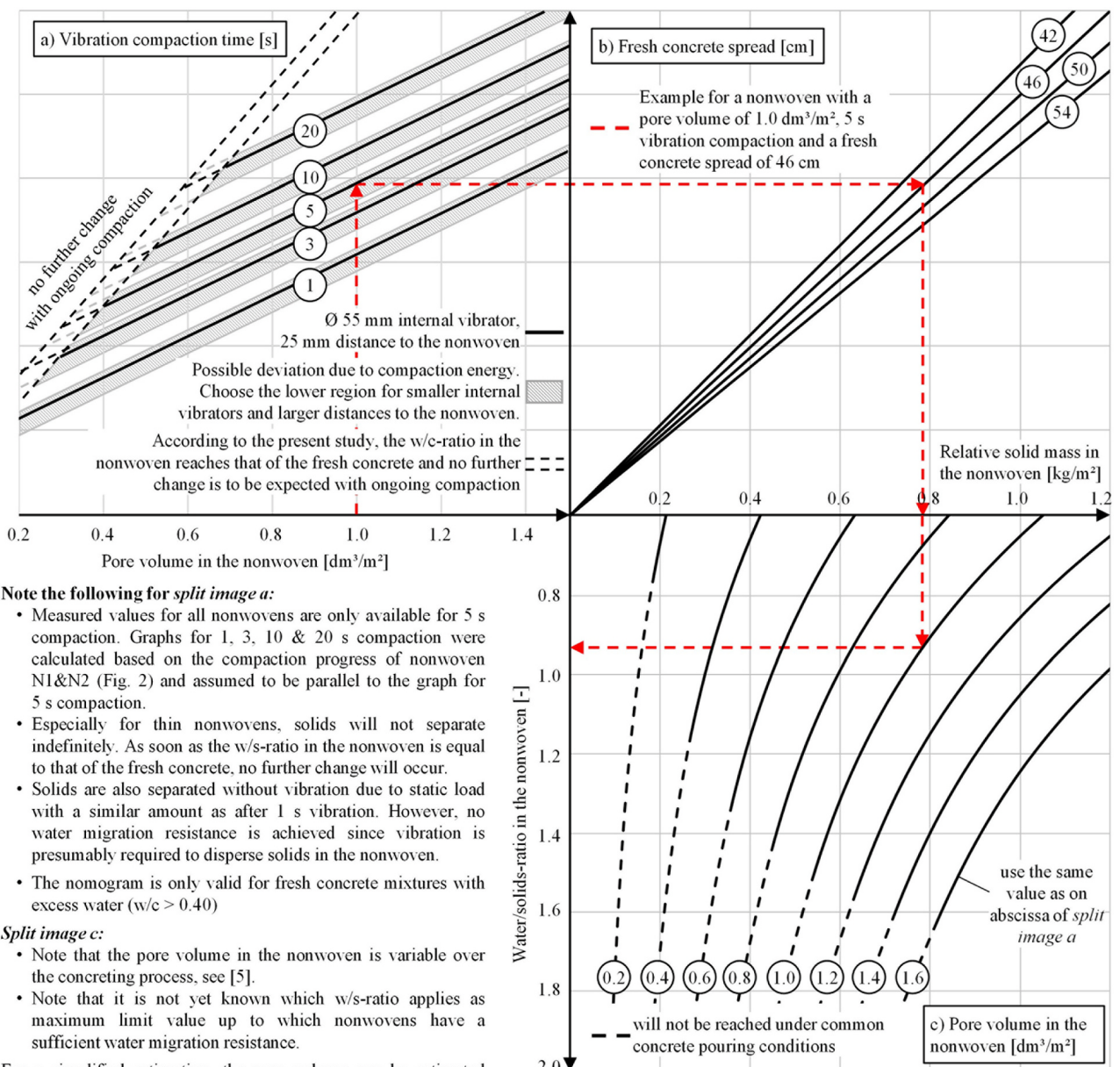
- The existing filter cake, formed during static loading, was loosened by the vibration compaction.
- Dynamic action is known to reduce the yield point of cement paste and dissolve interparticle forces [46], lowering filtration resistance.
- As the solid volume in the nonwoven increased, water from the nonwoven was possibly forced back upwards due to its lower density. As the water was squeezed back into the fresh concrete, it loosened the filter cake. The method of “backflows” or filter cake washing is used in filtration processes to loosen the filter cake in cyclic intervals [9].
- *Palmeira and Trejos* [17] argued for geotextiles that vibration moves particles within the nonwoven structure. A similar effect was observed in Chapter 3.5 for fresh concretes with low water contents, where vibration was needed to transport particles through the nonwoven. In this process, nonwoven fibers may be stimulated to vibrate.
- Nonwovens are compressed due to the fresh concrete, but are decompressed during vibration compaction [5]. So far, it is unclear how the thickness change affects the solid’s separation. Due to the relaxation effect during vibration compaction, pore sizes may expand, and permeability may increase again.

After 5 s vibration compaction, a high w/s-ratio remained in the nonwovens, ranging from 0.6 to 0.9 for the nonwovens N1 and N2. It was significantly higher than the w/c-ratio of the fresh concrete and contained about 15% inert fines from the aggregates. Evaluating this high w/s-ratio must consider two points: On the one hand, previous studies [4,5] have shown that the N1 and N2 nonwovens were

waterproof after 5 s of vibration compaction. On the other hand, Powers et al. [52] showed increasing permeability of hardened cement paste above w/c-ratios > 0.6, even when complete cement hydration was accomplished. It is not yet clear why nonwovens have a water migration resistance even with high w/s-ratios. A possible influence is an inhomogeneous solids distribution in the nonwoven resulting in locally fluctuating w/s-ratios, leading to nonwoven areas with w/s-ratios < 0.6. Also, the fiber-reinforced composite may have enhanced waterproofing, which needs further investigation.

With continued vibration compaction, the particle size decreased due to an increasingly compacted filter cake and embedded particles in the nonwoven (clogging). As a result, the permeability of the filter cake and the nonwoven presumably decreased over time and height. Similar effects have been observed for continuously loaded geotextiles [14,18,23].

In summary, the paste composition inside the nonwoven was variable in terms of water and solids content and solids composition (cement-aggregate ratio) due to the retention of sand particles in the upper nonwoven area. These properties varied with the loading condition (static/dynamic intrusion), time, and position in the nonwoven. Due to the variable paste composition, variable paste rheology must be expected. At the same time, the permeability of the nonwoven presumably changed due to clogging, resulting in



Note the following for split image a:

- Measured values for all nonwovens are only available for 5 s compaction. Graphs for 1, 3, 10 & 20 s compaction were calculated based on the compaction progress of nonwoven N1&N2 (Fig. 2) and assumed to be parallel to the graph for 5 s compaction.
- Especially for thin nonwovens, solids will not separate indefinitely. As soon as the w/s-ratio in the nonwoven is equal to that of the fresh concrete, no further change will occur.
- Solids are also separated without vibration due to static load with a similar amount as after 1 s vibration. However, no water migration resistance is achieved since vibration is presumably required to disperse solids in the nonwoven.
- The nomogram is only valid for fresh concrete mixtures with excess water (w/c > 0.40)

Split image c:

- Note that the pore volume in the nonwoven is variable over the concreting process, see [5].
- Note that it is not yet known which w/s-ratio applies as maximum limit value up to which nonwovens have a sufficient water migration resistance.

For a simplified estimation, the pore volume can be estimated from the nonwoven thickness and an average porosity of 0.86 for pre-applied mechanically bonded membranes (see Table 2).

Fig. 14. Nomogram for estimating the w/s-ratio in the nonwovens, based on the results of Chapter 3.1–3.7 and considering the relevant influences during concrete placement. Note that the nomogram is valid only for concretes with excess water (w/c > 0.40).

complex fluid flow processes in the nonwoven.

4.2. Recommendations for practice

The time until nonwovens were saturated with water during static loading depends on their pore volume, fresh concrete mixture's water retention capacity, and fresh concrete load. Normal site conditions would lead to saturation within a few minutes, so thin nonwovens will likely be saturated until vibration compaction starts. Especially for thick nonwovens, it appears advantageous to vibrate the concrete as early as possible to avoid high water contents in the nonwoven.

The separated solid mass especially depends on the nonwovens used, as higher pore volumes resulted in more separated solids. A similar effect was seen in Ref. [22], where thicker geotextiles separated a higher solid mass. It was argued that thicker nonwovens led to a slower stabilization of the filter cake, resulting in a lower filter cake compaction. Nevertheless, nonwovens with a high pore volume had increased w/s-ratios due to the high amount of water separating during static loading. Even with a long vibration time of 10 s, high w/s-ratios were present; longer compaction times are barely justifiable on a construction site. Nonwovens for pre-applied membranes should thus be selected with low pore volume, which corresponds to the finding in Ref. [5]. However, it is yet unclear how the pore volume affects the bond strength required in vertical applications, which should be investigated in further tests.

Another effect influencing solid's separation may be due to different manufacturing methods of nonwovens. Thin nonwovens are often thermally bonded on a calendar, while thick nonwovens tend to be mechanically bonded by hydroentanglement or needling. The different production processes result in variable surface and pore properties [53]. Furthermore, it was assumed in Ref. [5] that large pores running through the nonwoven (e.g., needle pores) favor filtration. However, no significant effects of these influences were observed in this study. Due to the filter cake, nonwoven N9 with large openings did not separate more solids, and the solid mass was determined in good correlation by the nonwovens pore volume.

The concrete placement, particularly the vibration compaction time, influenced the separated solid mass. Previous studies [4,5,50] identified a 2–3 s vibration time as sufficient for nonwovens up to 1.0 dm³/m² pore volume. However, the solid separation rate decreased with ongoing compaction time (see Fig. 3), presumably because the permeability of the filter cake and nonwoven were lowered due to clogging. Furthermore, the vertical distance between the internal vibrator and nonwoven as well as the diameter of the internal vibrator influenced the compaction progress [46]. relates a decreasing impact of an internal vibrator to smaller unbalanced masses and larger distances in the fresh concrete due to lower wave amplitudes. On nonwovens, smaller internal vibrators and increasing distances may have led to a less pronounced loosening of the filter cake resulting in slower solid separation.

Furthermore, increased fresh concrete workability led to an improved solid separation [4,50]. also observed an improving cement paste penetration in nonwovens of pre-applied membranes with an increased fresh concrete spread [1]. recommends a minimum fresh concrete spread of 42 cm, which appears justified as a higher fresh concrete spread ensured more solids in the nonwoven at constant vibration time.

Using the findings above, Fig. 14 shows a nomogram to estimate the w/s-ratios in the nonwoven, based on the separated solid mass from Fig. 12 and the relevant influences from fresh concrete spread and vibration compaction energy (Figs. 8 and 11). Note that the w/s-ratios were calculated based on the solid volume and the premise that the remaining volume in the nonwoven is filled with water. The solid volume was calculated according to Equation (2) based on the known solid mass (Fig. 12) and its density (Table 4). Furthermore, only the graph for 5 s compaction was measured across all nonwoven pore volumes (Fig. 12). Other compaction graphs were calculated based on the compaction progress for nonwoven N1 and N2 (Fig. 3). Note that the nomogram is only valid for concrete mixtures with excess water ($w/c > 0.40$). Also note the comments in Fig. 14.

4.3. Experimental limitations

Due to the experimental procedure and the samples used, the following limiting boundary conditions apply:

- The concreting tests were carried out with only one formwork size. Nevertheless, internal vibrators have different effective radii [46]. Thus, the solid masses using varying internal vibrators may deviate in reality from the values determined in this study.
- Only one grading curve, type of aggregate, and cement were included in the tests. Due to deviating fine fractions and particle size distributions, the formation of the filter cake and the separated solid masses may differ.
- No statement regarding a maximum w/s-ratio is possible yet, up to which the nonwovens have a waterproof bond. Further tests are necessary.
- No pressurized water tests have been performed, and the suitability of the different nonwovens has only been determined based on the separated solid mass.
- The tests were carried out in the laboratory at around 24 °C. Both cement paste rheology and polymer properties are strongly temperature-dependent.

5. Conclusions

This paper aims to determine the process and influences on paste infiltration during concrete placement to optimize nonwovens for pre-applied membranes and avoid defects due to incorrect concrete placement. The following conclusions can be drawn:

- The test stand exposed loose nonwovens to site typical concrete placements with an internal vibrator and allowed the analysis of the separated solids. The comparability to pre-applied membranes was verified using nonwovens on a sealing layer.
- After the fresh concrete is placed on the nonwoven, water and a limited solid mass separate during filter cake formation, subsequently, water continues to separate until the nonwoven is saturated.

- As vibration compaction begins, more solids penetrate the nonwovens, presumably as the filter cake is loosened by dynamic vibration. The w/s-ratio in the nonwovens is reduced, and excess water is squeezed back into the fresh concrete leading to further loosening of the filter cake. Also, vibration probably enhances the distribution of the solid particles in the nonwovens. The proposed working model was graphically summarized in Fig. 13.
- The solids particle size depends on the loading modality (static loading/vibration compaction), the duration, and the position in the nonwovens. The particle size decreases with longer vibration times and lower positions in the nonwovens.
- High w/s-ratios of 0.6–0.9 (by mass) were determined after 5 s vibration compaction for nonwovens known to be waterproof at this point. Further investigations must determine whether the solids distribution is uniform or the maximum w/s-ratio up to which nonwovens are waterproof.
- The separation of solids during vibration compaction is influenced, ordered by relevance, by the nonwovens pore volume, the compaction time, the fresh concrete spread, and the distance between the internal vibrator and the nonwovens. The diameter of the internal vibrator has a minor and other fresh concrete properties a negligible influence. Thus, compaction should be carried out as close to the nonwovens as possible for a few seconds using a fresh concrete mixture with good workability. To estimate the influence of changed concrete placement parameters, a nomogram was proposed in Fig. 14.
- New nonwovens for pre-applied membranes should be designed with a minimum pore volume and therefore be thin and of low porosity. However, this may be contrary to a good bond strength. Further investigations are necessary to investigate nonwoven properties for a good bond strength.

CRedit author statement

for the for the article „Heinlein, Freimann: Pre-applied mechanically bonded waterproofing membranes: Cement paste filtration process and influencing parameters”

The corresponding author Ulli Heinlein has acted in the following roles: Conceptualization, Methodology, Resources, Investigation, Formal Analysis, Writing – original draft, Writing – reviewing and editing.

The author Thomas Freimann has acted in the following roles: Funding acquisition, Writing – original draft.

Declaration of competing interest

The authors declare that they have no known competing financial interests or personal relationships that could have appeared to influence the work reported in this paper.

Data availability

Data will be made available on request.

Acknowledgment

The authors would like to thank Prof. Dr.-Ing. K.-Ch. Thienel (Universität der Bundeswehr München) for the inspiring discussions. The present work is supported by the Bavarian Academic Forum in the collegium “Infrastruktur-Bauen-Urbanisierung”.

References

- [1] E.V. Deutscher Beton- und Bautechnik-Verein, DBV-Heft 44 "Frischbetonverbundsysteme (FBV-Systeme) - Sachstand und Handlungsempfehlungen" Fassung Oktober 2018, Eigenverlag DBV, 2018.
- [2] BS 8102:2009-11-30, Code of Practice for Protection of below Ground Structures against Water from the Ground. British Standards Institution, London.
- [3] U. Heinlein, K.-C. Thienel, T. Freimann, Pre-applied bonded waterproofing membranes: a review of the history and state-of-the-art in Europe and North America, *Construct. Build. Mater.* 296 (2021), 123751, <https://doi.org/10.1016/j.conbuildmat.2021.123751>.
- [4] L. Meyer, S. Bilgin, S. Filusch, T. Freimann, U. Heinlein, K. Herrmann, *Bauwerksabdichtung mit Frischbetonverbundfolie - Grundlagen zur Erstellung eines Regelwerks für eine innovative Bauart: Abschlussbericht F 3183*, Fraunhofer IRB Verlag, Stuttgart, 2020.
- [5] U. Heinlein, T. Freimann, Pre-applied mechanical bonded waterproofing membranes: macroscopic nonwoven behavior during the concreting process, *J. Build. Eng.* 45 (2022), 103531, <https://doi.org/10.1016/j.jobe.2021.103531>.
- [6] I.M. Hutten, *Handbook of Nonwoven Filter Media*, Butterworth Heinemann an imprint of Elsevier Ltd, 2016. Kidlington, Oxford, Waltham, MA.
- [7] M. Stieß, *Mechanische Verfahrenstechnik - Partikeltechnologie 1*, third ed., Springer, 2009.
- [8] Verein Deutscher Ingenieure, VDI 2762-1 - Mechanical Solid-Liquid-Separation by Cake Filtration - Overview, 2006.
- [9] K. Luckert (Ed.), *Handbuch der mechanischen Fest-Flüssig-Trennung*, first ed., Vulkan-Verlag, Essen, 2016.
- [10] R.J. Barrett, Use of Plastic Filters in Coastal Structures, 10th Conference on Coastal Engineering, Tokyo, Japan, 1966, pp. 3–22.
- [11] B.R. Christopher, G.R. Fischer, Geotextile filtration principles, practices and problems, *Geotext. Geomembranes* 11 (4–6) (1992) 337–353, [https://doi.org/10.1016/0266-1144\(92\)90018-6](https://doi.org/10.1016/0266-1144(92)90018-6).
- [12] K. Liao, S. Bhatia, Geotextile tube: filtration performance of woven geotextile under pressure, *Proceedings of NAGS* (2005) 1–15.
- [13] S.M. Luettich, J.P. Giroud, R.C. Bachus, Geotextile filter design guide, *Geotext. Geomembranes* 11 (4–6) (1992) 355–370, [https://doi.org/10.1016/0266-1144\(92\)90019-7](https://doi.org/10.1016/0266-1144(92)90019-7).
- [14] A. Muthukumar, K. Ilamparuthi, Laboratory studies on geotextile filters as used in geotextile tube dewatering, *Geotext. Geomembranes* 24 (4) (2006) 210–219, <https://doi.org/10.1016/j.geotextmem.2006.03.002>.
- [15] ASTM D 1434-1982: Test Method for Determining Gas Permeability Characteristics of Plastic Film and Sheeting: American Society for Testing and Materials. <https://doi.org/10.1520/D1434-82R15E01>.
- [16] D. Cazzuffi, M.C. Mandaglio, N. Moraci, Hydraulic properties, behavior, and testing of geotextiles, in: *Geotextiles*, Elsevier, 2016, pp. 151–176.
- [17] E.M. Palmeira, H.L. Trejos Galvis, Opening sizes and filtration behaviour of nonwoven geotextiles under confined and partial clogging conditions, *Geosynth. Int.* 24 (2) (2017) 125–138, <https://doi.org/10.1680/jgein.16.00021>.

- [18] M.G. Gardoni, E.M. Palmeira, Microstructure and pore characteristics of synthetic filters under confinement, *Geotechnique* 52 (6) (2002) 405–418, <https://doi.org/10.1680/geot.2002.52.6.405>.
- [19] R.M. Koerner, G.R. Koerner, Lessons learned from geotextile filter failures under challenging field conditions, *Geotext. Geomembranes* 43 (3) (2015) 272–281, <https://doi.org/10.1016/j.geotextmem.2015.01.004>.
- [20] S. Bourges-Gastaud, G. Stoltz, F. Sidjui, N. Touze-Foltz, Nonwoven geotextiles to filter clayey sludge: an experimental study, *Geotext. Geomembranes* 42 (3) (2014) 214–223, <https://doi.org/10.1016/j.geotextmem.2014.03.002>.
- [21] Wilke M, Hangen H. Geotextile Container und Schläuche zur Entwässerung von Schlämmen: Funktionsprinzip - Abdichtungsmaßnahmen - Anwendungsmöglichkeiten. 27. Fachtagung 'Die sichere Deponie 2011 - Abdichtung von Deponien und Altlasten mit Kunststoffen'.
- [22] G. Stoltz, P. Delmas, C. Barral, Comparison of the behaviour of various geotextiles used in the filtration of clayey sludge: an experimental study, *Geotext. Geomembranes* 47 (2) (2019) 230–242, <https://doi.org/10.1016/j.geotextmem.2018.12.008>.
- [23] D.B. Narejo, R.M. Koerner, A dynamic filtration test for geotextile filters, *Geotext. Geomembranes* 11 (4–6) (1992) 395–400, [https://doi.org/10.1016/0266-1144\(92\)90021-2](https://doi.org/10.1016/0266-1144(92)90021-2).
- [24] Y.-S. Hong, C.-S. Wu, Filtration behaviour of soil-nonwoven geotextile combinations subjected to various loads, *Geotext. Geomembranes* 29 (2) (2011) 102–115, <https://doi.org/10.1016/j.geotextmem.2010.10.010>.
- [25] Övbb-Merkblatt, Weiche Betone". Österreichische Vereinigung für Beton und Bautechnik, 2009.
- [26] A.R. El Zein, Y. Vanhove, C. Djelal, O. Madec, P. Gotteland, Evaluation of internal bleeding in concrete foundation from the Terzaghi's effective stress postulate, *Mater. Struct.* 54 (6) (2021), <https://doi.org/10.1617/s11527-021-01828-1>.
- [27] C. Djelal, Y. Vanhove, A. Azzi, O. Madec, Recommendation for concrete mix design to prevent bleed channels on diaphragm walls, *Europ. J. Environ. Civil Eng.* (2020) 1–13, <https://doi.org/10.1080/19648189.2020.1713900>.
- [28] M.D. Larisch, K.G. Higgins, Y. Ainsworth, D.G. Toll, A.S. Osman, *Concrete Bleeding in Deep Foundations as a Result of Aggregate Grading, Piling, 2021, 2020*.
- [29] DBV-Merkblatt Besondere Verfahren zur Prüfung von Frischbeton. Fassung 01/2014. Deutscher Beton- und Bautechnikverein E.V. Berlin.
- [30] DIN EN 480-4 - 2006-03 Zusatzmittel für Beton, Mörtel und Einpressmörtel - Prüfverfahren - Teil 4: Bestimmung der Wasserabsonderung des Betons (Bluten); Deutsche Fassung.: (Beuth).
- [31] ASTM C232/C232M-20a Standard Test Method for Bleeding of Concrete. ASTM International;91.100.30.
- [32] W.F. Price, *Controlled Permeability Formwork*, CIRIA, London, 2000.
- [33] P.J. Schubel, N.A. Warrior, K.S. Elliott, An investigation into factors affecting the performance of composite controlled permeable formwork liners: Part II – filter medium, *Construct. Build. Mater.* 22 (11) (2008) 2235–2249, <https://doi.org/10.1016/j.conbuildmat.2007.08.006>.
- [34] H. Figueiras, S. Nunes, J.S. Coutinho, J. Figueiras, Combined effect of two sustainable technologies: self-compacting concrete (SCC) and controlled permeability formwork (CPF), *Construct. Build. Mater.* (23) (2009) 2518–2526, <https://doi.org/10.1016/j.conbuildmat.2009.02.035>.
- [35] S. Kothandaraman, S. Kandasamy, K. Sivaraman, The effect of controlled permeable formwork liner on the mechanical and durability properties of self compacting concrete, *Construct. Build. Mater.* (118) (2016) 319–326, <https://doi.org/10.1016/j.conbuildmat.2016.05.083>.
- [36] E. Nolan, P.A.M. Basheer, A.E. Long, Effects of three durability enhancing products on some physical properties of near surface concrete, *Construct. Build. Mater.* 9 (5) (1995) 267–272.
- [37] Z.Q. Yang, J.Z. Liu, W. Lin, J.P. Liu, D.G. Xu, Review of progress and applications of controlled permeability formwork in concrete engineering, *AMR (Adv. Magn. Reson.)* 821–822 (2013). <https://doi.org/10.4028/www.scientific.net/AMR.821-822.171>, 171–8.
- [38] ISO 13320:2020-01, *Particle Size Analysis - Laser Diffraction Methods*, Beuth, 2020-01.
- [39] DIN EN 1097-7:2008-06, Prüfverfahren für mechanische und physikalische Eigenschaften von Gesteinskörnungen - Teil 7: Bestimmung der Rohdichte von Füller - Pyknometer-Verfahren; Deutsche Fassung EN 1097-7:2008. Berlin: Beuth Verlag GmbH. <https://doi.org/10.31030/1426719>.
- [40] DIN EN 1849-2:2019-09, Abdichtungsbahnen - Bestimmung der Dicke und der flächenbezogenen Masse - Teil 2: Kunststoff- und Elastomerbahnen für Dachabdichtungen; Deutsche Fassung EN 1849-2:2019. Berlin: Beuth Verlag GmbH. <https://doi.org/10.31030/3042454>.
- [41] DIN EN ISO 12956:2020-05, Geotextilien und geotextilverwandte Produkte - Bestimmung der charakteristischen Öffnungsweite (ISO 12956:2019); Deutsche Fassung EN ISO 12956:2020. Berlin: Beuth Verlag GmbH. <https://doi.org/10.31030/3104672>.
- [42] DIN EN 12350-5:2019-09, Prüfung von Frischbeton - Teil 5: Ausbreitmaß; Deutsche Fassung EN 12350-5:2019. Berlin: Beuth Verlag GmbH. <https://doi.org/10.31030/3045714>.
- [43] DIN EN 12350-6:2019-09, Prüfung von Frischbeton - Teil 6: Frischbetonrohddichte; Deutsche Fassung EN 12350-6:2019. Berlin: Beuth Verlag GmbH. <https://doi.org/10.31030/3045731>.
- [44] J. Rickert, *Zeta-Potential und Rheologie von Zementleimen - Einfluss von Fließmittel sowie Hüttensand und Kalkstein*, *Betontechnische Berichte*, 2010-2012 (VDZ).
- [45] G. Spanka, H. Grube, G. Thielen, Wirkungsmechanismen verflüssigender betonzusatzmittel, *Beton* 45 (11) (1995) 802–808.
- [46] American Concrete Institute ACI Committee 309. Report on Behaviour of Fresh Concrete during Vibration. ACI 309.1R-08 2008.
- [47] M.T. Alonso, P. Schäffel, Das Wasserabsondern von Beton für Industrieböden. Laborergebnisse und Übertragbarkeit auf praktische Verhältnisse. TL.1, *beton* 64 (11) (2014) 455–460.
- [48] F. Dehn, O. Fischer, M. Orgass, Polypropylenfaserbeton (PP-faserbeton), in: K. Bergmeister, F. Fingerloos, J.-D. Wörner (Eds.), *Beton-Kalender 2017: Schwerpunkte: Spannbeton, Spezialbetone*, Ernst & Sohn, Berlin, 2017, pp. 473–489.
- [49] Krell J. Bluten von Beton. Nützlich oder möglichst zu vermeiden? VDB-information 117/12 2012.
- [50] U. Heinlein, T. Freimann, S. Bilgin, S. Filusch, L. Meyer, K. Herrmann, Frischbetonverbundsysteme – neue Erkenntnisse aus Forschung und Praxis, *Beton-Stahlbetonbau* (2020), <https://doi.org/10.1002/best.202000031>.
- [51] T. Freimann, U. Heinlein, Planung und Anwendung der Frischbetonverbundsysteme bei wasserundurchlässigen Baukonstruktionen aus Beton, in: K. Bergmeister, F. Fingerloos, J.-D. Wörner (Eds.), *Beton-Kalender 2018: Bautenschutz, Brandschutz*, Ernst & Sohn a Wiley brand, Berlin, Germany, 2018, pp. 227–258.
- [52] T.C. Powers, L.E. Copeland, J.C. Hayes, H.M. Mann, Permeability of Portland cement paste, *J. Am. Concr. Inst.* (1954).
- [53] H. Fuchs, W. Albrecht (Eds.), *Vliesstoffe: Rohstoffe, Herstellung, Anwendung, Eigenschaften, Prüfung*, second ed., Wiley-VCH, Weinheim, 2012.

9.4 Pre-applied mechanically bonded waterproofing membranes: Bond strength of nonwovens to concrete and influencing parameters

Reprint

Published in “Journal of Building Engineering”

Volume 68, 2023; DOI: 10.1016/j.job.2023.105837

Authors: U. Heinlein, T. Freimann



ELSEVIER

Contents lists available at ScienceDirect

Journal of Building Engineering

journal homepage: www.elsevier.com/locate/job

Pre-applied mechanically bonded waterproofing membranes: Bond strength of nonwovens to concrete and influencing parameters

Ulli Heinlein^{*}, Thomas Freimann

Technische Hochschule Nürnberg Georg Simon Ohm, 90489, Nürnberg, Germany

ARTICLE INFO

Keywords:

pre-applied waterproofing membranes
Blindside waterproofing
Fully-bonded waterproofing membranes
Nonwoven
Bond strength
Bonding
Tensile bond

ABSTRACT

Pre-applied bonded membranes are used for waterproofing on the outside of concrete basements and are installed prior to the reinforcement, e.g., on a formwork. They often use nonwovens as a bonding layer and must ensure a sufficient bond both during stripping and use. However, it is not yet known how the bond develops and how it depends on concrete placement conditions. Hence, this study tested ten nonwovens for their bond to concrete in pull-off tests according to DIN EN 1542, varying the fresh concrete and concrete placement. The bond strength for all nonwovens developed proportionally to the concrete tensile splitting strength at a factor of 18–56% and was, e.g., 0.40–0.78 MPa after two days. The development was approximated by a *fib* model code approach, with higher concrete tensile splitting strengths and lighter nonwovens resulting in better bond strengths. In comparison with the reference tests, the bond strength was reduced for larger distances to the internal vibrator (max. –35%), higher w/c ratios of the fresh concrete, and nonwovens with higher basis weights. Also, water movements and air voids deviated the bond strength of vertically oriented nonwovens by –25% to +35% compared to reference values. Video recordings and measurements of the w/s ratio in the nonwoven complemented the results and showed that the nonwovens behave similarly to Controlled Permeable Formworks and separate excess water from the fresh concrete. As a result, the w/c ratio of the cement paste in the bonding zone changes, affecting the bond strength.

1. Introduction

Pre-applied bonded membranes are used to waterproof concrete basements on the outside (positive side). They are installed before the reinforcement underneath a base slab, vertically on a soil retention system, or in a formwork. With the later placed fresh concrete, they form a bond, improving redundancy compared to loosely laid waterproofing membranes [1]. If the membrane has a defect, the bond prevents lateral water migration between the concrete surface and the membrane, preventing cracks in the concrete from getting saturated [2]. Additionally, a tensile bond develops and enables, e.g., formwork stripping. Ref. [3] gives further information on the mechanisms and types of pre-applied waterproofing membranes.

Pre-applied bonded membranes comprise a sealing layer and a bonding layer, the latter often made of nonwovens that must be filled with cement paste during concrete placement. Heinlein and Freimann [4] investigated this process of cement paste filling by placing fresh concrete on loose nonwovens inside a pressure chamber and measuring the solid and water mass in the nonwovens. Based

^{*} Corresponding author.

E-mail address: ulli.heinlein@th-nuernberg.de (U. Heinlein).

<https://doi.org/10.1016/j.job.2023.105837>

Received 8 November 2022; Received in revised form 19 December 2022; Accepted 5 January 2023

Available online 6 January 2023

2352-7102/© 2023 The Author(s). Published by Elsevier Ltd. This is an open access article under the CC BY-NC-ND license (<http://creativecommons.org/licenses/by-nc-nd/4.0/>).

on the results, a working model for cement paste filling was created. Immediately after the concrete is poured, water and a limited amount of fine particles are separated from the fresh concrete. During this process, a filter cake forms on the nonwovens, inhibiting further separation of solids but still allowing excess water to pass through, resulting in a high water/solids ratio (w/s ratio). During compaction, the filter cake is loosened, and more solids penetrate the nonwoven, pushing separated water back into the fresh concrete and lowering the w/s ratio inside the nonwoven. Low w/s ratios were argued to improve the waterproof bond and were achieved using nonwovens with low pore volumes and long compaction times.

Controlled Permeable Formworks (CPF) also use nonwovens and are placed on formworks to remove excess water and air voids from the concrete surface, e.g., to increase durability [5]. CPF consists of a filter element facing the fresh concrete and a drainage layer on its back, draining excess water and air outside the formwork [6], while cement particles are retained due to small opening widths of the filter element (4–35 μm) [7]. The amount of excess water depends on the w/c ratio of the fresh concrete and ranges between 0.7 and 2.5 l/m^2 at w/c 0.5 [8,9]. It separates even without vibration compaction, as has been observed using self-compacting concretes [10,11].

The bond mechanisms of pre-applied membranes to concrete were previously investigated by Meyer *et al.* [12]. Mechanically bonded membranes were installed horizontally with fresh concrete, compacted on a vibrating table, and tested in pull-off tests according to DIN EN 1542 [13]. Variations were made in concrete age (2, 7, 28 d), cement type, membrane type, and fresh concrete load by performing pull-off tests over a 2.5 m high column. The following results were found: bond strength was between 0.2 and 1.1 MPa; cement types with lower early strength showed lower bond strength till 7 d; prewetted nonwovens showed reduced bond strength, and higher fresh concrete load increased the bond strength. However, not all effects could be explained since the nonwoven properties were unknown and since the internal bond between the nonwovens and sealing layer was, in some cases, weaker than the bond to concrete, thus, determining the overall bond strength. Furthermore, Long and Paul [14] investigated the peel-strength bond between concrete and geotextiles. They found the vibration compaction of the fresh concrete increased the bond strength by 20%, prewetted geotextiles reduced the bond strength, and woven geotextiles had a weaker bond than nonwovens.

No other studies have been published on the bond strength of pre-applied membranes, and previous studies remain unclear on the relationship between bond strength and concrete strength and the influence of concrete placement and nonwoven properties. This article examines ten nonwovens in pull-off tests under varying concrete placement conditions. In addition, processes within the nonwovens during concrete placement were recorded. This allowed the identification of relevant influences due to concrete mixture, concrete placement and vibration, the type and properties of nonwovens, and the identification of pertinent processes inside the nonwovens. The results complement the existing working model of the cement paste filtration process, allowing recommendations for practice and selecting suitable nonwovens for pre-applied bonded membranes regarding bond strength.

2. Methods and materials

2.1. Methods

2.1.1. Setup and procedure

In order to examine the bond strength of nonwovens to concrete, ten loose nonwovens were installed with fresh concrete and tested in pull-off tests according to DIN EN 1542 [13]. The use of loose nonwovens allowed known nonwoven properties, variations independent of pre-applied membranes on the market, and prevented the adhesion between nonwoven and sealing layer from affecting the bond. Furthermore, pull-off tests were already used in Ref. [12] for testing the bond strength of pre-applied membranes and recommended in Ref. [1] since they simulate the loading during formwork stripping. However, two confounding factors were identified in own preliminary tests, if DIN EN 1542 was applied for loose nonwovens: First, loose nonwovens can be entirely encased in cement paste after concrete placement and compaction preventing the application of test stamps directly onto the nonwovens, and thus, the reliable determination of the bond strength in the bonding zone. Second, epoxy resin can penetrate through nonwovens during the application of test stamps and may bond to the cement paste of the concrete, falsifying the results.

In order to avoid these confounding factors, the nonwovens were initially laminated to a plastic film made of low-density polyethylene (LDPE, 125 μm thickness), reproducing the build-up of pre-applied membranes. First, epoxy resin was applied to the plastic film at around 50 g/m^2 . After curing, a second layer of epoxy resin was applied at about 50 g/m^2 , and the nonwoven was placed on top and lightly pressed down with a roller. This two-step procedure resulted in a full-surface bond between the nonwovens and the epoxy

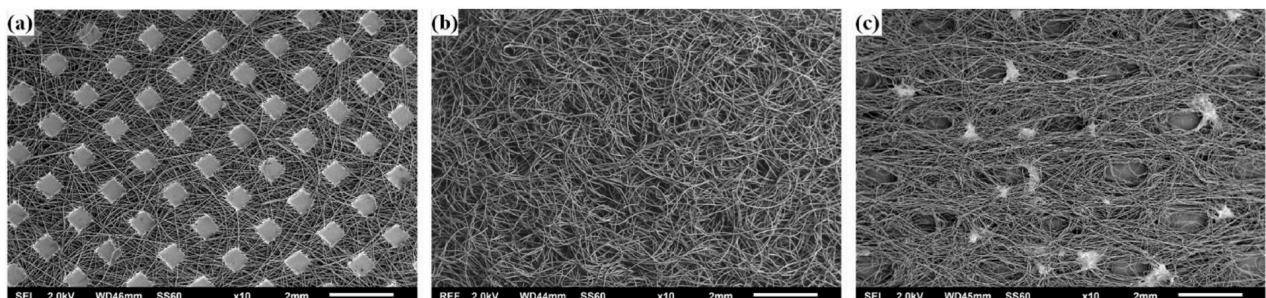


Fig. 1. The nonwoven surface was not changed by the lamination process using epoxy resin. SEM images of the nonwovens N4 with calendar bonding (a), N6 with needle bonding (b) and N9 with hydroentanglement (c) are shown.

resin and a closed surface on the reverse side. The nonwoven surface was not affected by the lamination process, as was verified using SEM images. Fig. 1 shows three various nonwoven surfaces bonded to the plastic film. The bond between the epoxy resin and plastic film ensured enough stability during concrete placement but was low enough to remove the plastic film after concrete hardening. Subsequently, a closed epoxy resin surface was present for applying the test stamps. The bond between the epoxy resin and nonwovens was sufficiently high for the pull-off tests, preventing the material strength from influencing the test results, as was the case in Refs. [12,15]. After the nonwovens were laminated, the tests followed the procedure shown in Fig. 2 and described below.

- **Formwork:** The specimens were installed with horizontal or vertical orientation on a formwork. The formwork was made waterproof; otherwise, separated excess water could leak out after concrete placement altering the fresh concrete composition.
- **Specimen size:** The size was selected according to DIN EN 1542 with dimensions of length/width $l/w = 300/300$ mm. In order to achieve proper compaction with the internal vibrator, the height of the specimens was set to 200 mm. For vertically oriented specimens, the height was set to 300 mm in order to provide the same test area as for horizontally oriented specimens.
- **Concrete placement:** The fresh concrete was poured with a hand shovel onto the specimen center. This was followed by a setting time of 15 min to simulate site conditions. The fresh concrete was then compacted with an internal vibrator ($\varnothing 55$ mm) for 0.5–10 s in the specimen center. To ensure exact vibration times, the internal vibrator was time programmed using a contactor, which was placed between the transducer and the vibrator and was operated using a programmable time-switching relay. Positions of the sampling given below refer to the axis of the internal vibrator.
- **Concrete curing:** The specimens were stripped after one day and cured underneath wrapping foil while the later test area was additionally covered by the laminated plastic film. The specimens were stored indoors at 23–25 °C until testing.
- **Pull-off tests:** At least five pull-off tests were carried out per specimen following DIN EN 1542. For preparation, the circumference of the test positions was drilled, then the plastic foil was removed, the test surface was lightly roughened, dried, and finally, steel stamps ($\varnothing 50$ mm) were affixed with a fast-curing epoxy resin. After curing, the pull-off tests were carried out with a stress rate of 0.05 MPa/s with the 'Proceq DY-206' automatic pull-off tester. If the specimens were younger than 1 d, the test positions were not drilled, as damage to the bond of the nonwovens could occur. Instead, the stamps were applied, and the nonwovens were subsequently cut. When positions of the pull-off tests are given below, they refer to the center of the test stamp.

2.1.2. Variations of the pull-off tests

A total of 304 specimens were tested, with at least 5 pull-off tests each to identify the influence of concrete mixture, placement, age, nonwovens, and the diameter of the internal vibrators. Variations were mainly investigated with nonwovens in horizontal orientation since the bond strength was then not affected by air voids. Table 1 lists the variations; Fig. 3 shows exemplarily a reference specimen with horizontal nonwoven orientation and a specimen with varying testing distances to the point of concrete placement and compaction.

2.1.3. Tensile splitting strength of concrete

In order to compare the bond strength with the concrete tensile strength, the tensile splitting strength was determined according to DIN EN 12390-6 [17]. Concrete cylinders with the dimensions $\varnothing/h = 150/300$ mm were used. For each concrete mixture and test date, three specimens were tested.

2.1.4. Approximation of the strength development

The development of the concrete tensile splitting strength was approximated in Chapter 3 according to the *fib* model code approach [18]. The approximation is designed for compressive strength and also exhibited a good fit for the results of the tensile splitting tests. Equation (1) describes the compressive strength $f_{cm}(t)$ over time for normal concretes according to the *fib* model code:

$$f_{cm}(t) = f_{cm} e^s \left[1 - \left(\frac{28}{t} \right)^{0.5} \right] \text{ [MPa]} \quad (1)$$

where f_{cm} is the mean compressive strength at 28 days in MPa, s is a unitless coefficient depending on the strength class of the cement,

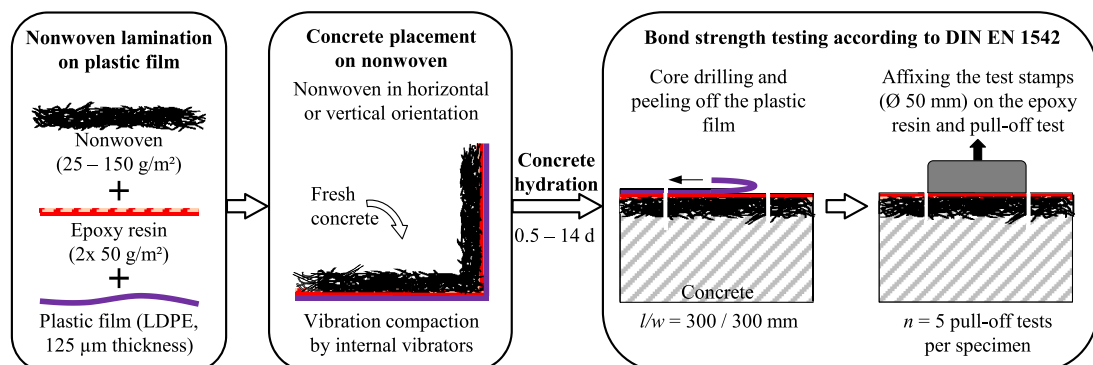


Fig. 2. Experimental procedure of the pull-off tests on concrete bonded nonwovens testing the bond strength.

Table 1
Methodological approach and experimental variation.

Test	Nonwoven orientation	Test parameters and deviations from the reference test	Specimen size l/w/h [mm]	No. of samples
Reference test	Horizontal (H)	Nonwovens N1&N2, concrete mixture 1 acc. to Tables 3 and 2 s vibration compaction (internal vibrator Ø 55 mm) 15 min after concrete pouring, 2 d concrete age	300/300/200	10
Concrete age	H	Testing after 0.5–14 d using concrete mixture 1&2 acc. to Table 3		74
Cement content	H	280/320/380 kg/m ³ cement content. Concrete mixtures 1&3–4 acc. to Table 3		24
w/c ratio	H	0.40/0.48/0.55/0.65 w/c ratio. Concrete mixtures 1&5–7 acc. to Table 3		28
Concrete workability	H	420/460/610 mm fresh concrete spread according to DIN EN 12350-5 [16]		20
Vibration compaction time	H	0/0.5/1/2/5/10 s vibration compaction time (internal vibrator Ø 55 mm)		32
Distance to and variation of internal vibrators	H	0/110/160/210/260/310 mm distance to internal vibrators with diameters Ø 30/45/55 mm	600/600/200	8
Nonwovens	H	N3–N10 with 25–150 g/m ² basis weight using concrete mixtures with w/c ratios 0.55 (0.5–7 d concrete age) and w/c 0.40 (2 d concrete age)	300/300/200	64
Video recording	H	Video recording of the horizontally oriented nonwoven N1 through acrylic glass during concrete placement and vibration compaction	500/500/200	1
Nonwovens	Vertical (V)	Nonwovens N1–N10 with vertical orientation	300/300/300	24
Vibration compaction time	V	0/1/2/5/10 s vibration compaction time (internal vibrator Ø 55 mm) using N1&N2 with vertical orientation		16
Fresh concrete load	V	0–1200 mm fresh concrete load by placing the nonwovens N1&N2 in a column formwork	300/300/1200	4
Video recording	V	Video recording of the vertically oriented nonwoven N1 through acrylic glass during concrete placement and vibration compaction		1

Table 2
Properties of the nonwovens before lamination to a plastic film [20].

Property	Unit	Individual mean values 10 tested products										Test method, number of samples per product, and average standard deviation \bar{s} in the test
		N1	N2	N3	N4	N5	N6	N7	N8	N9	N10	
Basis weight	g/m ²	64.3	97.1	23.7	52.9	116.9	153.4	109.8	37.3	60.3	86.8	6 samples per product, $\bar{s} = 8.2$ g/m ²
Thickness 0.5 kPa	mm	0.83	1.50	0.23	0.35	1.33	3.23	0.49	0.43	0.61	1.15	DIN EN 1849-2 [21]; 5 samples per product; $\bar{s} = 0.04$ mm
Thickness 2.0 kPa	mm	0.74	1.36	0.17	0.31	1.26	2.72	0.40	0.37	0.55	1.13	DIN EN 1849-2 [21]; 5 samples per product; $\bar{s} = 0.03$ mm
Thickness 15 kPa	mm	0.60	1.07	0.16	0.28	1.06	1.86	0.39	0.29	0.45	0.81	DIN EN 1849-2 [21]; 5 samples per product; $\bar{s} = 0.04$ mm
Fiber material		PP	PP	PP	PP	PP	PP	PP	PES	PES	PES	Manufacturer specification
Porosity at 15 kPa load, $\epsilon_{15\text{kPa}}$	[-]	0.88	0.90	0.84	0.80	0.88	0.91	0.69	0.91	0.90	0.92	$\epsilon_{15\text{kPa}} = 1 - \frac{m}{\rho T_{15\text{kPa}} A}$ (m : nonwoven basis weight, ρ : density of fibers, $T_{15\text{kPa}}$: thickness of the nonwoven at 15 kPa load; A : area)
Pore volume at 15 kPa load, $V_{15\text{kPa}}$	[dm ³ /m ²]	0.53	0.96	0.14	0.22	0.93	1.70	0.27	0.27	0.41	0.75	$V = \epsilon_{15\text{kPa}} T_{15\text{kPa}}$ ($\epsilon_{15\text{kPa}}$: porosity at 15 kPa load, $T_{15\text{kPa}}$: thickness of the nonwoven at 15 kPa load)
Type of nonwoven bonding		NP	NP	CB	CB	NP	NP	NP	HE	HE	HE	NP: Needle punching; CB: Calendar bonding; HE: Hydroentanglement

Table 3
Fresh concrete mixtures.

	Nr. of the mixture	Cement type	Cement content [kg/m ³]	Water content [kg/m ³]	w/c ratio	Aggregate A/B 32 [kg/m ³]
Reference	1	CEM II/A-LL 42.5 N	320	175	0.55	1847
	2	CEM III/A 42.5 N-LH	320	175	0.55	1847
Cement content	3	CEM II/A-LL 42.5 N	280	154	0.55	1937
	4	CEM II/A-LL 42.5 N	380	209	0.55	1707
w/c ratio	5	CEM II/A-LL 42.5 N	320	128	0.40	1971
	6	CEM II/A-LL 42.5 N	320	154	0.48	1903
	7	CEM II/A-LL 42.5 N	320	208	0.65	1761

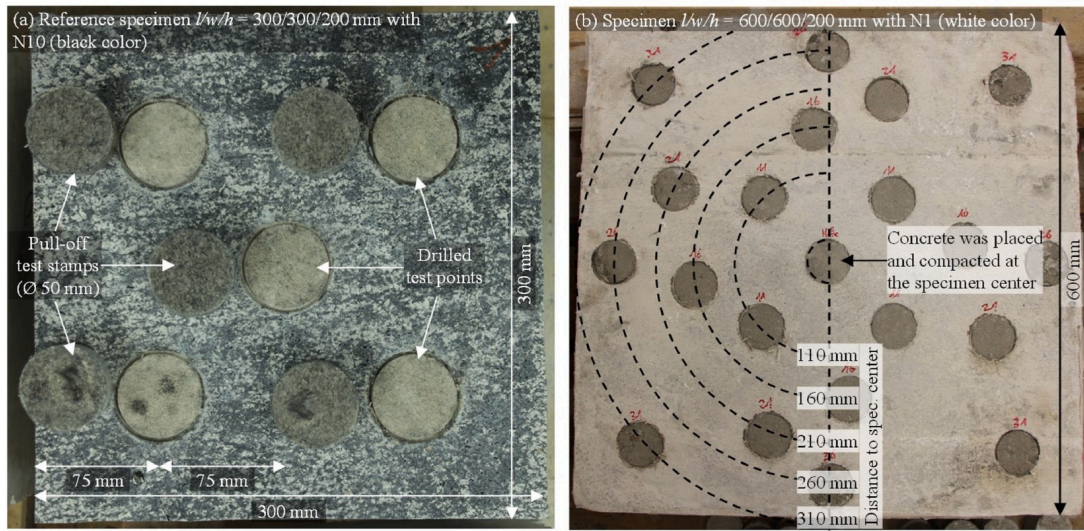


Fig. 3. Top view of a reference specimen with N10 with black color after testing (a) and a larger specimen with increasing testing distance to the point of concrete placement and compaction (b). (For interpretation of the references to color in this figure legend, the reader is referred to the Web version of this article.)

and t_T is the concrete age in days adjusted according to its temperature during curing. In order to approximate the tensile splitting strength in this paper, Equation (1) was adapted to Equation (2):

$$f_{ct,sp}(t) = f_{ct,sp} e^s \left[1 - \left(\frac{t}{t_T} \right)^{0.5} \right] \text{ [MPa]} \tag{2}$$

where $f_{ct,sp}$ is the concrete tensile splitting strength after 14 days as maximum test duration, and $f_{ct,sp}(t)$ is the tensile splitting strength over time. The concrete temperature during curing was considered using Equation (3):

$$t_T = \sum_{i=1}^n t_i e^{13.65} \frac{4000}{27a + T(t_i)} \text{ [d]} \tag{3}$$

where t_T is the temperature-adjusted concrete age in days, and $T(t_i)$ is the mean temperature in degrees Celsius during the time period t_i . The concrete temperature was recorded using embedded temperature sensors and a data logger with a measuring interval of 1 h. Two specimens were measured for each cement type. Also, the air temperature was recorded.

The bond strengths of the nonwovens showed proportionality to the concrete tensile splitting strength in Chapter 3. Thus, the bond strengths over time $f_{NW,pull-off}(t)$ were also approximated by the *fib* model code approach by shifting the tensile splitting strength using a unitless coefficient ν depending on the nonwoven in Equation (4):

$$f_{NW,pull-off}(t) = \nu f_{ct,sp}(t) \text{ [MPa]} \tag{4}$$

2.1.5. Determination of the w/s ratio in nonwovens

In Chapter 3.3, the ratio of water to solids (w/s ratio) within the nonwovens was determined across the specimen by measuring several subsamples. Before concrete placement, 25 disks with a diameter of 50 mm were punched out of a nonwoven at a distance to the specimen center of 0, 75, 100, 150, 175, and 225 mm. They were initially weighed, placed back into the overall nonwoven, and taped to the overall specimen on the reverse side to prevent leakage during concrete placement. The concrete was then placed and compacted as was done for bond strength specimens and immediately removed again. Finally, the disks were dried at 105 °C to determine the w/s ratio in the nonwoven according to Equation (5):

$$w / s = \frac{m_w}{m_s} \text{ [-]} \tag{5}$$

where m_w is the water mass, and m_s is the solid mass.

2.2. Materials

2.2.1. Nonwoven

Ten commercially available technical nonwovens were included in the tests (N1–N10). The nonwovens N1&N2 were included in all tests since they are used on commercially available pre-applied membranes. The nonwovens N3–N10 were used to investigate the textile influence and were chosen with different surface structures, weights, thicknesses, and types of bonding. The fundamental structural properties of the examined nonwovens were analyzed in Ref. [4] and presented in Table 2.

2.2.2. Concrete

Pre-applied membranes are usually installed with waterproof concrete. The reference concrete mixture contained a Portland limestone cement CEM II/A-LL 42.5 N with a cement content of 320 kg/m^3 , a w/c ratio of 0.55, and a grading curve A/B 32 ($k = 4.81$) with quartzitic round grain. The fresh concrete had a density of 2410 kg/m^3 according to DIN EN 12350-6 [17]. Furthermore, varying cement types, cement contents, and w/c ratios were tested and listed in Table 3 as fresh concrete mixtures 1–7. The spread of the fresh concrete mixtures was uniformly adjusted to 460 mm with a PCE-based superplasticizer, measured with the flow table test in DIN EN 12350-5 [16].

2.3. Internal vibrator

The concrete was compacted with high-frequency internal vibrators, as is typical for construction sites. An internal vibrator with a diameter of $\varnothing 55 \text{ mm}$ was used in all tests. Additionally, internal vibrators with $\varnothing 30 \text{ mm}$ and $\varnothing 45 \text{ mm}$ were used in the variation of concrete placement (Chapter 3.3). All internal vibrators were operated with a frequency of 200 Hz. The nominal power varied between 0.20 and 1.05 kW.

3. Results

3.1. Scatter of the bond strength

First, reference tests with horizontally and vertically oriented nonwovens were conducted to investigate the scatter. N1 and N2 were used to produce six specimens in horizontal orientation (in four concrete pours) and four specimens in vertical orientation (in two concrete pours). Fig. 4 shows the bond strength values being between 0.40 and 0.78 MPa and, thus, being similar to literature values in Ref. [12] with 0.40–0.93 MPa for comparable nonwovens and conditions. The scatter of the mean values is at a maximum of 0.17 MPa and thus sufficiently low compared to the influencing variables. Furthermore, the consistent results confirm a uniform lamination process of the nonwovens. It also became apparent from the N1 samples that the bond strength values depend on the nonwoven orientation during concrete placement.

The bond generally failed in the interface between the concrete surface and the nonwoven. For young specimens (<1d) and low concrete tensile strength, the nonwoven detached adhesively from the concrete surface. For older specimens, the failure was in the uppermost nonwoven layer as some fibers remained in the concrete and were pulled out of the nonwoven. The nonwoven disintegrated, the cement paste was released from the nonwoven and remained on the concrete surface as a sandy residue. Fig. 5 shows the concrete surface, and the disintegrated nonwoven for N1 and N2 two days after concrete casting.

3.2. Hardened concrete properties

The bond strength was evaluated depending on hardened concrete properties by varying the cement type and the curing time. Fig. 6 shows the bond strength and concrete tensile splitting strength over the concrete maturity for concrete mixture 1 using a CEM II (Fig. 6-a) and concrete mixture 2 using a CEM III (Fig. 6-b). The mathematical approach of the *fib* model code was used to approximate the splitting tensile tests via Equations (2) and (3) and the nonwoven bond strength via Equation (4) subsequent to the concrete setting. Table 4 lists the variables used for Equations (2) and (4), with the values s being close to the values given in the model code for the used cement types. Three observations can be made from Fig. 6.

- The concrete tensile splitting strength is approximated with a good fit using the mathematical approach of the *fib* model.

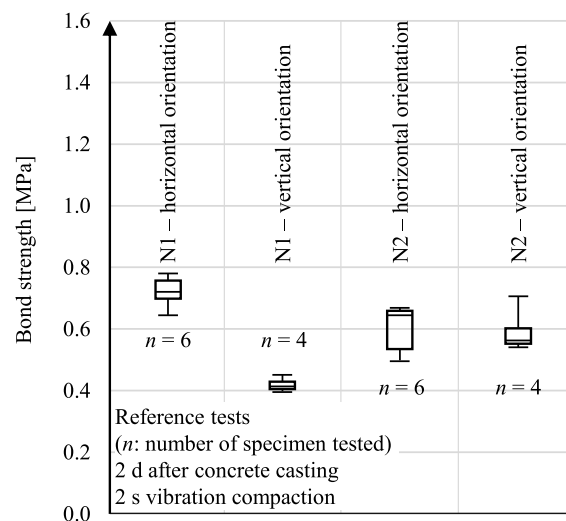


Fig. 4. Scatter of the bond strength in the reference tests. Whisker show max/min values.

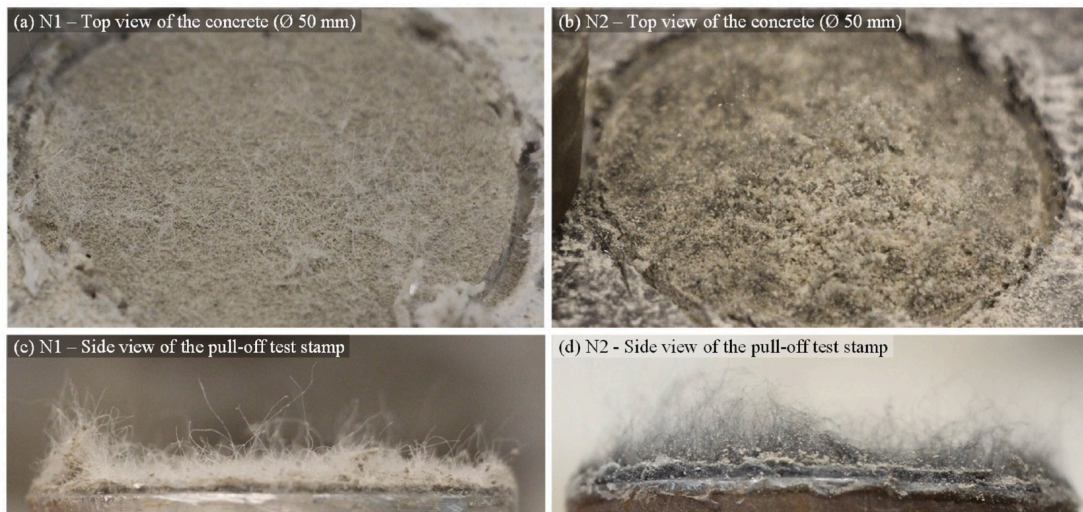


Fig. 5. Pull-off test specimens typically failed at the interface between the nonwoven and concrete in the upper nonwoven part, leaving some fibers in the concrete surface (a, b) and causing the nonwoven to disintegrate (c, d).

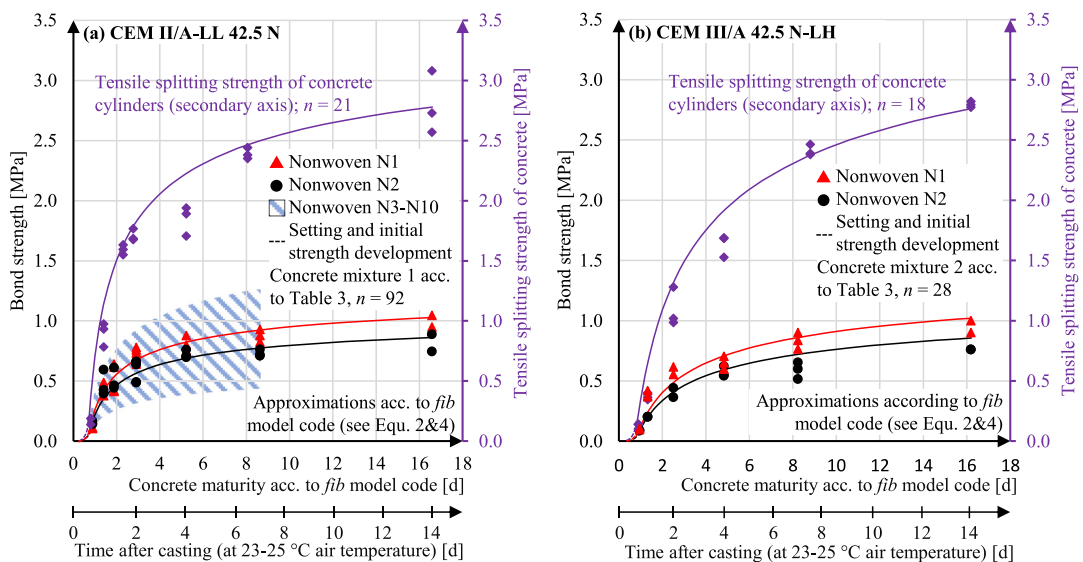


Fig. 6. Development of the bond strength compared to the concrete tensile splitting strength using a CEM II (a) or CEM III cement (b). Bond strength values are plotted against concrete maturity, which was determined according to Equation (3) according to the concrete temperature during curing. For comparison, the time after concrete placement is shown.

Table 4
Coefficients in Equations (2) and (4) to approximate the results in the tensile splitting and pull-off tests.

Cement type	Mean tensile splitting strength, 14 d after concrete casting $f_{ct,sp}$ for Equation 2	Cement-specific coefficient s in Equation 2	Nonwoven-specific coefficient v in Equation 4		
			Nonwoven N1	Nonwoven N2	Nonwoven N3-N10
CEM II/A-LL 42.5 N	2.79	0.25	0.37	0.31	0.18–0.52
CEM III/A 42.5 N-LH	2.71	0.42	0.37	0.31	–

- The nonwoven bond strength develops proportionally to the concrete tensile splitting strength. Equation (4) shows a good fit to the bond strength test results and is based merely on the shifting of the tensile splitting curve of the concrete.
- The nonwoven bond strength is lower than the concrete tensile splitting strength and ranges for all nonwovens in Fig. 6-a between 18 and 52% of the tensile splitting strength, as can be seen from coefficient ν in Table 4. The nonwovens show significant differences in absolute bond strength, demonstrating the relevance of the nonwoven properties.

The fresh concrete mixtures were varied according to Table 3. The influence of varying cement contents is shown in Fig. 7-a and of changing w/c ratios in Fig. 7-b. In particular, lower w/c ratios of the fresh concrete mixture lead to higher bond strength values. For example, N1 shows a bond strength of about 0.5 MPa at a w/c ratio of 0.65, increasing to 1.2 MPa at w/c 0.40. If, on the other hand, the cement contents were varied within reasonable limits for waterproof concrete, the bond strengths did only change slightly. The maximum difference in the mean values is 0.26 MPa for N1 and 0.17 MPa for N2 and is thus just above the scatter of 0.17 MPa from Chapter 3.1.

In order to further evaluate the proportionality between the bond and tensile splitting strength, they were plotted for equal test times against each other in Fig. 8. The regressions with good coefficients of determination (min $r^2 = 0.82$) confirm that the bond strength is significantly influenced by the concrete tensile splitting strength. However, results vary clearly between the different nonwovens. The slopes of the linear regressions were 0.39 for N1, 0.32 for N2, and between 0.18 and 0.56 for the nonwovens N3–N10. The slopes were also close to the coefficient ν in Table 4 and can be used to estimate nonwoven bond strength in relation to concrete splitting strength.

3.3. Concrete placement

Fig. 9 shows the influence of the fresh concrete spread (Fig. 9-a) and duration of vibration compaction (Fig. 9-b). The fresh concrete spread was adjusted using a PCE-based superplasticizer without further altering the mix design, having no effect on the bond strength. Longer vibration compactions also have a small influence but seem to cause a slight improvement in bond strength in both horizontally and vertically oriented nonwovens. Interestingly, even uncompacted specimens exhibit good bond strength values. Note that the small changes in bond strength are within the scatter of the reference tests.

During the tests, the bond strength at the specimen center was sometimes slightly higher than at the specimen edge. In order to investigate this influence more closely, the bond strength was determined with increasing distance to the internal vibrator on specimens with larger dimensions ($L/w/h = 600/600/200$ mm, see Fig. 3-b). The concrete was placed in the specimen center with a hand shovel and compacted with high-frequency internal vibrators with diameters of 30, 45, and 55 mm, as described in Chapter 2.2.3. The bond strength was measured two days after concrete casting and shown in Fig. 10-a for 0–310 mm distance between the pull-off test and the specimen center. For comparison, Fig. 10-b shows the w/s ratio measured in the nonwovens across specimens produced in the same way as the specimen for pull-off testing, as described in Chapter 2.1.5.

Fig. 10-a shows decreasing bond strength values with increasing distance from the specimen center. This effect seemed to be influenced by the concrete placement itself since even uncompacted specimens showed this trend. A possible explanation is the fresh concrete movement during concrete placement carrying more fine particles into the nonwoven at the specimen center. This effect was also observed visually after formwork striping with more cement paste within nonwovens at the specimen center and is available as Supplementary Fig. S1. Towards the edge of the specimen, the bond strength decreased with an increasing difference between vibrated and non-compacted samples. Especially internal vibrators with larger diameters and nominal powers showed enhancing effects at the specimen edges. Note that the small internal vibrator with $\varnothing 30$ mm had no observable compaction effect at the specimen edge and was limited to a vibration diameter of around 300 mm, corresponding to around 150 mm in Fig. 10. Simultaneously, the w/s ratio in

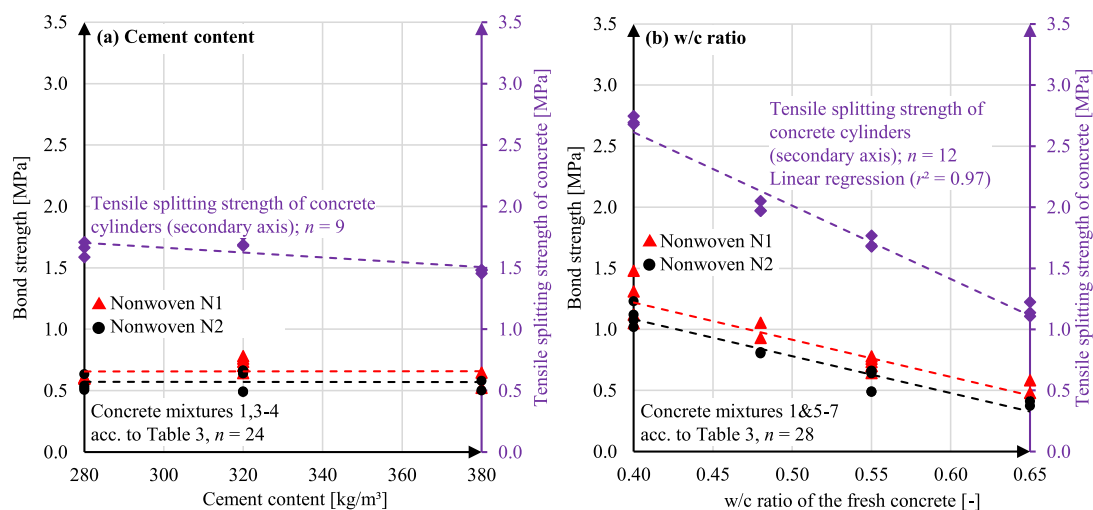


Fig. 7. Bond strength for concrete mixtures with varying cement content (a) or w/c ratio (b) compared to the concrete tensile splitting strength, two days after concrete casting.

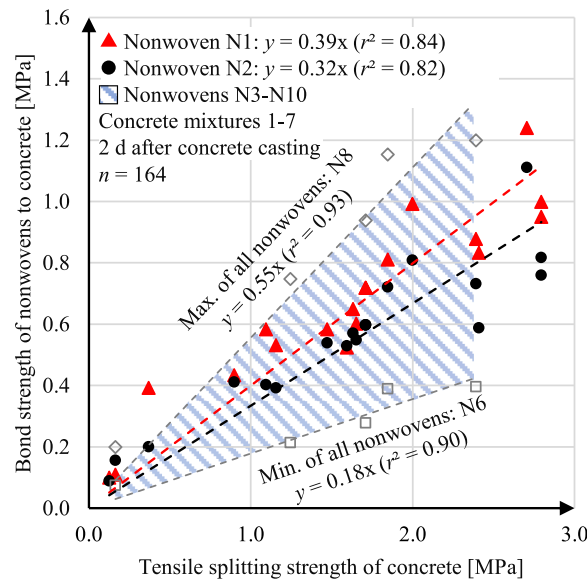


Fig. 8. Comparison of the bond strength of nonwovens to the tensile splitting strength of concrete for N1–N10.

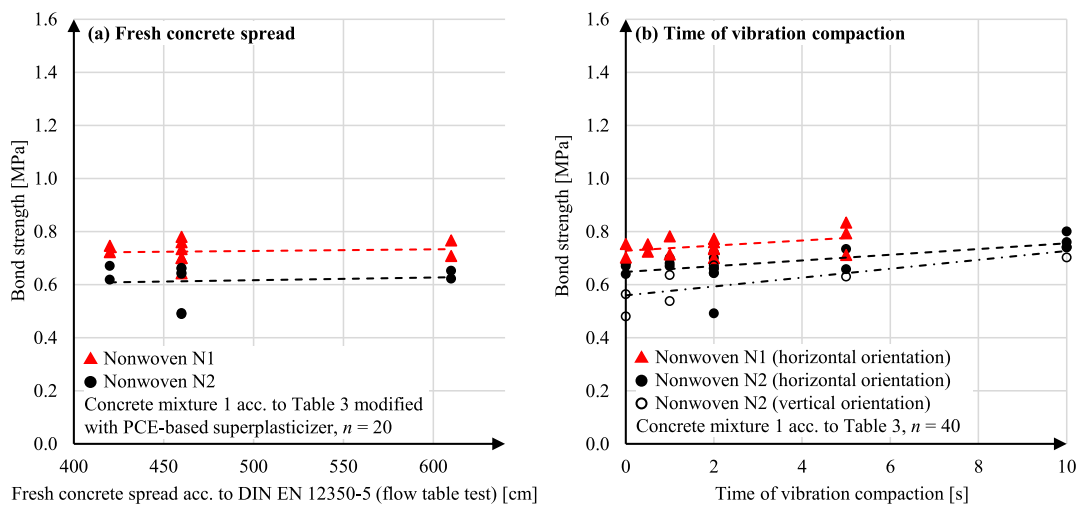


Fig. 9. Bond strength with varying fresh concrete spread (a) or vibration compaction time (b) two days after concrete casting.

Fig. 10-b was indirectly proportional to the bond strength of Fig. 10-a. In the center of the specimen, where better bond strength values were measured, the w/s ratio was lower - towards the edge of the specimen, the w/s ratio increased. Also, the nonwoven N2 yielded significantly higher w/s ratios than N1, corresponding to the lower bond strength values. Vibration compaction reduced the w/s ratios, with internal vibrators with larger diameters achieving more pronounced effects. The results of Fig. 10-a and 10-b suggest that the w/s ratio in the nonwoven influences the bond strength values.

3.4. Nonwoven properties

Fig. 11 displays the bond strength of the nonwovens N1–N10 during sustained hydration time. All nonwovens show a similar trend, like N1 and N2, with a development proportional to the concrete tensile splitting strength. Nevertheless, the absolute bond strength varied considerably and was, e.g., at 1.2 MPa for the nonwoven N8 and at 0.4 MPa for the nonwoven N6 after 7 days. In order to evaluate the influence of different material properties, the bond strength values after two days were plotted against different nonwoven properties. The regression with the best coefficient of determination is presented in Fig. 12-a with nonwovens with higher basis weights having lower bond strengths with a relatively mean coefficient of determination of $r^2 = 0.69$ [22]. The regression against thickness at 2 kPa load led to a low coefficient of determination of $r^2 = 0.48$; against pore volume of $r^2 = 0.39$.

Previous results suggest an influence of the nonwovens w/s ratio on the bond strength (see Fig. 10). However, the w/s ratio is influenced itself by the nonwovens pore volume as it controls the separable amount of excess water [20]. To separate these two

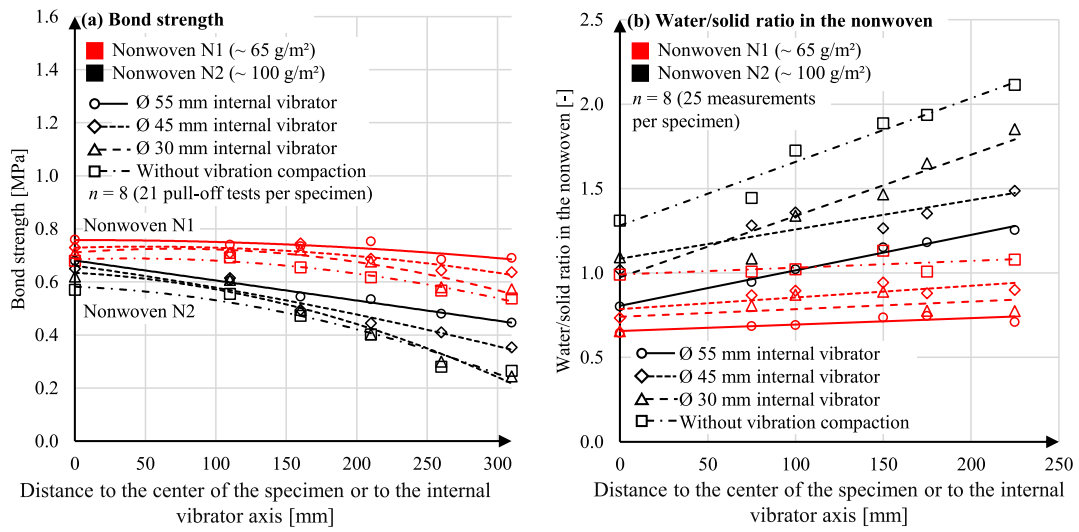


Fig. 10. Bond strength with increasing distance from the internal vibrator and location of concrete placement (a) and corresponding water/solid ratios in the nonwovens (b) two days after concrete casting.

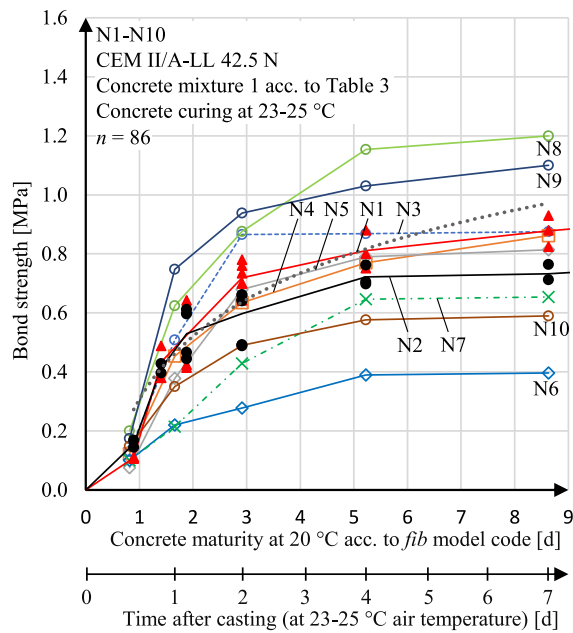


Fig. 11. Development of bond strength of the nonwovens N1–N10 during ongoing concrete hydration.

influences, the tests used for Fig. 12-a were repeated using a fresh concrete mixture that can be assumed without or with very low excess water with a w/c of 0.40. Then, the w/s ratios in all nonwovens approximately correspond to the w/c ratio of the fresh concrete. The resulting bond strengths are shown in Fig. 12-b, with the nonwovens now exhibiting small differences in the bond strength or slightly higher values for nonwovens with higher basis weights. Especially the bond strength of heavier nonwovens improved due to a lower w/c ratio. In comparison with Fig. 12-a, the bond strength values were plotted against basis weights leading to a poor correlation ($r^2 = 0.28$). A slightly better but still poor correlation was obtained versus nonwoven pore volume ($r^2 = 0.48$).

3.5. Nonwoven orientation

When the nonwovens were arranged vertically during concrete placement, they reached a lower bond strength on average. In Fig. 13, they were compared with the bond strength in horizontal orientation. According to a linear regression among all nonwovens, the bond strength in vertical orientation was, on average, 25% lower than in the horizontal orientation. Visible reasons for the lower bond strength values in the vertical area were voids, water channels, and cement paste washouts at the lower half of the specimen. The

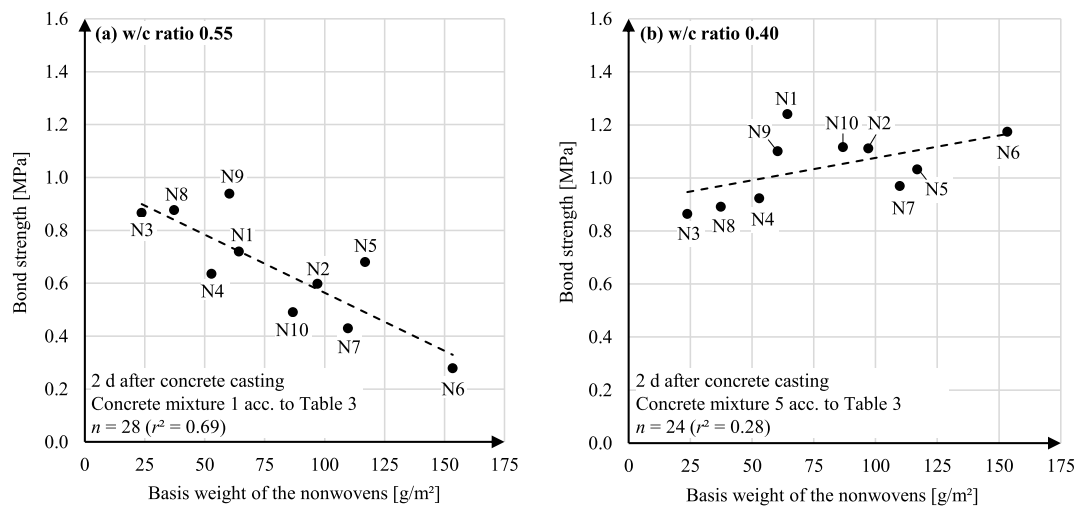


Fig. 12. Bond strength of nonwovens N1–N10 using a practice-oriented fresh concrete mixture with w/c 0.55 (a) and a fresh concrete mixture that can be assumed without or with very little excess water with w/c 0.40 (b).

washouts indicated water movements on top or within the nonwovens during concrete placement. However, it could not be determined yet which nonwovens are more sensitive to washouts when exposed to water movements.

3.6. Processes within nonwovens during concrete placement

In order to further investigate the processes within the nonwovens during concrete placement, the nonwoven N1 with a transparent sealing layer was filmed in a formwork made of acrylic glass. It was installed on a column with dimensions $l/w/h = 300/300/1200$ mm and sealed at the edges with silicone. Additionally, three dots of water-soluble color powder were applied to the nonwoven to visualize water movements, with the powder having a red to green color, depending on its dilution. Fig. 14 shows the different stages during and after concrete placement as described below.

1. During concrete placement, excess water separates from the fresh concrete and flows down in the nonwoven, as is evident from the color movements. After a few minutes, the water concentrates at the base of the column inside the nonwoven as standing water. Note that this was only possible because the formwork was sealed.
2. During concrete compaction, solids penetrate the nonwoven, as seen from the changing nonwoven color. As a result, water is displaced, partly rises to the top of the formwork due to its lower density, and partially mixes with the cement paste. Also, water channels become visible in the lower third of the column.
3. After final compaction, further upward water movements are visible, as indicated by a color difference marked in Fig. 14. However, it is unclear whether the water moves within the nonwoven due to the lower density compared to cement paste or between the laminated nonwoven and the acrylic glass due to a leaking sealing.

After two days, pull-off tests were carried out over the column height at 80 mm intervals (see Fig. 15). At the column head, the bond strength corresponds to the values of the reference tests in horizontal orientation, e.g., 0.75 MPa for N1 at the column compared to the reference with 0.72 MPa. Towards the center of the column at 500 mm fresh concrete height, the values increase by 30–40% and reach 0.98 MPa for N1. Towards the base of the column, the values decrease again to about 0.5 MPa. In comparison, the reference bond strength values in the vertical arrangement are between 0.4 and 0.6 MPa for the nonwovens N1 and N2. The discussion follows in Chapter 4.

The nonwoven N1 was also recorded in a horizontal arrangement, available as Supplementary Fig. S2. Before concrete placement, water moved to and collected at the specimen edges. During compaction, excess water was displaced to the specimen edge and rose upwards along the formwork. This led to water channels and washouts of the cement paste on the concrete surface, which were visible after stripping. After compaction, minor water movements occurred, similar to the column test in Fig. 14, from the specimen edge towards the center of the specimen. These movements were probably due to water movements within capillaries in unfilled nonwoven parts, diffusion processes between the water-rich specimen edge and the specimen center, or an ongoing excess water filtration from the fresh concrete in unfilled nonwoven parts.

4. Discussion

4.1. Processes during concrete placement

The recorded processes during concrete placement documented in Fig. 14 and S1 match the cement paste filtration process in Ref. [20], with excess water and a limited amount of solids separating before concrete compaction. The recordings also reveal separated excess water filling the nonwovens and being displaced during vibration compaction. In addition, water movements were

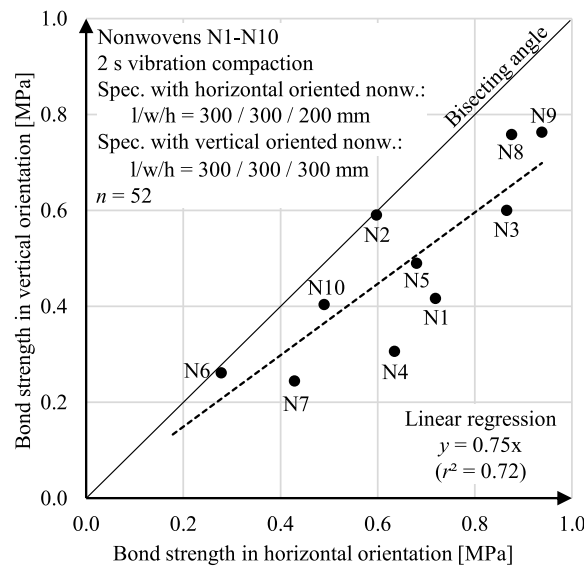


Fig. 13. Comparison of the bond strength values of the nonwovens N1–N10 in horizontal and vertical arrangement two days after concrete casting.

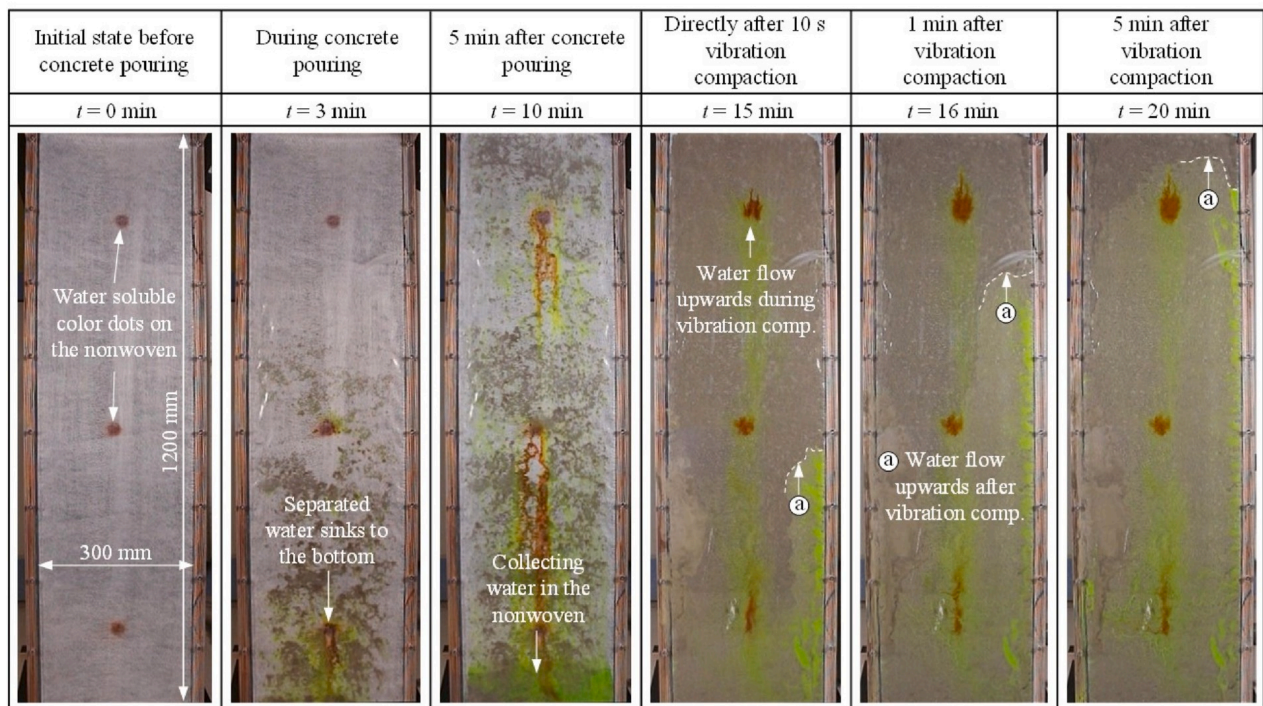


Fig. 14. –Nonwoven N1 during and after concrete placement. Noticeable is the flow of separated excess water in the nonwoven before and after concrete compaction. The reason for the water movement after vibration compaction is unclear.

visible after compaction in vertically arranged nonwovens, with water rising to the top. These processes in the nonwovens can partially be compared with Controlled Permeable Formworks (CPF), which separate excess water using a nonwoven filter, drain it off at the back and remove it outside the formwork, while cement particles are retained by small pore radii (4–35 μm) [7]. Unlike CPF, however, the sealing layer of pre-applied membranes prevents excess water from draining out. In contrast, the water is displaced within the nonwovens or squeezed back into the fresh concrete during concrete compaction.

4.2. Water content in the bonding zone

The investigated bonding layer is made of a nonwoven filled with cement paste. Thus, it is plausible that the cement properties

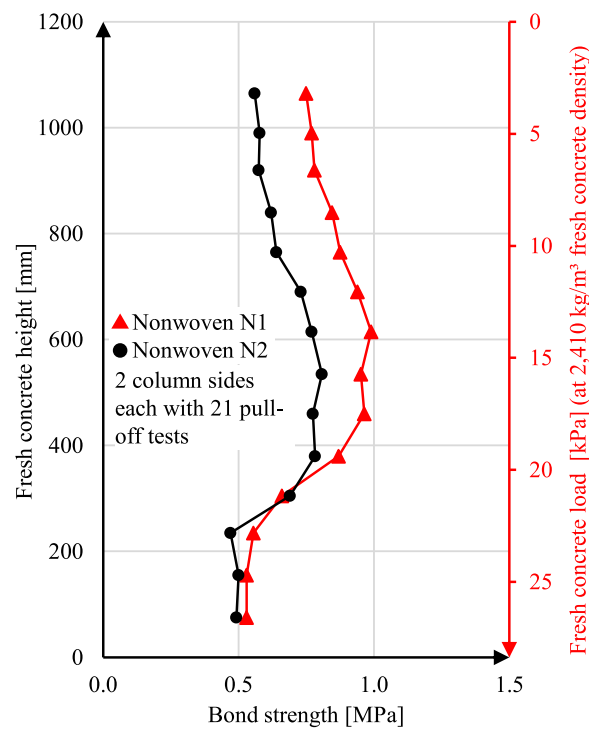


Fig. 15. Bond strength measured on a column in relation to the fresh concrete height or the fresh concrete load two days after concrete casting.

partly influence the physical performance of the bonding layer, and the cement strength influences the bond strength. Simultaneously, the cement strength is influenced by the w/c ratio according to Abrams Law (see Fig. 7-b or [23,24]). In combination with the water movements during concrete placement, the following can be postulated: water movements during concrete placement lead to varying w/c ratios in the nonwovens and the adjacent fresh concrete, which influence the strength of the cement matrix in the bonding zone, which in turn affects the bond strength. The following points support this hypothesis.

- Lower w/c ratios of the fresh concrete lead to higher bond and tensile splitting strength (see Fig. 7-b).
- The bond strength is lower in areas of higher w/s ratios in the nonwovens (see Fig. 10).
- Vibration compaction improves the bond strength, especially at the specimen edges, as accumulated excess water is displaced upward along the formwork.
- Pre-applied membranes with prewetted nonwovens exhibited reduced bond strength in Ref. [12]. Similarly, prewetted geotextiles had reduced peel strength values to concrete in Ref. [14].

The hypothesis is also supported by the bond strength among the tested nonwovens in Fig. 12 and the results across the column in Fig. 15. Heavier nonwovens yield lower bond strength values using a fresh concrete mixture with a w/c ratio of 0.55 (Fig. 12-a) - but at least equivalent bond strength values with w/c 0.40 (Fig. 12-b). At the same time, nonwovens with higher pore volumes are known to remove more excess water for w/c > 0.40 [20]. It is plausible that heavier nonwovens separate more excess water during concrete pouring, which changes the w/c ratio in the bonding zone during vibration compaction, reducing the matrix strength and, thus, the bond strength.

The bond strength values across the column also fit the hypothesis of changing w/s ratios in the bonding zone. If the bond strengths of the column are compared with those at varying w/c ratios in the fresh concrete of Fig. 7-b, the w/c ratio at the column center corresponds to 0.48–0.50. Comparable to CPF, water was separated, the w/c ratio in the adjacent fresh concrete was lowered, and its strength was increased [25,26]. At the same time, water separation is faster at higher fresh concrete loads [4], which explains the increasing bond strength towards the column center. In contrast, the column base corresponds to a w/c of 0.60, which can be explained by the collecting water, which is not completely displaced upward but is also pushed back into the fresh concrete raising the w/c ratio and reducing the matrix strength in the bonding zone.

The influence of the fresh concrete load on the bond strength was already investigated in Ref. [12] using a column with 2.5 m height. The membrane with the nonwoven N1 showed a strength increase of about 50% between the column base and top (one pull-off test). Here, the strength increased by about 35% at a fresh concrete height of 0.7 m. Lower bond strength values at the base were not determined in Ref. [12], probably because the first measuring point was between 150 and 450 mm from the bottom and because a standard column formwork was used, allowing excess water to drain out of the formwork.

4.3. Recommendations for practice

The bond strength develops proportionally to the concrete's tensile splitting strength and was between 0.28 and 0.94 MPa two days after concrete casting using a CEM II/A-LL 42.5 N. The values were comparable to Ref. [12], where the bond strength values of six mechanical bonded pre-applied membranes were between 0.40 and 0.93 MPa after two days using a CEM II/A-LL 32.5 R. Subsequently, the strength development slowed down and was at 23% between 2 and 7 d in Ref. [12] - here at 27% under comparable conditions. Note that these values were determined in an indoor climate between 20 and 25 °C and that the bond strength development is strongly temperature-dependent according to Ref. [15], comparable to the strength development of concrete. However, the bond strength is still clearly below the concrete tensile splitting strength. Since the debonding generally occurred at the interface between the nonwoven and the concrete surface, it is plausible that the nonwoven fibers lead to a weakening of the cement paste as they are mostly arranged parallel to the concrete surface (see Fig. 1).

Bond strength was present even without compaction, presumably as solids entered the nonwovens during filter cake formation leading to an interlocking of the upper nonwoven fibers with the concrete. Nevertheless, the bond strength depends on the installation position of the fresh concrete and is lower at specimen edges. During vibration, the bond improves at the edges during vibration compaction as water accumulations are displaced. Internal vibrators with larger diameters exhibited a greater improvement of the tensile bond strengths at the specimen edges, presumably due to higher amplitudes and a larger vibration radius. In contrast, the smaller internal vibrator with \varnothing 30 mm had no more compaction effect at the specimen edge with $l/w = 600/600$ mm. On site, however, compaction over the entire area is recommended since there is no defined location of fresh concrete placement. The fresh concrete should also be compacted quickly to avoid water accumulation, and base and corner areas should be compacted appropriately to displace existing water accumulations from the membranes.

The bond strength development follows the fib model code after introducing a nonwoven-specific coefficient v , which allows a rough estimation of the bond strength on-site based on the concrete tensile splitting strength and the nonwoven properties using Figs. 8 and 12-b. At a practical w/c ratio of 0.55, the bond strength is around 0.18–0.56 of the concrete's tensile splitting strength with lighter nonwovens bonding better than heavier ones. On top of that, differences according to the nonwovens' orientation and location must be considered. If nonwovens are oriented horizontally, bond strength values are influenced by the distance to the point of concrete pouring and can be 35% below reference values at the specimen edge, even after good vibration compaction. For nonwovens in vertical orientation, air voids, water channels, and separating excess water due to fresh concrete load influence the bond strengths between –25% (Fig. 13) to +35% (Fig. 15) of the reference values. In order to formulate stripping times for pre-applied membranes, acting forces, e.g., at fasteners, have to be known. However, little research is available on this topic, so the recommendation on the stripping time of Ref. [28] remains valid. In good weather conditions ($T \geq 20$ °C) and cement types with medium or rapid strength development, pre-applied membranes should remain stripped for 2 d.

For the development of new pre-applied membranes, nonwovens with low pore volumes are recommended in Ref. [19, 27] as they accumulate less excess water. In this article, nonwovens with higher pore volumes tend to show higher bond strength values at a w/c ratio of 0.40 ($r^2 = 0.48$). This trend can be explained physically since nonwovens with a higher pore volume are usually mechanically bonded by needling or hydroentanglement and thus have rougher surfaces and more fibers in the z-direction than calendared nonwovens. As a result, they interlock better with the matrix [30]. At a practice-oriented w/c ratio of 0.55, however, nonwovens with higher basis weights yield lower bond strength values since they accumulated more excess water, lowering the matrix strength in the bonding zone. Since the development of new pre-applied membranes must consider standard fresh concrete mixtures with a w/c of 0.5–0.6, nonwovens with low basis weights are recommended.

4.4. Experimental limitations

Due to the experimental procedure and the samples used, the following limiting boundary conditions apply.

- The tests were carried out in the laboratory at 23–25 °C. Both the concrete hydration and plastic properties are strongly temperature dependent.
- Only one grading curve and type of aggregate were included in the tests. According to Ref. [12], the aggregate size has a minor influence on bond strength.
- No comparative investigations were carried out on commercially available pre-applied bonded membranes. Comparative results were derived from Ref. [12].
- Only dry and clean nonwovens were included in the tests. On construction sites, weather and dirt are present as non-negligible influencing variables.

5. Conclusions

This paper aims to determine the bond strength values of nonwovens with concrete and the influence of fresh and hardened concrete properties to optimize nonwovens for pre-applied membranes and avoid defects due to incorrect concrete placement. The following conclusions can be drawn.

- Specimens with laminated nonwovens show bond strength values in the reference tests comparable to literature values. At the same time, the results are not influenced by the material strength of the pre-applied membrane.
- In pull-off tests, debonding generally occurs in the interface between nonwoven and concrete surface within the uppermost nonwoven layer. Some nonwoven fibers remain in the concrete, pull out of the nonwoven and lead to the nonwoven disintegration.

The failure location can possibly be related to a weakened cement matrix, which is caused by the nonwoven fibers that are mostly arranged parallel to the concrete surface.

- Nonwovens' bond strength is proportional to the tensile splitting strength of concrete as the bond strength increases with increasing tensile splitting strength, e.g., due to a reduced w/c ratio in the fresh concrete mixture.
- Nonwovens' bond strength also develops proportionally to the tensile splitting strength and can be described in good approximation using the *fib* model code for compressive strength development and a nonwoven-specific coefficient. The bond strength is between 18 and 56% of the tensile splitting strength for fresh concrete with w/c 0.55 - with lighter nonwovens showing higher bond strengths.
- Modified fresh concrete spread due to varying amounts of PCE superplasticizer and changed vibration compaction times have little influence on the bond strength. Even without vibration compaction, a bond is achieved, most likely as solids enter the nonwovens during filter cake formation. However, vibration compaction improves the bond strength in edge and corner areas as water accumulations are displaced.
- If the nonwovens are horizontally oriented, an increasing distance to the point of concrete pouring leads to decreasing bond strength values. At the same time, the w/s ratios in the nonwovens increase.
- With vertically arranged nonwovens, excess water sinks in the nonwovens during the concrete placement, as observed in video recordings. In the same areas, the bond strength improves. However, vertical nonwoven areas with standing water showed reduced bond strength values, most likely because the water is squeezed back into the fresh concrete during vibration compaction. In practical applications, water can drain out of formworks and, thus, is unlikely to change the bond strength.
 - In summary, the behavior of nonwovens during concrete placement can be described in comparison with Controlled Permeable Formworks. The nonwovens separate excess water from the fresh concrete that fills the nonwovens and moves during and after compaction. A higher water-to-solids ratio in the bonding zone reduces the cement matrix strength and, thus, the bond strength. For the development of pre-applied membranes, nonwovens with low basis weights are recommended regarding improved bond strength since they accumulate less excess water in the nonwovens.

CRedit author statement

The corresponding author [Ulli Heinlein](#) has acted in the following roles:

Conceptualization, Methodology, Resources, Investigation, Formal Analysis, Writing – original draft, Writing – reviewing and editing.

The author [Thomas Freimann](#) has acted in the following roles:

Funding acquisition, Writing – reviewing and editing.

Declaration of competing interest

The authors declare that they have no known competing financial interests or personal relationships that could have appeared to influence the work reported in this paper.

Data availability

Data will be made available on request.

Acknowledgment

The authors would like to thank Prof. Dr.-Ing. K.-Ch. Thienel (Universität der Bundeswehr München) for the inspiring discussions. The present work is supported by the Bavarian Academic Forum in the collegium "Infrastruktur-Bauen-Urbanisierung".

Appendix A. Supplementary data

Supplementary data to this article can be found online at <https://doi.org/10.1016/j.jobe.2023.105837>.

References

- [1] Deutscher Beton- und Bautechnik-Verein E.V. DBV-Heft 44, Frischbetonverbundsysteme (FBV-Systeme) - Sachstand und Handlungsempfehlungen" Fassung Oktober 2018, Eigenverlag DBV, 2018.
- [2] BS 8102:2009-11-30, Code of Practice for Protection of below Ground Structures against Water from the Ground. British Standards Institution, London.
- [3] U. Heinlein, K.-C. Thienel, T. Freimann, Pre-applied bonded waterproofing membranes: a review of the history and state-of-the-art in Europe and North America, *Construct. Build. Mater.* 296 (2021), 123751, <https://doi.org/10.1016/j.conbuildmat.2021.123751>.
- [4] U. Heinlein, T. Freimann, Pre-applied mechanically bonded waterproofing membranes: cement paste filtration process and influencing parameters, *J. Build. Eng.* (2022), 105385, <https://doi.org/10.1016/j.jobe.2022.105385>.
- [5] W.F. Price, *Controlled Permeability Formwork*, CIRIA, London, 2000.
- [6] P.J. Schubel, N.A. Warrior, K.S. Elliott, M. Jones, An Investigation into the critical factors affecting the performance of composite controlled permeable formwork liners: Part I – drainage medium, *Construct. Build. Mater.* 22 (7) (2008) 1551–1559, <https://doi.org/10.1016/j.conbuildmat.2007.03.030>.

- [7] Z.Q. Yang, J.Z. Liu, W. Lin, J.P. Liu, D.G. Xu, Review of progress and applications of controlled permeability formwork in concrete engineering, *Adv. Mater. Res.* (2013) 821–822, 171–8, <https://doi.org/10.4028/www.scientific.net/AMR.821-822.171>.
- [8] F. Serafini, Concrete Form Liner (US 5,824,347) United States Patent, 1998. <https://depatisnet.dpma.de/DepatisNet/depatisnet?action=pdf&docid=US000005824347A>.
- [9] R. Beddoe, The effect of formwork linings on surface concrete, in: 28th Research Colloquium DAfStb, Technische Universität München, 1993.
- [10] H. Figueiras, S. Nunes, J.S. Coutinho, J. Figueiras, Combined effect of two sustainable technologies: self-compacting concrete (SCC) and controlled permeability formwork (CPF), *Construct. Build. Mater.* (23) (2009) 2518–2526, <https://doi.org/10.1016/j.conbuildmat.2009.02.035>.
- [11] S. Kothandaraman, S. Kandasamy, K. Sivaraman, The effect of controlled permeable formwork liner on the mechanical and durability properties of self compacting concrete, *Construct. Build. Mater.* (118) (2016) 319–326, <https://doi.org/10.1016/j.conbuildmat.2016.05.083>.
- [12] L. Meyer, S. Bilgin, S. Filusch, T. Freimann, U. Heinlein, K. Herrmann, Bauwerksabdichtung mit Frischbetonverbundfolie - Grundlagen zur Erstellung eines Regelwerks für eine innovative Bauart: Abschlussbericht F 3183, Fraunhofer IRB Verlag, Stuttgart, 2020.
- [13] DIN EN 1542:1999-07, Produkte und Systeme für den Schutz und die Instandsetzung von Betontragwerken - Prüfverfahren - Messung der Haftfestigkeit im Abreiβversuch; Deutsche Fassung EN 1542:1999. Berlin: Beuth Verlag GmbH. <https://doi.org/10.31030/8086119>.
- [14] J.H. Long, S.L. Paul, Bond strength between geotextiles and concrete, *Geotext. Geomembranes* 8 (1989) 113–132.
- [15] P. Schreiber, Frischbetonverbundtechnologie - Vergleichende Untersuchungen zum Einfluss des Betonalters auf die Haftspannung in der Grenzschicht von vertikal applizierten FBV-Systemen, Unpublished Master Thesis at the Technical University in Nuremberg, Germany, 2019.
- [16] DIN EN 12350-5:2019-09, Prüfung von Frischbeton - Teil 5: Ausbreitmaß; Deutsche Fassung EN 12350-5:2019. Berlin: Beuth Verlag GmbH. <https://doi.org/10.31030/3045714>.
- [17] DIN EN 12350-6:2019-09, Prüfung von Frischbeton - Teil 6: Frischbetonrohndichte; Deutsche Fassung EN 12350-6:2019. Berlin: Beuth Verlag GmbH. <https://doi.org/10.31030/3045731>.
- [18] fib Model Code for Concrete Structures, *fédération internationale du béton/International Federation for Structural Concrete (fib)*, Ernst & Sohn, Berlin, 2010.
- [19] U. Heinlein, T. Freimann, Pre-applied mechanical bonded waterproofing membranes: cement paste filtration process and influencing parameters, *J. Build. Eng.* 62 (2022). <https://doi.org/10.1016/j.job.2022.105385>.
- [20] DIN EN 1849-2:2019-09, Abdichtungsbahnen - Bestimmung der Dicke und der flächenbezogenen Masse - Teil 2: Kunststoff- und Elastomerbahnen für Dachabdichtungen; Deutsche Fassung EN 1849-2:2019. Berlin: Beuth Verlag GmbH. <https://doi.org/10.31030/3042454>.
- [21] G. Kundt, H. Krentz, *Ä. Glass, Epidemiologie und Medizinische Biometrie (Epidemiology and Medical Biometry)*, Shaker Verlag, Aachen, 2011, p. 246.
- [22] S.B. Singh, P. Munjal, N. Thammishetti, Role of water/cement ratio on strength development of cement mortar, *J. Build. Eng.* 4 (2015) 94–100, <https://doi.org/10.1016/j.job.2015.09.003>.
- [23] Bonzel J, Dahms J. Der Einfluß des Zements, des Wasserzementwertes und der Lagerung auf die Festigkeitsentwicklung des Betons. *Betontechnische Berichte*; 66:115–138.
- [24] L. Basheer, S.V. Nanukkuttan, P.A.M. Basheer, The influence of reusing 'Formtex' controlled permeability formwork on strength and durability of concrete, *Mater. Struct.* 41 (8) (2008) 1363–1375, <https://doi.org/10.1617/s11527-007-9335-9>.
- [25] P.J. Schubel, N.A. Warrior, K.S. Elliott, An investigation into factors affecting the performance of composite controlled permeable formwork liners: Part II – filter medium, *Construct. Build. Mater.* 22 (11) (2008) 2235–2249, <https://doi.org/10.1016/j.conbuildmat.2007.08.006>.
- [26] U. Heinlein, T. Freimann, S. Bilgin, S. Filusch, L. Meyer, K. Herrmann, Frischbetonverbundsysteme – neue Erkenntnisse aus Forschung und Praxis, *Beton-Stahlbetonbau* (2020), <https://doi.org/10.1002/best.202000031>.
- [27] U. Heinlein, T. Freimann, Pre-applied mechanical bonded waterproofing membranes: macroscopic nonwoven behavior during the concreting process, *J. Build. Eng.* 45 (2022), 103531, <https://doi.org/10.1016/j.job.2021.103531>.
- [28] P.K. Patnaik, P.T.R. Swain, S.K. Mishra, A. Purohit, S. Biswas, Recent developments on characterization of needle-punched nonwoven fabric reinforced polymer composites – a review, *Mater. Today Proc.* 26 (2020) 466–470, <https://doi.org/10.1016/j.matpr.2019.12.086>.

Supplementary Data to the publication:

Heinlein, U., Freimann, T.: Pre-applied mechanically bonded waterproofing membranes: Bond strength of nonwovens to concrete and influencing parameters.



Fig. S1 – After the fresh concrete was placed on nonwoven N2 in the center of the specimen ($l/w/h = 600/600/200$ mm) without vibration compaction, more cement paste was visible in the specimen center

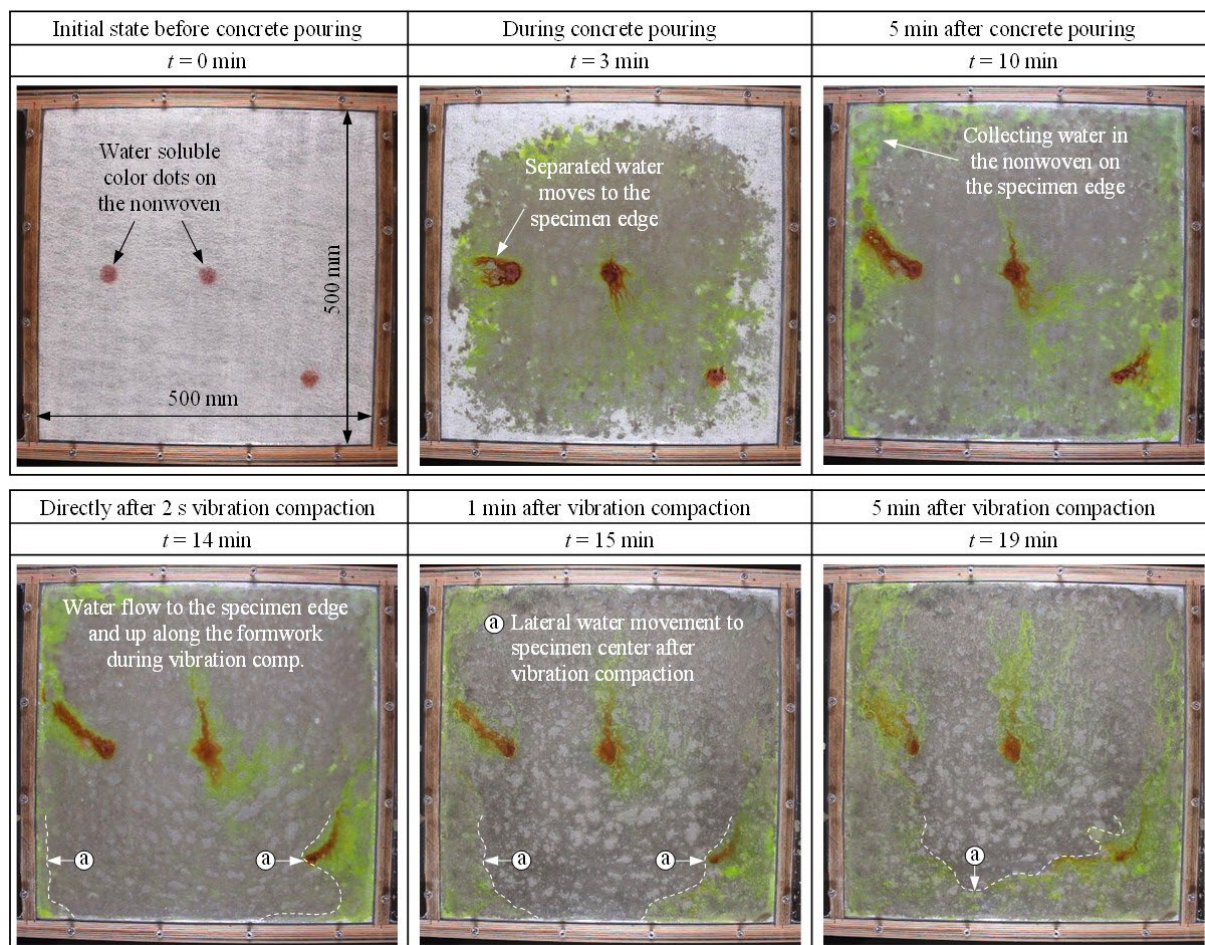


Fig. S2 – Filmed processes in the horizontally oriented nonwoven N1 during and after concrete placement.

10 Appendix A

Fig. A1 illustrates selected processes in the production of nonwovens.

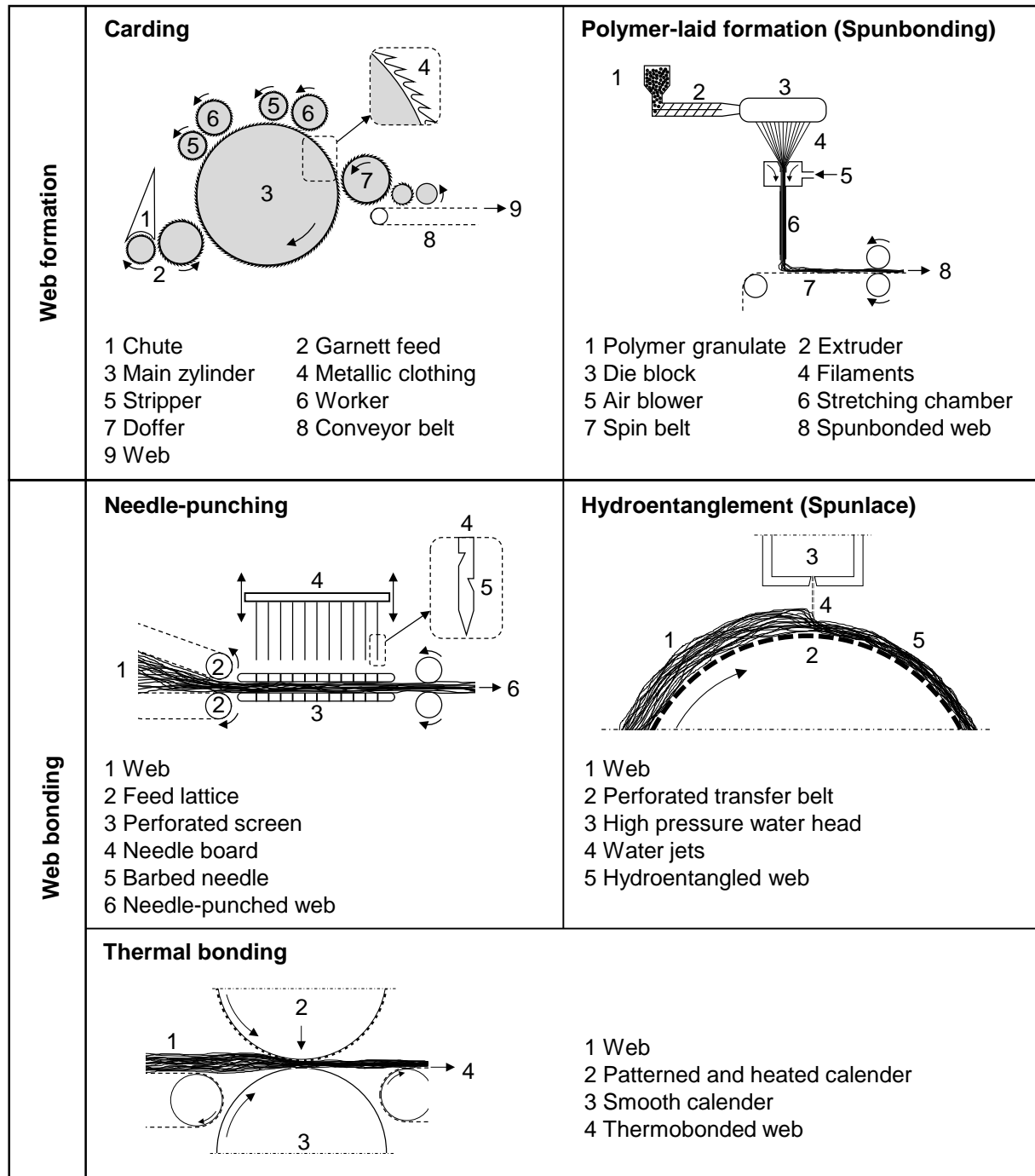


Fig. A1 - Illustration of selected processes in the formation and bonding of nonwovens (based on [56])

11 Appendix B

A list of all publications prepared during the doctorate:

2023

- **Heinlein, U.** *Mechanisch-adhäsive Frischbetonverbundsysteme: Untersuchungen zur Verbundentwicklung und Haftzugfestigkeit.* Beton- und Stahlbetonbau 118 (2023). Ernst & Sohn a Wiley brand, <https://doi.org/10.1002/best.202300034>
- **Heinlein, U.**, Freimann, T. *Pre-applied mechanically bonded waterproofing membranes: Bond strength of nonwovens to concrete and influencing parameters.* Journal of Building Engineering 2023;68:105387. <https://doi.org/10.1016/j.jobee.2023.105837>.

2022

- Freimann, T., **Heinlein, U.** *Planung und Anwendung von Frischbetonverbundsystemen bei wasserundurchlässigen Baukonstruktionen aus Beton.* In: Bergmeister K, Fingerloos F, Wörner J-D (Hrsg.). Beton-Kalender 2023: Wasserundurchlässiger Beton; Brückenbau. Berlin, Germany: Ernst & Sohn a Wiley brand; 2022.
- **Heinlein, U.**, Freimann, T. *Pre-applied mechanically bonded waterproofing membranes: Cement paste filtration process and influencing parameters.* Journal of Building Engineering 2022;62:105385. <https://doi.org/10.1016/j.jobee.2022.105385>.
- **Heinlein, U.**, Freimann, T. (Technische Hochschule Nürnberg) DE10 2021 105 112 A1. Prüfanordnung und Verfahren zur Prüfung von Frischbetonverbundsystemen auf laterale Wasserbewegungen. Offenlegungsschrift.
- Krause, H-J., Horstmann, M., Hohmann, R., Zitzelsberger, T., Freimann, T., **Heinlein, U.**, Frisch, J. *Planungsprozesse für erfolgreiche WU-Betonkonstruktionen – Empfehlungen aus der Praxis.* Beton- und Stahlbetonbau 2022;117(6):383–96. <https://doi.org/10.1002/best.202200032>.
- **Heinlein, U.**, Freimann, T. *Pre-applied mechanical bonded waterproofing membranes: Macroscopic nonwoven behavior during the concreting process.* Journal of Building Engineering 2022;45:103531. <https://doi.org/10.1016/j.jobee.2021.103531>.
- **Heinlein, U.**, Freimann, T. *Industrial concrete floors: Evaluation of electrostatic dissipative properties according to IEC 61340-4-1.* Construction and Building Materials 2022;329:127162. <https://doi.org/10.1016/j.conbuildmat.2022.127162>.

2021

- **Heinlein, U.**, Thienel, K-C., Freimann, T. *Pre-applied bonded waterproofing membranes: A review of the history and state-of-the-art in Europe and North America.* Construction and Building Materials 2021;296:123751. <https://doi.org/10.1016/j.conbuildmat.2021.123751>.

2020

- Meyer, L., Bilgin, S., Filusch, S., Freimann, T., **Heinlein, U.**, Herrmann, K. *Bauwerksabdichtung mit Frischbetonverbundfolie - Grundlagen zur Erstellung eines Regelwerks für eine innovative Bauart.* Abschlussbericht F 3183. Stuttgart: Fraunhofer IRB Verlag; 2020.
- **Heinlein, U.**, Fraundorfer, A., Katona, S., Wimmer, M. *Herstellung gekrümmter tragender Betonbauteile auf einem formflexiblen Schalungswerkzeug.* Beton- und Stahlbetonbau 2020;115(8):576–85. <https://doi.org/10.1002/best.201900103>.
- **Heinlein, U.**, Freimann, T., Bilgin, S., Filusch, S., Meyer, L., Herrmann, K. *Frischbetonverbundsysteme – Neue Erkenntnisse aus Forschung und Praxis.* Beton- und Stahlbetonbau 2020. <https://doi.org/10.1002/best.202000031>.

- **Heinlein, U.**, Freimann, T., Bilgin, S., Filusch, S., Meyer, L., Herrmann, K. *Frischbetonverbundsysteme – Neue Erkenntnisse aus einem Forschungsvorhaben*. DBV-Rundschreiben 265, Juli 2020

2019

- Fraundorfer, A., Wimmer, M., **Heinlein, U.**, Katona, S. *CAD-gestützte Schalungsmodule. Herstellung komplexer Betonbauteile*. Technik in Bayern 05/2019
- **Heinlein, U.**, Freimann, T. Verwendung von Frischbetonverbundsystemen an befahrenen WU-Sohlplatten in Tiefgaragen. Diskussionspapier. In: 1) Hohmann (Hrsg.): Tagungsband 3. Dortmunder Bauforum. Tiefgaragen und Parkhäuser. März 2019. 2) Freimann (Hrsg.): Tagungsunterlage 13. Nürnberger Bauseminar. Parkbauten und Tiefgaragen. März 2019.

2018

- Freimann, T., **Heinlein, U.** *Planung und Anwendung der Frischbetonverbundsysteme bei wasserundurchlässigen Baukonstruktionen aus Beton*. In: Bergmeister K, Fingerloos F, Wörner J-D (Hrsg.). Beton-Kalender 2018: Bautenschutz, Brandschutz. Berlin, Germany: Ernst & Sohn a Wiley brand; 2018, p. 227–258.
- Freimann, T., **Heinlein, U.** *Frischbetonverbundtechnologie. Verbundmechanismus und Hinweise zur fachgerechten Ausführung*. Beton- und Stahlbetonbau 2018;113(5):368–84. <https://doi.org/10.1002/best.201700098>.
- Freimann, T., **Heinlein, U.** *Fachgerechte Ausführung von Frischbetonverbundsystemen*. BauPortal, Heft 2. 2018. BG Bau.
- Freimann, T., **Heinlein, U.** *Bauen mit Frischbetonverbundsystemen – Chance oder Risiko? Was ist bei der Planung und Bauausführung mit Frischbetonverbundsystemen unbedingt zu beachten?* In: Freimann, Hohmann (Hrsg.) WU-Konstruktionen richtig geplant und ausgeführt. Tagungsband 12. Nürnberger Bauseminar 2018.
- Freimann, T., **Heinlein, U.** *Aktuelle Hinweise zur Verwendung und fachgerechten Ausführung von Frischbetonverbundsystemen*. DBV-Regionaltagung Nürnberg 2018.